AD/A-005 392

LOW SPEED WIND TUNNEL INVESTIGATION OF A .09 SCALE, NAVY MODEL T-2C SUBSONIC JET TRAINER AIRCRAFT, FROM -8 TO +83 DEGREES ANGLE-OF-ATTACK

A. J. Schuetz, et al

Naval Air Development Center

Prepared for:

Director of Navy Laboratories

31 December 1973

DISCLAIMER NOTICE

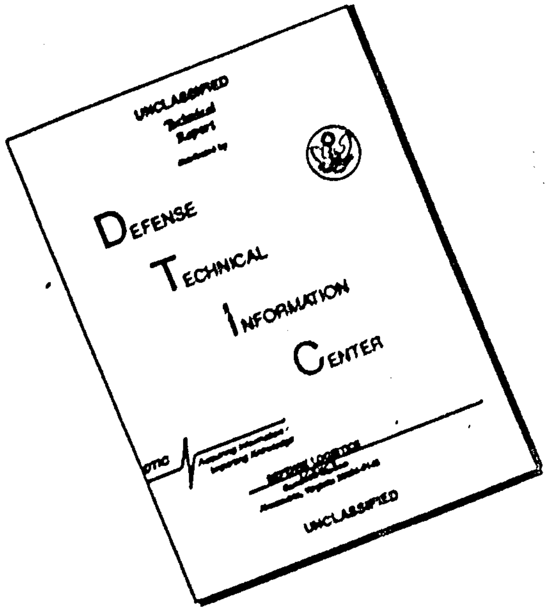

THIS DOCUMENT IS BEST QUALITY AVAILABLE. THE COPY FURNISHED TO DTIC CONTAINED A SIGNIFICANT NUMBER OF PAGES WHICH DO NOT REPRODUCE LEGIBLY.

NADC-73259-30

NOTICES

REPORT NUMBERING SYSTEM - The numbering of technical project reports issued by the Naval Air Development Center is arranged for specific identification purposes. Each number consists of the Center acronym, the calendar year in which the number was assigned, the sequence number of the report within the specific calendar year, and the official 2-digit correspondence code of the Command Office or the Functional Department responsible for the report. For example: Report No. NADC-73015-40 indicates the fifteenth Center report for the year 1973, and prepared by the Crew Systems Department. The numerical codes are as follows:

CODE	OFFICE OR DEPARTMENT
00	Commander, Naval Air Development Center
01	Technical Director, Naval Air Development Center
02	Program and Fiscal Management Department
03	Anti-Submarine Warfare Program Office
04	Remote Sensors Program Office
05	Ship and Air Systems Integration Program Office
10	Naval Air Facility, Warminster
20	Aero Electronic Technology Department
30	Air Vehicle Technology Department
40	Crew Systems Department
50	Systems Analysis and Engineering Department
81	Administration and Technical Services Department
85	Computer Services Department

PRODUCT ENDORSEMENT - The discussion or instructions concerning commercial products herein do not constitute an endorsement by the Government nor do they convey or imply the license or right to use such products.

APPROVED BY: ______________________ DATE: 31 December 1973

P. D. STOGIS
Commander, USN
Deputy Director, AVTD

UNCLASSIFIED

SECURITY CLASSIFICATION OF THIS PAGE (When Data Entered)

REPORT DOCUMENTATION PAGE		READ INSTRUCTIONS BEFORE COMPLETING FORM
1. REPORT NUMBER NADC-73259-30	2. GOVT ACCESSION NO.	3. RECIPIENT'S CATALOG NUMBER AD/A 005 312
4. TITLE (and Subtitle) LOW SPEED WIND TUNNEL INVESTIGATION OF A .09 SCALE, NAVY MODEL T-2C SUBSONIC JET TRAINER AIRCRAFT, FROM -8 TO +83 DEGREES ANGLE-OF-ATTACK		5. TYPE OF REPORT & PERIOD COVERED FINAL REPORT 6. PERFORMING ORG. REPORT NUMBER
7. AUTHOR(s) A. J. Schuetz D. B. Bailey		8. CONTRACT OR GRANT NUMBER(s)
9. PERFORMING ORGANIZATION NAME AND ADDRESS Air Vehicle Technology Department (Code 30) Naval Air Development Center Warminster, Pa. 18974		10. PROGRAM ELEMENT, PROJECT, TASK AREA & WORK UNIT NUMBERS IR TASK R000-01-01/MF-9-01
11. CONTROLLING OFFICE NAME AND ADDRESS Director of Naval Laboratories Department of the Navy Washington, D. C. 20390		12. REPORT DATE 31 December 1973 13. NUMBER OF PAGES 185
14. MONITORING AGENCY NAME & ADDRESS(if different from Controlling Office)		15. SECURITY CLASS. (of this report) UNCLASSIFIED 15a. DECLASSIFICATION/DOWNGRADING SCHEDULE

16. DISTRIBUTION STATEMENT (of this Report)

Approved for public release, distribution unlimited.

17. DISTRIBUTION STATEMENT (of the abstract entered in Block 20, if different from Report)

18. SUPPLEMENTARY NOTES

PRICES SUBJECT TO CHANGE

19. KEY WORDS (Continue on reverse side if necessary and identify by block number)

Low Speed Wind Tunnel Testing
Aircraft High Angles-Of-Attack
Stability and Control

20. ABSTRACT (Continue on reverse side if necessary and identify by block number)

The aerodynamic stability and control characteristics of a .09 scale T-2C model have been investigated in the NASA-Ames 12-foot pressure wind tunnel. The T-2C is a straight, fixed-wing Navy jet trainer aircraft manufactured by the Columbus Division of Rockwell International Corporation. The data span angles-of-attack from -8 to 83 degrees and sideslip angles of -10 to 30 degrees for various deflections of the ailerons, rudder, and elevator. The data are judged to be sufficient in quality and quantity to fully define the static aerodynamic characteristics of the T-2 aircraft in low speed flight.

DD FORM 1 JAN 73 1473

UNCLASSIFIED

SECURITY CLASSIFICATION OF THIS PAGE (When Data Entered)

A C K N O W L E D G E M E N T S

This wind tunnel test would not have been possible without the cooperation of several corporations and government agencies. The authors are indebted to NASA-Ames for the use of the 12-foot pressure wind tunnel, to McDonnell-Douglas Corporation for the use of their balances and stings, and to NASA-Langley for the use of the original T-2 model, subsequently modified substantially by Atkins and Merrill, Inc.

The authors wish to express their thanks to all the personnel of the various corporations and agencies who assisted in the performance of the test. The following individuals deserve particular thanks for their especially significant contributions: Mr. Daniel Petroff (technical monitor's representative, NASA-Ames), Mr. David Banducci (supervisory engineer, ARO, Inc.), Mr. Odell Sapp (project engineer, ARO, Inc.), Mr. Richard Walrose (associate project engineer, ARO, Inc.), Mr. Randy Nelson (equipment engineer, Naval Ship Research and Development Center), Messrs. Dale Atkinson and Richard Cassidy (modelmakers, Atkins and Merrill, Inc.), and Mr. William Bihrle (consultant, Bihrle Applied Research, Inc.).

SUMMARY

The objective of this investigation was the determination of the full-scale static aerodynamic stability and control characteristics of the T-2B/C aircraft. To accomplish this objective, tests were conducted in the NASA-Ames 12-foot pressure wind tunnel using a .09 scale T-2C model.

The T-2C is a straight, fixed wing Navy jet trainer aircraft manufactured by the Columbus Division of Rockwell International. A YT-2B, aerodynamically identical to the T-2C, is currently assigned to NAVAIRDEVCEN for research and development purposes. It has been gathering flight time history data for use in parameter identification technique development and for use as baseline data for a proposed variable-stability conversion. In order to use the flight data for either of these purposes, however, it is first necessary to have complete, accurate wind tunnel data.

A variety of wind tunnel operating conditions were evaluated in preliminary tests. The results of these tests indicated that the bulk of the data should be collected at a Mach number of 0.2 and a Reynolds number of 6 million per foot. The data span angles-of-attack from -8° to 83° and sideslip angles from -10° to +30°. Various deflections of ailerons, rudder, and elevator were investigated independently and in combination. Only full control deflections were used at angles-of-attack greater than 40°.

In general, the data presented in this report are judged to be sufficient to fulfill the objective of the investigation. Complete determination of static aerodynamic characteristics, however, is not sufficient for complete modeling or simulation of the aircraft, and it is recommended that every effort be made to obtain dynamic wind tunnel data in the near future.

TABLE OF CONTENTS

LIST OF FIGURES

LIST OF FIGURES (CONT)

LIST OF FIGURES (CONT)

LIST OF FIGURES (CONT)

LIST OF TABLES

SYMBOLS, ABBREVIATIONS, AND DEFINITIONS

b	wing span, feet
$\bar{c}$	mean wing chord, feet
C_A	coefficient of axial force, axial force/qS
C_D	coefficient of drag, drag/qS
C_L	coefficient of lift, lift/qS
C_{L_α}	change in lift coefficient with angle-of-attack (lift curve slope), 1/deg
C_ℓ	coefficient of rolling moment, rolling moment/qbs
C_{ℓ_β}	change in rolling moment coefficient with sideslip angle (effective dihedral derivative), 1/deg
$C_{\ell_{\delta_a}}$	change in rolling moment coefficient with deflection of aileron, 1/deg
C_m	coefficient of pitching moment, pitching moment/$qS\bar{c}$
C_{m_α}	change in pitching moment coefficient with angle-of-attack (static stability derivative), 1/deg
$C_{m_{\delta_e}}$	change in pitching moment coefficient with deflection of elevator, 1/deg
C_N	coefficient of normal force, normal force/qS
C_n	coefficient of yawing moment, yawing moment/qSb
C_{n_β}	change in yawing moment coefficient with sideslip angle (static directional stability derivative), 1/deg
$C_{n_{\delta_r}}$	change in yawing moment coefficient with deflection of rudder, 1/deg
C_Y	coefficient of sideforce, sideforce/qS
C_{Y_β}	change in sideforce coefficient with sideslip angle, 1/deg
M	mach number, velocity/speed of sound
q	dynamic pressure, pounds/square foot
Re	reynolds number, 1/foot or dimensionless
S	wing area, square feet

SYMBOLS, ABBREVIATIONS, AND DEFINITIONS (CONT)

GREEK SYMBOLS

α	angle-of-attack, relative to fuselage reference line, degrees
β	angle-of-sideslip, degrees (positive for airplane nose left relative to wind)
ΔC_L	change in coefficient of lift
ΔC_ℓ	change in coefficient of rolling moment
ΔC_m	change in coefficient of pitching moment
ΔC_n	change in coefficient of yawing moment
ΔC_Y	change in coefficient of sideforce
δ_a	aileron deflection, degrees (positive for right aileron trailing edge down, with left aileron trailing edge up)
δ_e	elevator deflection, degrees (positive trailing edge down)
δ_r	rudder deflection, degrees (positive trailing edge left)

ABBREVIATIONS

A&M	Atkins and Merrill, Inc., Ashland, Mass.
ARO	Arnold Research Organization, Moffett Field, Ca.
BAR	Bihrle Applied Research, Inc., Oyster Bay, N.Y.
B.L.	Butt Line
C.G.	Center of Gravity
FRP	Fuselage Reference Plane
F.S.	Fuselage Station, inches
MDC	McDonnell Douglas Corp., St. Louis, Mo.
NAVAIRDEVCEN	Naval Air Development Center, Warminster, Pa.
R.L.	Reference Line
W.L.	Water Line

SYMBOLS, ABBREVIATIONS, AND DEFINITIONS (CONT)

AXES SYSTEMS

Body Axis System: Origin at Center of Gravity; X-axis parallel to fuselage reference line, located within the plane of symmetry, positive forward; Y-axis perpendicular to plane of symmetry, positive toward right wing; Z-axis perpendicular to both X-axis and Y-axis, positive downward.

Stability Axis System: Same as Body System except that X-axis is aligned with tunnel axis, positive forward; so that Z-axis is perpendicular to tunnel axis, positive downward.

Note: The Body Axis System is used for the majority of the presentations of lateral-directional data in this report. Some data are presented in both axes systems as a convenience to the user. The Stability Axis System (lift, drag) is emphasized for the longitudinal data, but Body system (normal force, axial force) presentations are included as a convenience.

INTRODUCTION

The objective of this investigation was the determination of the full-scale static aerodynamic characteristics of the T-2B/C aircraft. Specifically, the changes in all aerodynamic forces and moments, due to changes in angles of attack and sideslip and deflections of control surfaces, were to be determined. Thus the investigation was of the stability and control type, rather than performance or component design analysis. The results of these tests will serve as a data base for several Naval Air Development Center (NAVAIRDEVCEN) research programs.

BACKGROUND

Two research programs in progress at NAVAIRDEVCEN involve the operation of a Navy T-2B/C aircraft. One program is the development of a variable stability research vehicle based on the T-2 airframe; the other program includes the evaluation and development of several different methods for the identification of airframe stability and control parameters from flight test data. Neither research program can be properly executed without complete, accurate wind tunnel data for the basic T-2. The previously available wind tunnel data for the T-2 were entirely inadequate - they covered only the low angle-of-attack region and they actually applied only to the T-2A, whose aft lower fuselage is substantially different from the T-2B/C.

The parameter identification research program intends to eventually develop a high angle-of-attack parameter identification method. In pursuit of this goal, several identification methods will be used to analyze T-2B flight data from (1) unstalled flight, (2) flight in the vicinity of the stall, and (3) spinning flight. In order to reach valid conclusions concerning the effectiveness of these methods, it is necessary that the full-scale aerodynamic characteristics of the T-2B are known to a high order of accuracy over a range of angles-of-attack from the negative stall angle (about -10°) to the largest angle-of-attack encountered in spins (near 90°). Since the focal point of the parameter identification research is the departure condition, characteristics just above and below stall angle-of-attack, over a large sideslip range, are of special interest.

EQUIPMENT DESCRIPTION

MODEL

A .09 scale model of the Navy/Rockwell International T-2C was used for this investigation. The model had been constructed originally by Atkins and Merrill, Inc., of Ashland, Mass., for use by the NASA Langley Research Center, NAVAIRDEVCEN returned the model to A&M for major modifications in preparation for this test. The model was of all-aluminium construction, weighing approximately ninety pounds. The intent of the design and construction was to model, as closely as possible, the features of the YT-2B aircraft currently assigned to NAVAIRDEVCEN. This aircraft is identical to the production T-2B (for which geometric parameters are given in Appendix B), with the exception

that the YT-2B is equipped with a noseboom. A scaled noseboom was therefore added to the model. Since baseline fuselage drag was not regarded as an important factor in these tests, it was decided not to construct elaborate flow-through ducts simulating actual inlet flow. Instead the inlet contours were faired along the fuselage.

Figures 1 through 4 provide detailed information on the geometry of the model.

Available control surface deflections were as follows:

(1) Elevator Deflection, δ_e +15, +5, 0, -5, -10, -15, -25 degrees

(2) Rudder Deflection, δ_r 0, ±7, ±15, ±25 degrees

(3) Aileron Deflection, δ_a 0, ±3, ±6, ±12 degrees (measured from an original uprigged trailing edge position of 3.0 degrees)

A leveling surface was located on the model for convenient zero reference of model pitch and roll. Photographs of the model installed in the tunnel are presented in figures 5 and 6.

STINGS AND SUPPORT SYSTEM

The basic support system used for this test in the NASA-Ames 12-foot pressure tunnel was the "Northrop High Angle" system. The cylindrical structural member extending upward from the tunnel floor is capable of independent movements of two modes such that changes in model pitch (angle-of-attack) and yaw (sideslip) may be accomplished by remote control. Unfortunately, the mechanism which creates this movement protrudes somewhat into the tunnel, causing some flow disturbance. This flow disturbance was analyzed in reference (a). To obtain the entire desired range of angle-of-attack, it was necessary to test in three support configurations, using a variety of stings and other support system hardware.

In sting configuration 001, the MDC F-4 straight sting (No. 32-031048) entered the model from the rear, as shown i . figure 7. This configuration was used to gather data from -8 to +40 degrees angle-of-attack.

For angles-of-attack from 35 to 55 degrees, sting configuration 002 was used. In this configuration the lower support system was identical to 001, but the MDC F-4 bent sting (No. 32-013049) was interposed between the straight sting and the model. The bent sting entered the model from above, through the area which corresponds to the canopy of the aircraft, and was bent toward the rear, so that the balance was installed in the reverse of the usual orientation. The installation is shown in figure 8.

Sting configuration 003, for angles-of-attack from 62 to 83 degrees, differed from 002 only in the deletion of the "dog-leg" in the lower support system. This configuration is illustrated in figure 9.

Model pitch attitude (angle-of-attack) was directly determined by a "dangleometer" (a simple gravity device to measure angular position) mounted in the nose of the model. Model yaw attitude (sideslip), however, was calculated by applying sting deflection corrections to the setting of the support mechanism.

BALANCE

A six component 2.0 inch diameter Task internal balance (MK XXIA) was used for force and moment measurements for test runs in sting configuration 001, but an electrical problem within the balance dictated the substitution of the identical MK XXIB balance for sting configurations 002 and 003. The internal balance fit, with a light press-fit, into the balance block, which was the keystone of the model structure. One end of the balance was firmly bolted to the sting, so that the balance-to-balance-block interface would bear all forces and moments transmitted from the model to the support system. To assure that no direct contact between the model and the support system took place, a fouling circuit was added to the installation to alert the tunnel operator to any model-sting fouling. The balance was limited to a normal force of 7000 pounds, a sideforce of 3000 pounds, an axial force of 450 pounds, and a rolling moment of 5000 inch-pounds.

A pressure measurement was made in the model cavity between the dangleometer and the forward end of the balance. This measurement data was used for the calculation of correction factors for the balance and dangleometer readings.

TEST OUTLINE AND PROCEDURES

A matrix of model attitudes, control surface deflections, and tunnel operating conditions was formulated to meet the objective of the tests. In view of the importance of tunnel operational efficiency, this matrix was reorganized into an effecient run schedule. Time restrictions, hardware limitations, and preliminary results obtained during the test motivated some changes to the run schedule as the test progressed. The record of the test runs as actually done is given as Appendix A.

While angles-of-attack and sideslip were varied by remote control during a run, changes in control deflection and/or sting configuration required access to the test section, so that the tunnel air had to be returned to atmospheric pressure and zero velocity. Control surfaces were re-positioned by changing the brackets which held the control surface to the model. Following each such change, the tunnel air was pressurized and then brought up to speed by the fan drive system. Before each run took place, bolt holes and other surface irregularities in the model were carefully smoothed or filled with wax or plaster.

To compensate for model vibration, each data point was automatically taken three times, then the readings were averaged to results in a single data point.

All correction factors and axis system transformations were applied to the data by an ARO computer program.

DETERMINATION OF OPERATING CONDITIONS

To permit straightforward evaluation of the effects of changes in model attitude and control surface deflections, it was necessary that the bulk of the data be gathered with a constant set of tunnel operating conditions. Preliminary tests were done in the wind tunnel and evaluated to determine these conditions, rather than relying on a priori selection.

REYNOLDS NUMBER EFFECTS

The maximum Re (Reynolds number) available in the NASA-Ames 12-foot pressure tunnel (when operating at $M = .2$) was 6.0×10^6/ft. This tunnel Re corresponds to a model Re of 4.0×10^6, based on mean aerodynamic chord. Test runs were made at a range of tunnel Re from the 6.0×10^6/ft maximum to 1.0×10^6/ft. The latter is a common tunnel Re for tests in unpressurized tunnels. It was expected that a critical Re (above which Re effects would be insignificant) would exist within this range. See reference (b) for a complete explanation of this phenomenom.

Plots of C_L, C_D, and C_m as a function of Re for various angles-of-attack are given as figures 10, 11, and 12 respectively. It can be seen in figure 10 that C_L tends to increase with Re up to Re = 3×10^6/ft, and then level off. The exception is $\alpha = 16°$, at which C_L continues to increase with Re across the entire range. It would appear from figure 11 that C_D is essentially constant with respect to Re, except for a slight tendency to increase with Re at $\alpha = 40°$. As shown in figure 12, C_m tends to be constant with respect to Re for $\alpha = 8, 12°$, and C_m becomes slightly more negative with increasing Re at $\alpha = 0, 16, 20, 40°$. The slope of the C_m vs. Re relationship for $\alpha = 16, 20°$ is more shallow above Re = 3×10^6/ft than below.

These results tend to indicate that although a critical Re seems to exist at approximately 3×10^6/ft, some data in the post-stall region ($\alpha = 16, 20°$) continue to be a function of Re throughout the available range. The report of the BAR (Bihrle Applied Research) consultant supported these observations (see Appendix C). On the basis of these results, it was determined that the majority of the data would be generated at Re = 6×10^6/ft.

MACH NUMBER EFFECTS

Operating at $M = .4$, the maximum available Re was 4×10^6/ft. Thus the comparison of $M = .4$ operation to operation at $M = .2$ was conducted at Re = 4×10^6/ft. The investigation was limited by structural problems with the model at the higher operating temperature and dynamic pressure associated with $M = .4$ operation.

Lift coefficient as a function of angle-of-attack is shown in figure 13 for both Mach numbers. The following differences may be observed: (1) the slope of the pre-stall C_L vs. α curve is slightly increased at M = .4, (2) the maximum lift coefficient obtained at M = .4 is smaller, and occurs at a lower angle of attack, than the $C_{L_{MAX}}$ obtained for M = .2.

The curves for C_D vs. α for the two Mach numbers, given in figure 14, do not reveal any differences between the two test conditions. In figure 15, however, the plots of C_m vs. α show that pitching moment is slightly more negative for M = .4 between $\alpha = 14°$ and $\alpha = 18°$.

In view of the previously discussed need for operation at Re = 6 X 10^6/ft, which is not possible at M = .4, and the hardware difficulties encountered in operation at M = .4, it was decided that data collection would proceed at M = .2. The limited data collected at M = .4 is expected to be quite useful in the process of estimating the full scale aircraft characteristics from the wind tunnel information.

GRIT (TRANSITION STRIP) EFFECTS

To assure that the flow over the wings and other components "trips" (becomes turbulent) at the appropriate point, it is common practice to utilize transition strips, which consist of carborundum grit glued to the surface of the model. A detailed discussion of the use of transition strips may be found in reference (b). The strip size, grit size, and strip locations for this test, as determined by BAR, are given in Table I.

Figures 16 and 17 show C_L vs. α for the model with and without grit, for sideslip angles of 0° and 30°, respectively. The only obserable difference between the "grit on" and "grit off" cases is a slightly decreased C_L for the "grit on" case at post-stall angles of attack at $\beta = 0°$. Corresponding curves for drag coefficient are given in figures 18 and 19. It would appear that the only effect of grit on drag is a slight increase in drag for the "grit on" case at angles-of-attack below stall.

The effects of the transition strips appear to be so minor that "grit on" and "grit off" data may be used interchangeably, and it was decided that grit would not be used for tests with sting configurations 002 and 003. The section of the BAR report dealing with repeatability in general and grit effects in particular is given in Appendix C.

RESULTS AND DISCUSSION

All of the data presented in this section were obtained at the M = .2, Re = 6 X 10^6/ft tunnel condition, and represent the best available information. Although comments will be made on significant aspects of the graphical relationships and on the general validity of the data, no efforts will be made to explain (or speculate concerning) the various apparent irregularities

and inconsistencies which inevitably occur in data collected in large quantities. Some of the obvious trends in the T-2 aerodynamic characteristics will be discussed as the results are presented. However, no attempt will be made at interpretation of the data, since the interpretation process is a function of the application. Instead the data will be left in a general format suitable for a variety of applications. The most generally interesting and useful relationships within the data will be graphed in this report, but an inspection of the run schedule will reveal that many additional relationships could be extracted and plotted for specific applications.

BASIC AIRCRAFT, LONGITUDINAL CHARACTERISTICS

This section is devoted to the effects of changes in angles-of-attack and sideslip, with control surfaces fixed in the undeflected position, on the longitudinal aerodynamic characteristics.

Figure 20 shows one of the most basic and most important relationships: lift coefficient as a function of angle-of-attack for various sideslip angles. At zero sideslip, an abrupt stall can be seen at approximately 14° angle-of-attack. With increasing sideslip, the stall becomes much less abrupt, with reduced $C_{L_{MAX}}$ (occurring at a higher angle-of-attack), and has a substantially higher C_L in the immediate post-stall angle-of-attack (or α) region than for zero sideslip. In the pre-stall α region, the C_L vs. α relationship (lift curve slope) is quite linear, with decreasing slope as sideslip increases. A corresponding graph of C_N (normal force coefficient) as a function of angle-of-attack has been included (figure 21) for use in analyses for which body-oriented axes are more appropriate.

It can be seen from figure 22 that drag coefficient increases in an essentially linear fashion with increasing angle-of-attack in the post-stall region, with little variation due to changes in sideslip. The corresponding axial force graph, figure 23, deserves some comment because of its unusual appearance. Measurements of axial force are subject to considerable inaccuracy because the net axial force is the difference between a positive drag force ($C_D \cos \alpha$) and a negative lift force ($C_L \sin \alpha$). Since these forces are often nearly equal, the axial force is relatively small, and the axial force coefficient scale on figure 23 has been expanded considerably relative to the usual scale for drag (compare, for instance, to figure 22). A "drag polar" showing lift coefficient as a function of drag coefficient, for sideslip angles of 0° and 30°, is given in figure 24 for the full range of angle-of-attack investigated. This graph does not present new information, but is presented as a convenience to the user. The pre-stall region of the C_L vs. C_D relationship is enlarged in figure 25.

Pitching moment is shown as a function of angle-of-attack in figure 26. It can be seen that pitching moment generally tends to become more negative with increasing angle-of-attack, but some local slope reversals do occur. These regions of positive slope indicate static instabilities of the aircraft and are therefore quite significant. At zero sideslip, a positive slope

exists for angles of attack between 18° and 20°, and at sideslip angles of 20° or greater a positive slope may be seen between 25° and 35° angle-of-attack. The C_L vs. C_m relationship is shown in figure 27, and an expanded view of the pre-stall region is given in figure 28.

Several aerodynamic relationships are essentially linear for pre-stall angles-of-attack, and therefore lend themselves to the extraction of stability derivatives from the data. In figure 29 C_{L_α} is shown as a function of sideslip angle, and a similar curve is given for C_{m_α} in figure 30. In both cases, the function has a maximum magnitude at zero sideslip, and decreases quite significantly with increasing magnitude of sideslip angle.

Some aerodynamic characteristics of the T-2B for pre-stall angles-of-attack were estimated by the aircraft manufacturer in Appendix I of reference (c). The estimate of C_{L_α} is .082/degree, which agrees exactly with the C_{L_α} of figure 29, for the zero sideslip case. When corrected for center-of-gravity location, the estimate of C_{m_α} is -.017/deg, which is quite close to the zero sideslip C_{m_α} of -.018 given in figure 30.

Reference (d) contains previous estimates of T-2B drag characteristics. The estimate of C_{D_0} is .023, while it may be concluded from figure 25 that C_{D_0} for these tests was .014. In fact, a comparison of the reference (d) drag polar with the current test drag polar (both are shown in figure 25) clearly indicates a significantly smaller amount of drag on the model used in these tests, but the shapes of the drag polars are quite similar. As previously stated, these tests were oriented toward stability and control information, rather than performance information, so the shape of the drag polar is considerably more important that the offset relative to other estimates. The most probable cause of the drag polar offset is the smoothing of the fuselage in the area of the inlets on the current model.

BASIC AIRCRAFT, LATERAL-DIRECTIONAL CHARACTERISTICS

Sideforce coefficient is plotted as a function of sideslip angle for selected angles-of-attack in figure 31. For a symmetric model and symmetric wind tunnel flow-field, the sideforce coefficient whould clearly be zero at a sideslip angle of zero. For the 001 sting mount this condition does prevail, but such is not the case for the 002 and 003 sting mounts. A direct comparison may be made on the figure 31 graph for 40° angle-of-attack. This plot shows that the C_Y vs. β function is both translated and rotated (i.e., it has a steeper slope) when the 002 sting mount is substituted for the 001. It is possible that the sting, entering the model through the upper surface of the forward portion of the fuselage, disrupts the flow over the vertical tail, which may still create some sideforce at very high angles-of-attack. Somewhat more plausible is the hypothesis that the model was simply mounted out of alignment on the 002 sting, thus shifting the scale of sideslip angle which is measured at the base of the support system. This theory is supported by the

observation that the zero sideforce intercept (approximately -3° sideslip) is independent of angle-of-attack.

Sideforce data are shown for two elevator settings, since elevator position could conceivably change the air flow pattern over the vertical tail. It is apparent from figure 31, however, that sideforce characteristics are not dependent upon elevator position.

Rolling moment due to sideslip, known as dihedral effect, may be evaluated from figures 32 and 33. Figure 32 shows rolling moments measured in body axes, while figure 33 shows the same data after transformation to the stability axis system. The aircraft exhibits positive dihedral effect (i.e., the slope of C_ℓ vs. β is negative) throughout the angle-of-attack range, except that a slope reversal occurs for small sideslip angles at 15° α, which is the stall angle-of-attack. In addition to the slope reversal, a non-zero rolling moment exists at zero sideslip for angles-of-attack from 15° to 30°, indicating that the air flow over the model is asymmetric in the post-stall situation. The lack of flow symmetry may result from subtle asymmetries in the model, or curvature of the basic flow in the tunnel, or asymmetric vortex conditions on the model. The slope of the C_ℓ vs. β curve (body axis) for small sideslip angles is shown as a function of angle-of-attack in figure 37. While some inconsistency exists in the data with respect to the different sting mounts used, there is a definite trend of increasing dihedral effect with increasing angle-of-attack throughout the entire range of test conditions.

Yawing moment coefficient is plotted as a function of sideslip angle (for angles between -10° and ±10°) for various angles-of-attack in figures 34 and 35 (body axis system and stability axis system, respectively). In the body axis system, the relationship between C_n and β is positive for pre-stall angles-of-attack and for α's greater than 50°. For the remaining range of angle-of-attack, C_n is either constant or does not seem to vary in any consistent fashion with sideslip angle. The graphs for 30° and 40° angle-of-attack show little agreement between sting 001 data and sting 002 data. As in the case of rolling moment, some non-zero yawing moments were recorded at zero sideslip and post-stall angles-of-attack. Relatively large positive yawing moments were also found for zero sideslip at angles-of-attack of 62° and 72°.

In figure 38 the slope of the C_n vs. β relationship, for those cases possessing sufficiently linearity for the concept of "slope" to be applicable, is shown as a function of angle-of-attack. It would appear that the aircraft has a high degree of natural directional stability except for the angle-of-attack region between 15° and 40°, in which there is essentially no stability.

No consistent effect of elevator position is observable in the data for rolling, yawing, or sideforce effects.

ELEVATOR EFFECTNESS

For angles-of-attack below 40°, the ability of the elevator to create

pitching moments was thoroughly investigated. Figure 39 shows pitching moment coefficient as a function of elevator deflection for various angles-of-attack. For pre-stall (i.e., less than 15°) angles-of-attack, this functional relationship is quite linear for elevator deflections between +10° and -15°. Beyond +10° deflection the incremental effectiveness is reduced significantly, and deflections more negative than -15° are useless or worse. For angles-of-attack from 18° to 40°, elevator effectiveness is still roughly linear for small elevator deflections, but the magnitude of the effectiveness (i.e., the slope of the curve) is reduced to about half of its value for pre-stall angles-of-attack. The elevator effectiveness for small deflections is plotted in figure 40 as a function of angle-of-attack.

Referring again to figure 39, it is clear that increasing angle-of-attack tends to increase the incremental effectiveness of large negative deflections. At 40° angle-of-attack, for instance, the pitching moment coefficient change due to deflection of the elevator from 0° to -25° is nearly twice the change which is obtained by a deflection from 0° to -15°.

The change in lift coefficient due to full negative, and positive, elevator deflection is shown in figures 41 and 42, respectively, for the full range of angle of attack.

Figure 43 shows the change in pitching moment coefficient due to deflection of the elevator from 0° to -25°, for rudder deflections of 0° and +25° (full left rudder) and sideslips of 0° and 30°. Similar data for elevator deflection from 0° to -15° is given in figure 44, but no data are available for varying rudder deflection or for angles-of-attack beyond 55°. Several significant observations may be made about the data presented on these figures. Most important, under no circumstances does elevator effectiveness become zero. With increasing angle-of-attack, elevator effectiveness increases until stall, then decreases steadily beyond stall. In the 30° sideslip condition, elevator effectiveness for negative control deflection is significantly reduced (relative to the zero sideslip case) for angles-of-attack greater than 20°. For positive deflections, however, the most significant effectiveness reduction due to sideslip occurs for angles-of-attack less than 10°. Rudder position seems to have no significant, consistent effect on elevator effectiveness.

AILERON EFFECTIVENESS

Rolling moment coefficient as a function of aileron deflection is shown in figure 45 for various angles-of-attack up to 40°, and sideslip angles of 0°, -10°, and 10°. Time did not permit the use of intermediate negative aileron deflections during the test period, so results are shown in figure 45 only for positive aileron deflections. For angles-of-attack below 14°, the relationship of C_l vs. δ_a is relatively linear, with a negative slope, as would be expected. Beyond stall angle-of-attack, however, an unusual pattern develops. The curves for +10° and -10° sideslip angles remain well-behaved, being nearly linear but with slightly decreased slopes relative to pre-stall conditions. At zero sideslip a significant rolling moment exists at zero aileron deflection for several angles-of-attack. At 15°, 16°, 18°, and 20° angle-of-attack, the rolling moment coefficient for 3° aileron deflection is

excessively positive, yielding a C_l vs. δ_a slope which is positive, indicating a control reversal. At 16° angle-of-attack, the zero offset is so large that a control reversal is indicated for the entire positive deflection range.

The slope of the C_l vs. δ_a relationship ($C_{l_{\delta_a}}$, the aileron effectiveness derivative) is plotted as a function of angle-of-attack in figure 46. As mentioned above, the relationship is rather nonlinear for angles-of-attack from 14° to 20°, so that $C_{l_{\delta_a}}$ cannot be accurately measured in this region.

Dealing with aileron effectiveness over the entire angle-of-attack range, the change in rolling moment coefficient due to full aileron deflection is shown in figures 47 and 48 (for positive and negative deflections, respectively). A general trend exists for aileron effectiveness to decrease with angle-of-attack. The data for positive deflections shows control reversals at 16° and 30° angles-of-attack, a large discrepancy between sting 001 and 002 results for angles-of-attack between 30° and 40°, and a great deal of data scatter for angles-of-attack beyond 65°. The data for negative deflections are considerably more consistent, showing some irregularity for angles-of-attack from 15° to 30°, and, again, a great deal of scatter for angles-of-attack beyond 65°.

Considering the various irregularities present in the aileron effectiveness data, it is difficult to reach specific conculsions. In general, it would appear that the ailerons are effective control surfaces for the angle-of-attack range up to 65°, except that their behavior seems somewhat irregular and unpredictable for angles-of-attack from 16° to 20°.

Yawing moments due to aileron deflections are quite significant for some aircraft. Yawing moment coefficients for the T-2 as a function of positive aileron deflections, for various angles-of-attack and three sideslip angles, are given in figure 49. It is clear from these graphs that aileron deflections cause essentially no yawing moment except in the 15° to 20° angle-of-attack range. Within this narrow range, positive aileron deflections tend to cause positive yawing moments, and some data points indicate that the yawing moment coefficients due to full aileron deflection might be as large as the yawing moment coefficient due to a 10° sideslip.

The change in yawing moment coefficient due to full aileron deflection is shown in figures 50 and 51 (for positive and negative aileron deflections, respectively) as a function of angle-of-attack for two sideslip angles. Considerable scatter is evident in the data, and only very general observations can be made. Positive deflections cause positive yawing moments in most cases, and negative deflections cause negative moments. This relationship is known as "aileron adverse yaw". Angle-of-attack variation seems to have little effect on the magnitude of the yawing moment coefficients created by aileron deflections, and there also seems to be no consistent difference between the zero sideslip and 30° sideslip cases.

RUDDER EFFECTIVENESS

Yawing moment coefficient is shown in figure 52 as a function of positive rudder deflection. For angle-of-attack below 14°, and from 25° to 40°, the

functional relationship is very well behaved: the yawing moment is zero for zero sideslip and zero deflection, the curve has a negative slope, and the relationship is linear for the entire deflection range. For angles-of-attack between 14° and 25°, small zero deflection offsets do exist, and the data points exhibit some scatter. Only one data point (18° angle of attack, 7° rudder deflection) indicates a control reversal, but data scatter alone may account for the displacement of this data point. The slope of the C_n vs. δ_r relationship ($C_{n_{\delta_r}}$, the rudder effectiveness derivative) is plotted in figure 53 with angle-of-attack as the independent variable. Rudder effectiveness is seen to be essentially invariant with angle-of-attack in the pre-stall region. The effectiveness is also nearly constant in the post-stall region, but at a value which corresponds to less than half the pre-stall effectiveness.

Data for yawing moment coefficient created by full rudder deflection are presented in figures 54 and 55 (for positive and negative deflections, respectively) as a function of angle-of-attack. These data appear to be rather clean (i.e., free from scatter and irregularities) except in the sting overlap region (35° to 40° angle-of-attack). With increasing angle-of-attack, the yawing moments are initially constant (for pre-stall angles-of-attack), then drop relatively rapidly to a lower level, and then slowly taper off to zero over the remainder of the angle-of-attack range (25° to 83°).

In the process of producing yawing moments, the rudder also produces sideforce which may have a significant effect on aircraft dynamics. Sideforce coefficient is shown in figure 56 as a function of rudder position, for various angles-of-attack (below 40°) and sideslip. For all the conditions shown in figure 56, sideforce increases in essentially a linear fashion with increasing positive rudder deflection. At several angles-of-attack, some sideforce was recorded for zero sideslip and zero rudder deflection, but no pattern is discernable and data scatter is the most plausible explanation.

The change in sideforce coefficient due to full rudder deflection as a function of angle-of-attack (for zero sideslip and 30° sideslip) is given in figures 57 and 58 (for positive and negative deflections respectively). The data trends are quite similar to those of the yawing moment data, and most of the same comments apply. Certainly the most curious feature of the data is the large magnitude, and sudden reversal in sign, of the sideforce due to negative rudder deflection for 30° sideslip at angles-of-attack near 40°. The number of data points involved in this phenomenom would seen to be large enough to rule out data scatter or other random measurement error as the cause of the unusual results.

Since the rudder is located above the roll axis of the T-2, rudder deflection also produces a rolling moment. This direct, static rolling moment must not be confused with the dynamic rolling moment due to dihedral effect following sideslip excursion due to rudder deflection. It is this dynamic rolling moment, rather than the static moment, which causes the rudder to be more effective roll control device than the ailerons at some flight conditions.

The coefficient of the static rolling moment is given in figure 59 as a function of rudder deflection for various angles-of-attack and sideslip angles

of 10°, 0°, and -10°. At pre-stall angles-of-attack, positive rudder deflections cause positive rolling moments in essentially a linear fashion. The effect, however, is quite small relative to the dihedral effect due to 10° sideslip. Near stall angle-of-attack, dihedral effect decreases considerably, but is still large compared to the rudder rolling effect. The roll due to rudder is difficult to evaluate near stall (angles-of-attack of 15° and 16°) for zero sideslip because the data are quite erratic, although the data for sideslip angles of 10° and -10° seem consistent. For post-stall angles-of-attack, there is essentially no change in rolling moment as a result of rudder deflection.

One of the more interesting aspects of the data shown in figure 59 is the frequent occurence of substantial zero offsets, i.e., non-zero rolling moment coefficients at zero rudder deflection and zero sideslip. The offsets range from zero to -.013. They are always negative, but seem to have no clear dependence on angle-of-attack. These rolling moment coefficients at zero deflection and zero sideslip are far too large to be attributed to random measurement error, and must result from asymmetric airflow.

The changes in rolling moment coefficient due to full rudder deflections are given in figures 60 and 61 (for positive and negative deflections, respectively). The data are quite scattered, and only general conclusions can be reached. Positive rudder deflections tend to cause positive rolling moments, and negative deflections tend to produce negative moments. Little variation with angle-of-attack is observable, and 30° sideslip angle data are noticeably different from zero sideslip data only for angles-of-attack above 50°.

STING INTERFERENCE EFFECTS

As explained earlier, it was necessary to use three different sting support configurations to span the entire angle-of-attack range from -8° to +83°. Stings 002 and 003 differed only with respect to the lower support. A change from 002 to 003 should only have a very minor effect on the aerodynamics of the model, since the model will be located in a different position in the tunnel, and the tunnel flow field is not perfectly uniform. A change from 001 to 002, however, could have large effects on the airflow over the model, since the point of entry of the sting into the model is substantially different.

An examination of the results reveals that large discontinuities did occasionally occur in the angle-of-attack range for which data was obtained with both stings 001 and 002. In figures 21 and 22, for instance, the value of C_L and C_D obtained from sting 001 data (in the 30° to 40° angle-of-attack range) are noticeably larger than the comparable values obtained from 002 data. In some cases, however, rapid changes in aerodynamics occurring at angle-of-attack between 30° and 40° are not due to sting interference effects. The change in lift coefficient due to full negative elevator deflection (figure 41), and the change in rolling moment coefficient due to full positive aileron deflection (figure 47) are examples of the latter situation, since sting 001 data points exist on both sides of the apparent discontinuities.

CONCLUSIONS AND RECOMMENDATIONS

CONCLUSIONS

1. The data presented in this report are sufficient in quantity and quality to fully define the static aerodynamic characteristics of the T-2 aircraft in low speed flight for purposes of computer simulation or reference values for parameter identification from flight test data.

2. The lack of data for dynamic conditions and for power effects cause the results presented herein to be insufficient for <u>complete</u> simulation of the flight of a T-2 aircraft.

3. The T-2 exhibits a linear pre-stall lift curve, terminated by an abrupt stall at approximately 15° angle-of-attack.

4. For zero sideslip, static pitch instability is present only for angles-of-attack between 18° and 20°.

5. The T-2 exhibits positive dihedral effect throughout the angle-of-attack range, except that a slope reversal occurs for small sideslip angles at 15° angle of attack.

6. The T-2 aircraft seems to have a relatively high natural yaw stability for angles-of-attack below 15° or above 40°. At angles-of-attack between 15° and 40°, however, the yaw stability seems to be essentially zero.

7. Elevator effectiveness is essentially constant with increasing angles-of-attack until the stall angle (15°) is achieved. At stall, the effectiveness drops sharply to approximately half its pre-stall value. Effectiveness then decreases slowly with increasing angle-of-attack, but under no conditions is the effectiveness reduced to zero or reversed in sign.

8. For angles-of-attack below 14° or between 35° and 65°, aileron effectiveness is relatively high. At other angles-of-attack the effectiveness is difficult to assess accurately, but it is clear that the ailerons are less effective in the 14° to 35° angle-of-attack region than at other angles-of-attack.

9. In general, the T-2 ailerons exhibit adverse yaw, but the effect is small and difficult to measure accurately.

10. The yaw effectiveness of the rudder varies with respect to angle-of-attack in the same fashion as the elevator effectiveness variation. Beyond 70° angle-of-attack the effectiveness is essentially zero.

11. Positive rudder deflections tend to cause positive rolling moments and vice versa, but the effect is small and difficult to measure accurately.

12. All data taken in the 30° to 40° angle-of-attack range should be used with caution, since some discrepancies exist between data obtained with the 001 sting configuration and those obtained with the 002 configuration.

RECOMMENDATIONS

1. The utility of the data obtained in this investigation would be greatly enhanced if dynamic data, i.e., variation of aerodynamic forces and moments due to pitch, roll, and yaw rates, could be obtained with the same wind tunnel model. Therefore it is recommended that every effort be made to obtain dynamic data in the near future.

REFERENCES

(a) Hauenstein, F. M., Influence of Northrop High Angle Support Fairing ("Bump") on Flow in the Ames 12-Foot Pressure Wind Tunnel Test Section, ARO, Inc., TM 37, 8 Feb 72

(b) Pope, A., and Harper, J. J., Low Speed Wind Tunnel Testing, John Wiley & Sons, Inc., New York, 1966

(c) Anon., Estimated Flying Qualities for T-2B Trainer Airplane, North American Aviation, Columbus Division, Report NA64H-845, 1 Dec 1964

(d) Elliot, D. W., Substantiating Data Report Based on Flight Test Data for the T-2B Trainer Powered with Two J69-P-6 Engines, North American Aviation, Columbus Division, Report NA64H-536, 9 Jun 1964

GENERAL ARRANGEMENT OF 9% T-2C WIND TUNNEL MODEL

WING AREA, S	$= 2.064\ FT^2$
MAC, $\bar{C}_W$	= 0.667 FT.
ASPECT RATIO	= 5.07
NACA AIRFOIL	$= 64_1$ A212 (SCALED TO .09)
ROOT CHORD, C_r	= 0.856 FT.
TIP CHORD, C_τ	= 0.423 FT.
DIHEDRAL, T_W	= + 3.0 DEG.

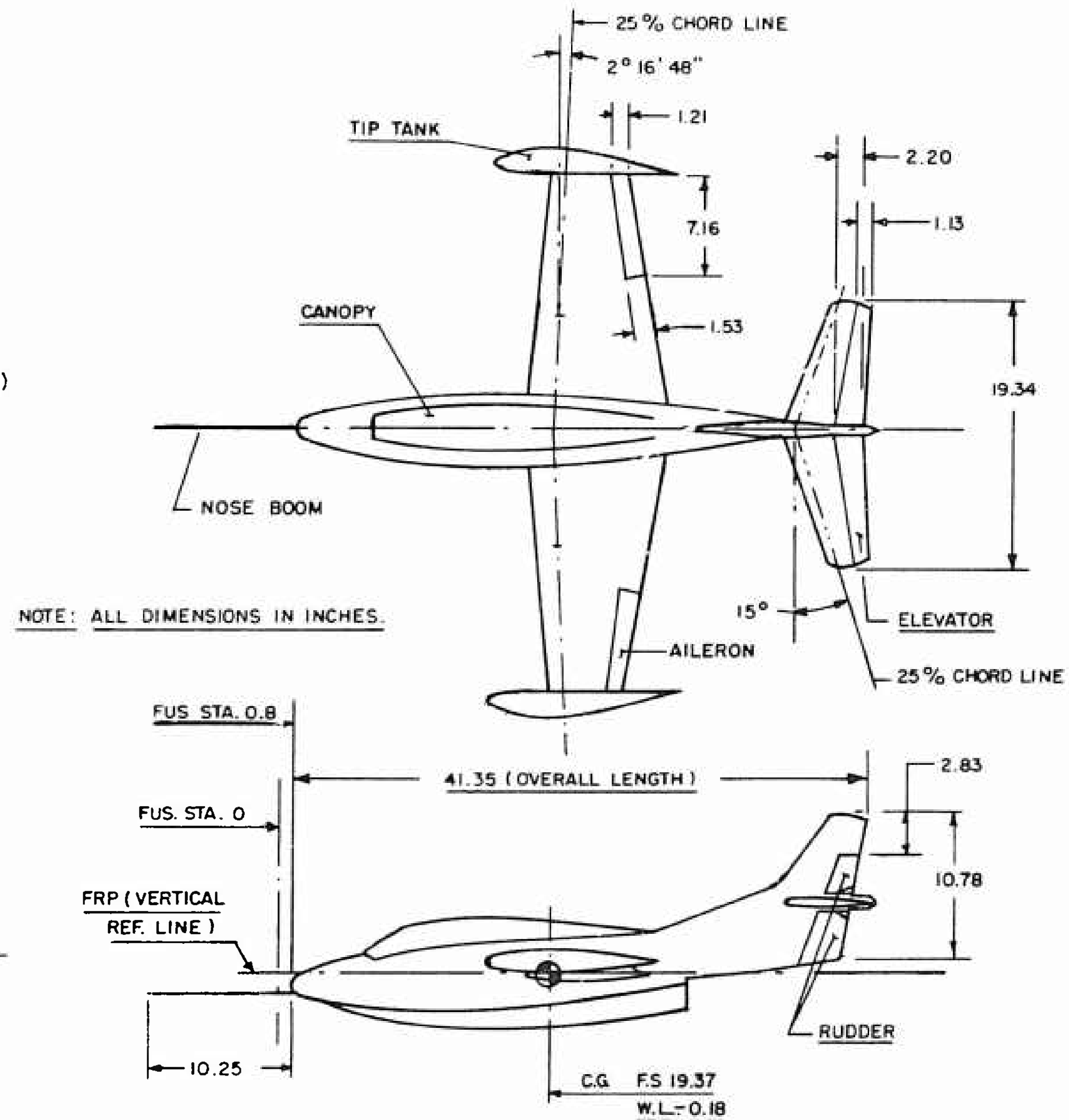

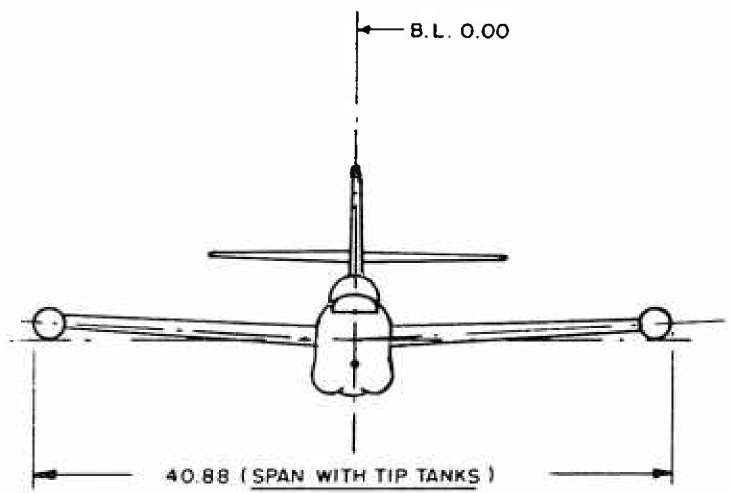

FIGURE 1. GENERAL ARRANGEMENT OF .09 SCALE T-2C WIND TUNNEL MODEL

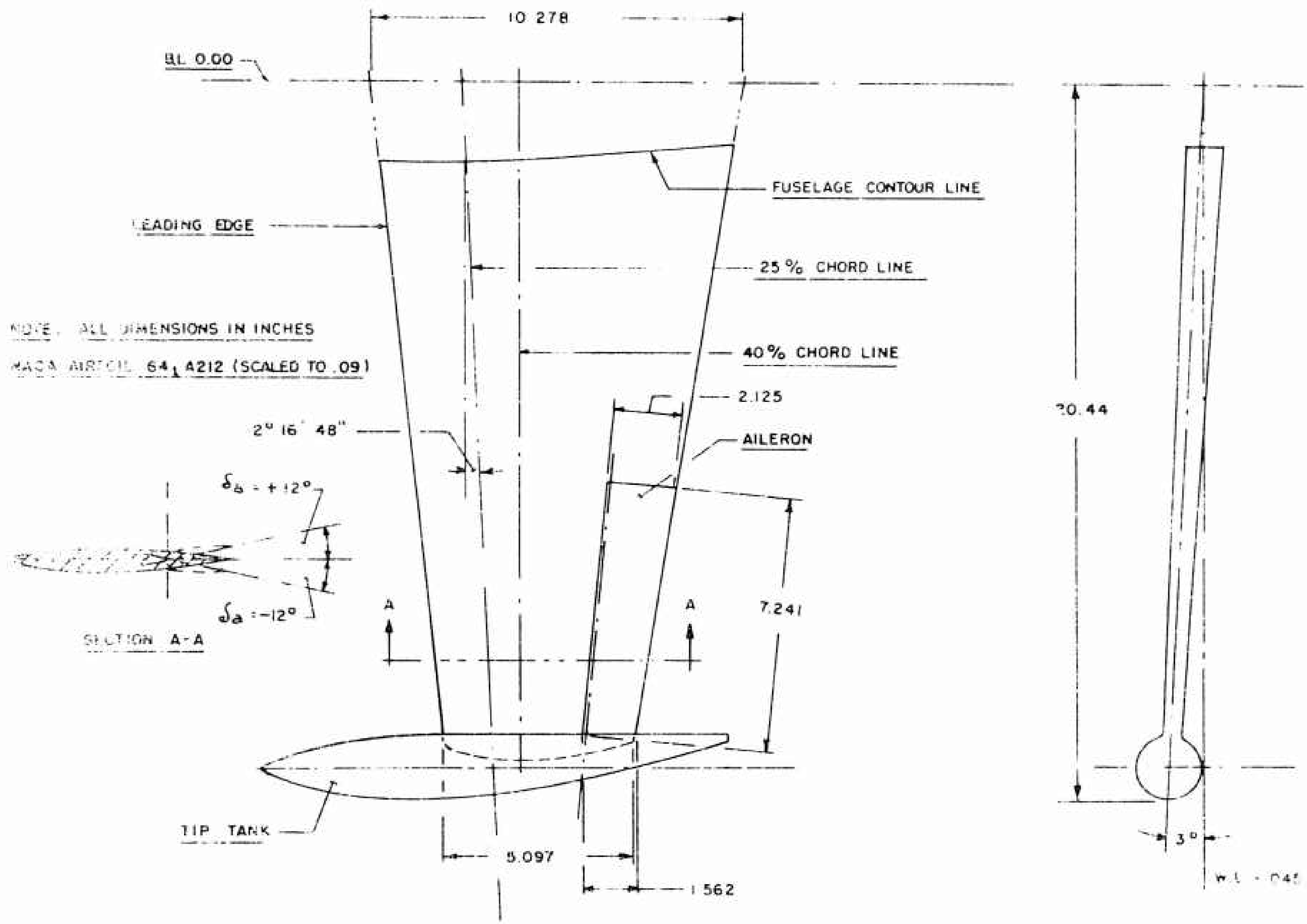

FIGURE 2. WING DETAIL OF .09 SCALE T-2C MODEL

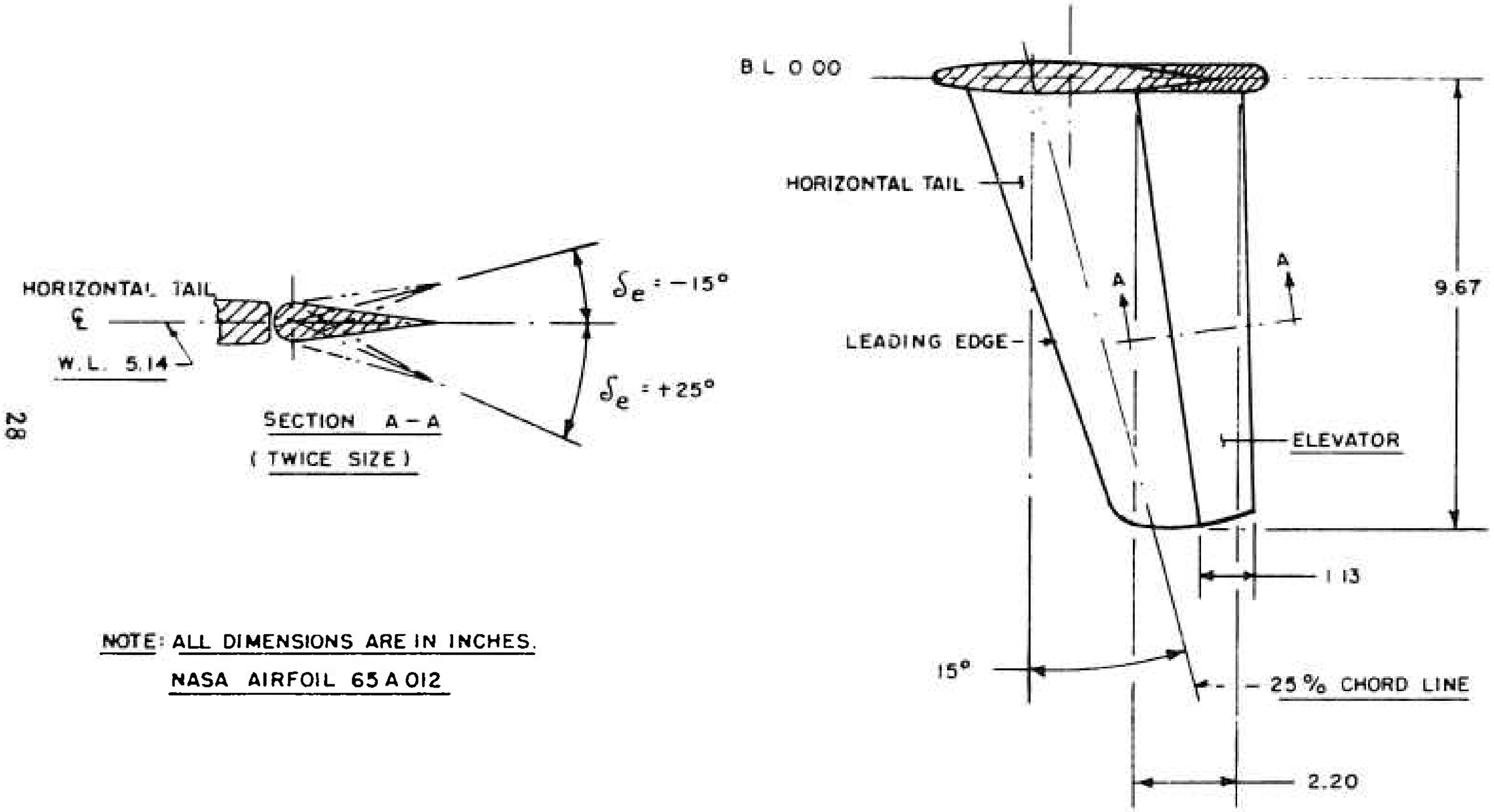

FIGURE 3. HORIZONTAL TAIL DETAIL OF .09 SCALE T-2C MODEL

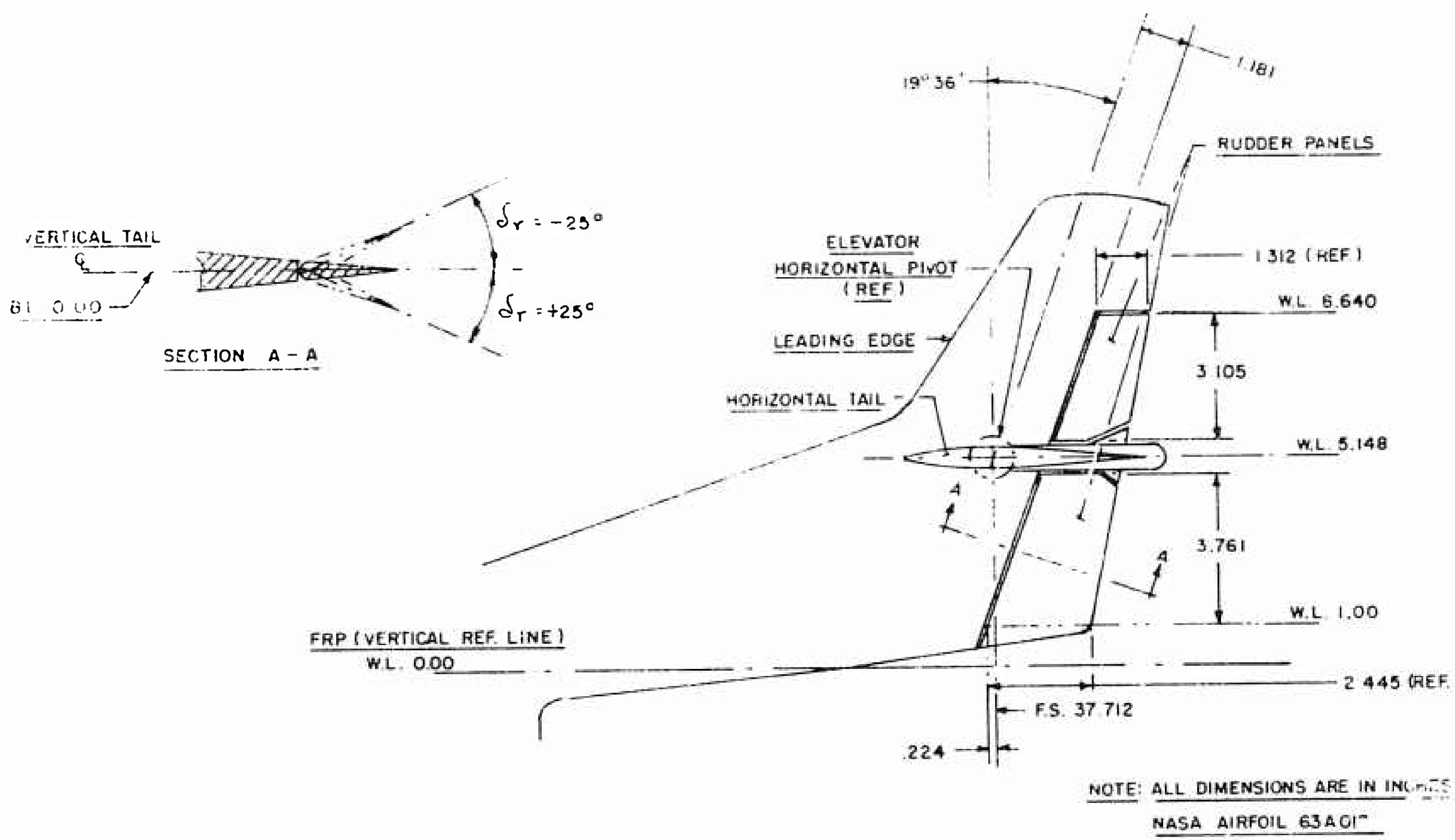

FIGURE 4. VERTICAL TAIL DETAIL OF .09 SCALE T-2C MODEL

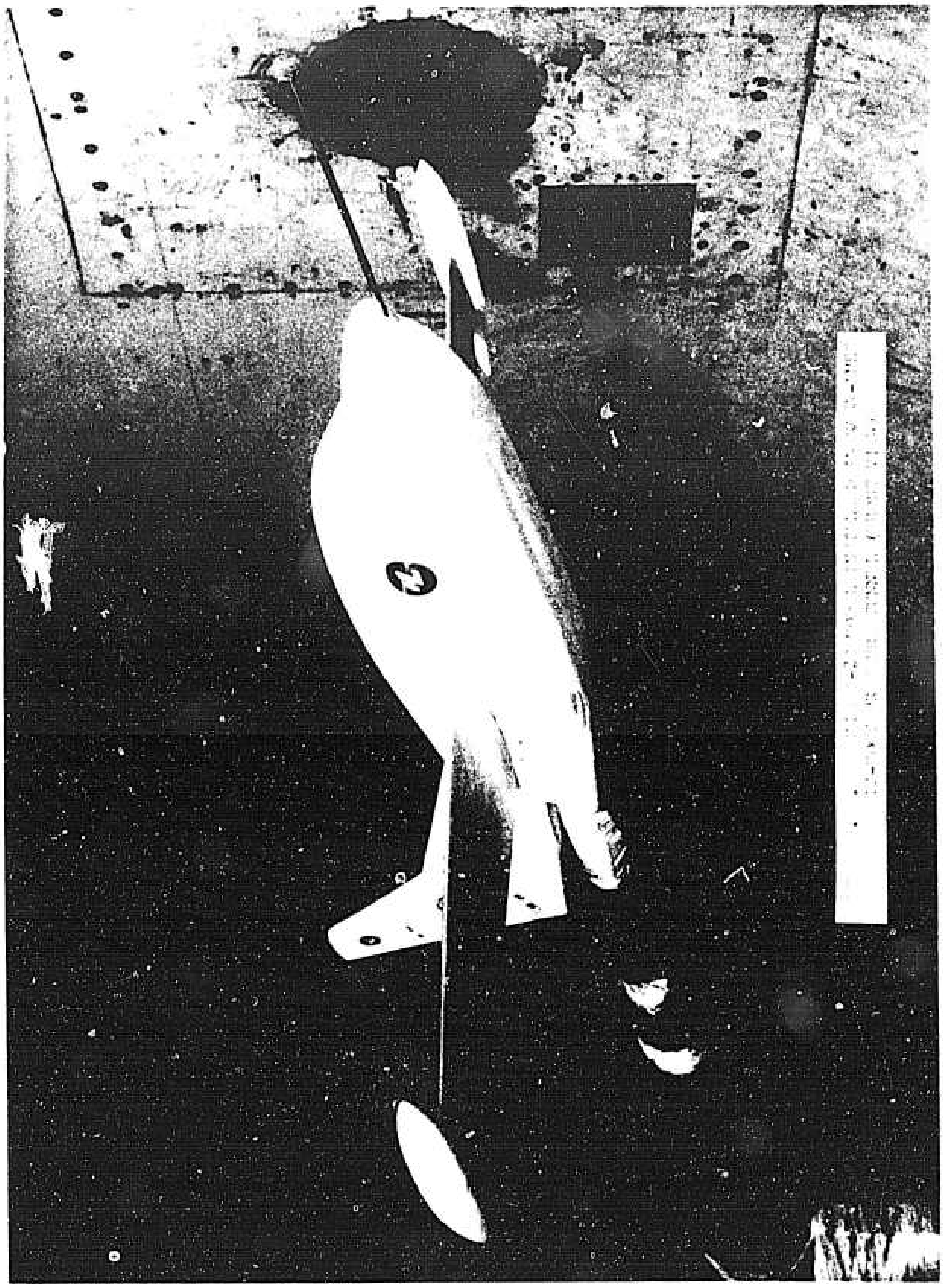

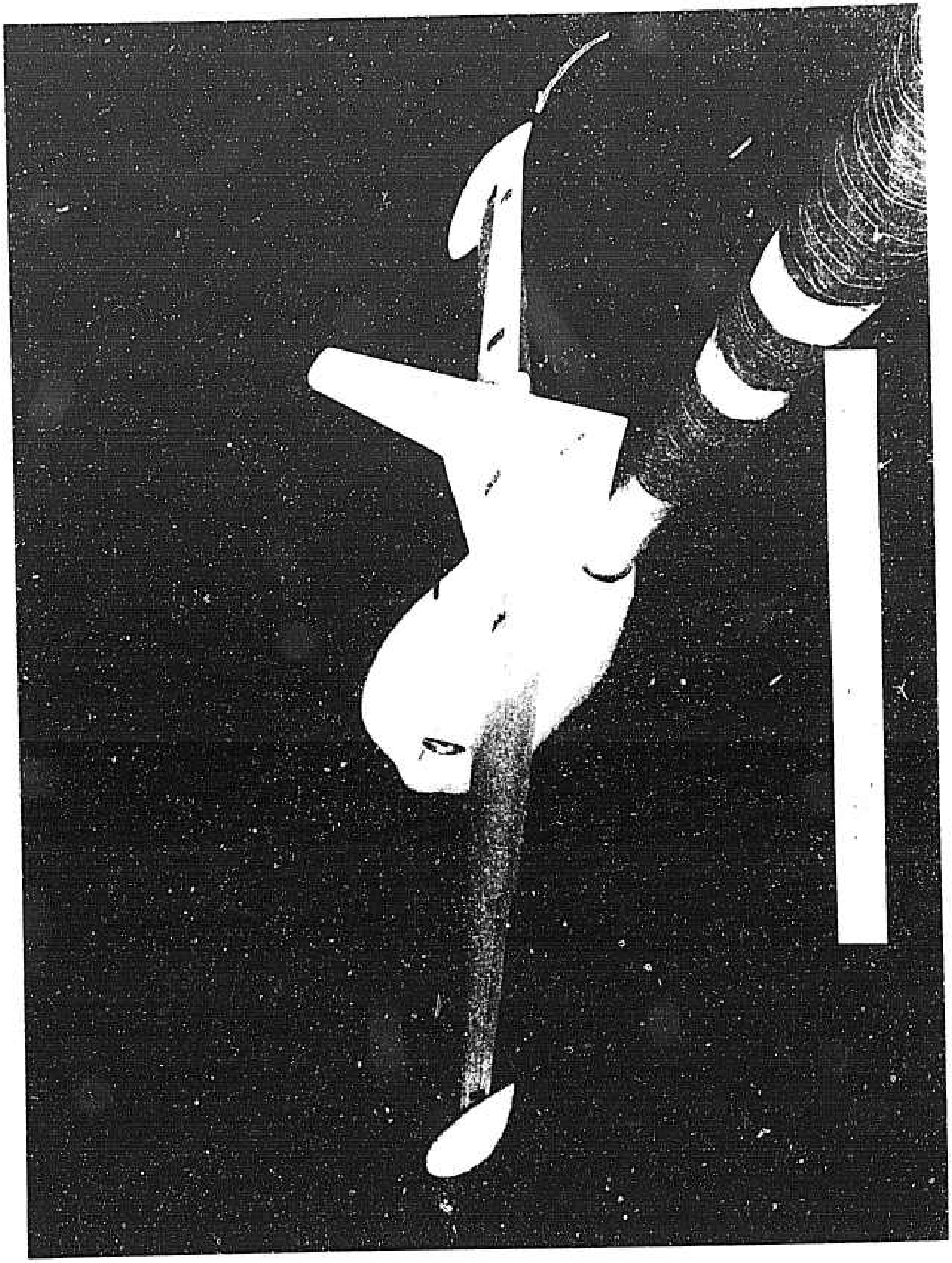

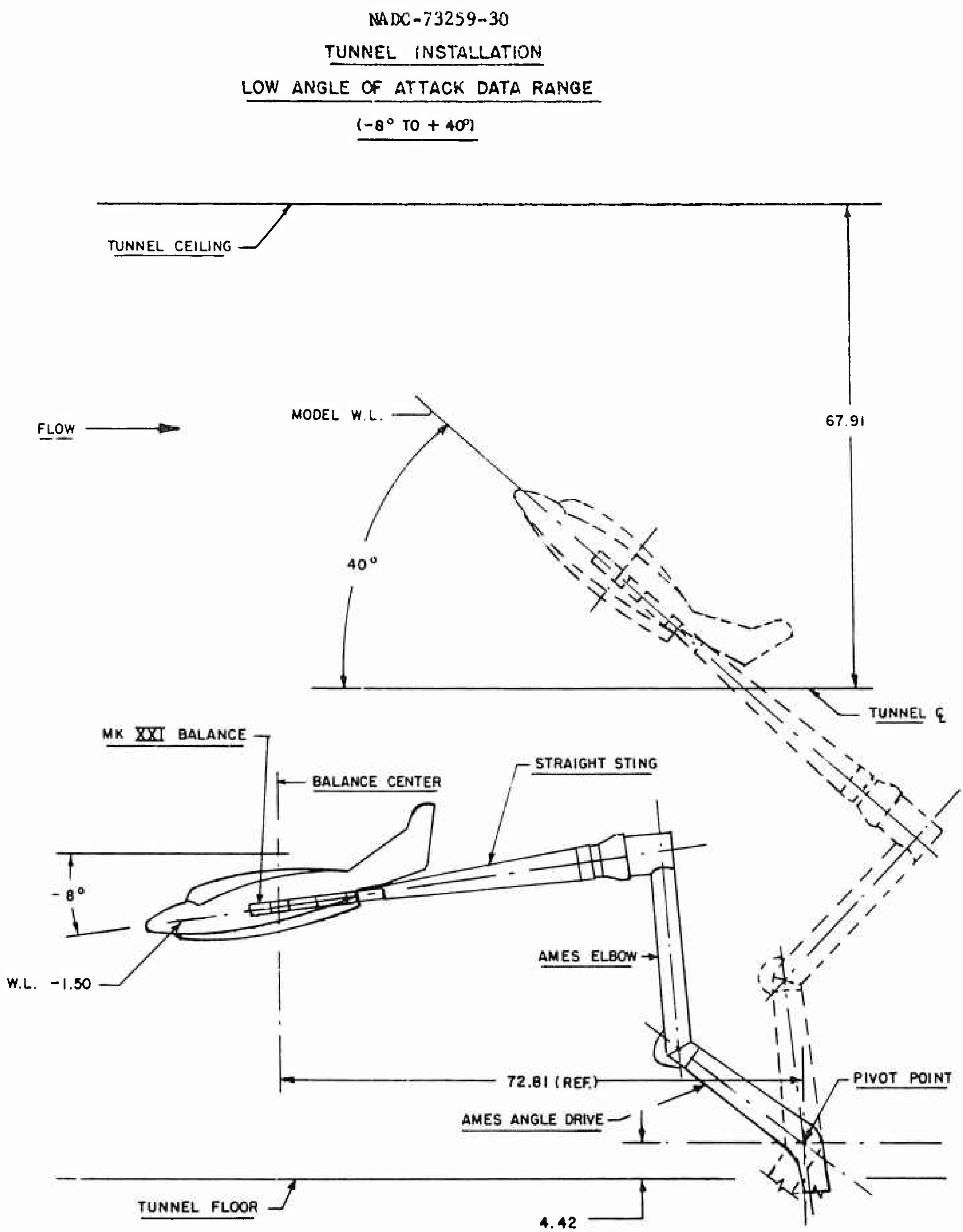

FIGURE 7. WING TUNNEL STING INSTALLATION (STING CONFIGURATION 001, LOW ANGLE-OF-ATTACK DATA RANGE)

TUNNEL INSTALLATION

INTERMEDIATE ANGLE OF ATTACK DATA RANGE

(40° TO 55°)

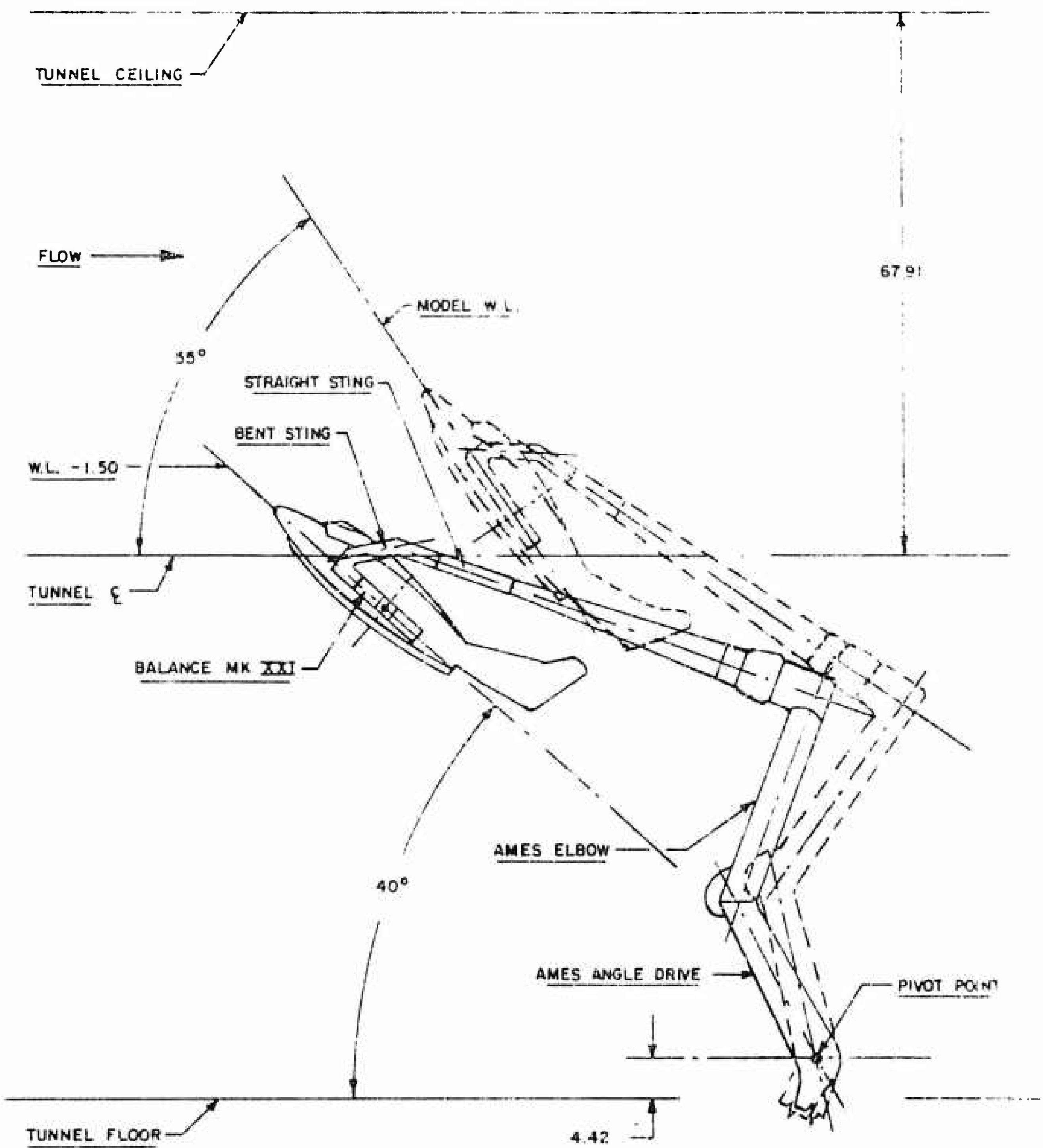

FIGURE 8. WIND TUNNEL STING INSTALLATION (STING CONFIGURATION 002, INTERMEDIATE ANGLE-OF-ATTACK DATA RANGE)

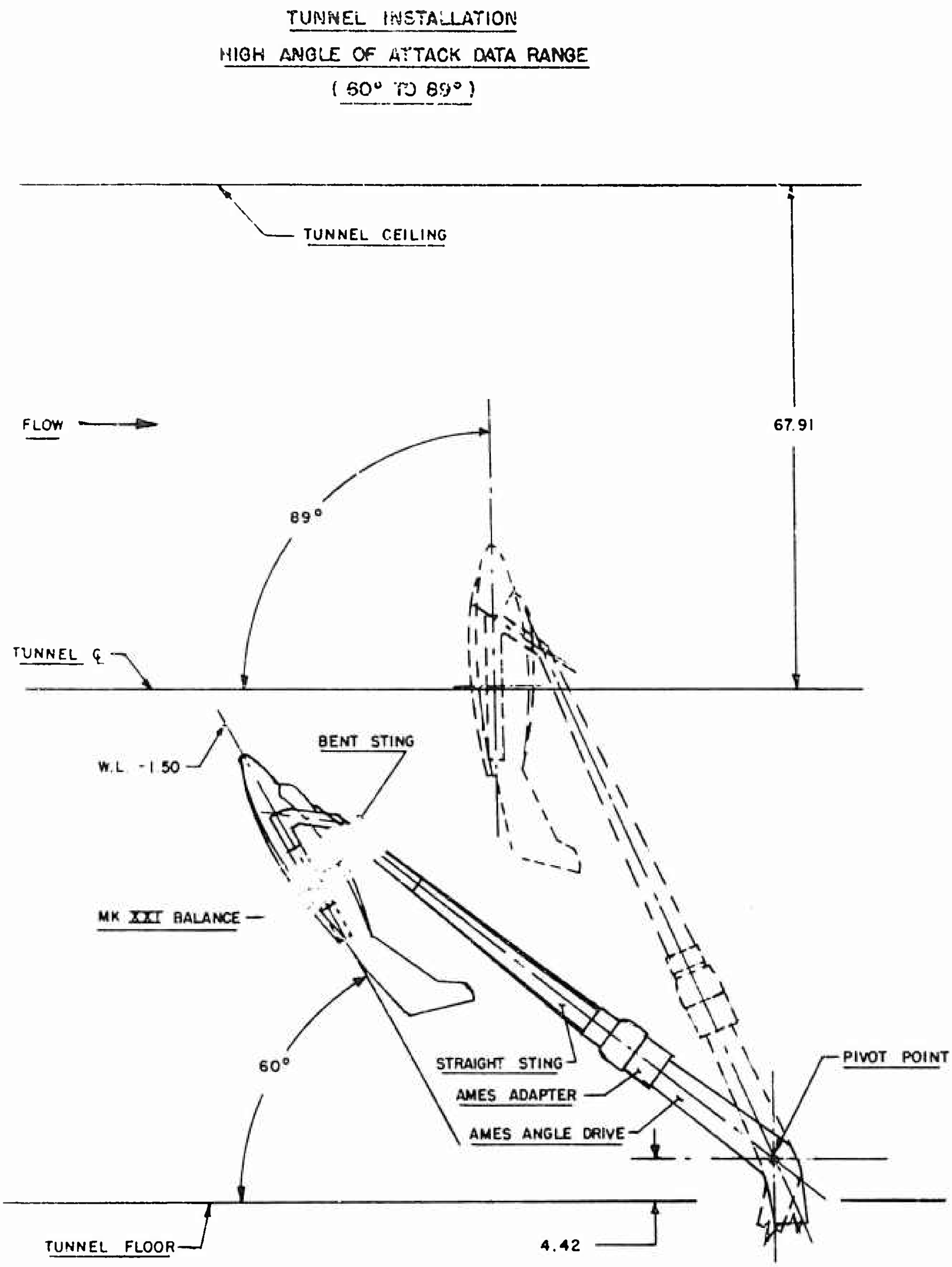

FIGURE 9. WIND TUNNEL STING INSTALLATION (STING CONFIGURATION 003, HIGH ANGLE-OF-ATTACK DATA RANGE)

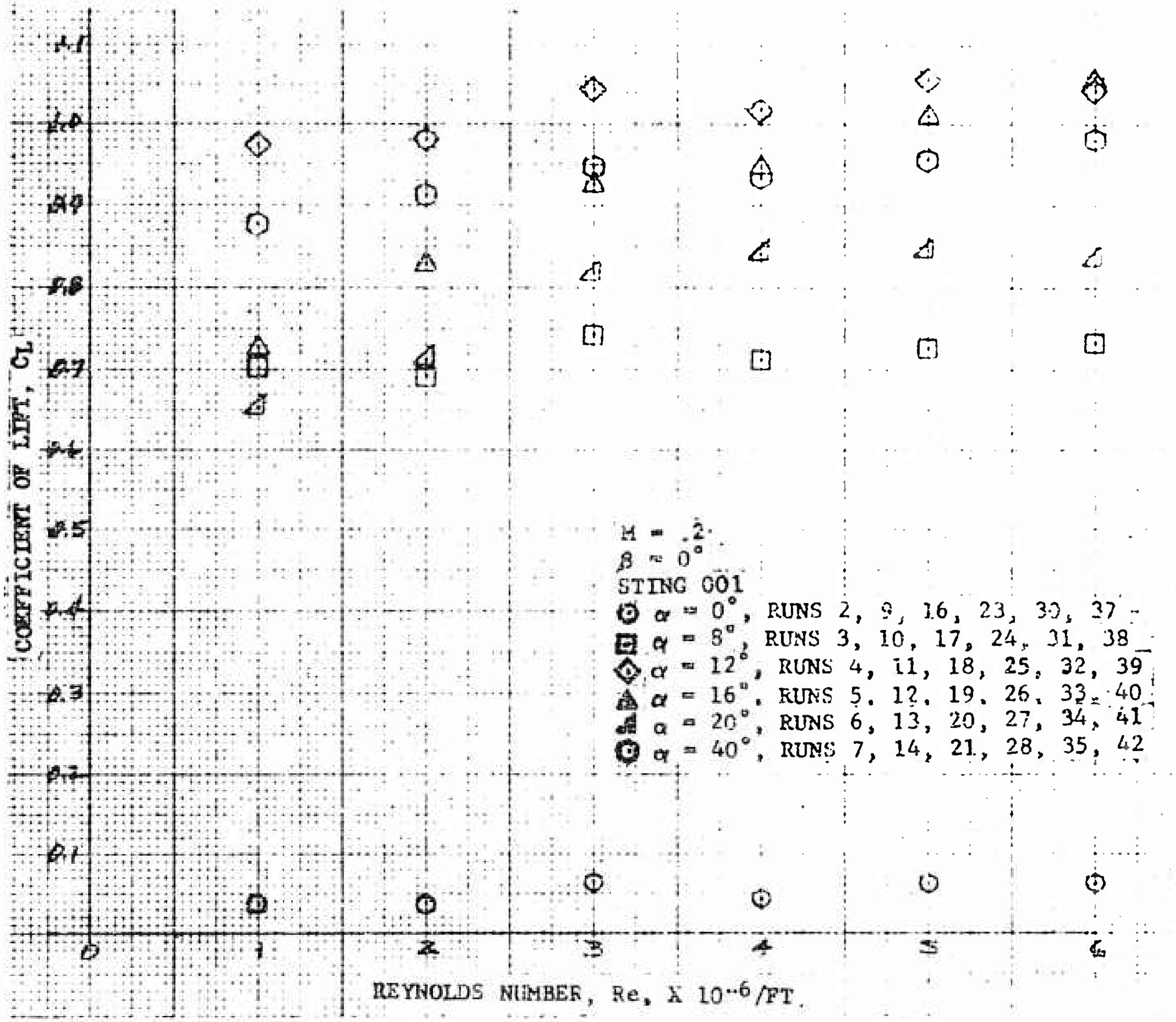

FIGURE 10. COEFFICIENT OF LIFT VERSUS REYNOLDS NUMBER FOR VARIOUS ANGLES-OF-ATTACK

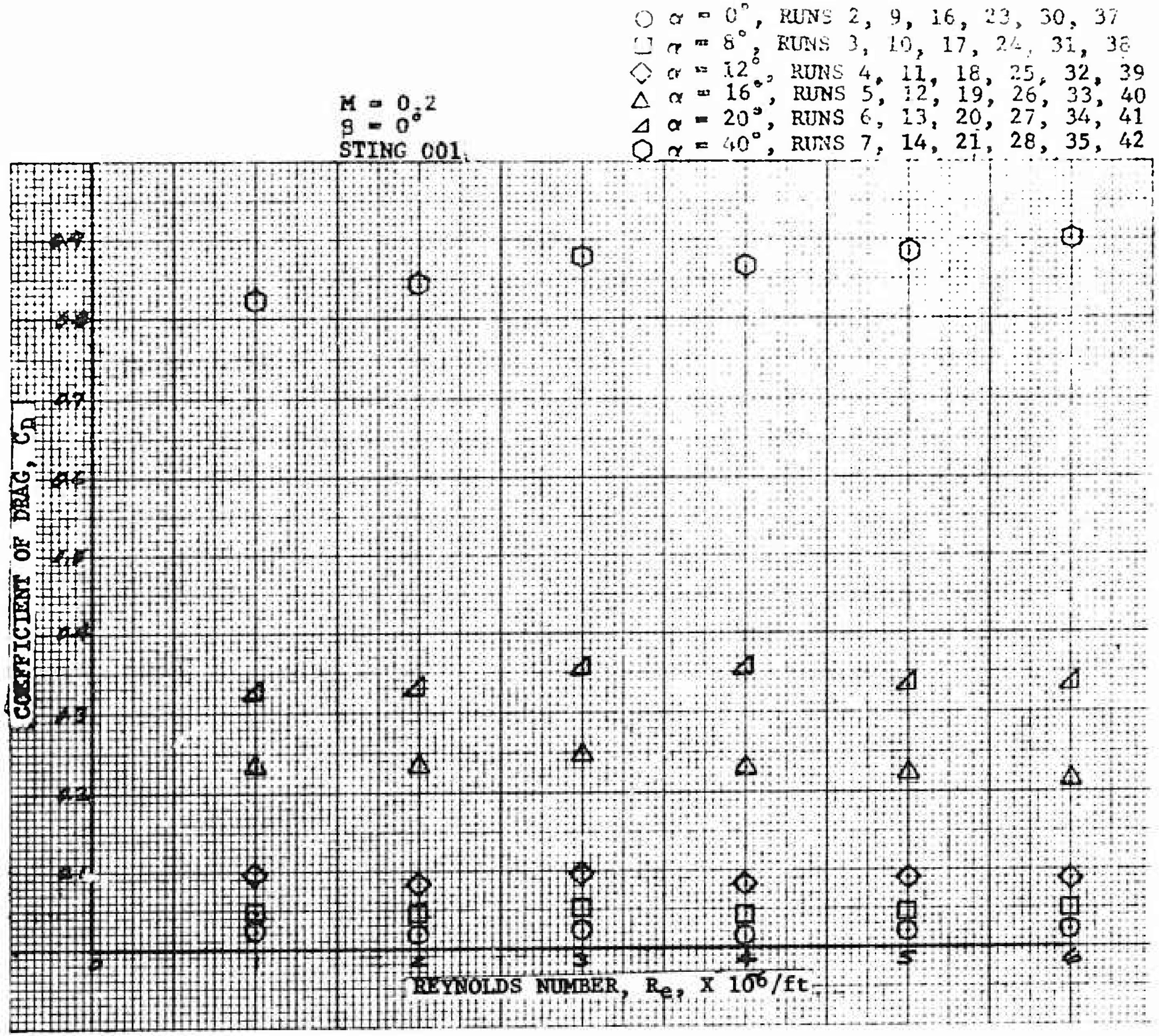

FIGURE 11. COEFFICIENT OF DRAG VERSUS REYNOLDS NUMBER FOR VARIOUS ANGLES-OF-ATTACK

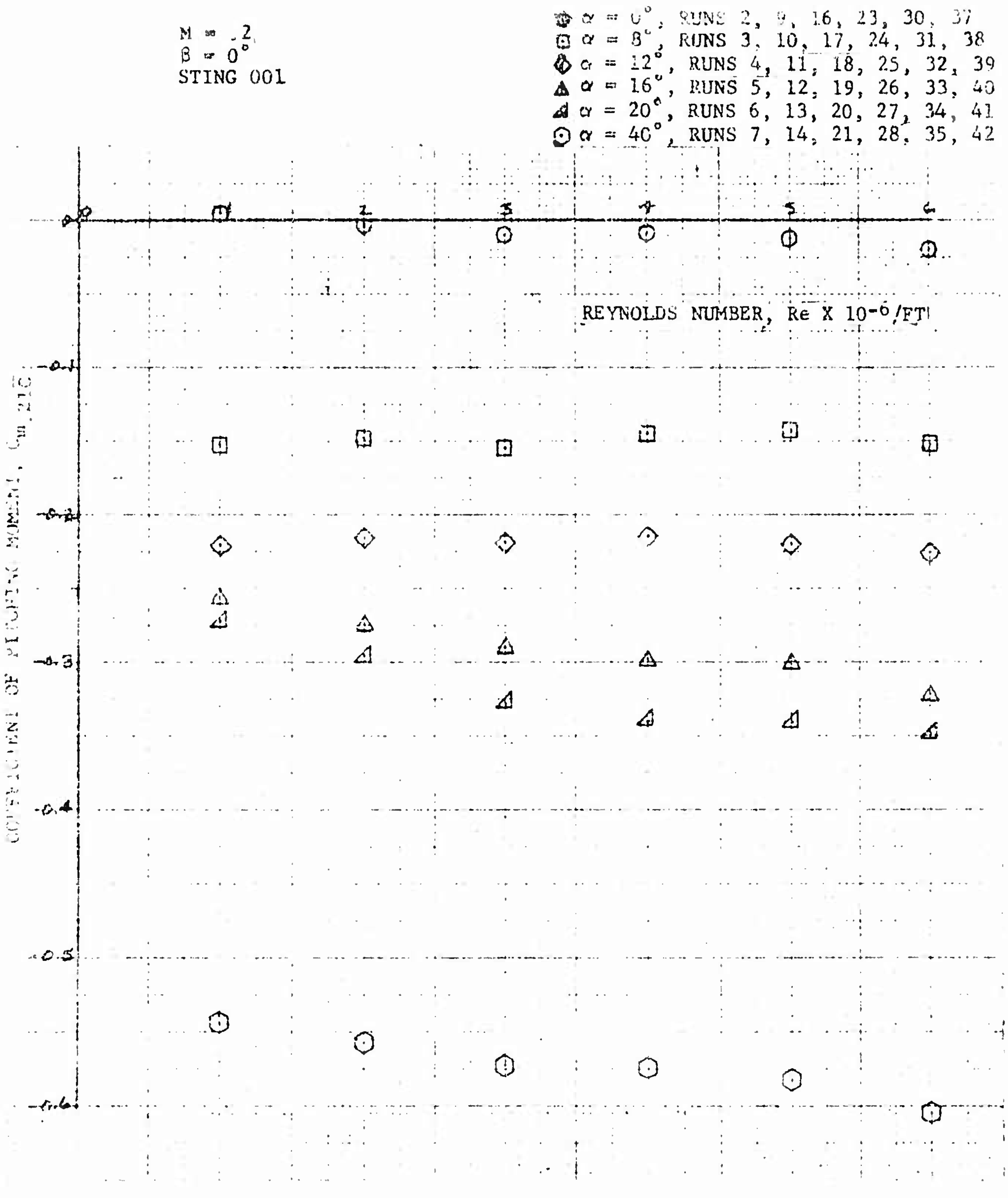

FIGURE 12. COEFFICIENT OF PITCHING MOMENT VERSUS REYNOLDS NUMBER FOR VARIOUS ANGLES-OF-ATTACK

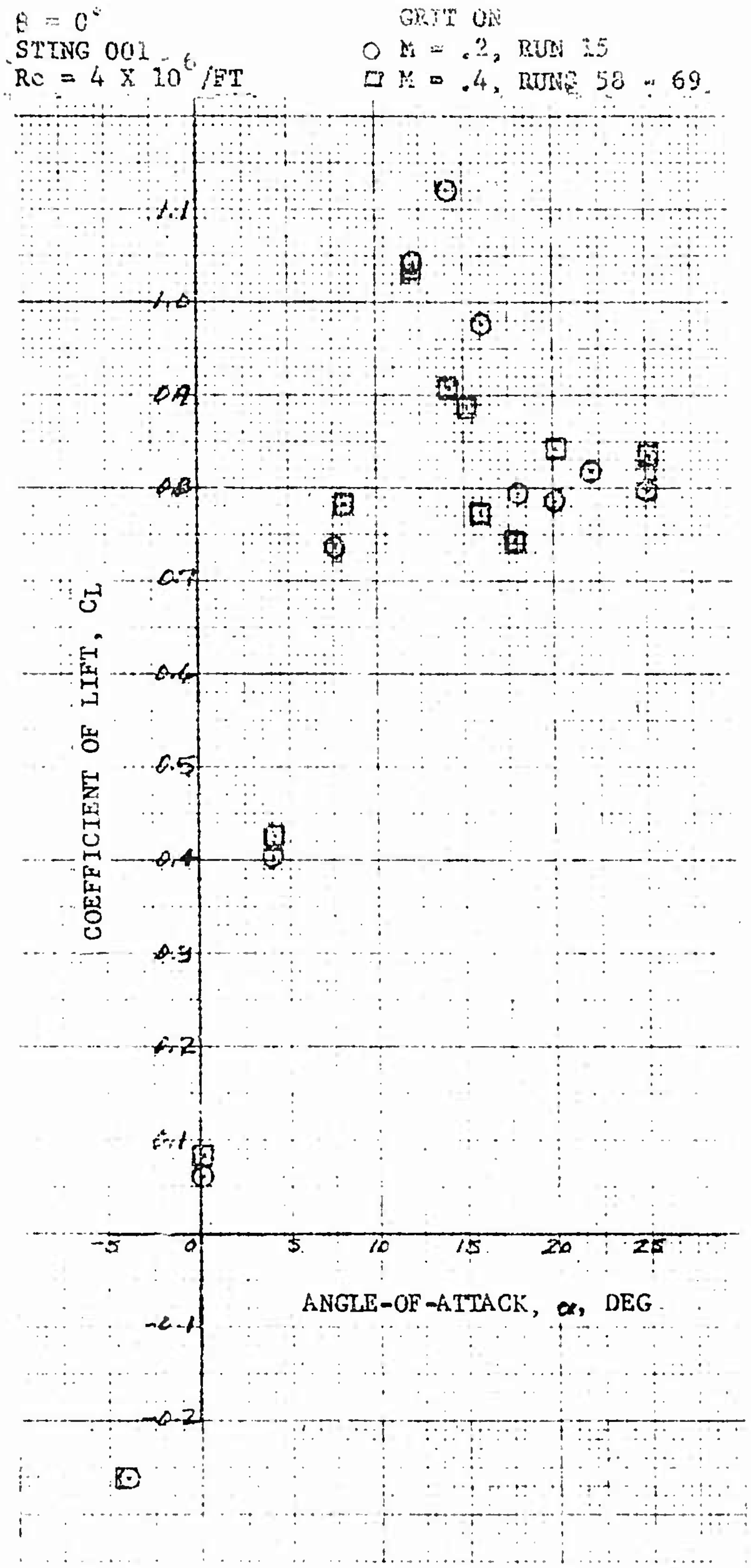

FIGURE 13. COEFFICIENT OF LIFT VERSUS ANGLE-OF-ATTACK FOR MACH NUMBER VARIATION

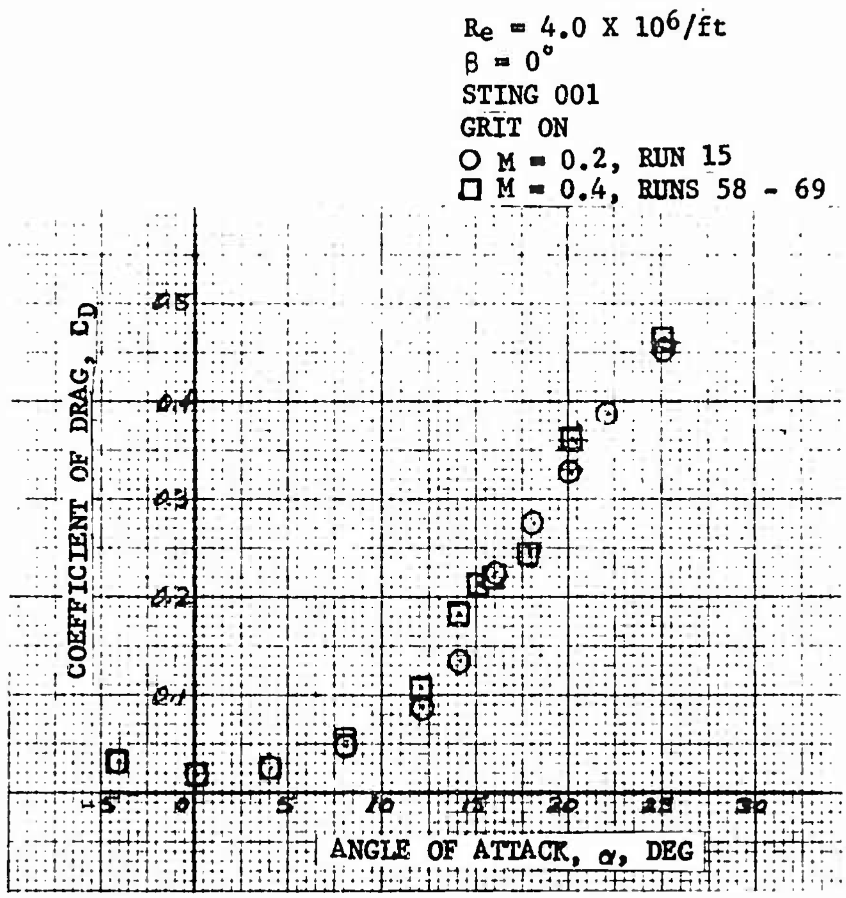

FIGURE 14. COEFFICIENT OF DRAG VERSUS ANGLE-OF-ATTACK FOR MACH NUMBER VARIATION

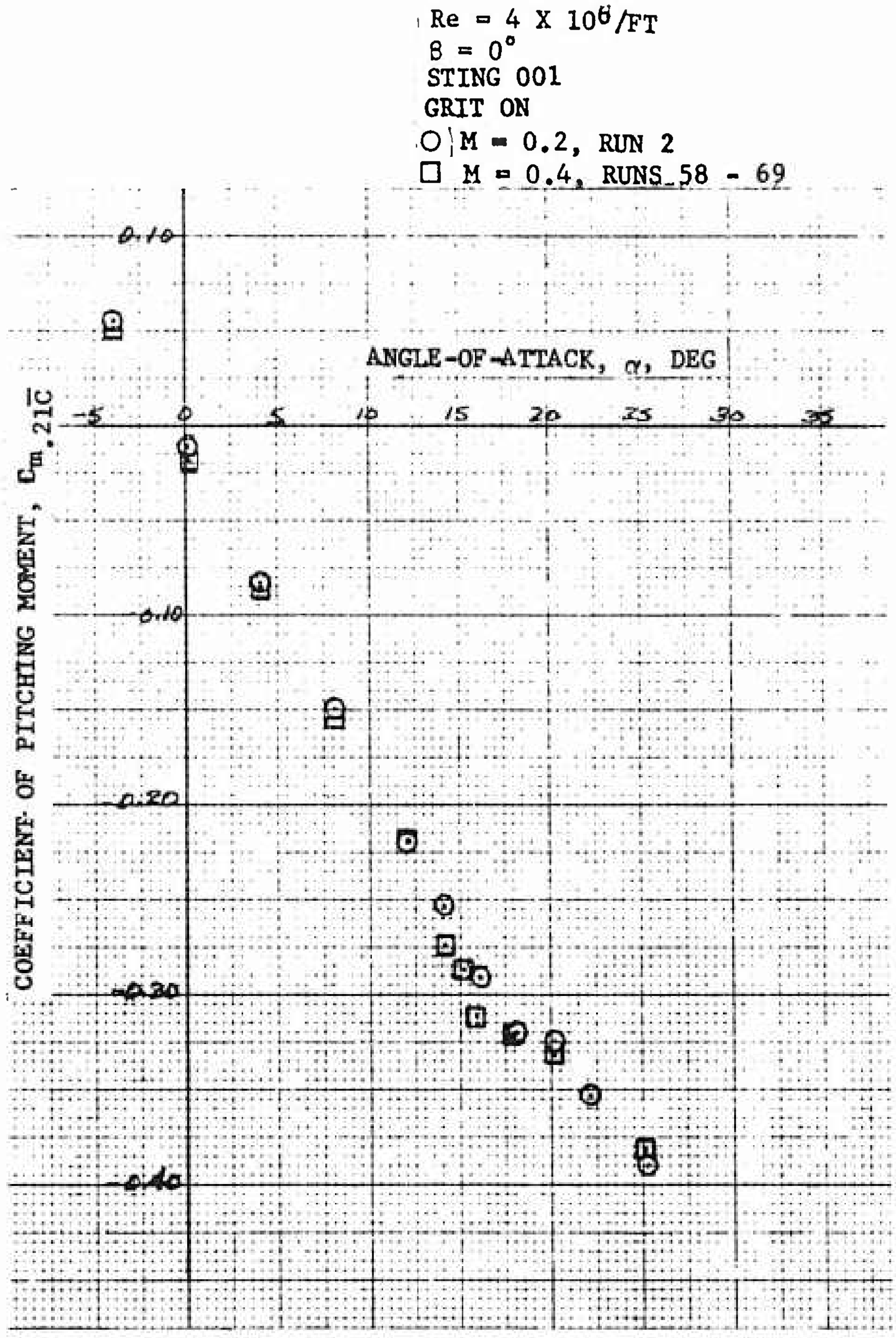

FIGURE 15. COEFFICIENT OF PITCHING MOMENT VERSUS ANGLE-OF-ATTACK FOR MACH NUMBER VARIATION

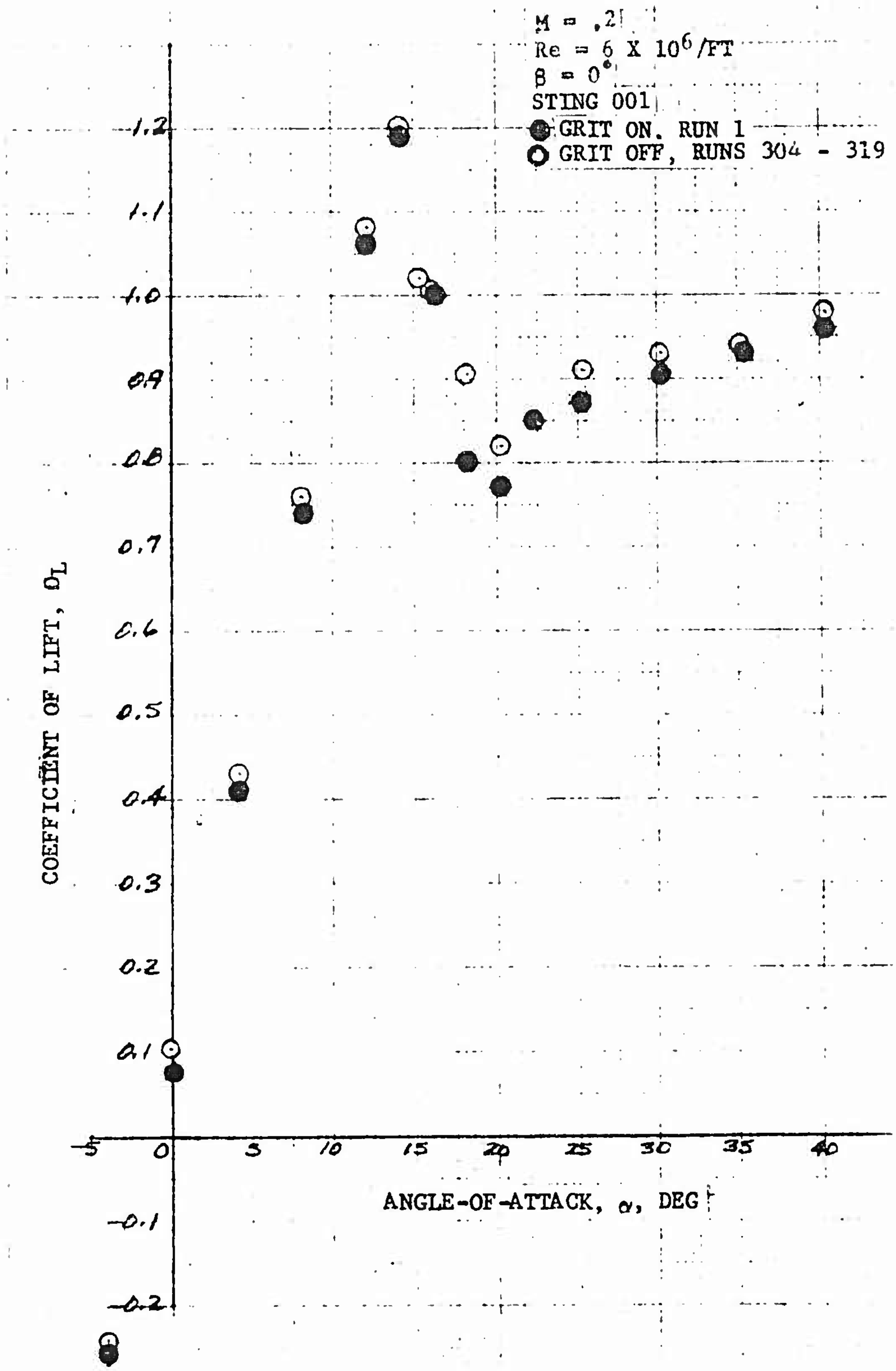

FIGURE 16. COEFFICIENT OF LIFT VERSUS ANGLE-OF-ATTACK (GRIT ON AND OFF, β = 0°)

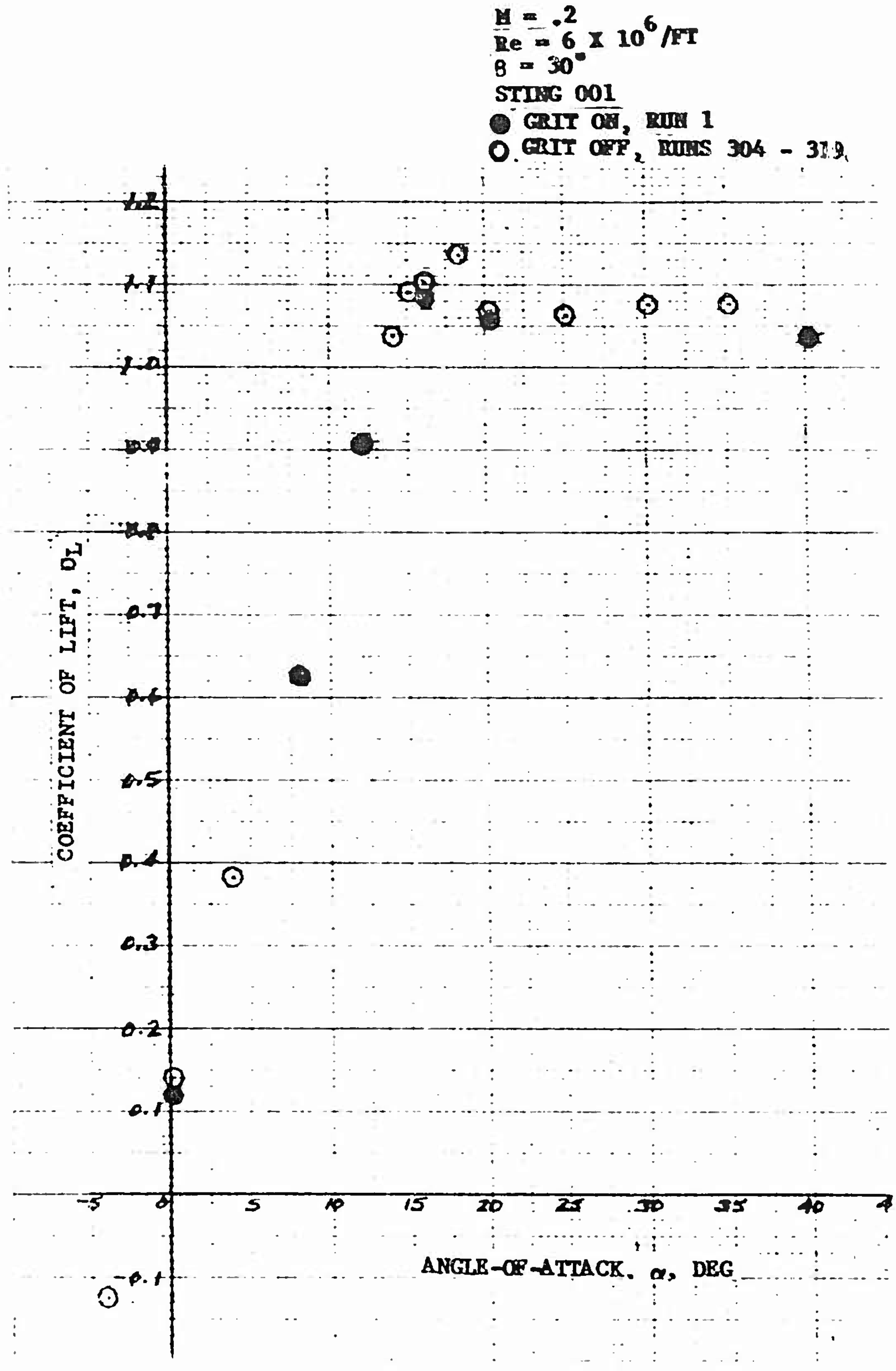

FIGURE 17. COEFFICIENT OF LIFT VERSUS ANGLE-OF-ATTACK
(GRIT ON AND OFF)

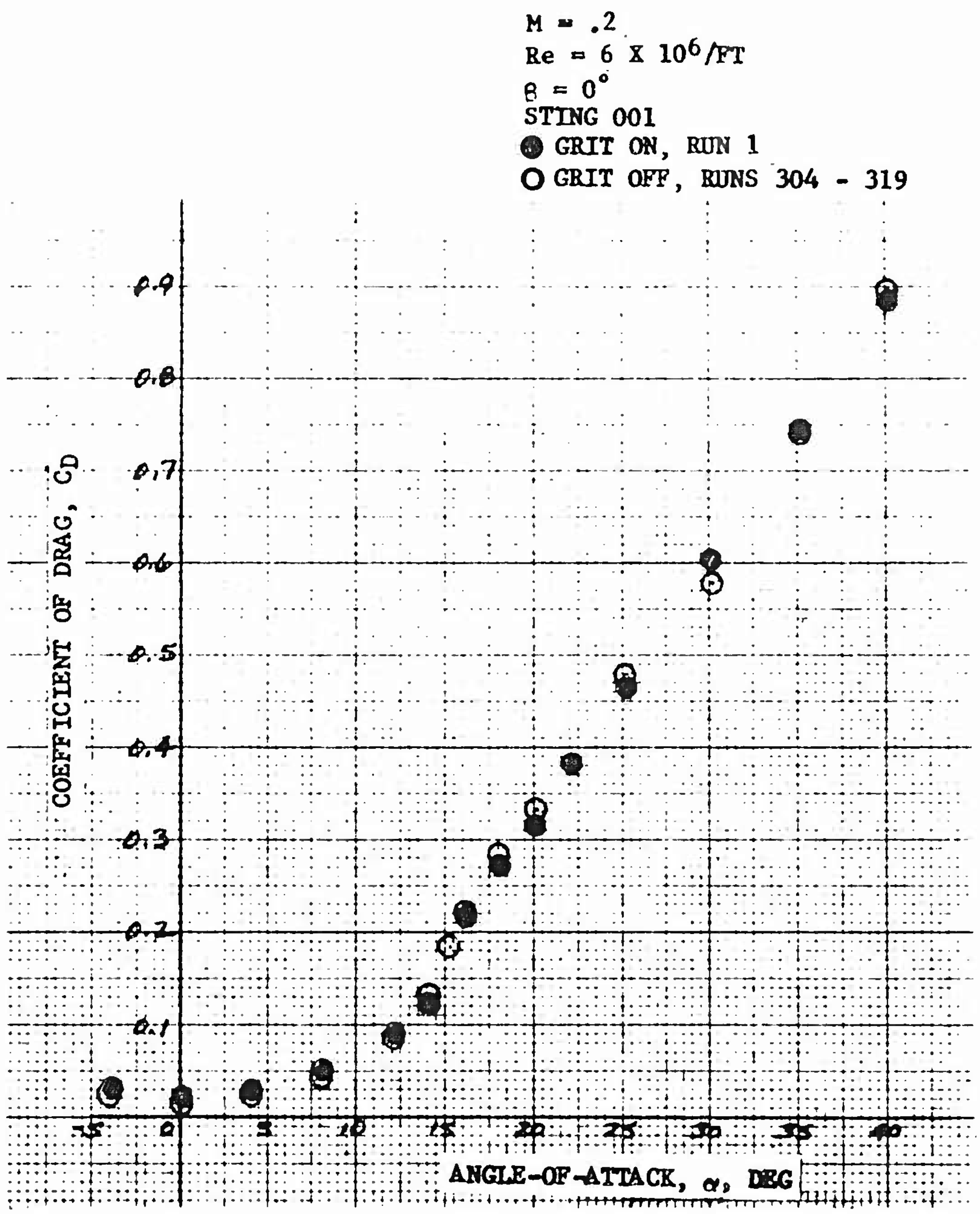

FIGURE 18. COEFFICIENT OF DRAG VERSUS ANGLE-OF-ATTACK (GRIT ON AND OFF, β = 0°)

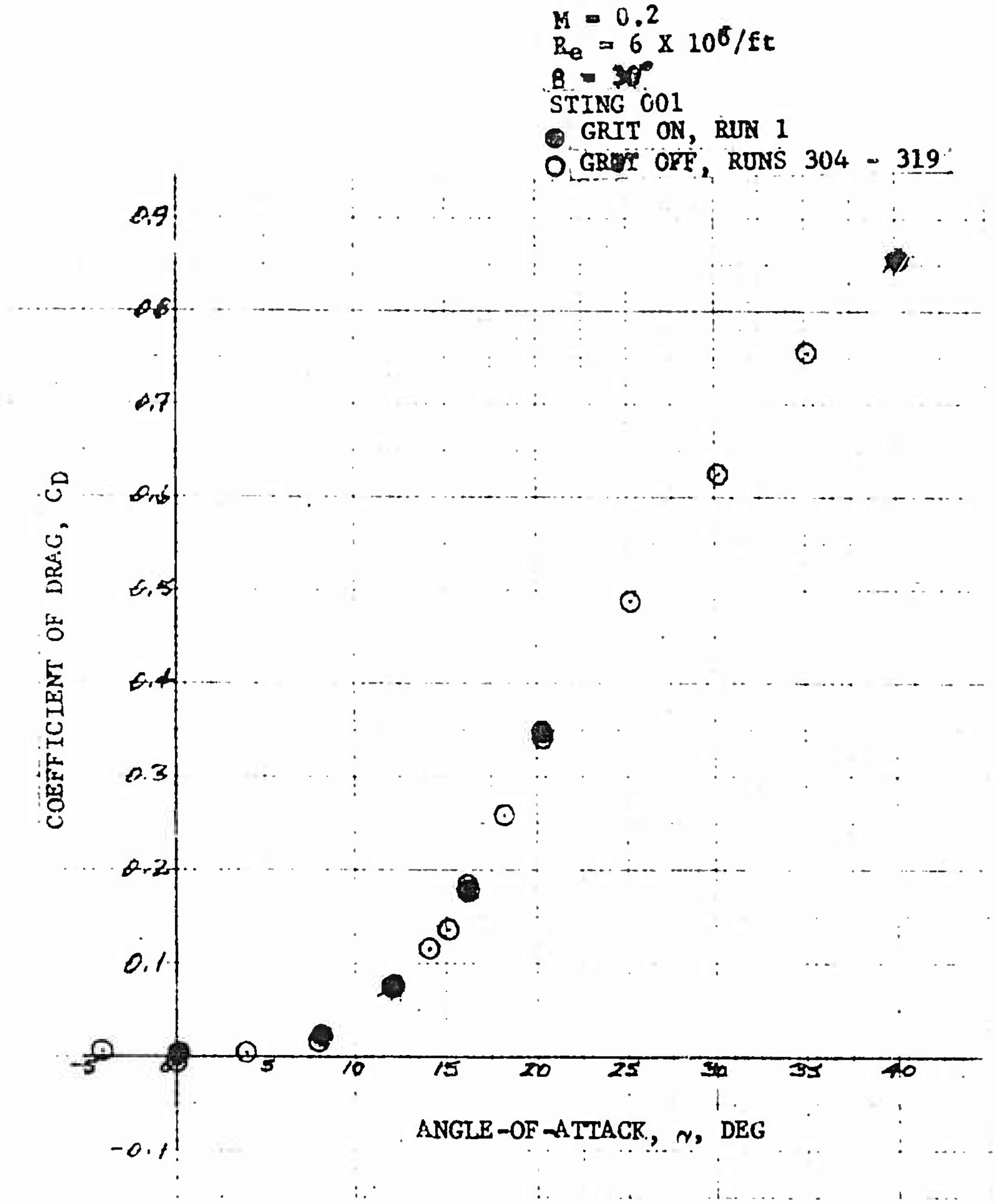

FIGURE 19. COEFFICIENT OF DRAG VERSUS ANGLE-OF-ATTACK (GRIT ON AND OFF, β = 30°)

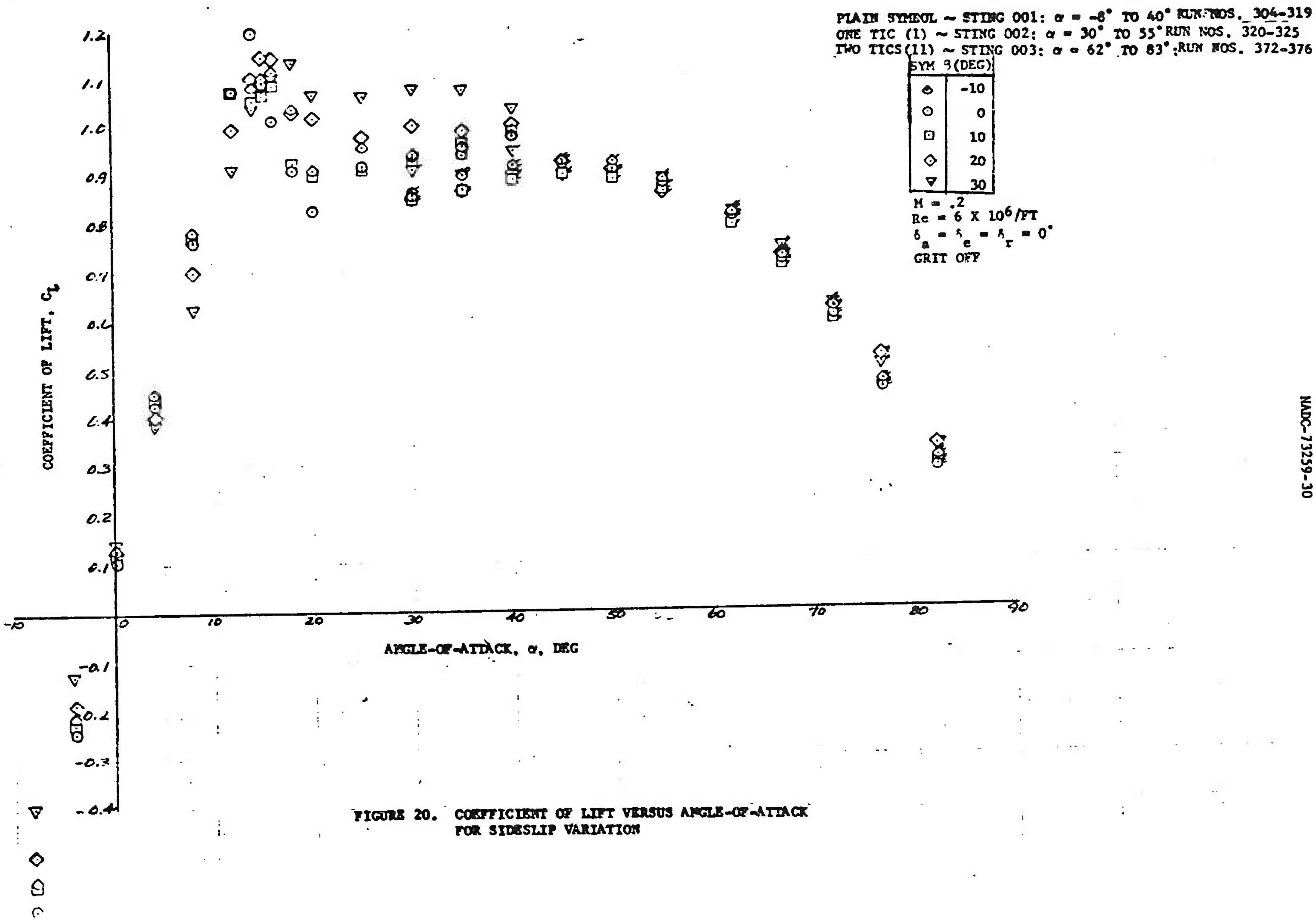

FIGURE 20. COEFFICIENT OF LIFT VERSUS ANGLE-OF-ATTACK FOR SIDESLIP VARIATION

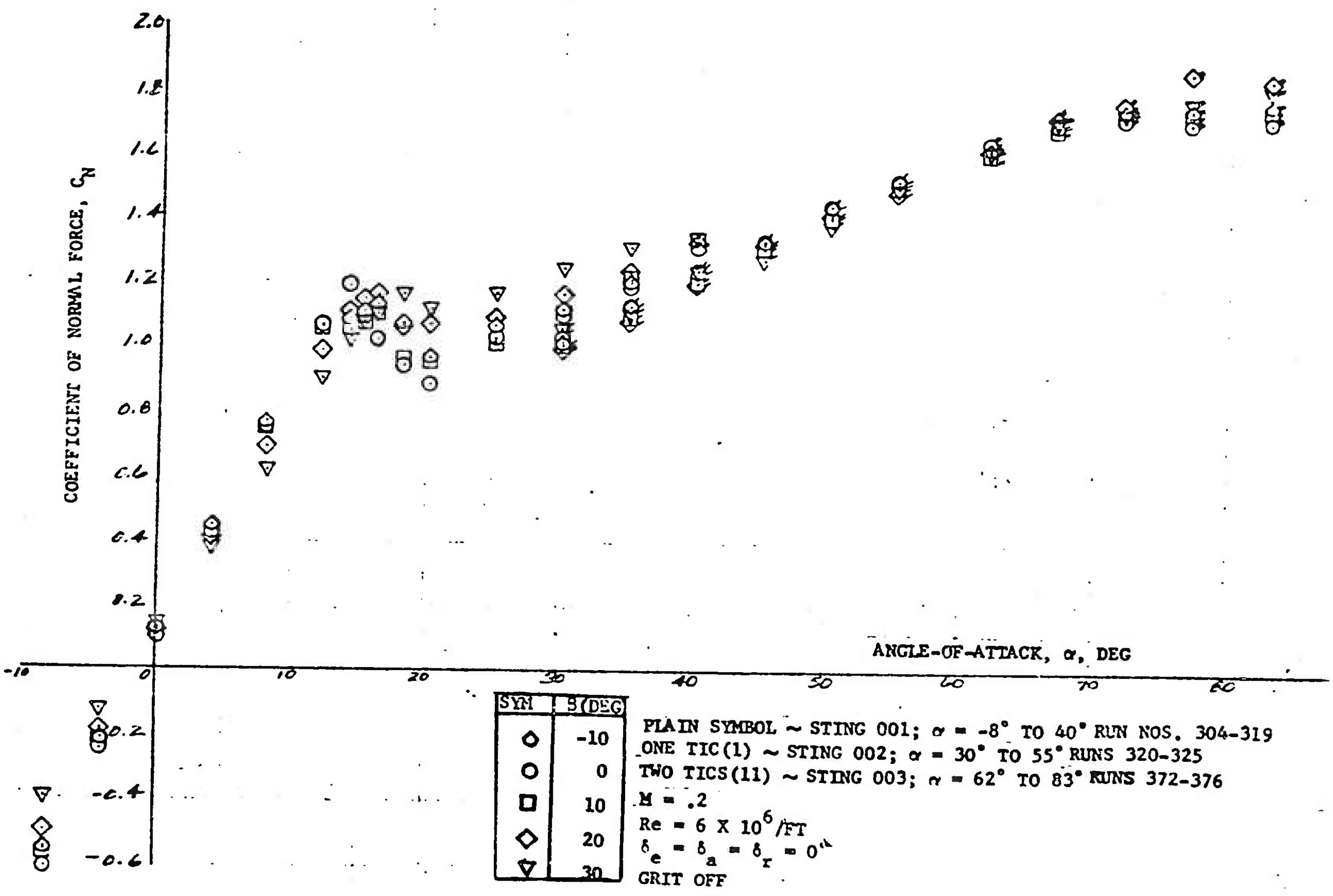

FIGURE 21. COEFFICIENT OF NORMAL FORCE VERSUS ANGLE-OF-ATTACK FOR SIDESLIP VARIATION

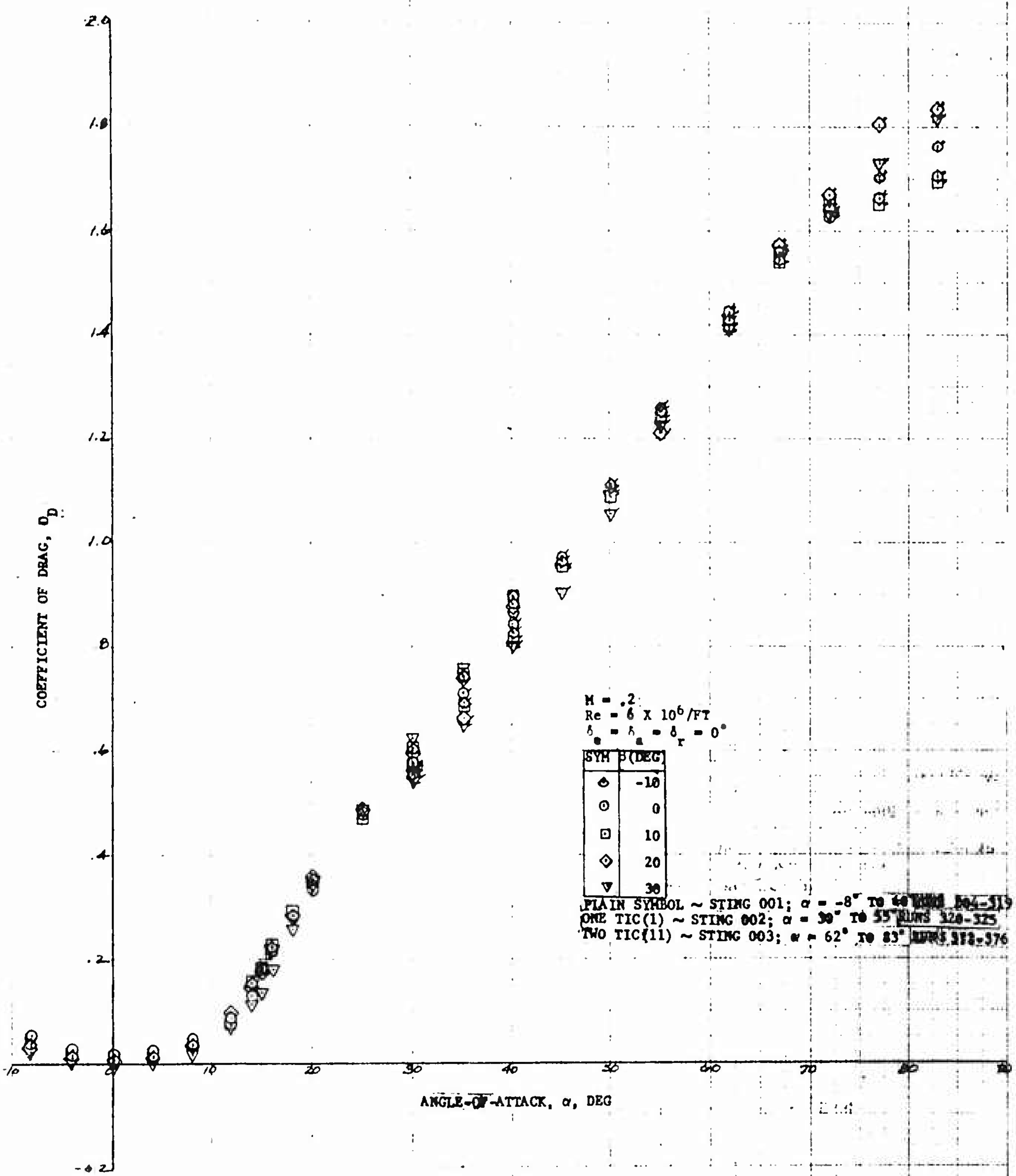

FIGURE 22. COEFFICIENT OF DRAG VERSUS ANGLE-OF-ATTACK FOR SIDESLIP VARIATION

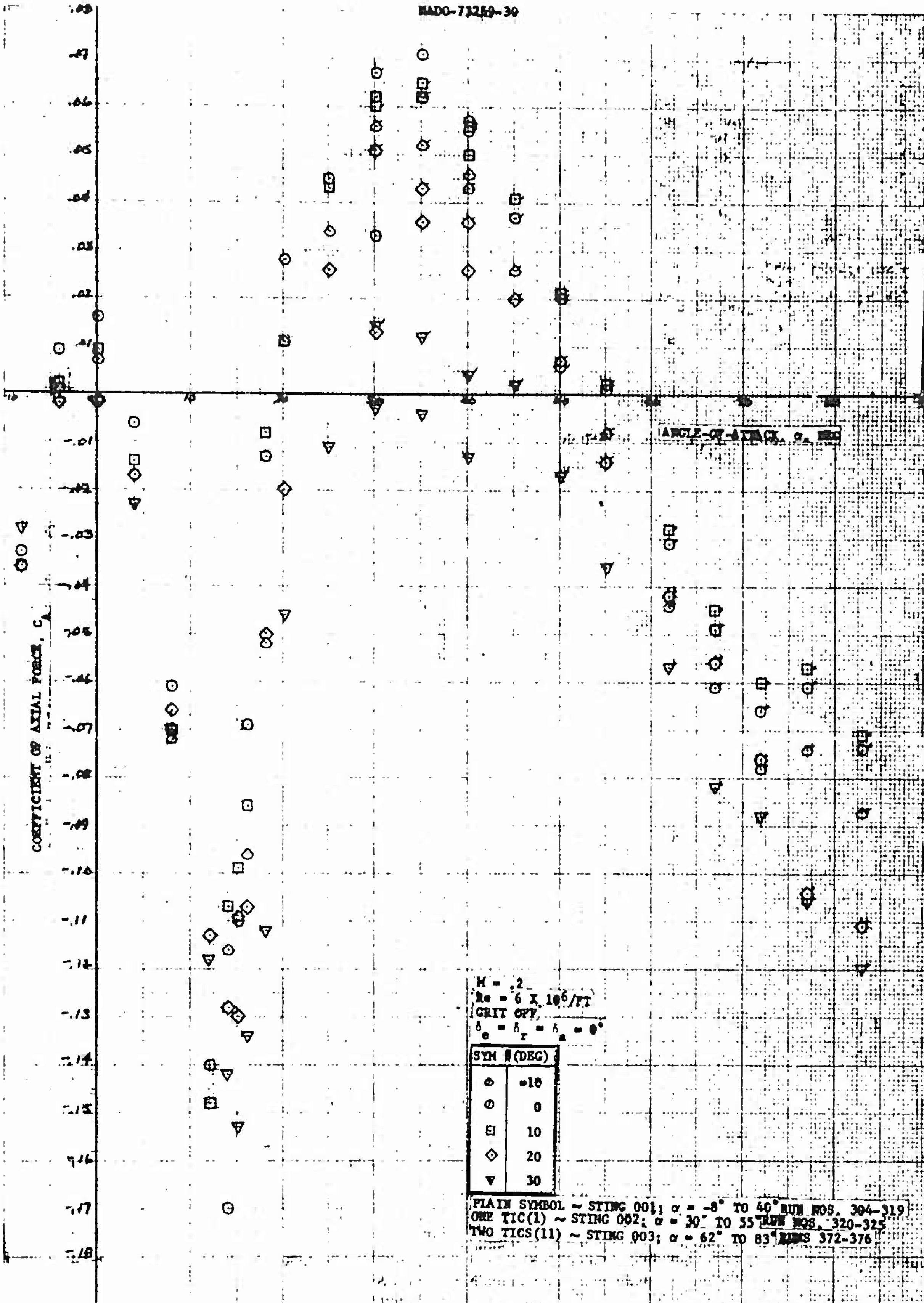

FIGURE 23. COEFFICIENT OF AXIAL FORCE VERSUS ANGLE-OF-ATTACK FOR SIDESLIP VARIATION

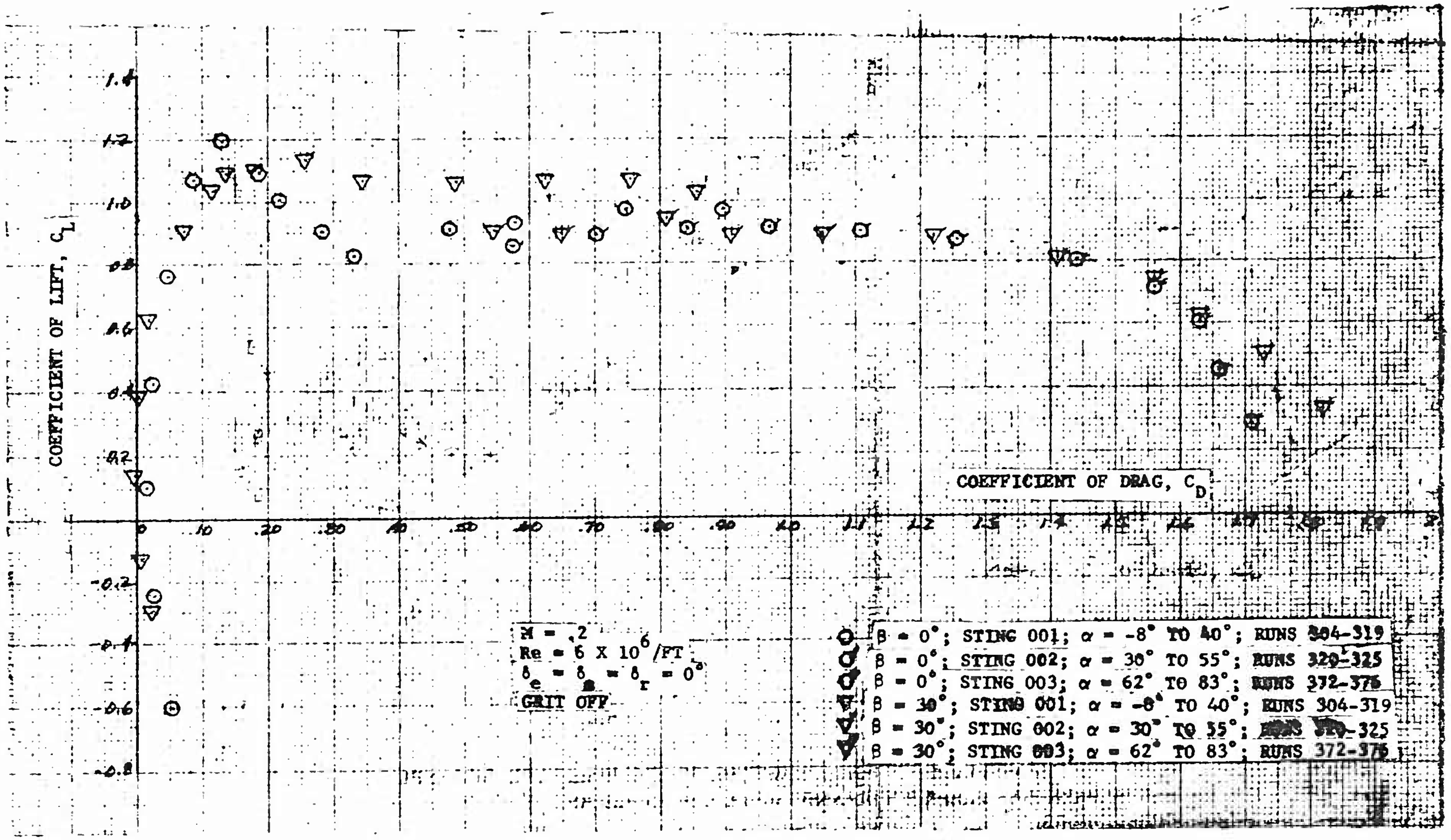

FIGURE 24. COEFFICIENT OF LIFT VERSUS COEFFICIENT OF DRAG FOR FULL RANGE OF ANGLE-OF-ATTACK

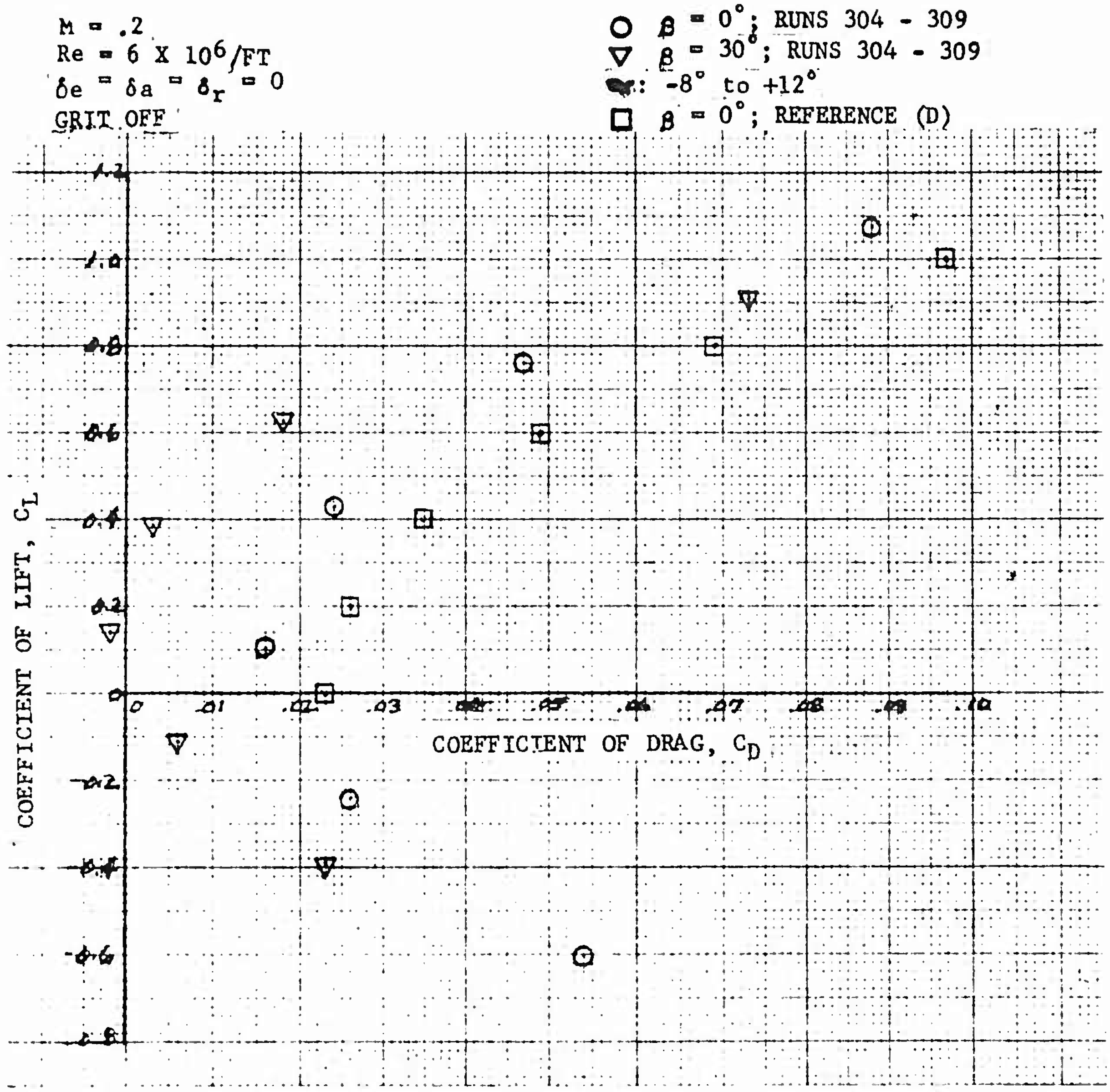

FIGURE 25. COEFFICIENT OF LIFT VERSUS COEFFICIENT OF DRAG FOR LOW ANGLES-OF-ATTACK

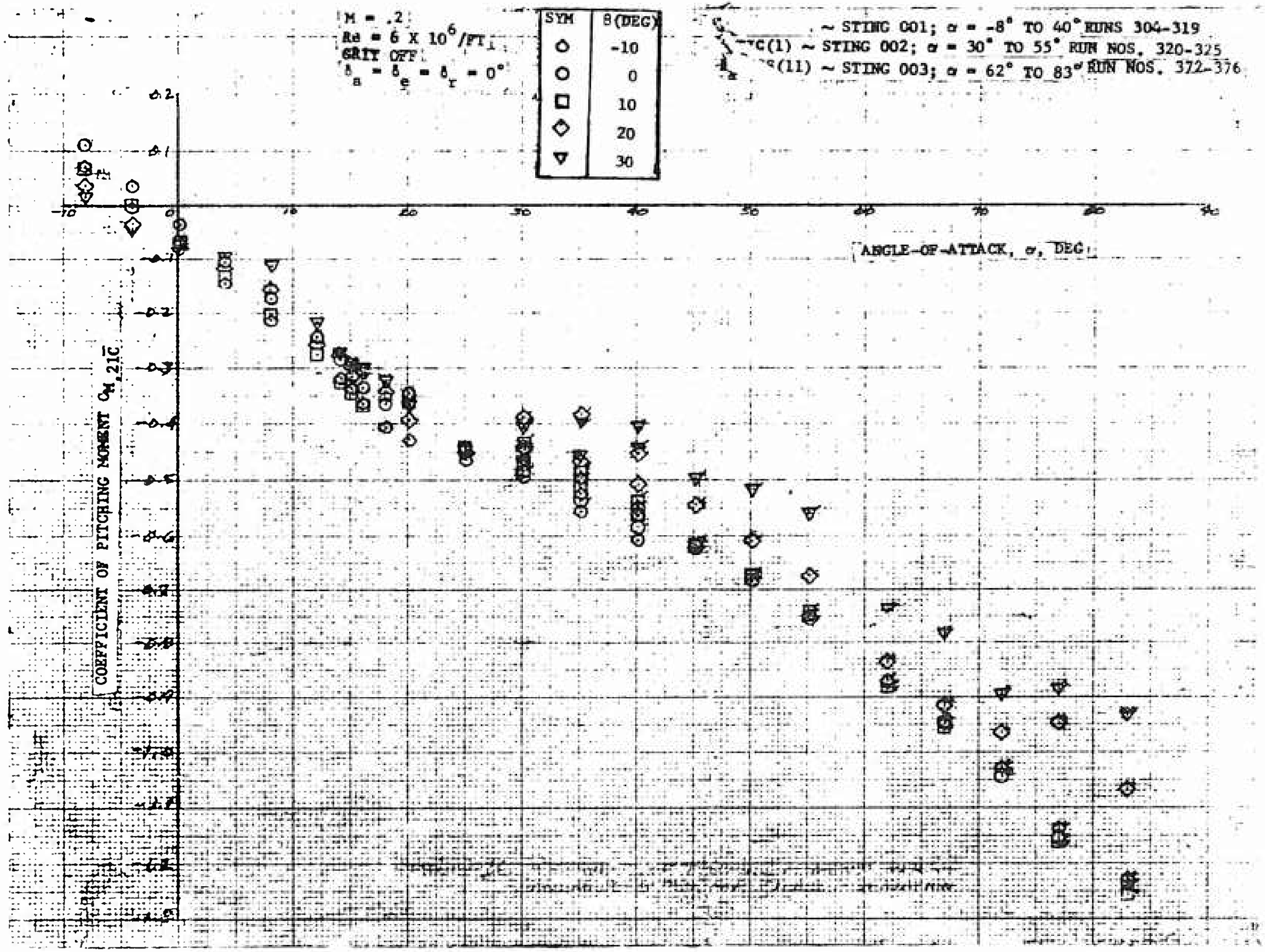

FIGURE 26. COEFFICIENT OF PITCHING MOMENT VERSUS ANGLE-OF-ATTACK FOR SIDESLIP VARIATION

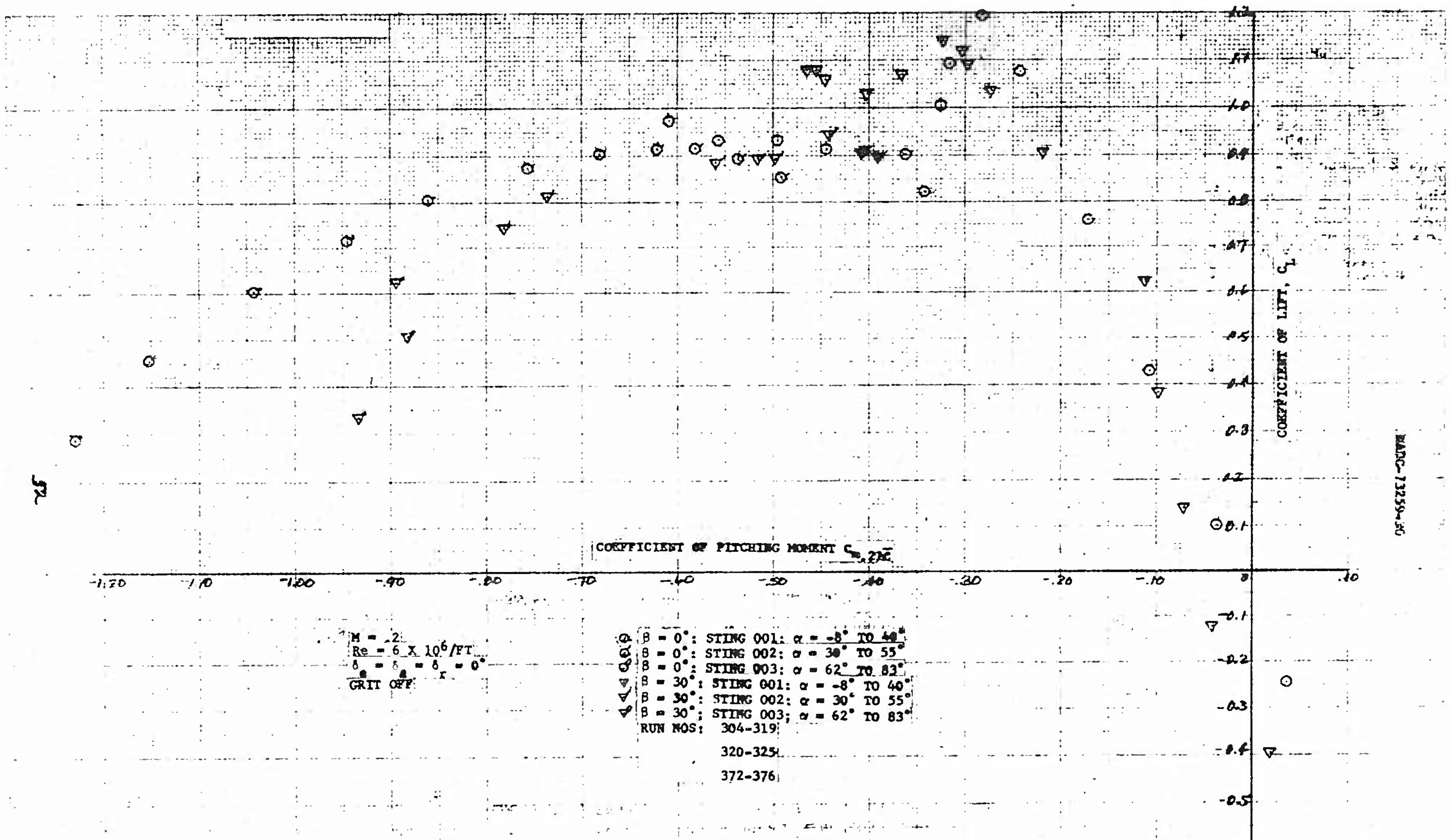

FIGURE 27. COEFFICIENT OF LIFT VERSUS COEFFICIENT OF PITCHING MOMENT FOR FULL RANGE OF ANGLE-OF-ATTACK

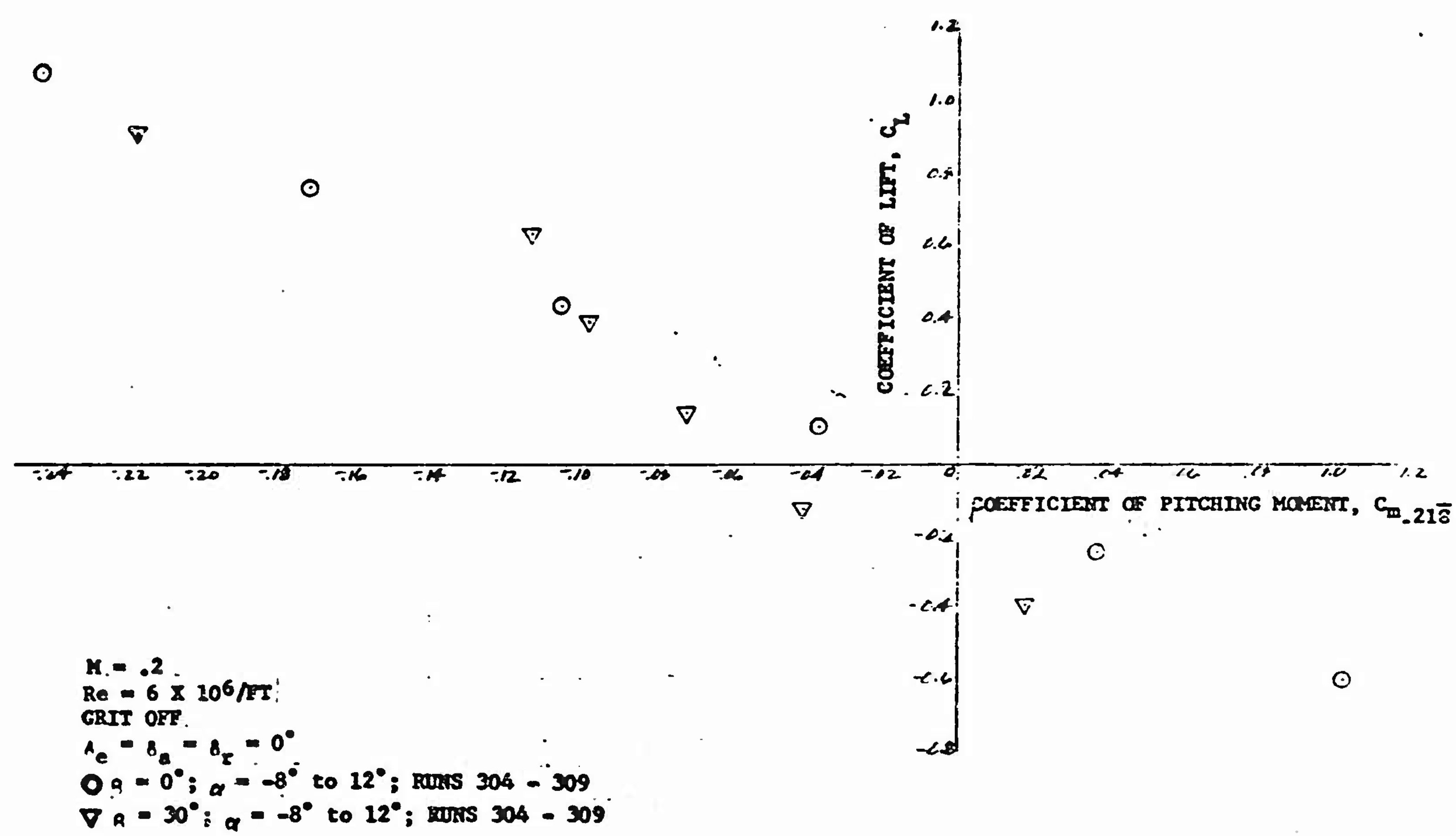

FIGURE 28. COEFFICIENT OF LIFT VERSUS COEFFICIENT OF PITCHING MOMENT FOR LOW ANGLES-OF-ATTACK

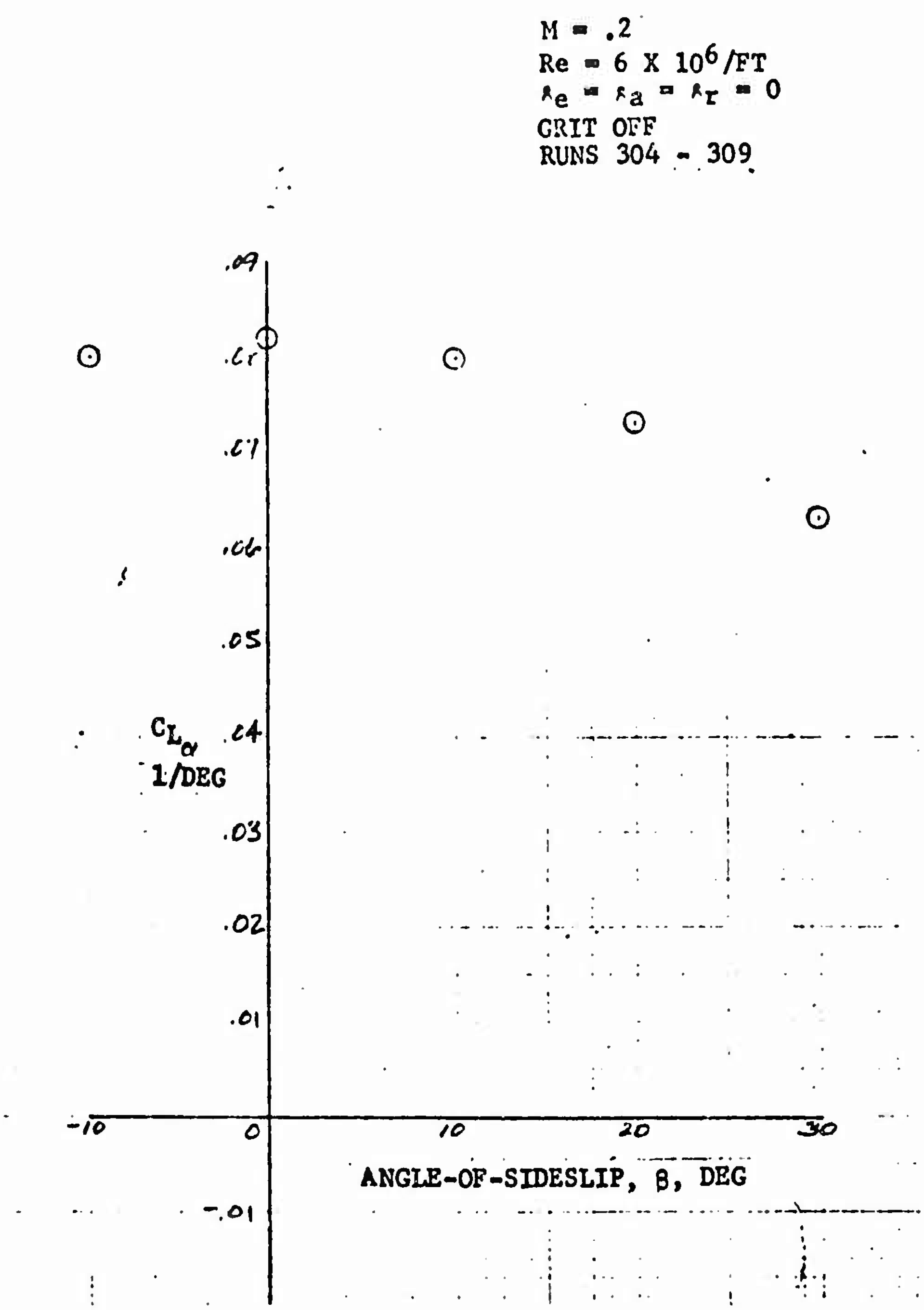

FIGURE 29. LIFT CURVE SLOPE, C_{L_α}, VERSUS ANGLE-OF-SIDESLIP, β

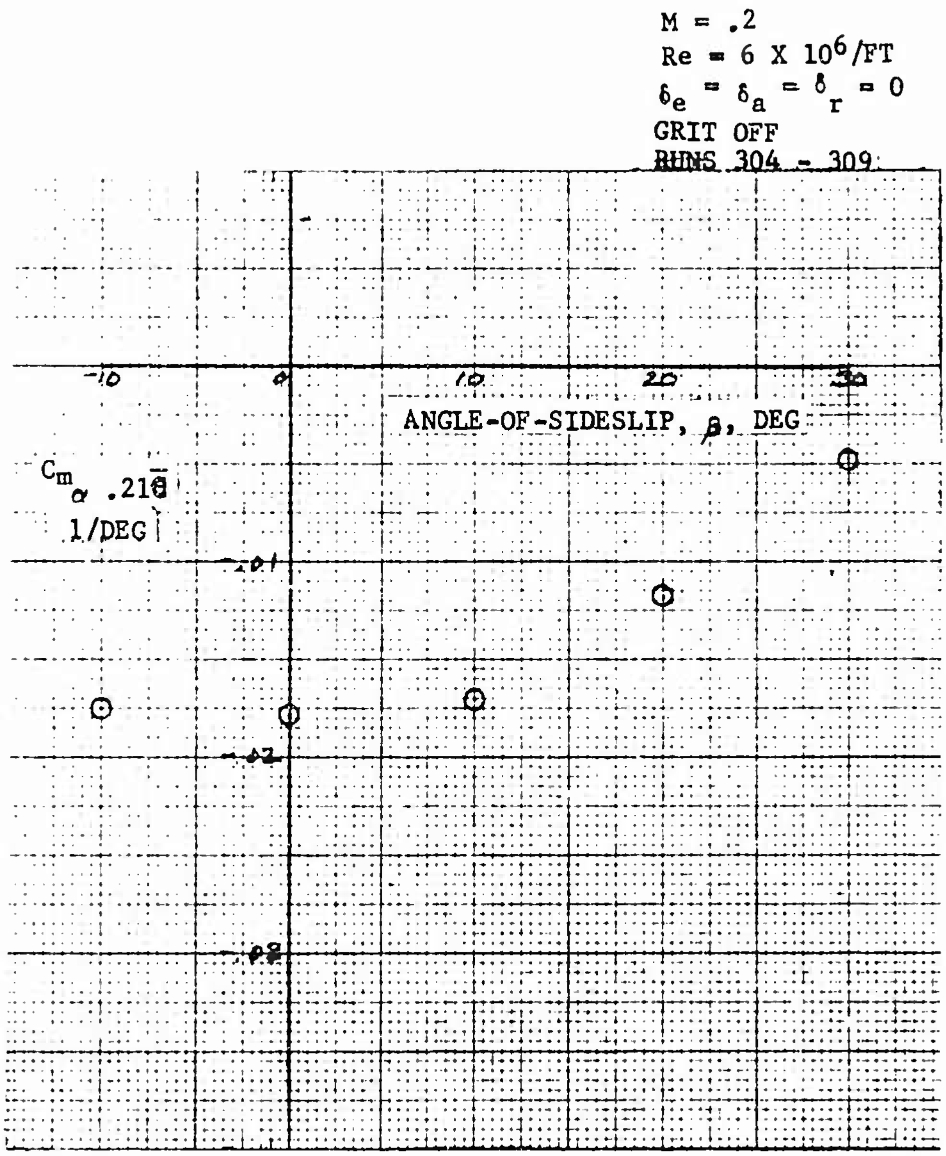

FIGURE 30. PITCHING MOMENT CURVE SLOPE, C_{m_α}, VERSUS ANGLE-OF-SIDESLIP, β

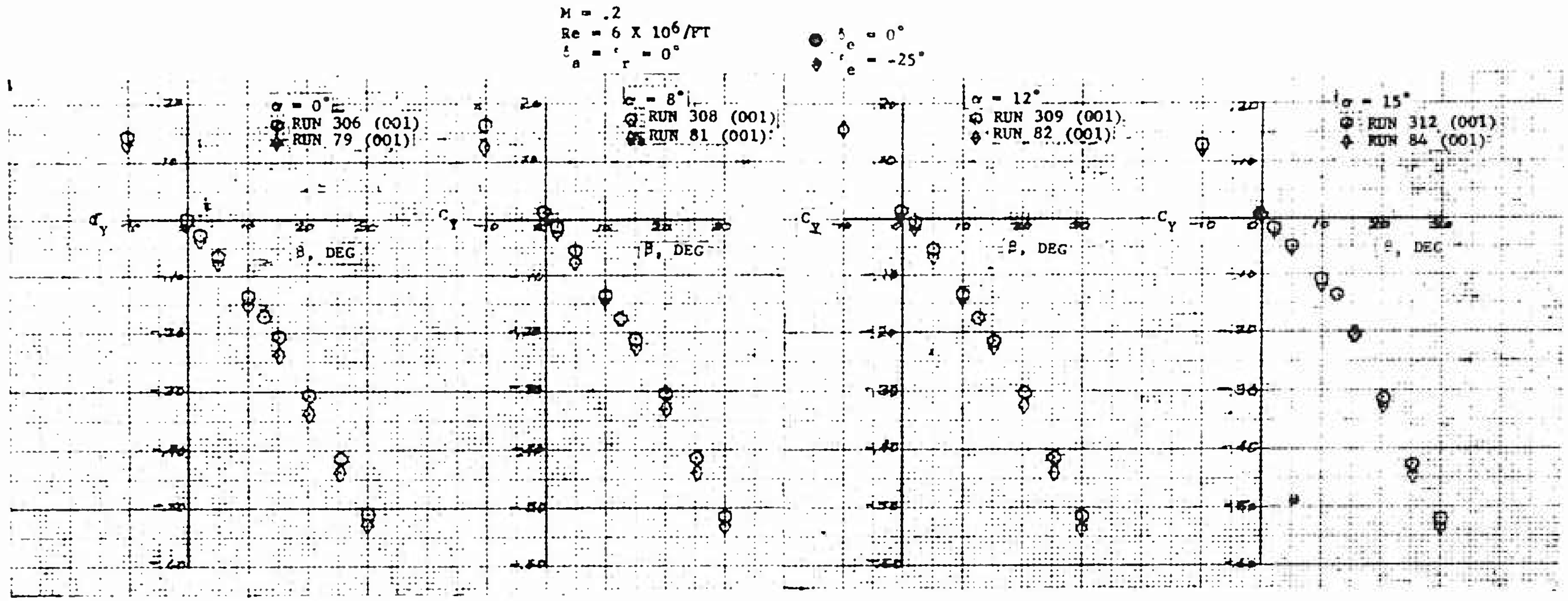

FIGURE 31. COEFFICIENT OF SIDE FORCE VERSUS ANGLE-OF-SIDESLIP FOR VARIOUS ANGLES-OF-ATTACK AND TWO ELEVATOR DEFLECTIONS

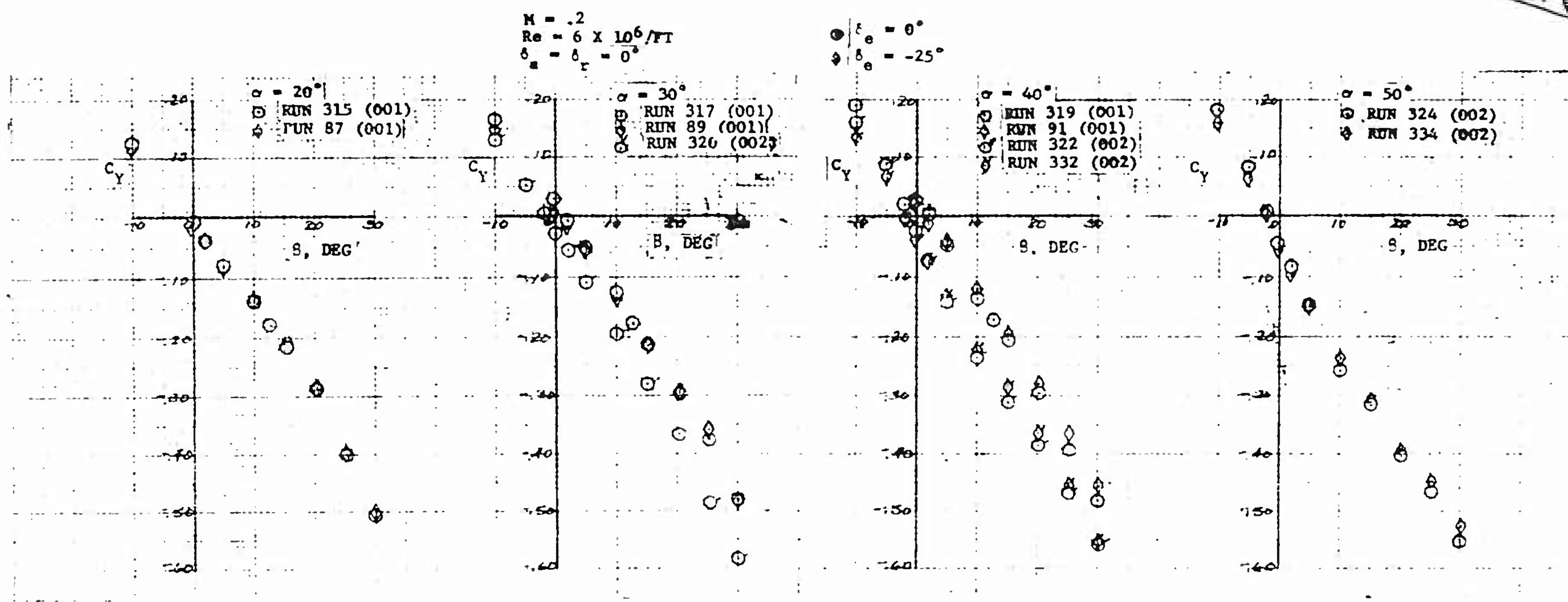

FIGURE 31. COEFFICIENT OF SIDE FORCE VERSUS ANGLE-OF-SIDESLIP FOR VARIOUS ANGLES-OF-ATTACK (CONT) AND TWO ELEVATOR DEFLECTIONS

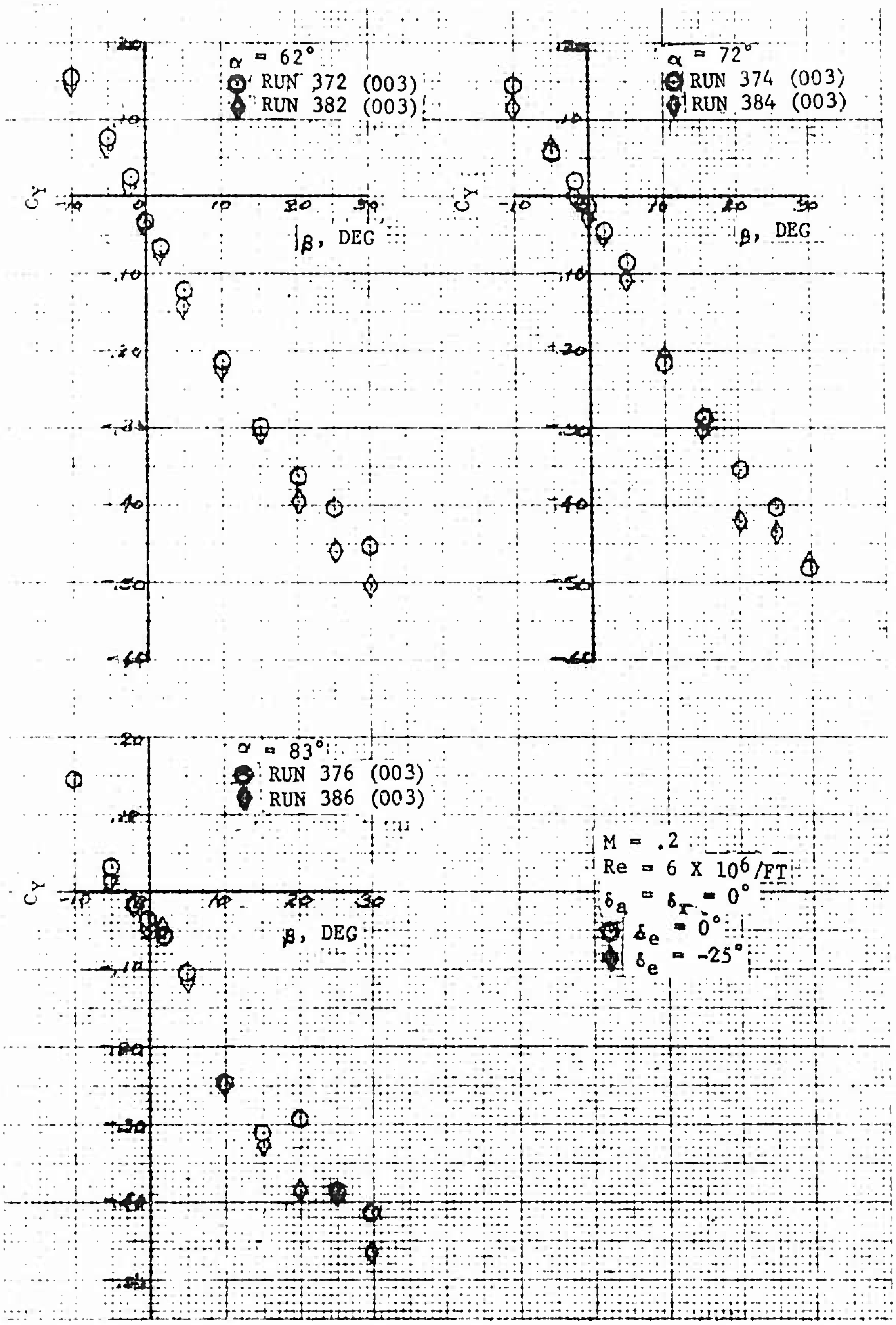

FIGURE 31. (CONT) COEFFICIENT OF SIDEFORCE VERSUS ANGLE-OF-SIDESLIP FOR VARIOUS ANGLES-OF-ATTACK AND TWO ELEVATOR DEFLECTIONS

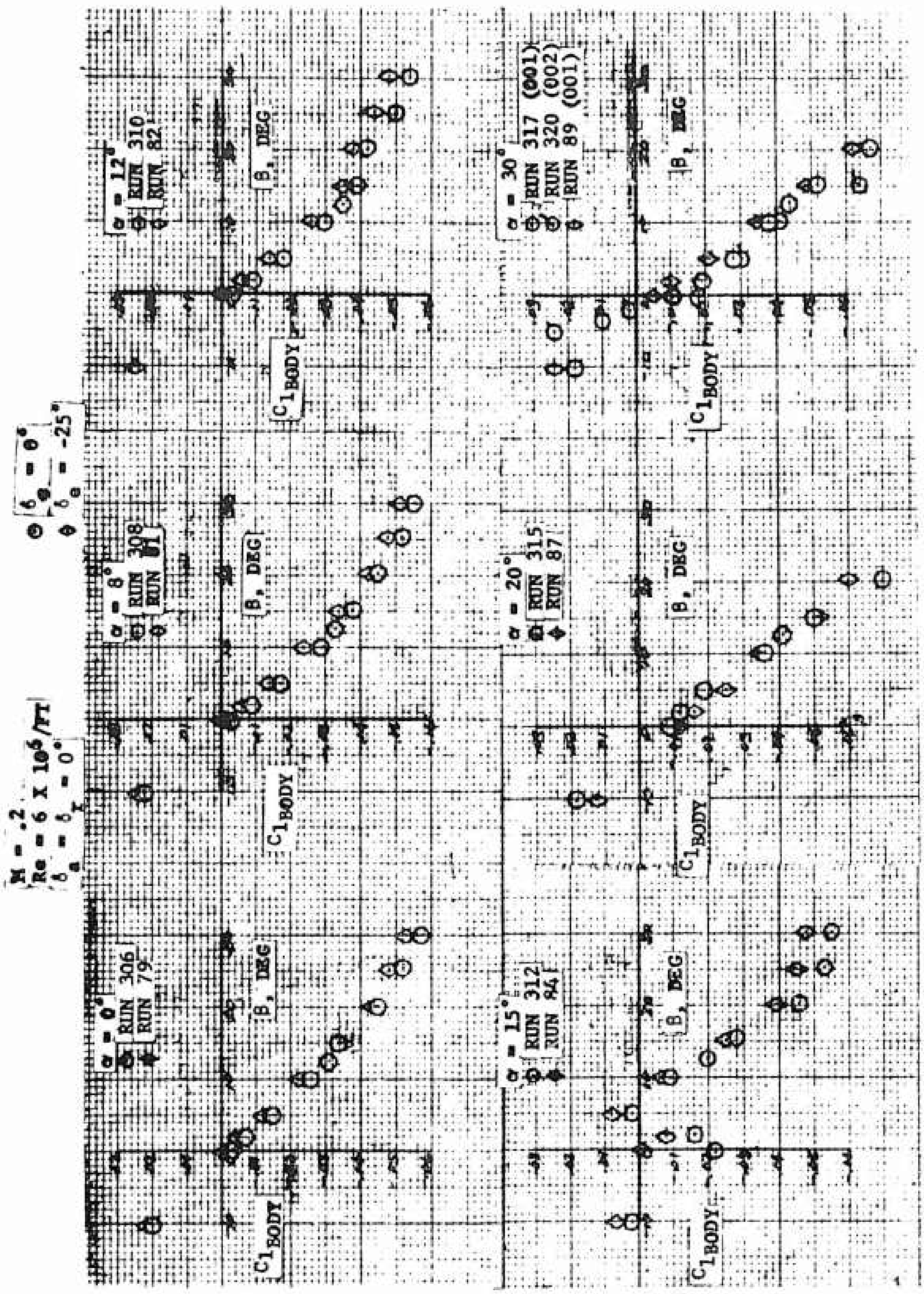

FIGURE 32. COEFFICIENT OF ROLLING MOMENT VERSUS ANGLE-OF-SIDESLIP FOR VARIOUS ANGLES-OF-ATTACK AND TWO ELEVATOR DEFLECTIONS (BODY AXIS SYSTEM)

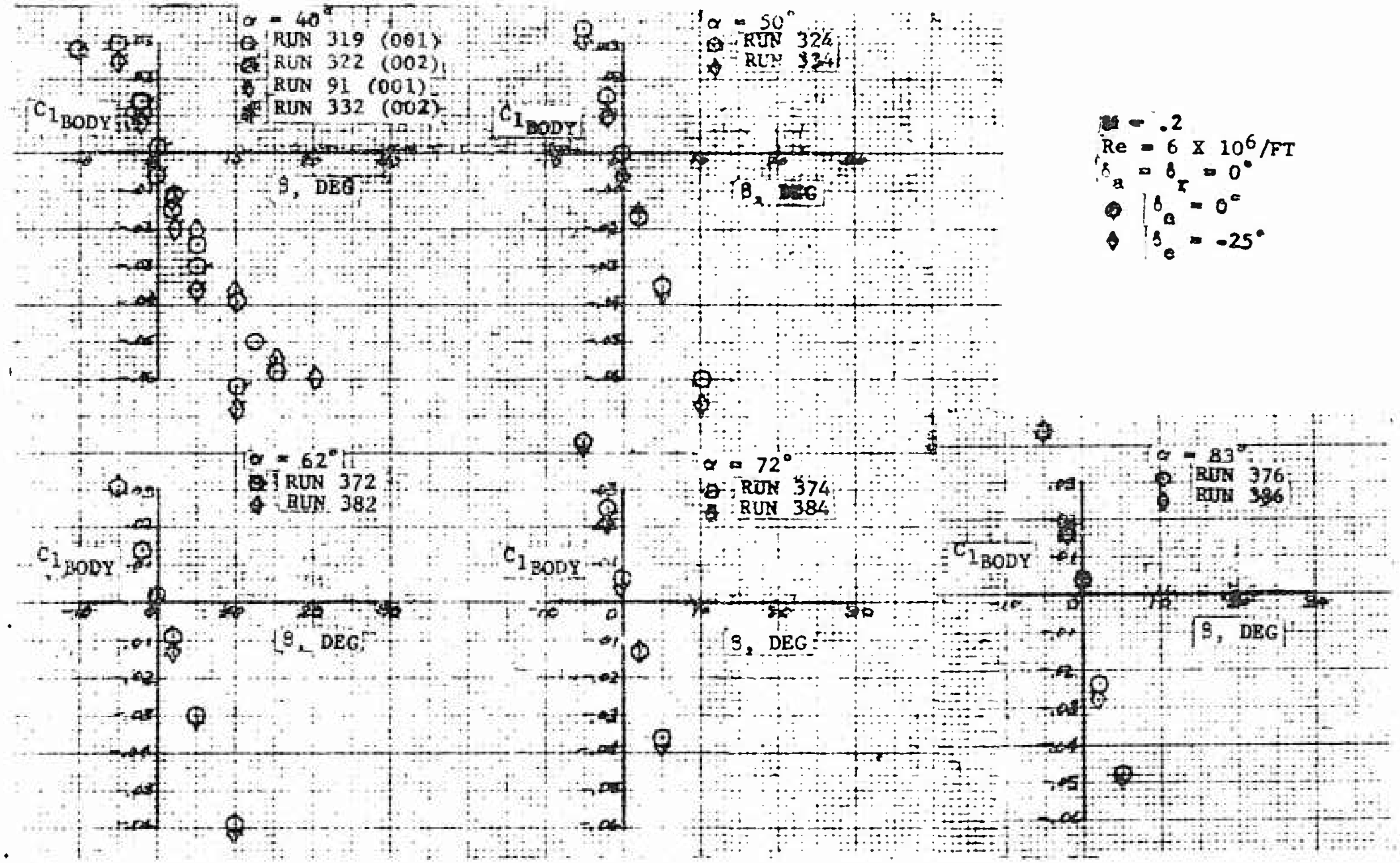

FIGURE 32. COEFFICIENT OF ROLLING MOMENT VERSUS ANGLE-OF-SIDESLIP FOR VARIOUS ANGLES-OF-ATTACK AND TWO ELEVATOR DEFLECTIONS (BODY AXIS SYSTEM) (CONT)

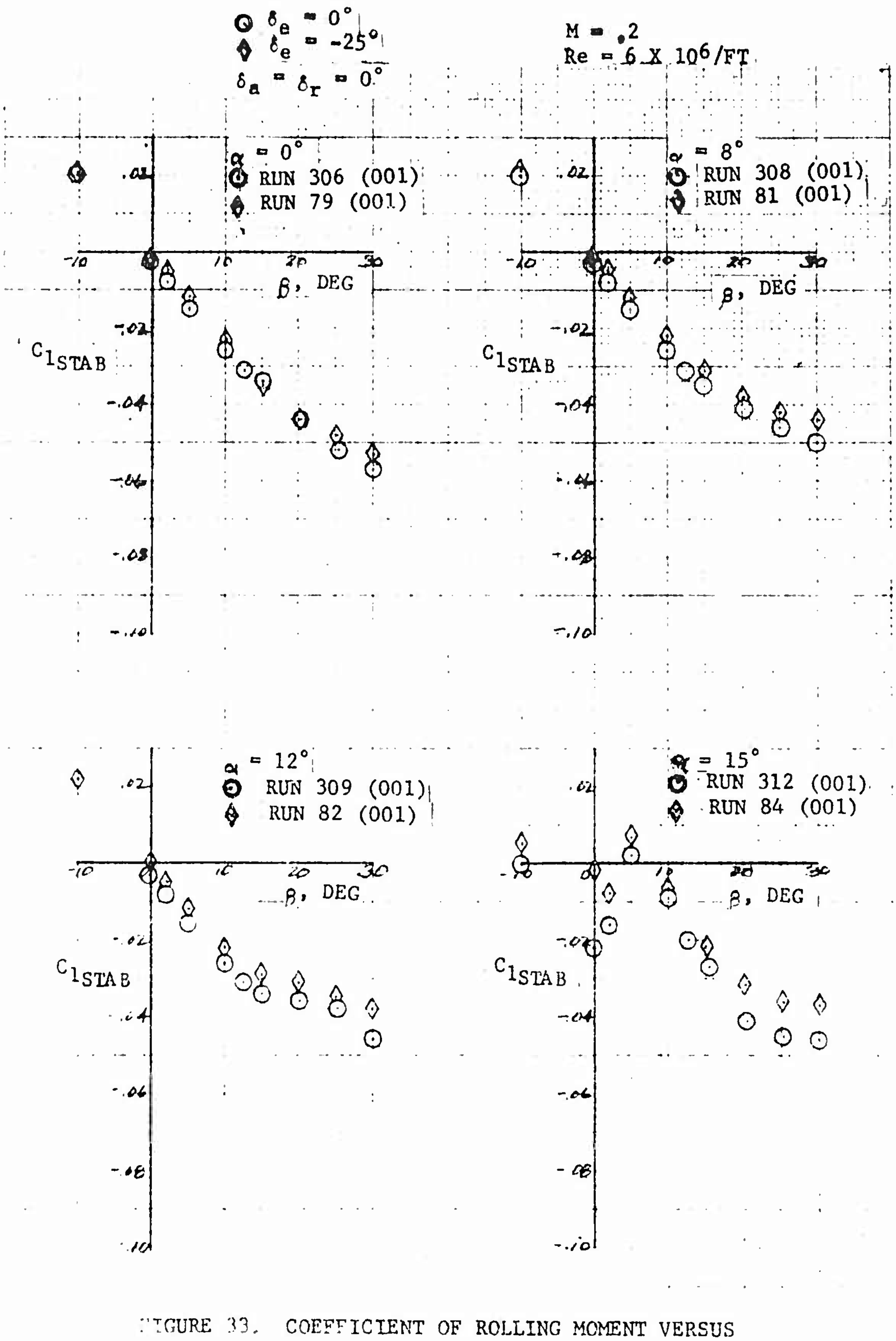

FIGURE 33. COEFFICIENT OF ROLLING MOMENT VERSUS ANGLE-OF-SIDESLIP FOR VARIOUS ANGLES-OF-ATTACK AT TWO ELEVATOR DEFLECTIONS (STABILITY AXIS SYSTEM)

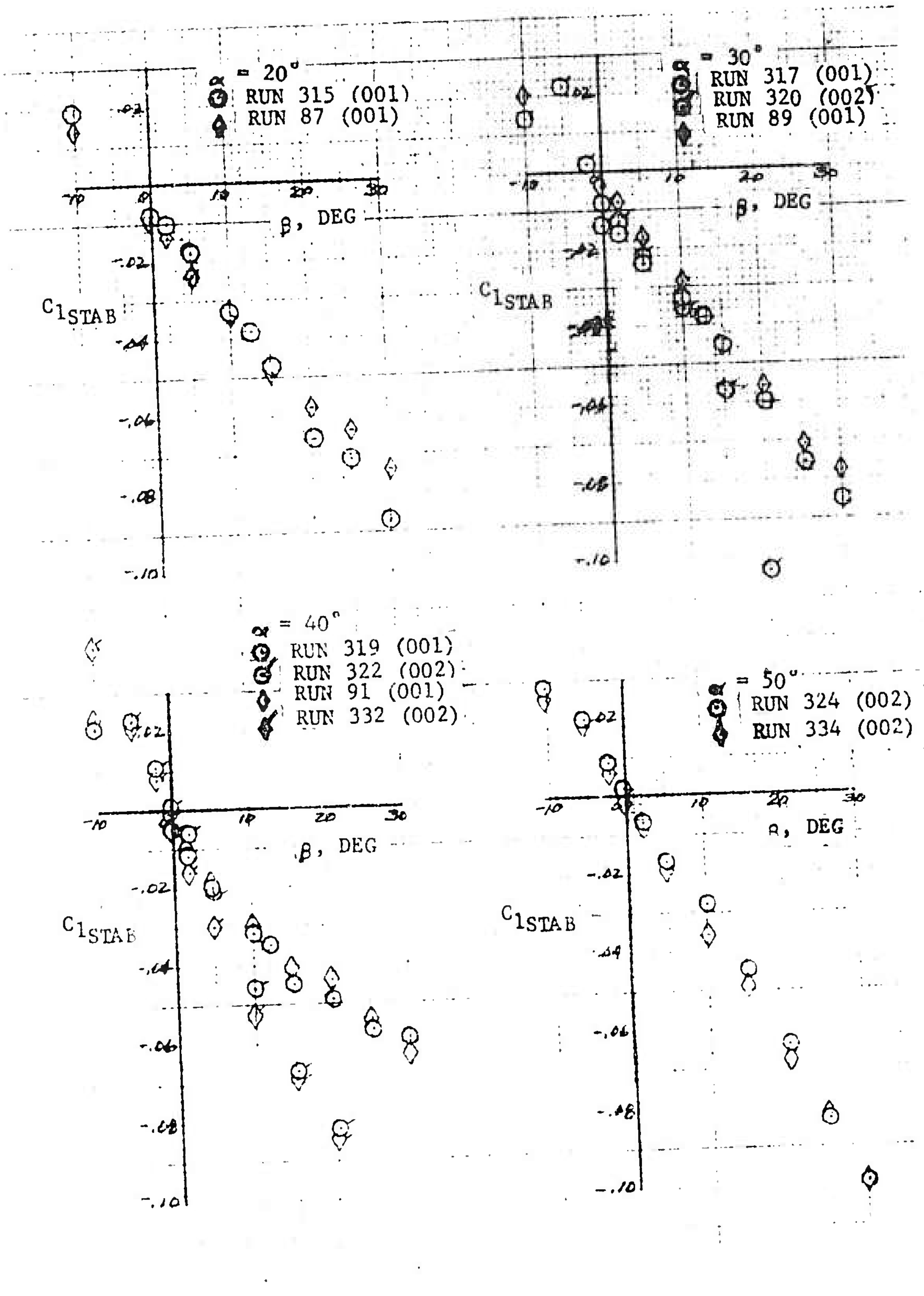

FIGURE 33. (CONT) COEFFICIENT OF ROLLING MOMENT VERSUS ANGLE-OF-SIDESLIP FOR VARIOUS ANGLES-OF-ATTACK AT TWO ELEVATOR DEFLECTIONS (STABILITY AXIS SYSTEM)

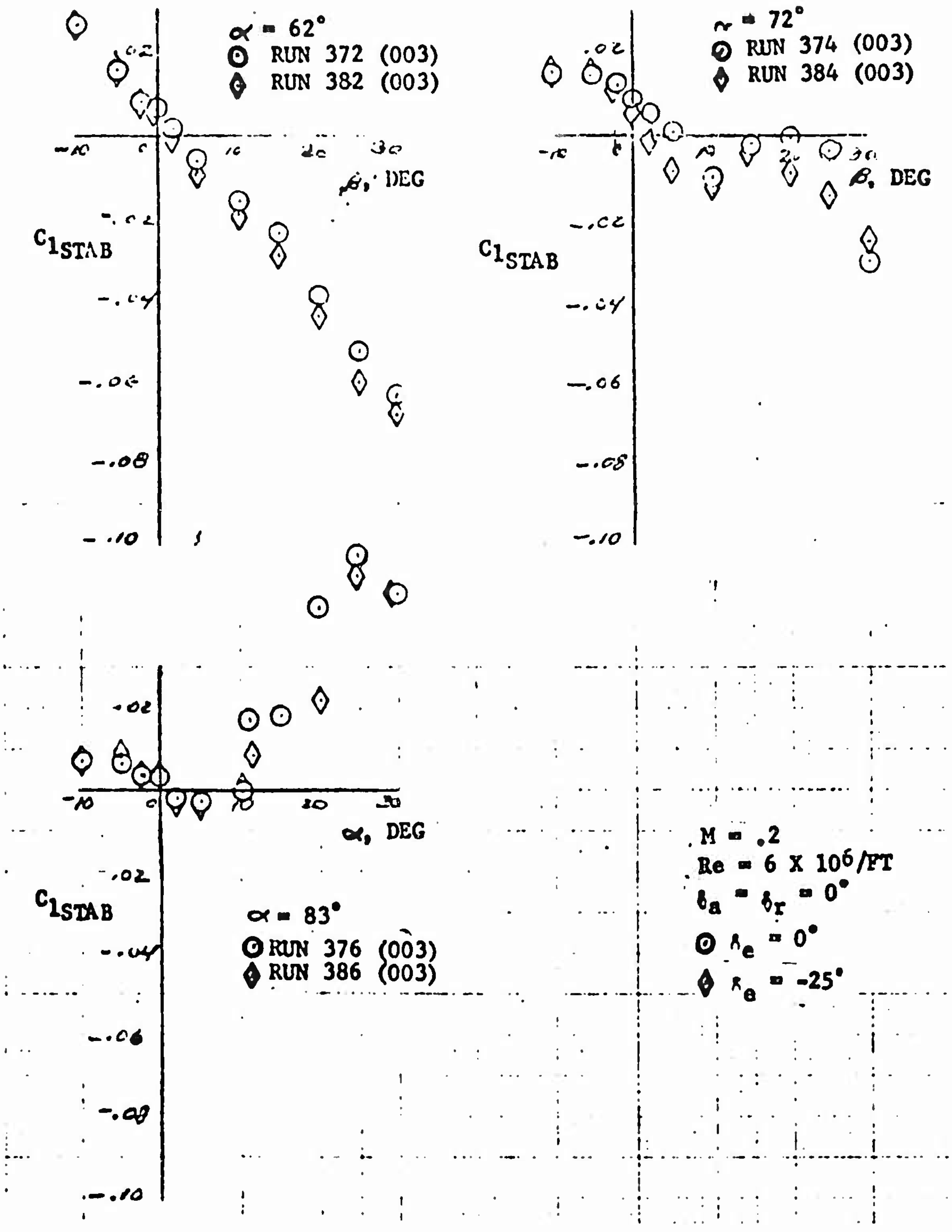

FIGURE 33. (CONT) COEFFICIENT OF ROLLING MOMENT VERSUS ANGLE-OF-SIDESLIP FOR VARIOUS ANGLES-OF-ATTACK AT TWO ELEVATOR DEFLECTIONS (STABILITY AXIS SYSTEM)

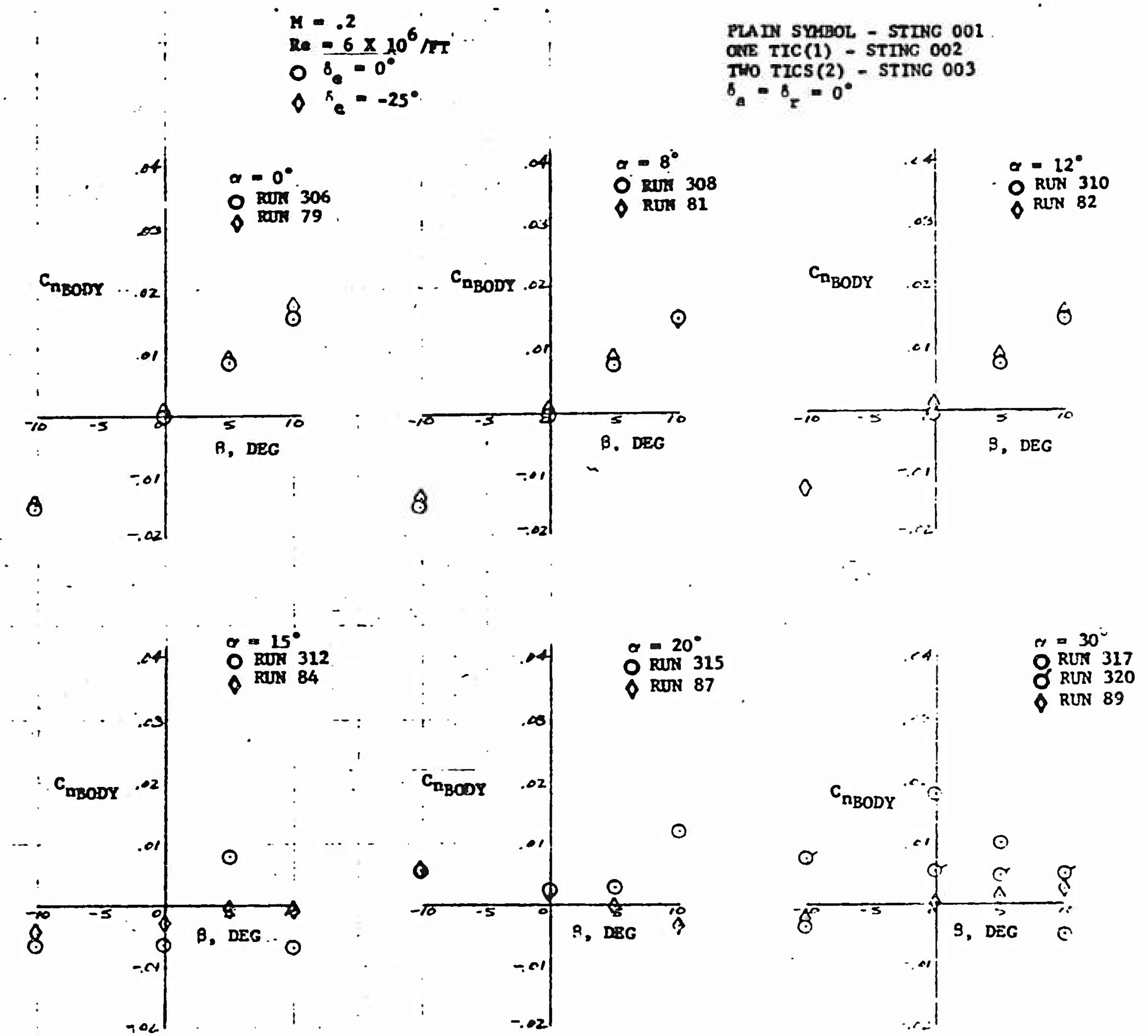

FIGURE 34. COEFFICIENT OF YAWING MOMENT VERSUS ANGLE-OF-SIDESLIP FOR VARIOUS ANGLES-OF-ATTACK AND TWO ELEVATOR DEFLECTIONS (BODY AXIS SYSTEM)

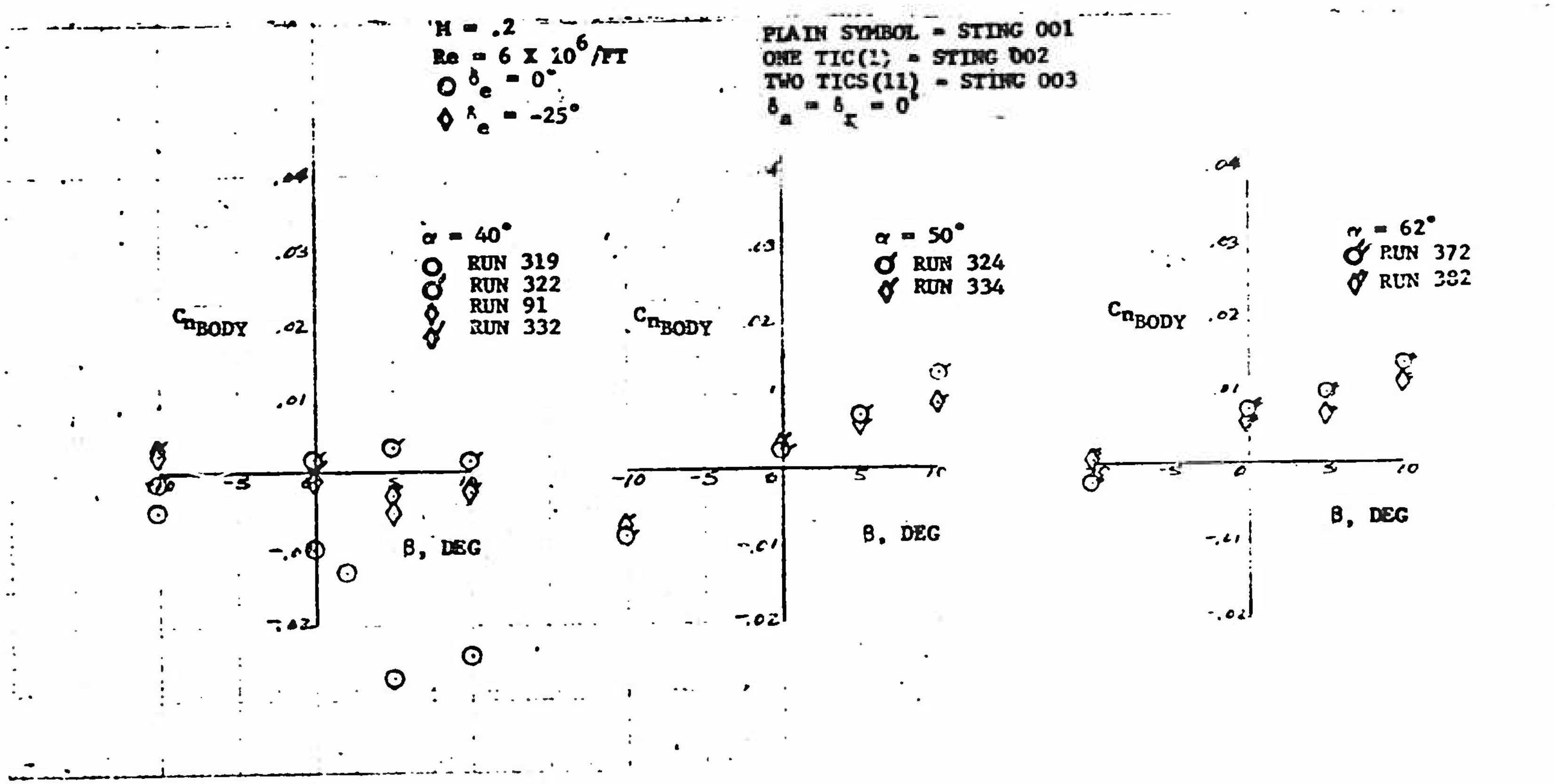

FIGURE 34. (CONT) COEFFICIENT OF YAWING MOMENT VERSUS ANGLE-OF-SIDESLIP FOR VARIOUS ANGLES-OF-ATTACK AND TWO ELEVATOR DEFLECTIONS (BODY AXIS SYSTEM)

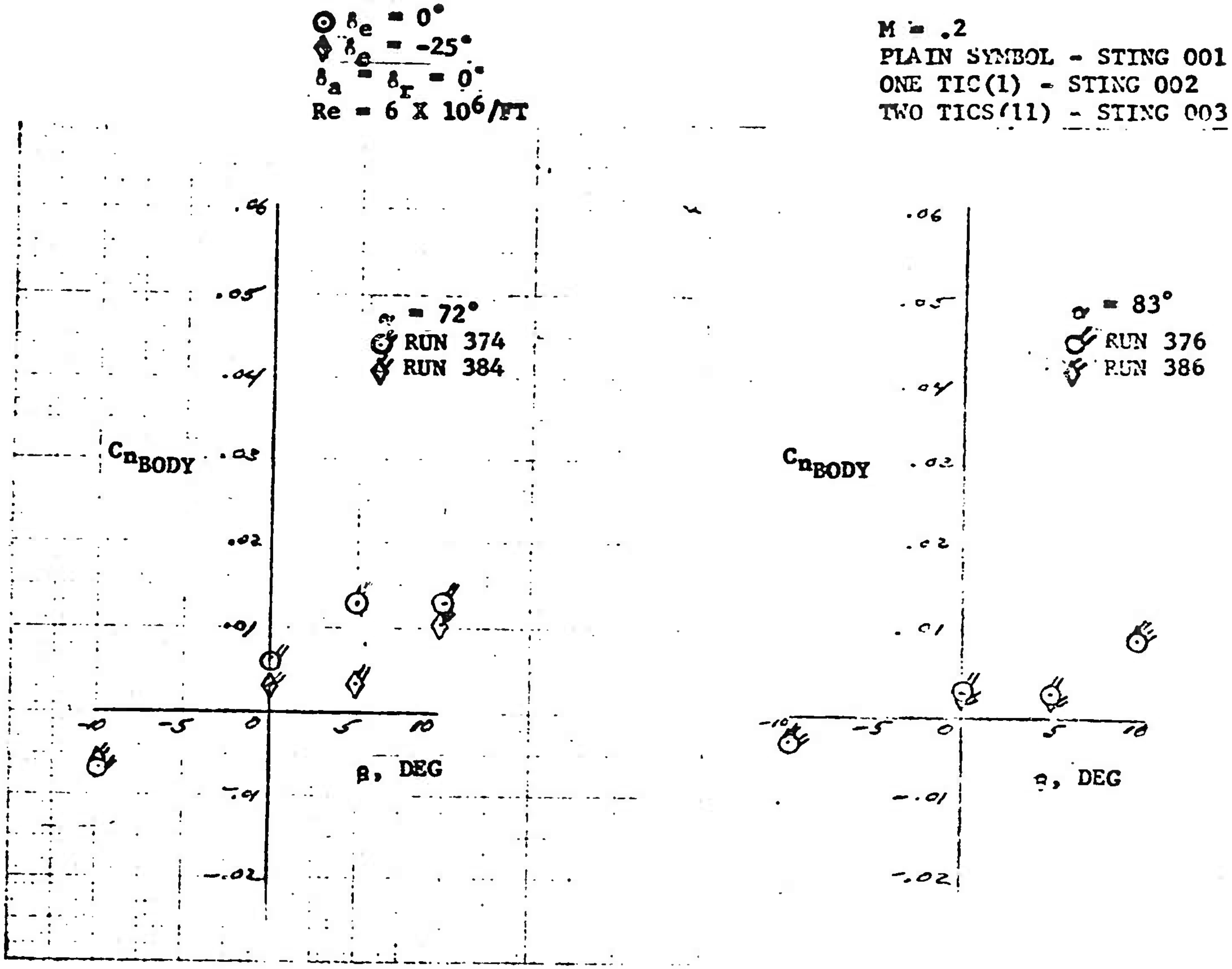

FIGURE 34. (CONT) COEFFICIENT OF YAWING MOMENT VERSUS ANGLE-OF-SIDESLIP FOR VARIOUS ANGLES-OF-ATTACK AND TWO ELEVATOR SETTINGS (BODY AXIS SYSTEM)

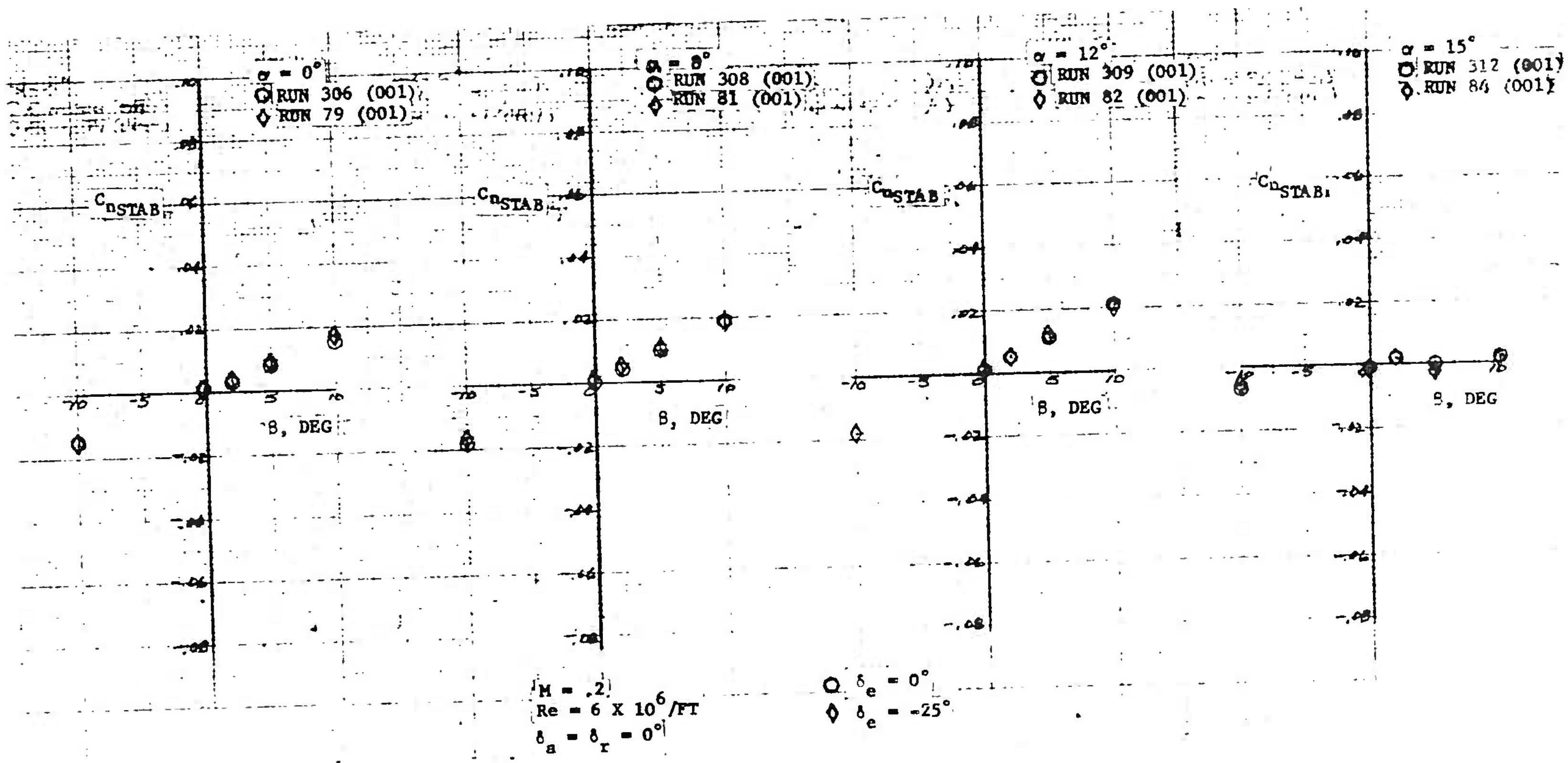

FIGURE 35. COEFFICIENT OF YAWING MOMENT VERSUS ANGLE-OF-SIDESLIP FOR VARIOUS ANGLES-OF-ATTACK AND TWO ELEVATOR DEFLECTIONS (STABILITY AXIS SYSTEM)

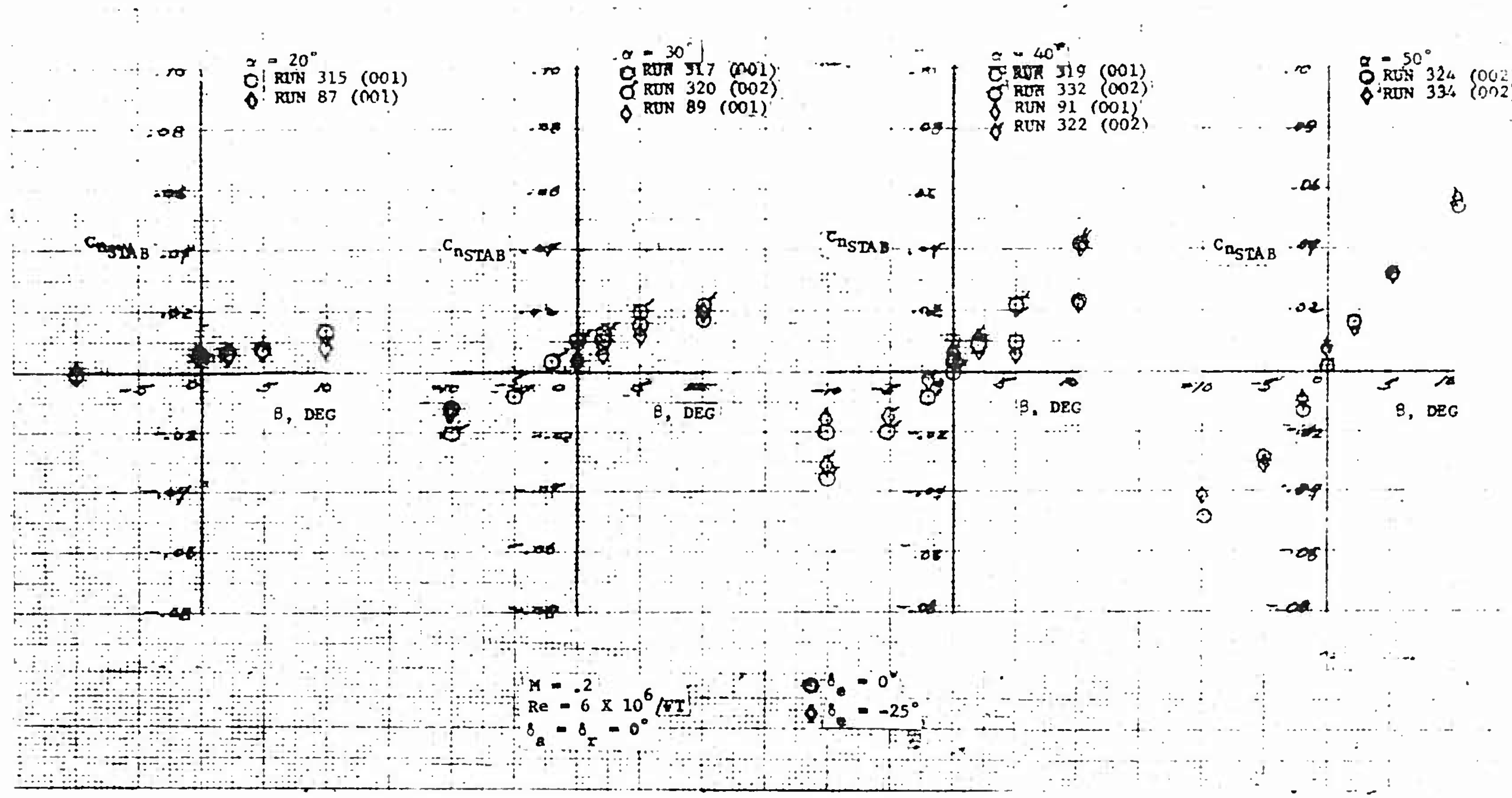

FIGURE 35. COEFFICIENT OF YAWING MOMENT VERSUS ANGLE-OF-SIDESLIP FOR VARIOUS ANGLES-OF-ATTACK AND TWO ELEVATOR DEFLECTIONS (CONT) (STABILITY AXIS SYSTEM)

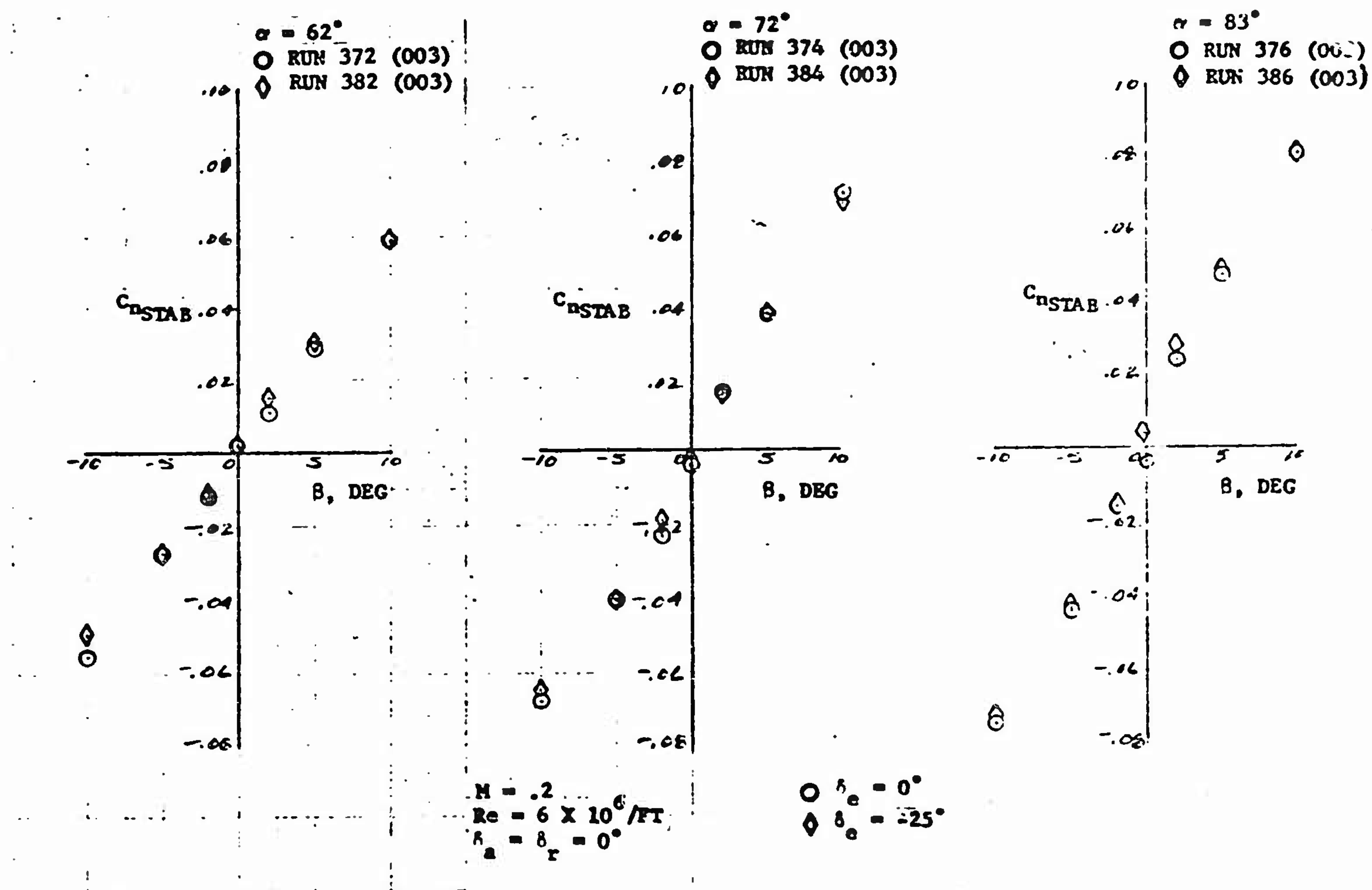

FIGURE 35. COEFFICIENT OF YAWING MOMENT VERSUS ANGLE-OF-SIDESLIP FOR VARIOUS ANGLES-OF-ATTACK AND TWO ELEVATOR DEFLECTIONS (STABILITY AXIS SYSTEM) (CONT)

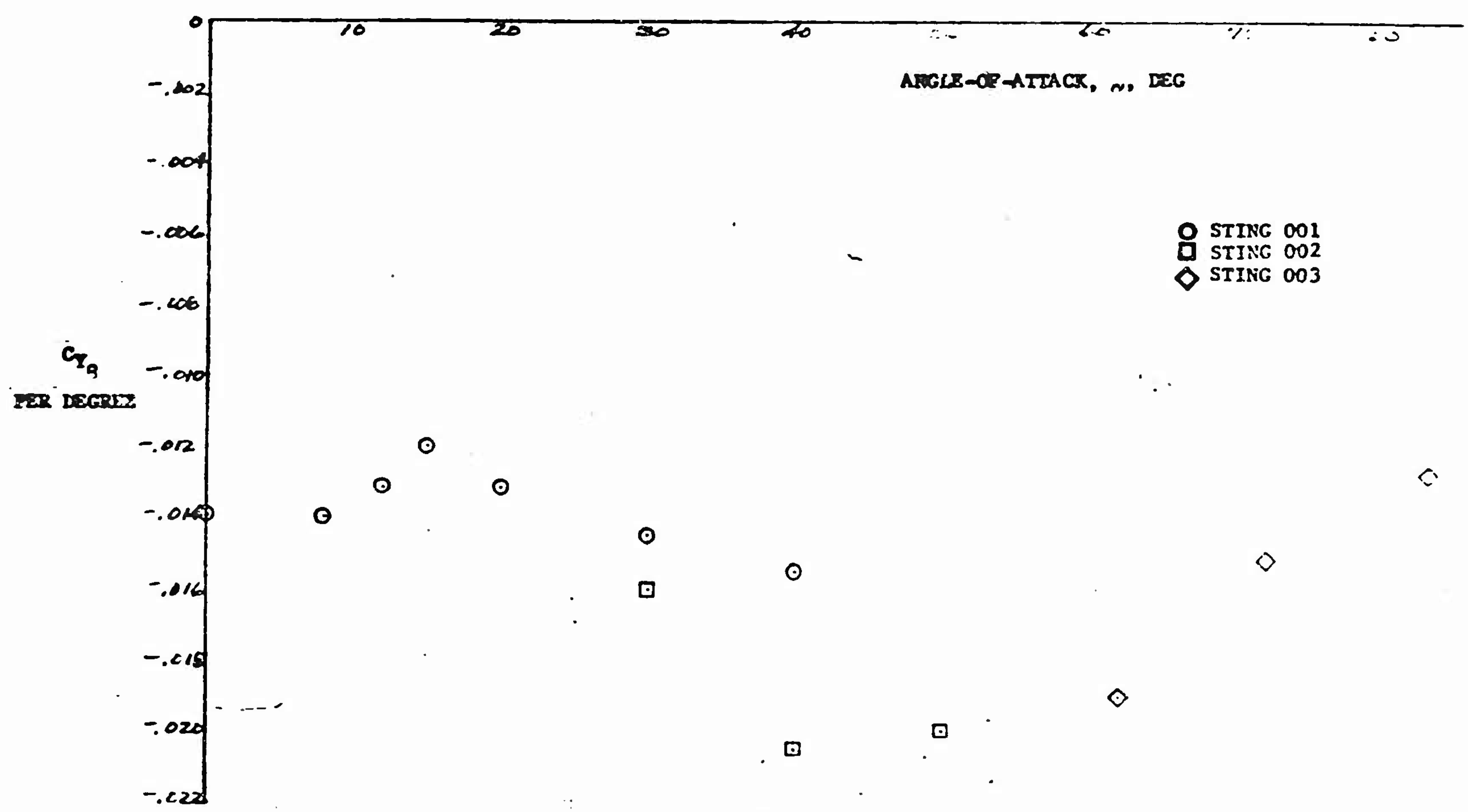

FIGURE 36. SIDEFORCE DAMPING DERIVATIVE VERSUS ANGLE-OF-ATTACK

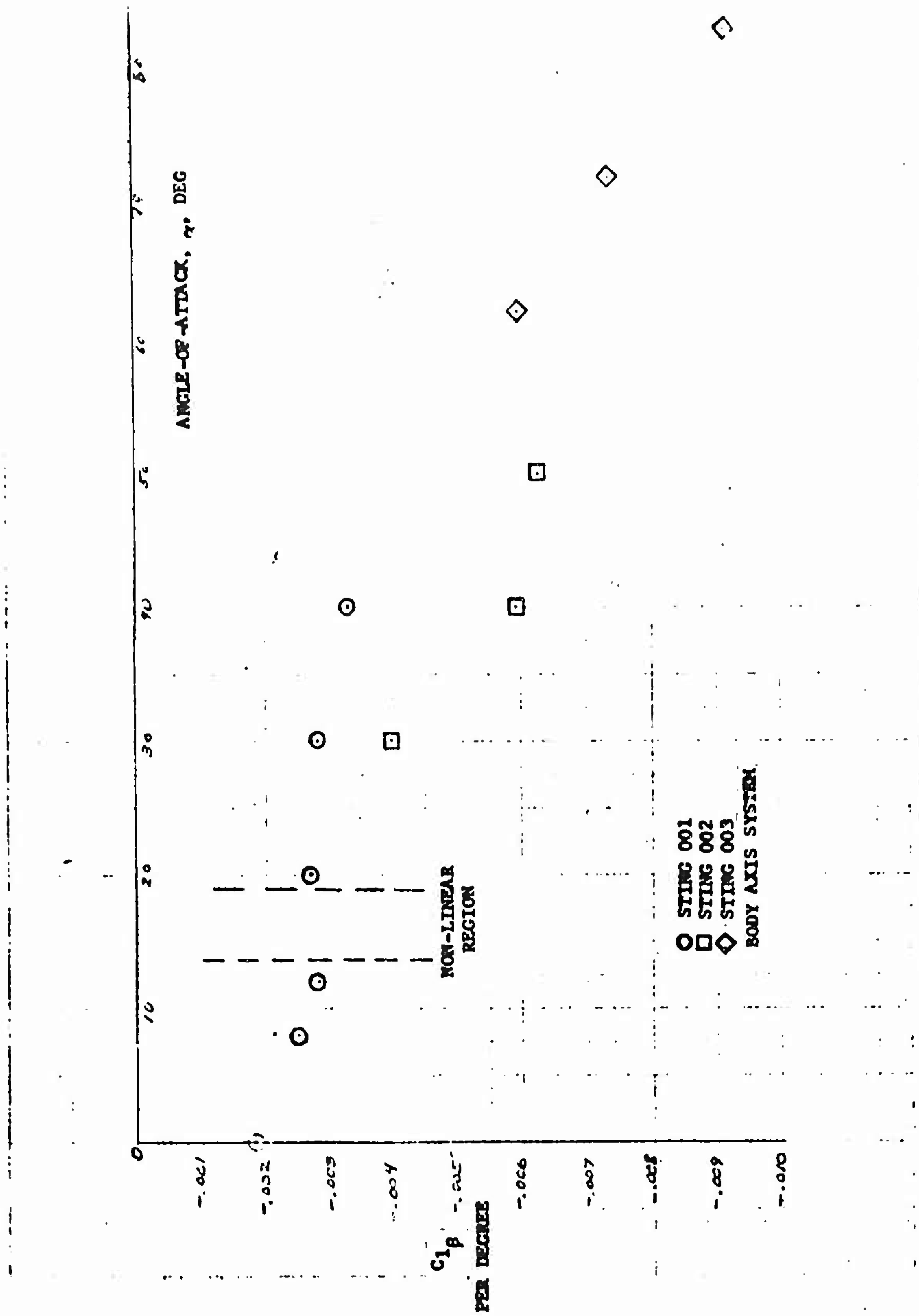

FIGURE 37.. EFFECTIVE DIHEDRAL DERIVATIVE VERSUS ANGLE-OF-ATTACK

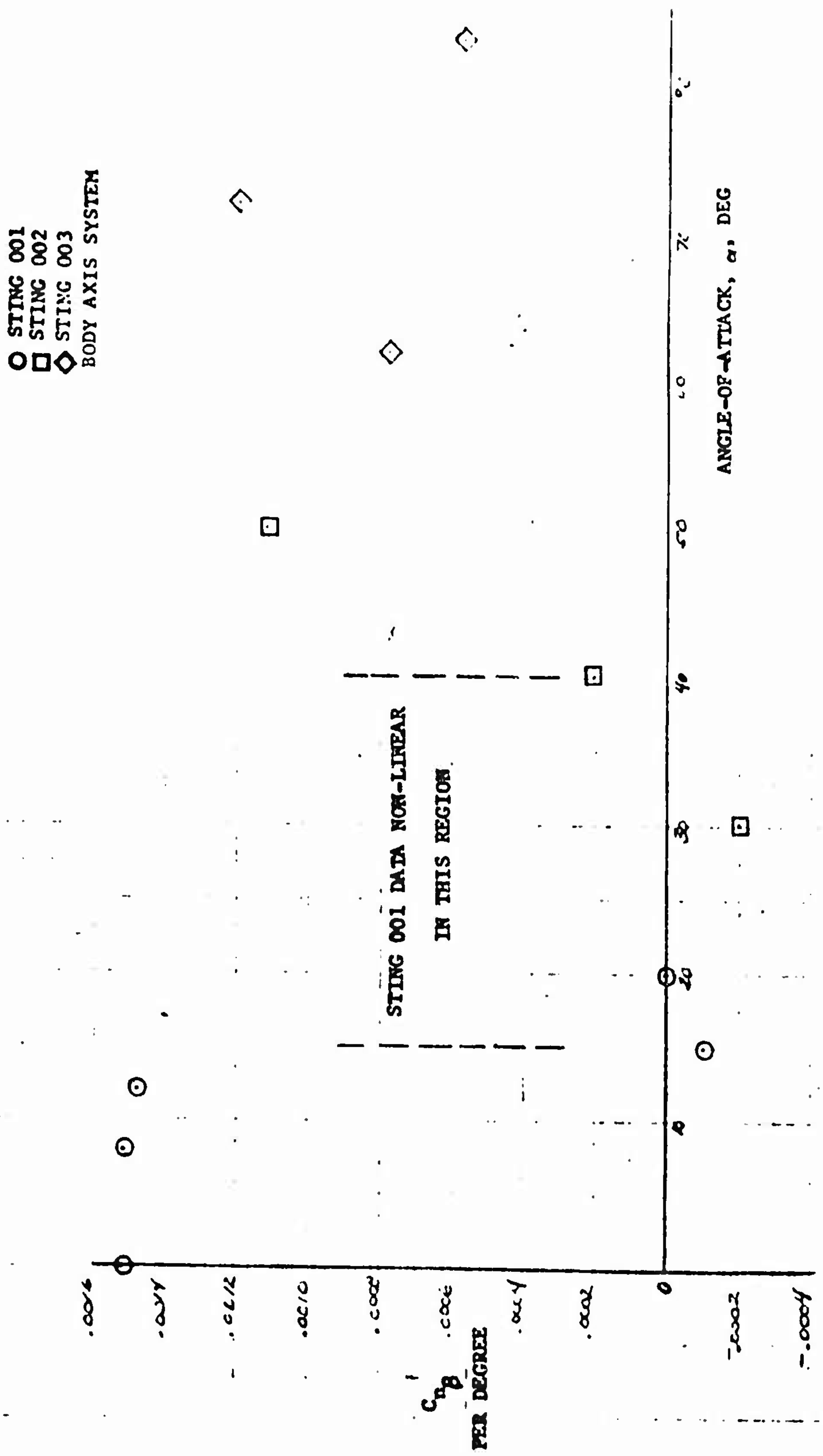

FIGURE 38. STATIC DIRECTIONAL STABILITY DERIVATIVE VERSUS ANGLE-OF-ATTACK

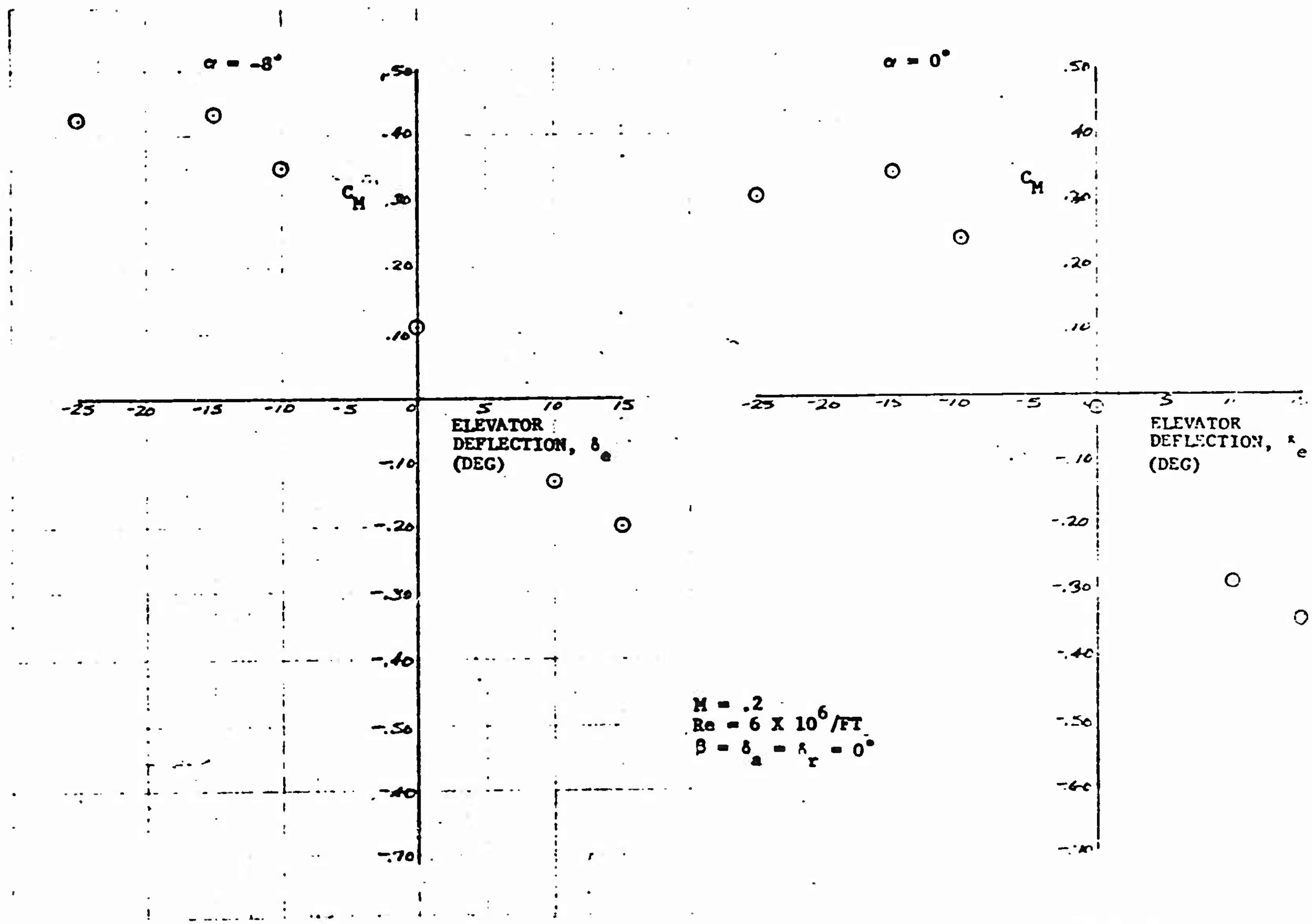

FIGURE 39. COEFFICIENT OF PITCHING MOMENT VERSUS ELEVATOR DEFLECTION FOR VARIOUS ANGLES-OF-ATTACK

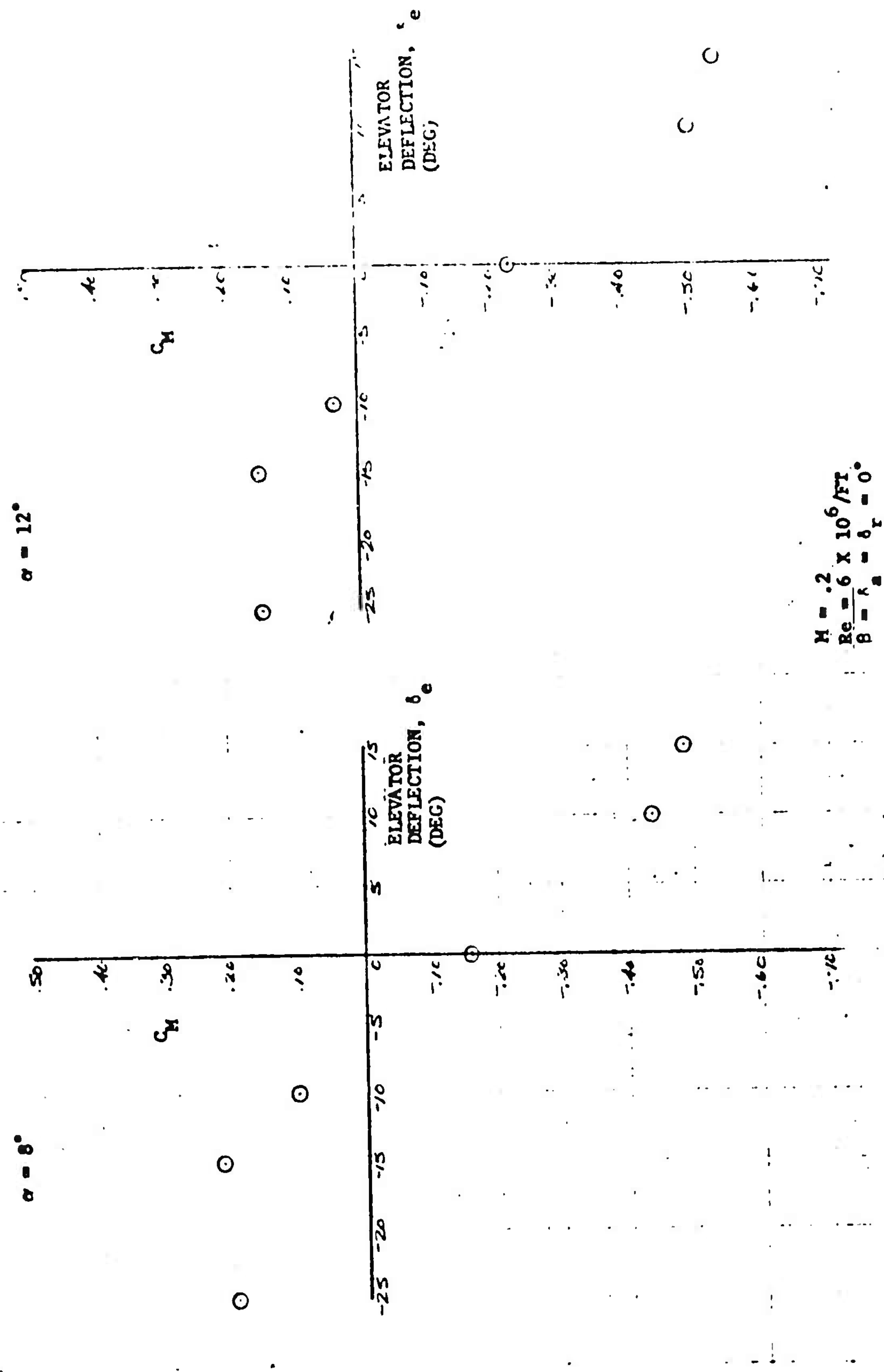

FIGURE 39. COEFFICIENT OF PITCHING MOMENT VERSUS ELEVATOR DEFLECTION FOR VARIOUS ANGLES-OF-ATTACK (CONT)

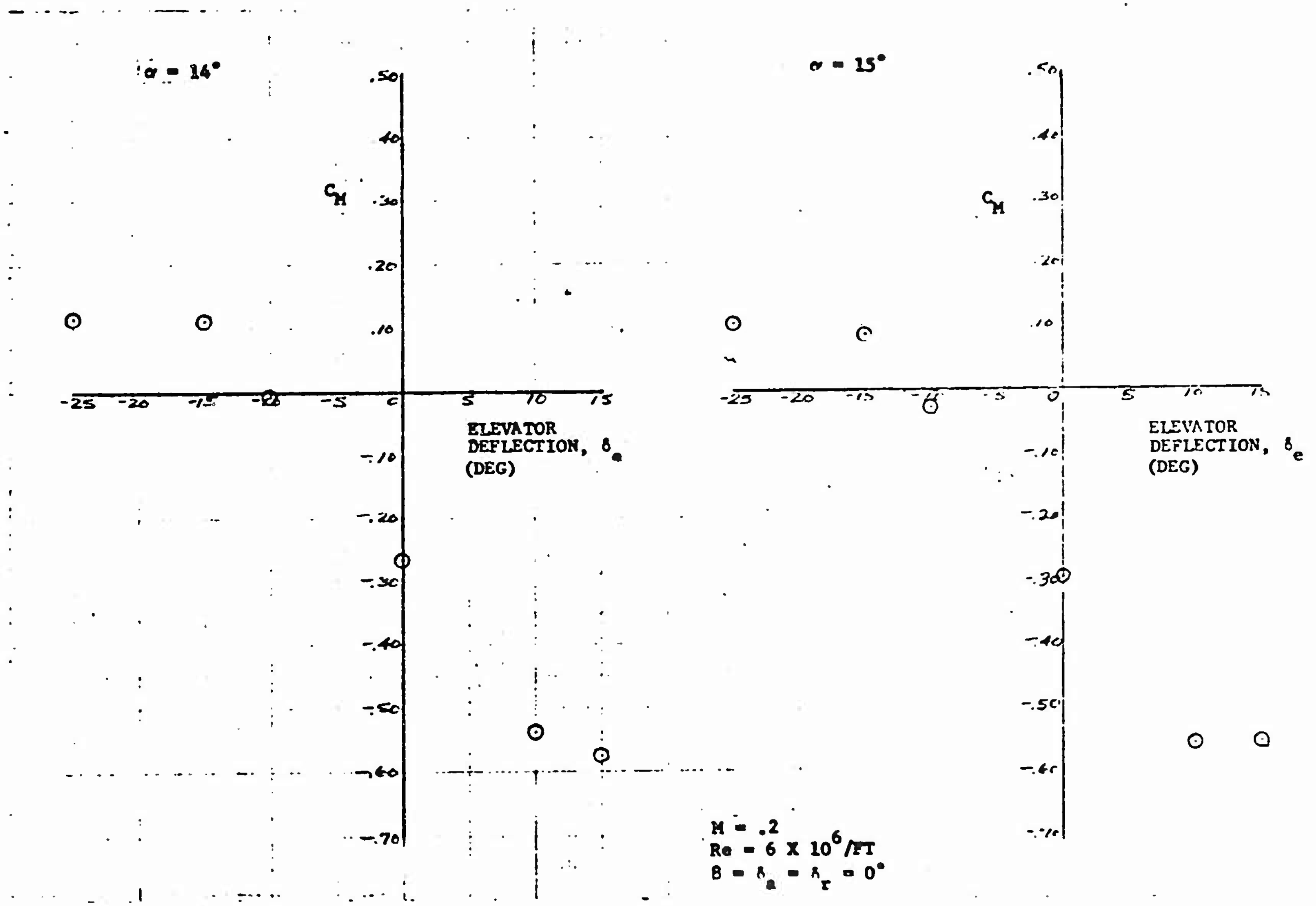

FIGURE 39. COEFFICIENT OF PITCHING MOMENT VERSUS ELEVATOR DEFLECTION FOR VARIOUS ANGLES-OF-ATTACK (CONT)

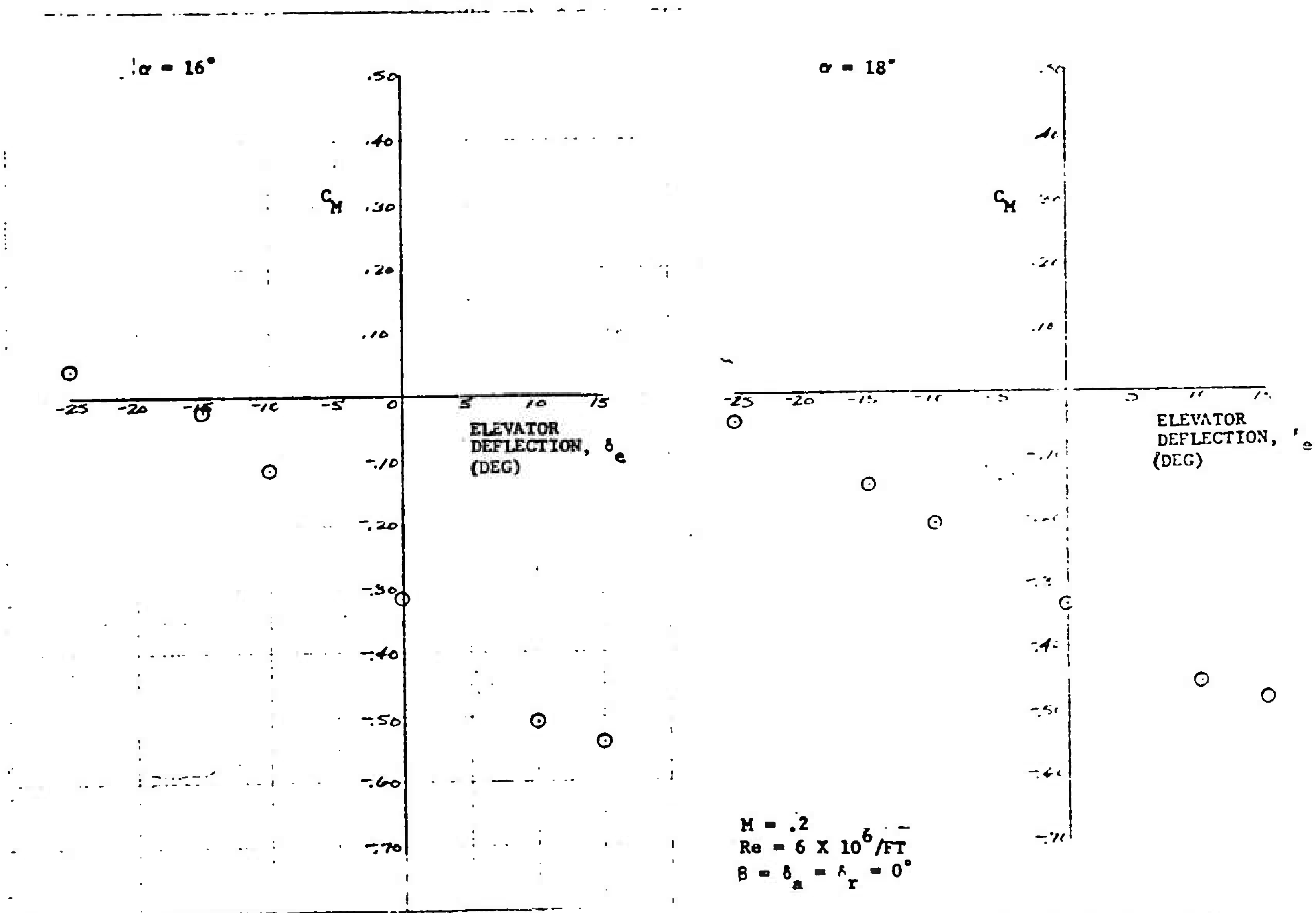

FIGURE 39. COEFFICIENT OF PITCHING MOMENT VERSUS ELEVATOR DEFLECTION FOR VARIOUS ANGLES-OF-ATTACK (CONT)

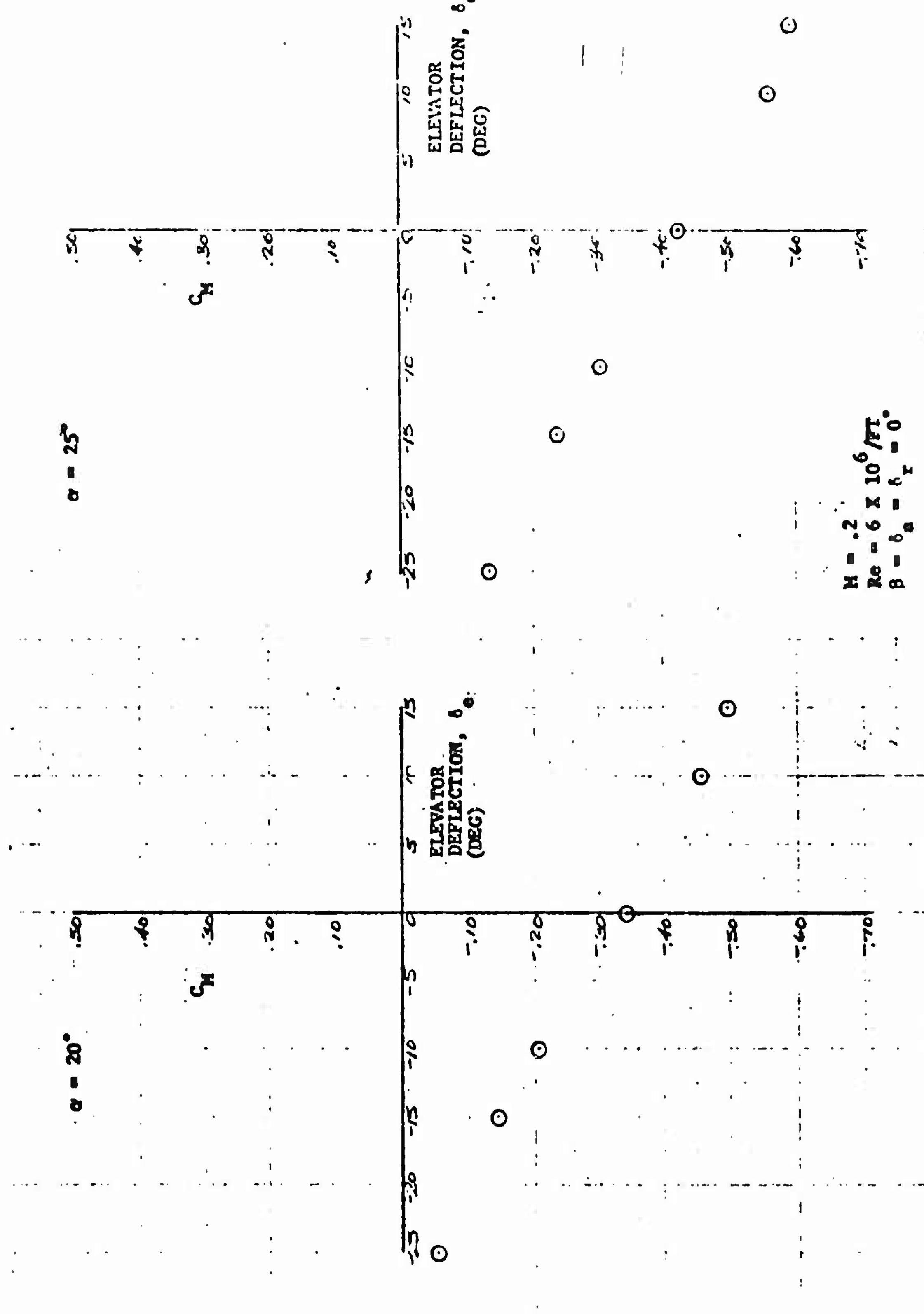

FIGURE 39. COEFFICIENT OF PITCHING MOMENT VERSUS ELEVATOR DEFLECTION FOR VARIOUS ANGLES-OF-ATTACK (CONT)

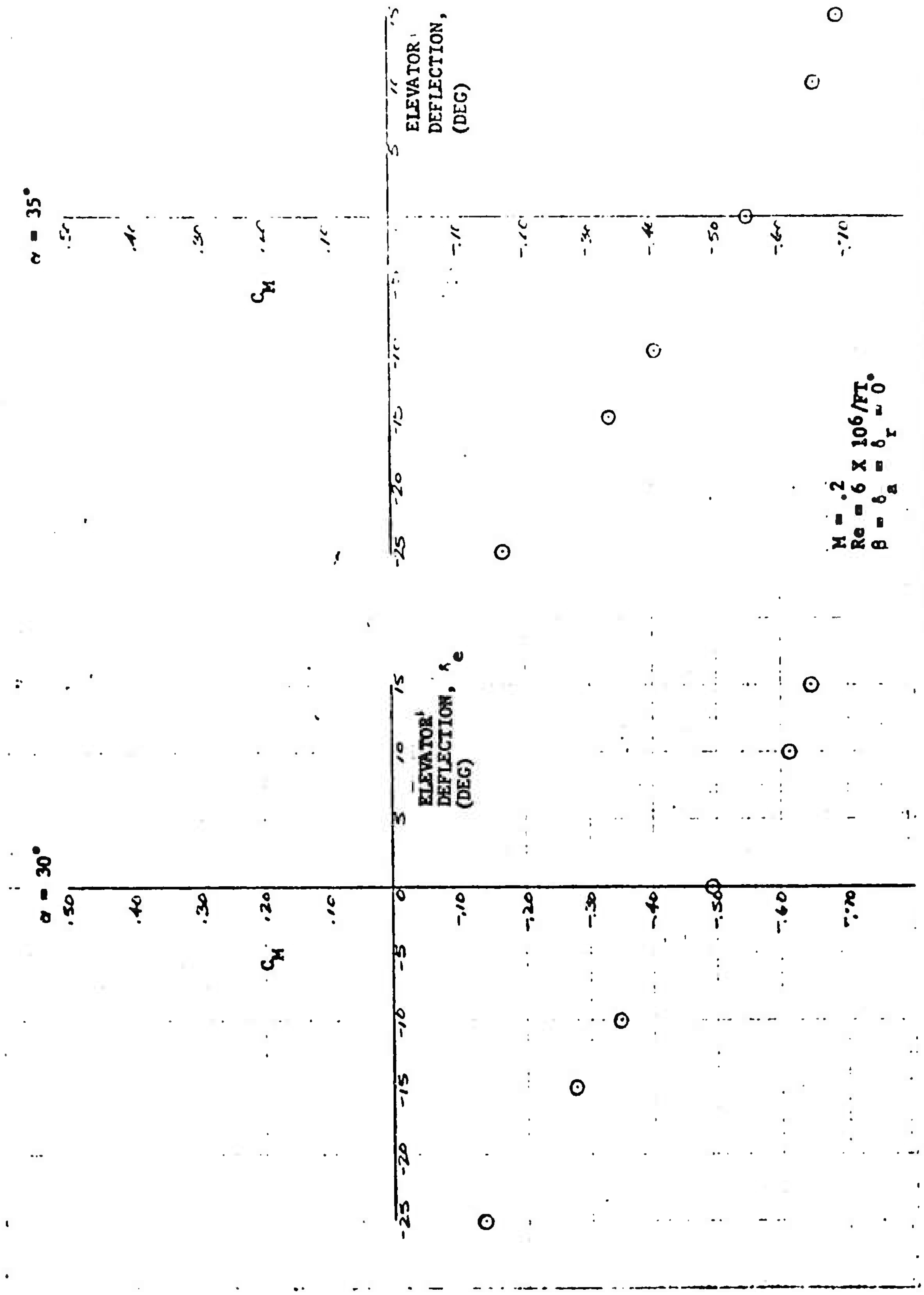

FIGURE 39. COEFFICIENT OF PITCHING MOMENT VERSUS ELEVATOR DEFLECTION FOR VARIOUS ANGLES-OF-ATTACK (CONT)

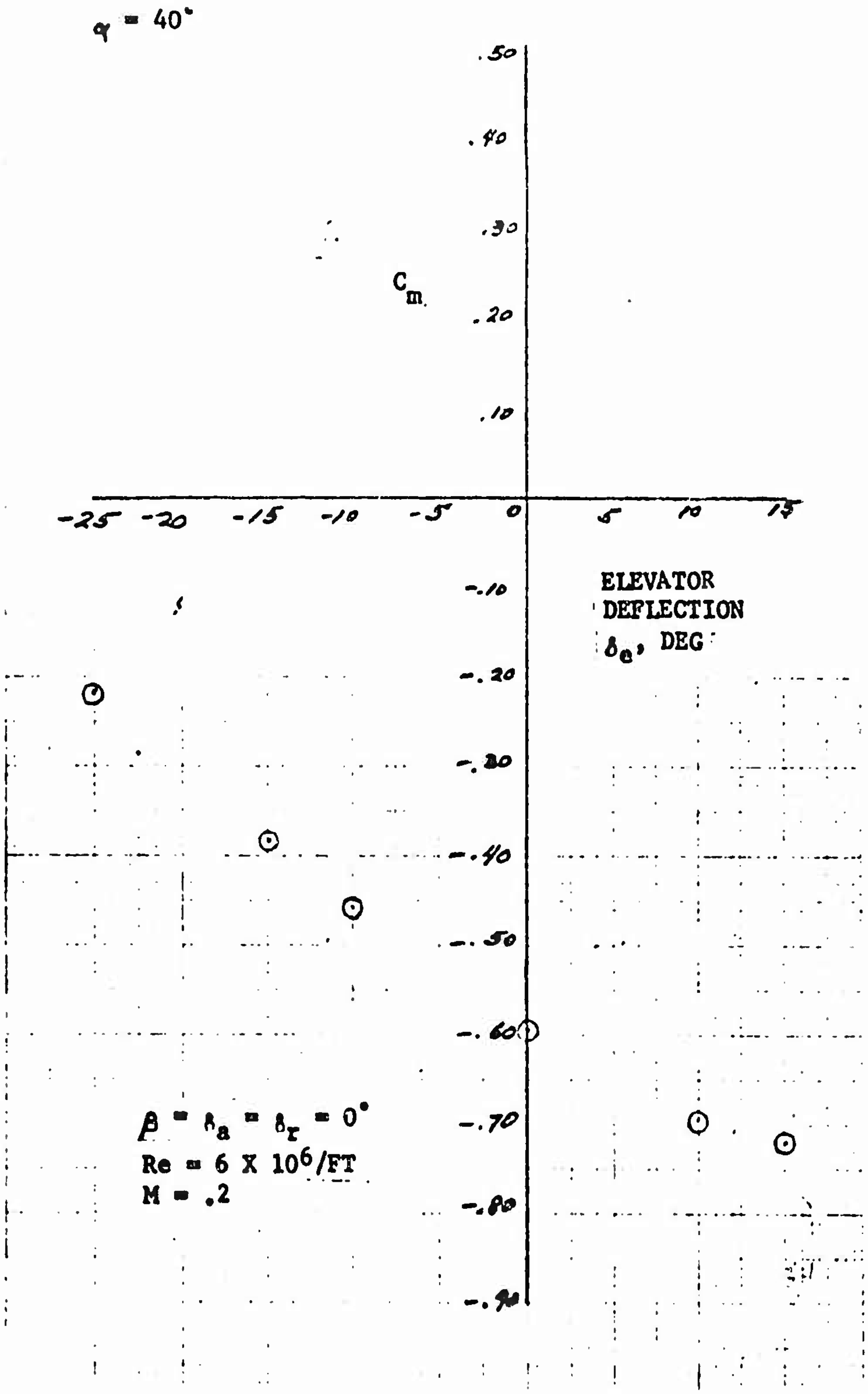

FIGURE 39. COEFFICIENT OF PITCHING MOMENT VERSUS ELEVATOR
(CONT) DEFLECTION FOR VARIOUS ANGLES-OF-ATTACK

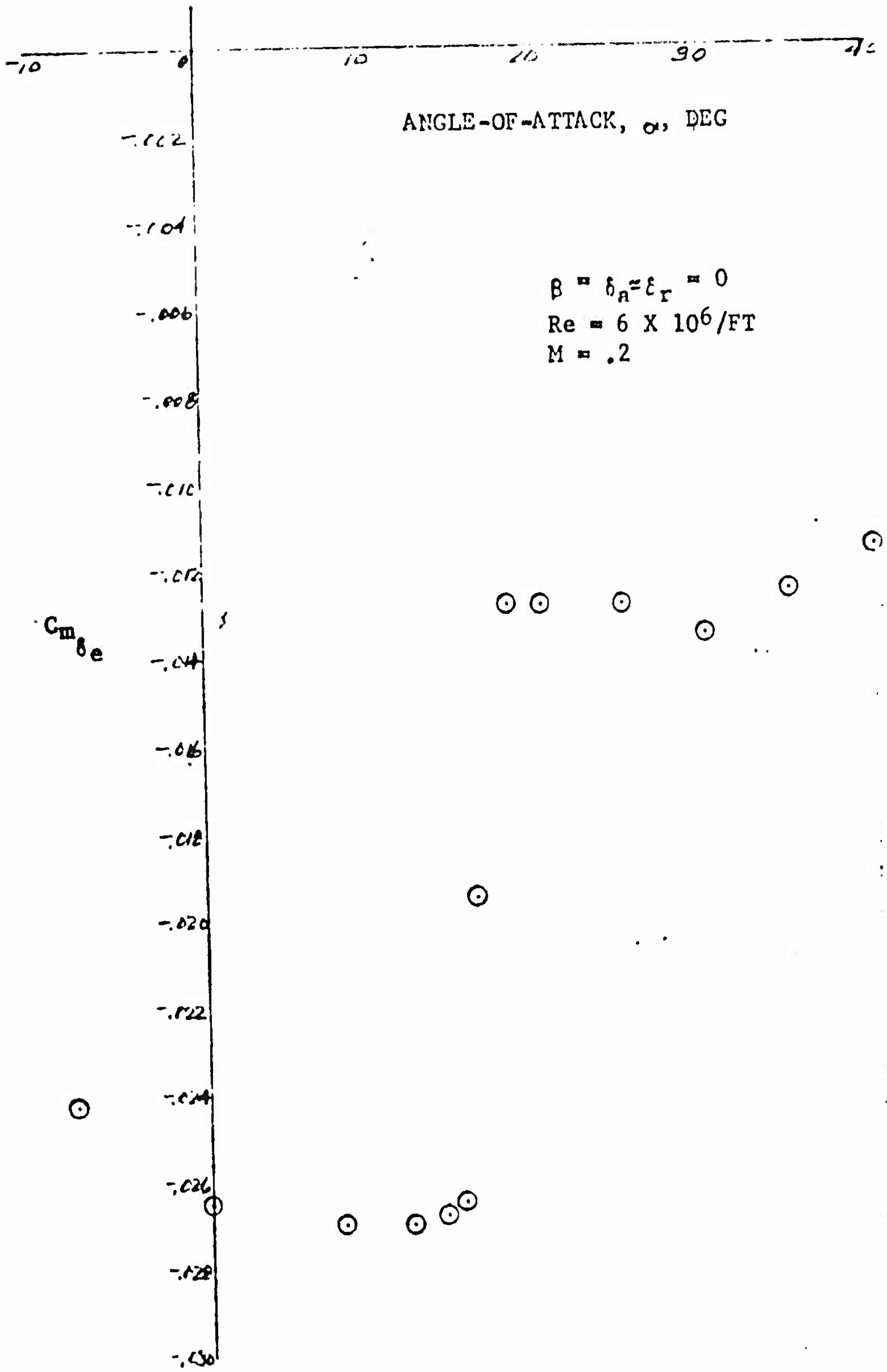

FIGURE 40. ELEVATOR EFFECTIVENESS VERSUS ANGLE-OF-ATTACK

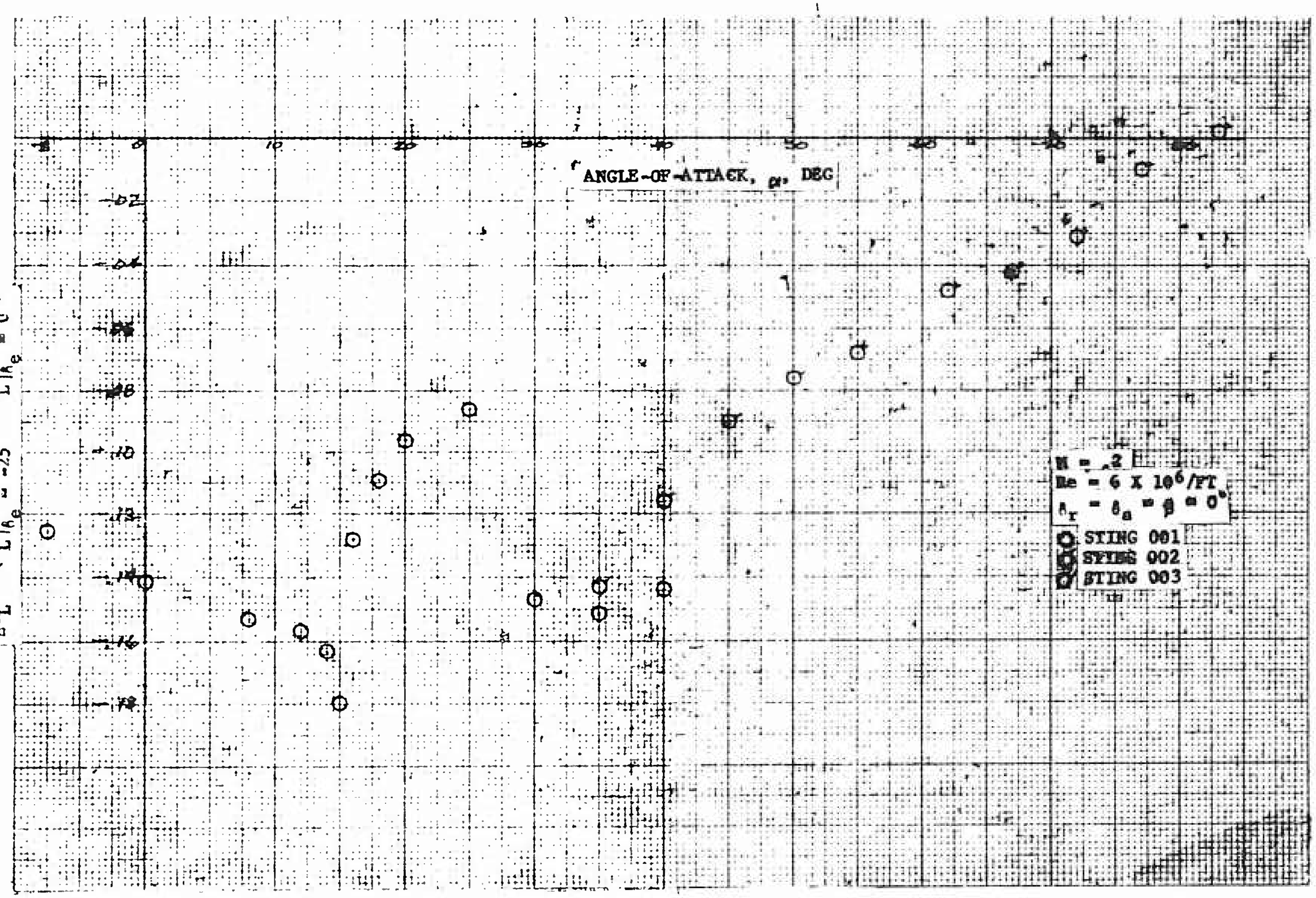

FIGURE 4K. CHANGE IN LIFT COEFFICIENT DUE TO FULL NEGATIVE ELEVATOR DEFLECTION VERSUS ANGLE-OF-ATTACK

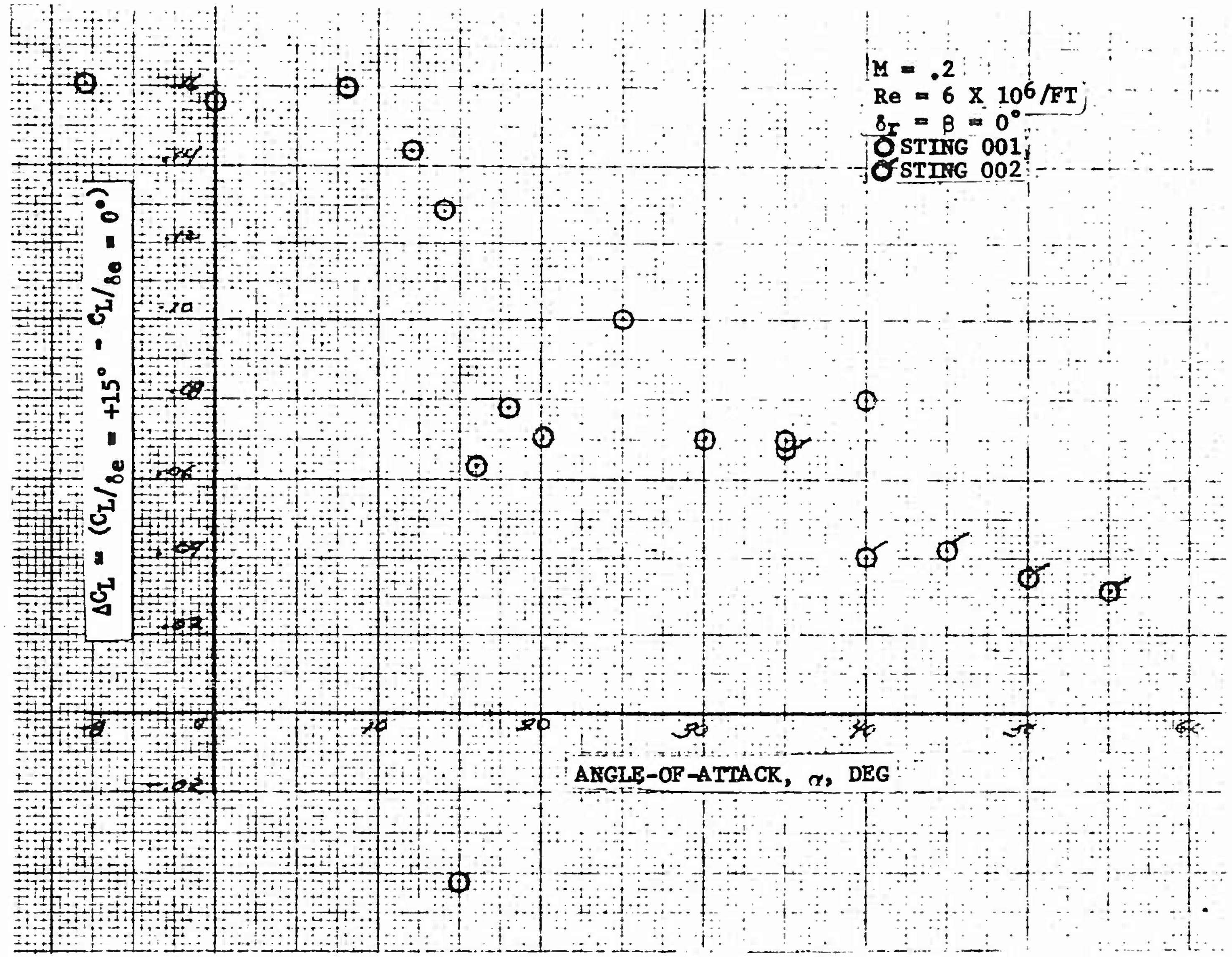

FIGURE 42. CHANGE IN LIFT COEFFICIENT DUE TO FULL POSITIVE ELEVATOR DEFLECTION VERSUS ANGLE-OF-ATTACK

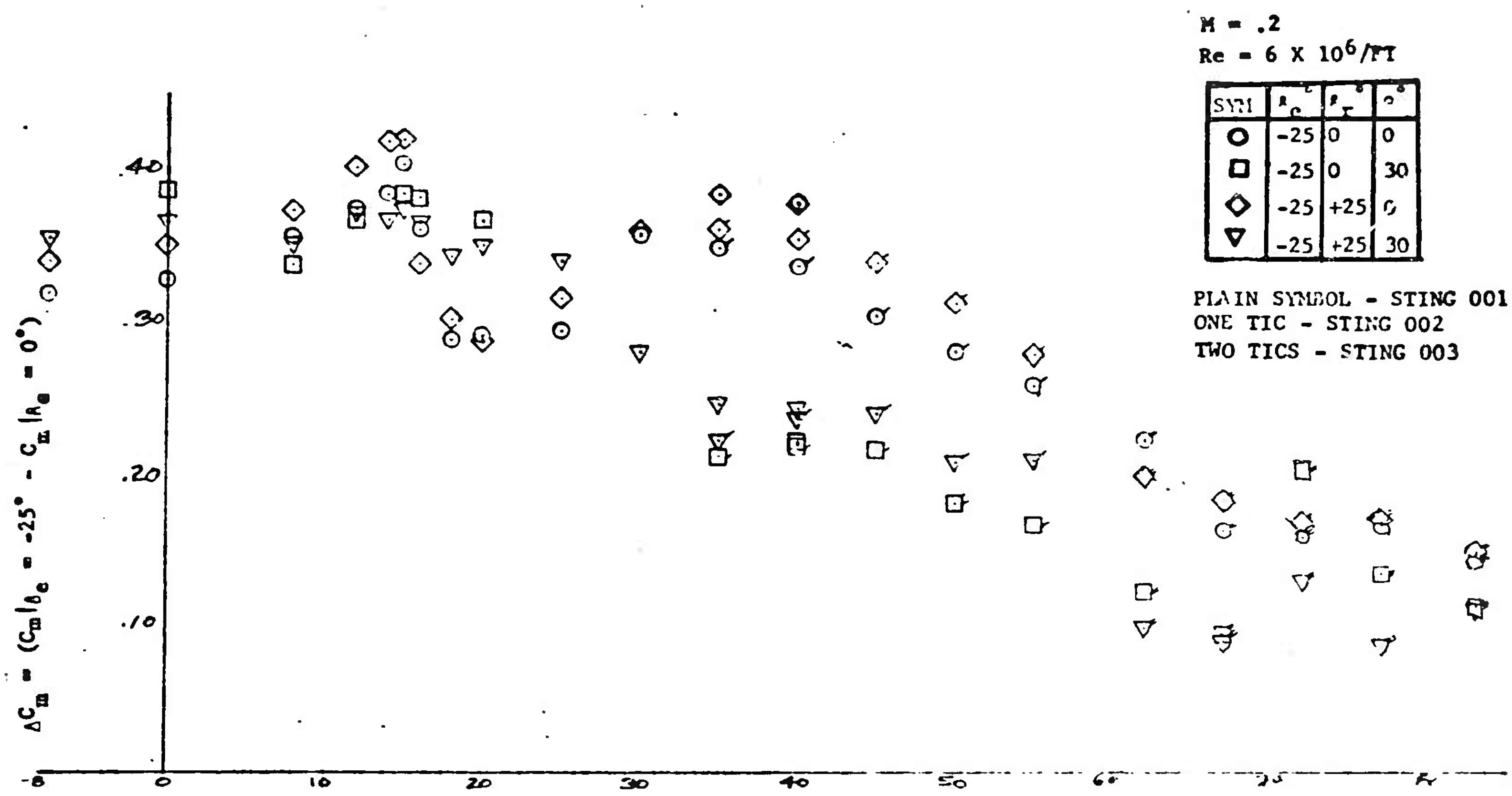

FIGURE 43. CHANGE IN PITCHING MOMENT COEFFICIENT DUE TO FULL NEGATIVE ELEVATOR DEFLECTION VERSUS ANGLE-OF-ATTACK FOR VARIOUS RUDDER DEFLECTIONS AND SIDESLIP ANGLES

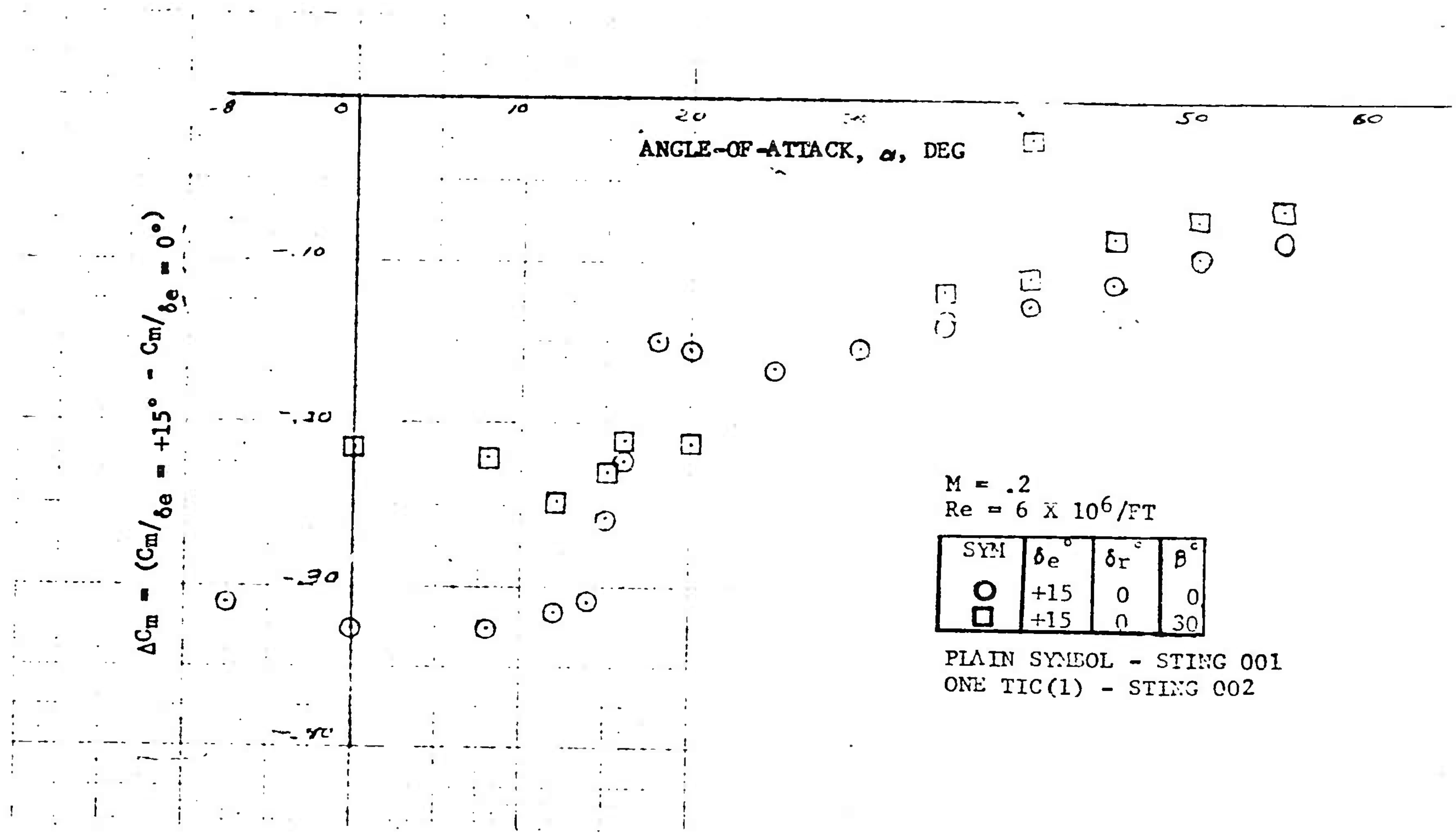

FIGURE 44. CHANGE IN PITCHING MOMENT COEFFICIENT DUE TO FULL POSITIVE ELEVATOR DEFLECTION VERSUS ANGLE-OF-ATTACK FOR TWO SIDESLIP ANGLES

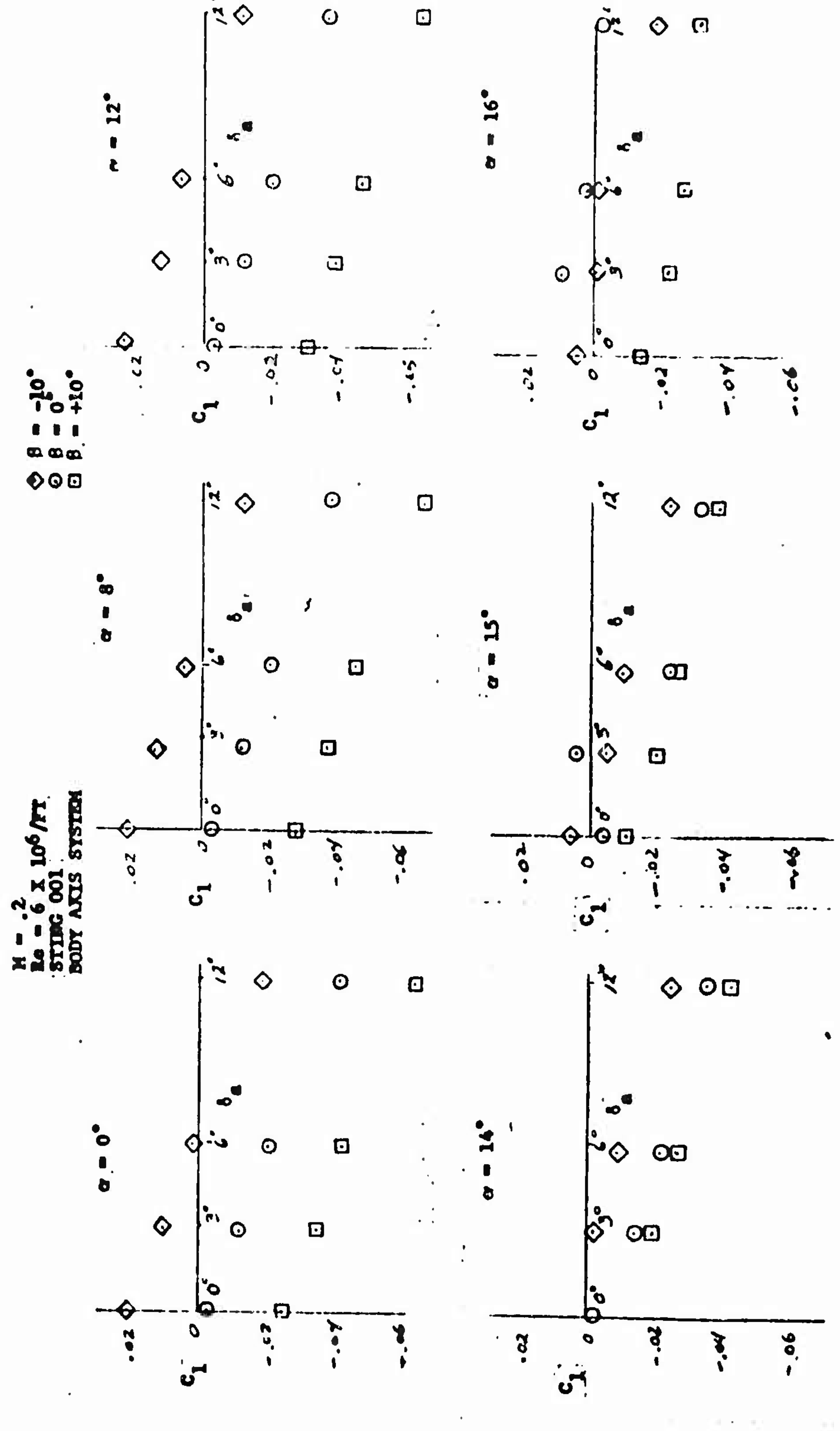

FIGURE 45. ROLLING MOMENT COEFFICIENT VERSUS AILERON DEFLECTION FOR VARIOUS ANGLES-OF-ATTACK (AT THREE SIDESLIP ANGLES)

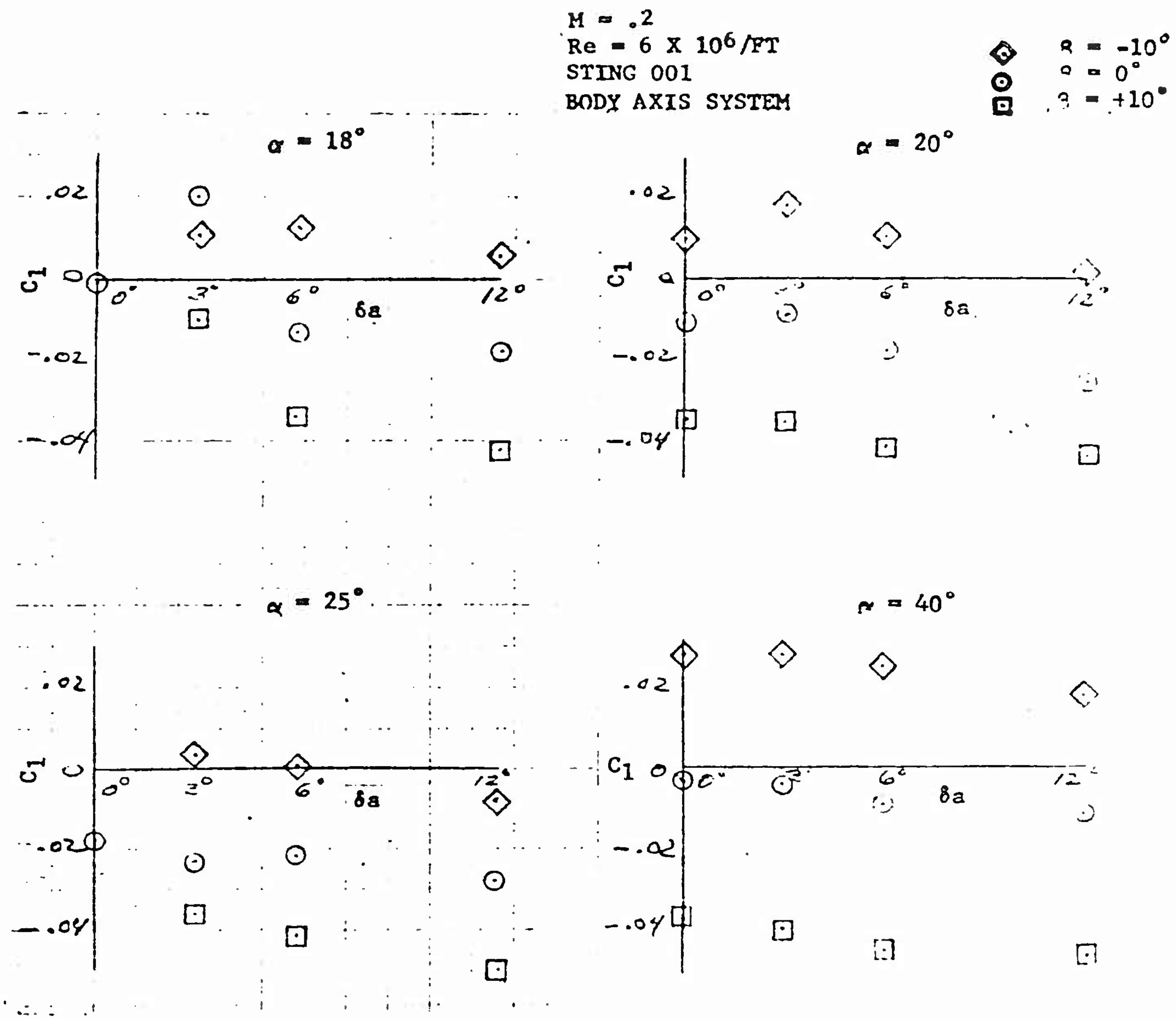

FIGURE 45. ROLLING MOMENT COEFFICIENT VERSUS AILERON DEFLECTION FOR VARIOUS ANGLES-OF-ATTACK (AT THREE SIDESLIP ANGLES) (CONT.)
(CONT.)

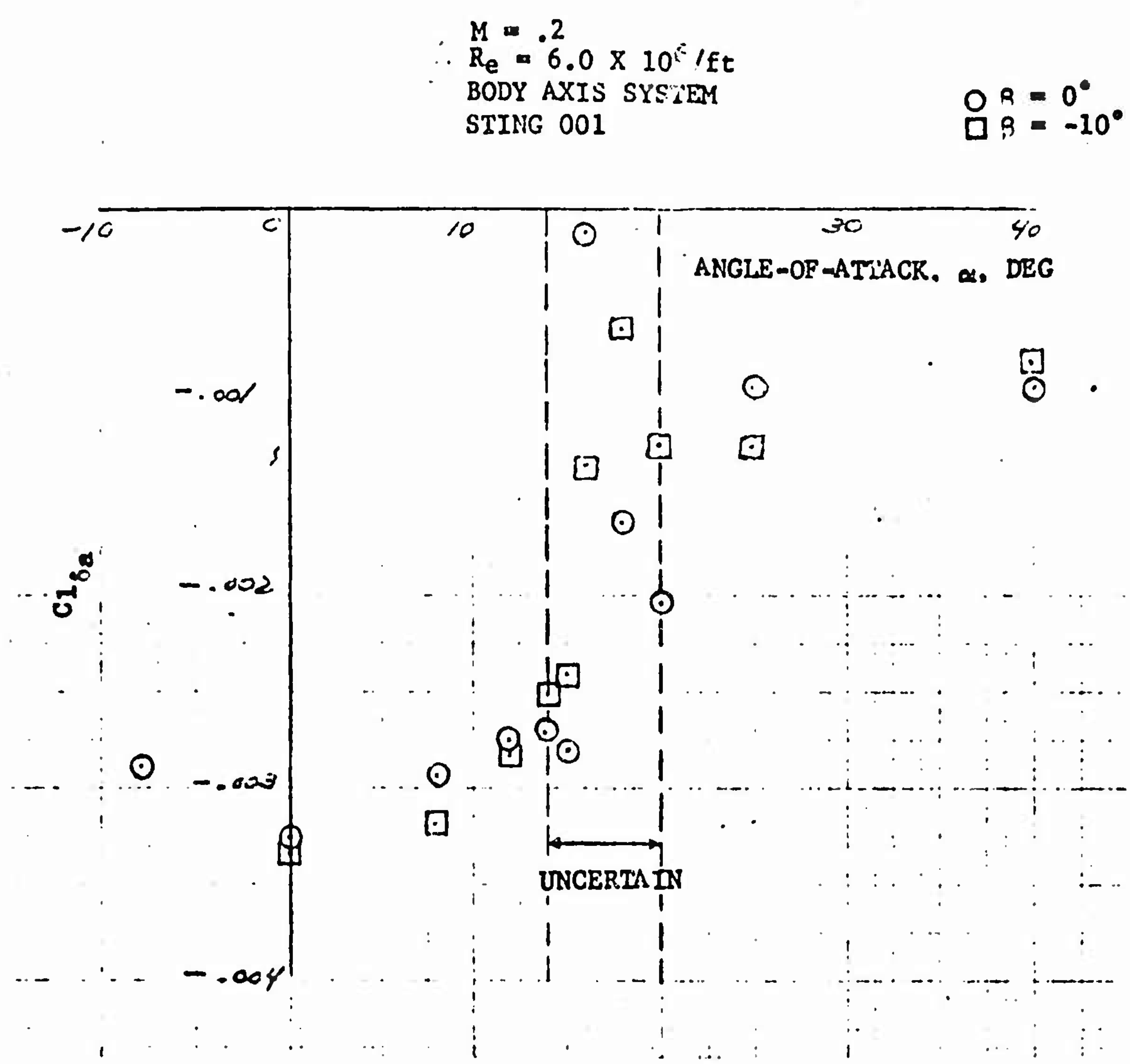

FIGURE 46. AILERON EFFECTIVENESS VERSUS ANGLE-OF-ATTACK
(FOR TWO SIDESLIP ANGLES)

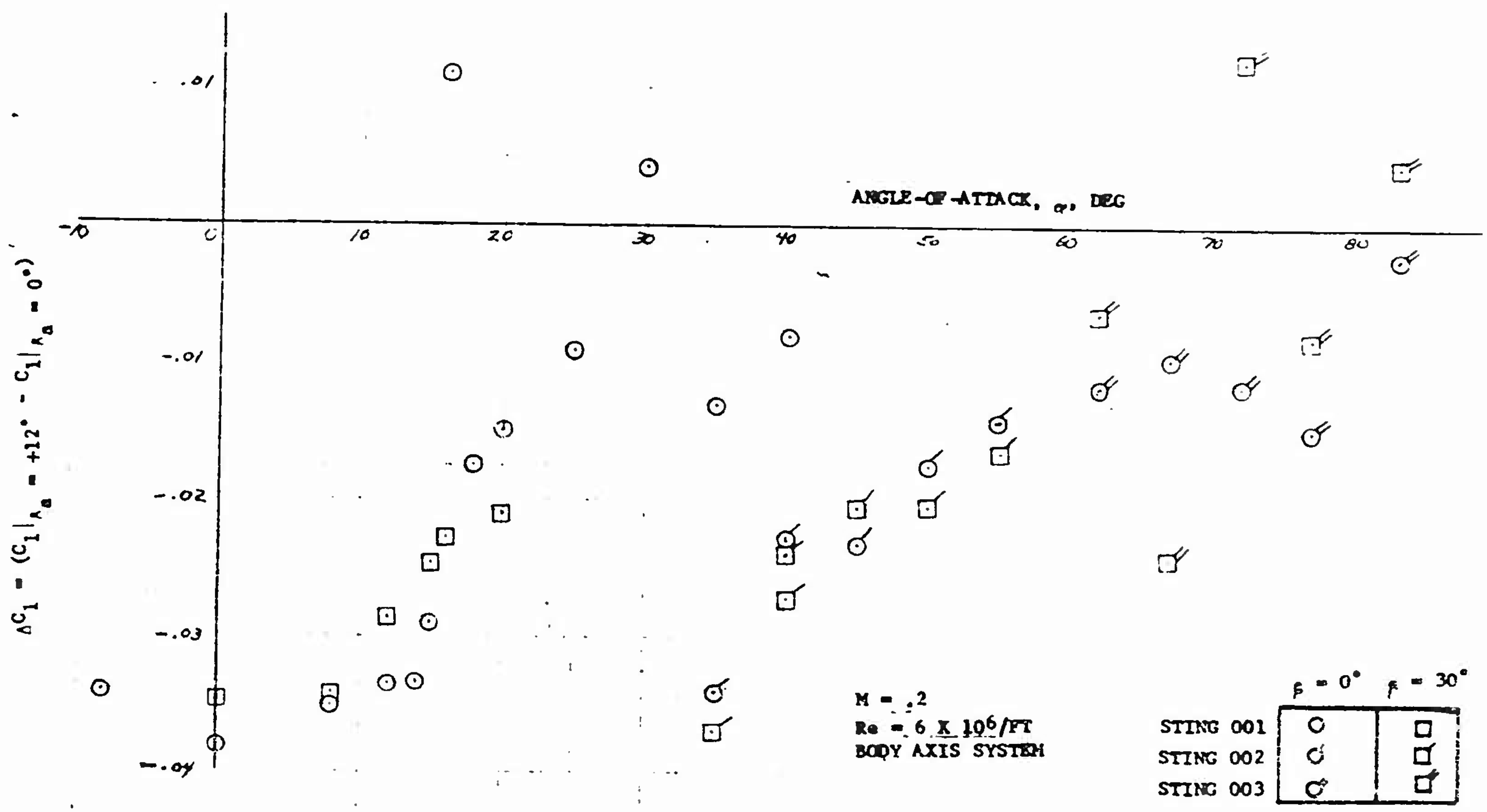

FIGURE 47.. CHANGE IN ROLLING MOMENT COEFFICIENT DUE TO FULL POSITIVE AILERON DEFLECTION VERSUS ANGLE-OF-ATTACK (FOR TWO SIDESLIP ANGLES)

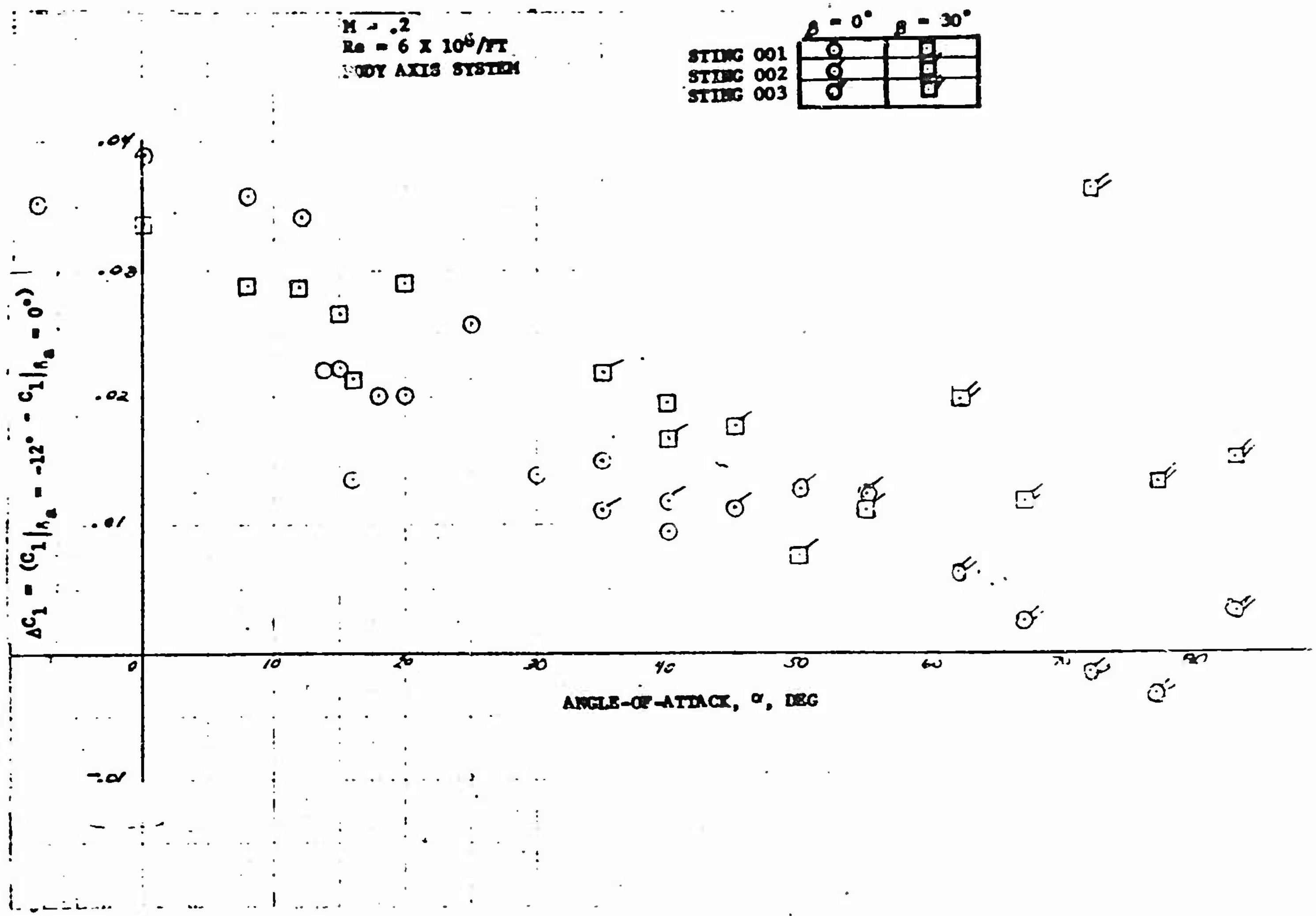

FIGURE 48. CHANGE IN ROLLING MOMENT COEFFICIENT DUE TO FULL NEGATIVE AILERON DEFLECTION VERSUS ANGLE-OF-ATTACK (FOR TWO SIDESLIP ANGLES)

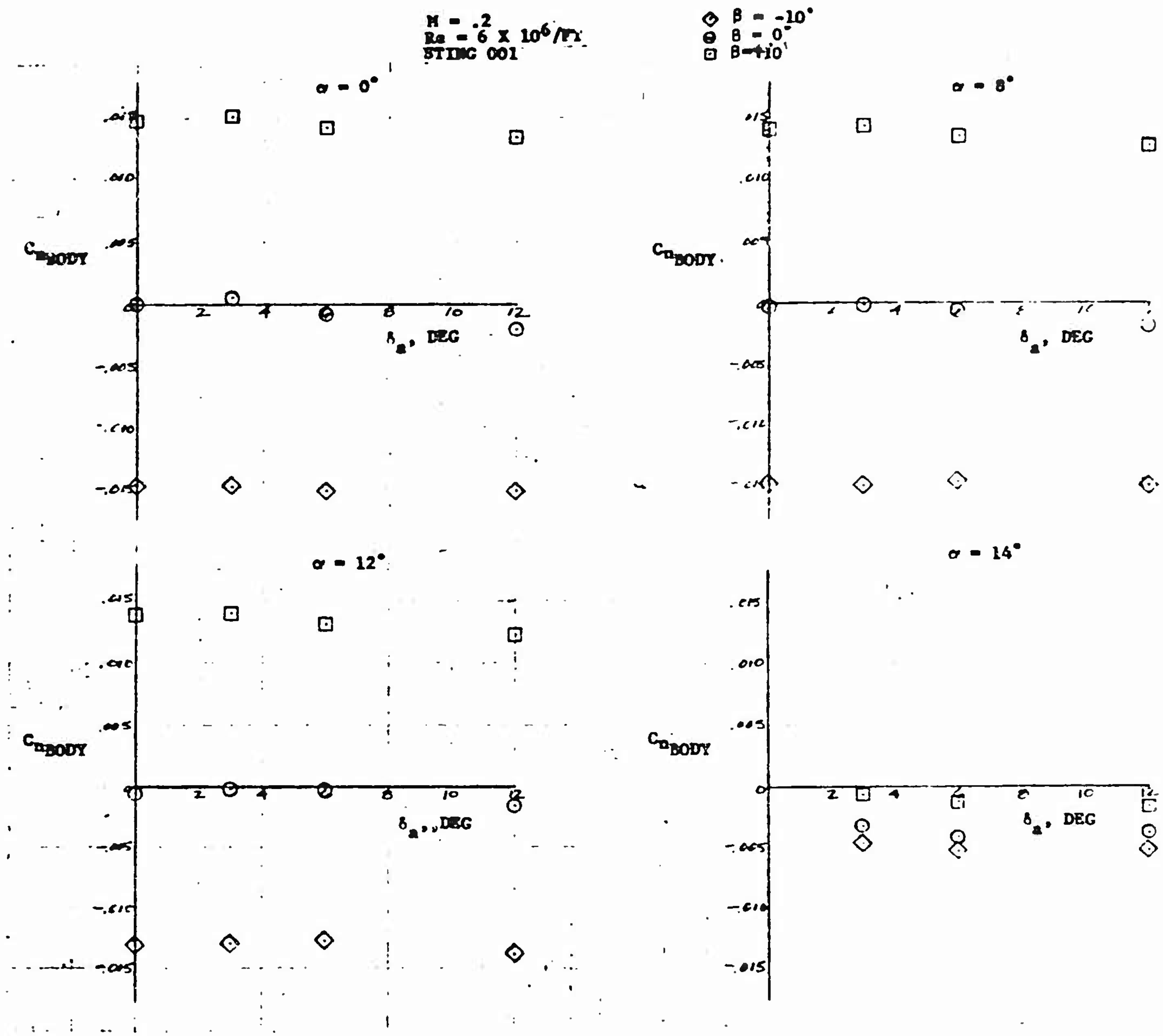

FIGURE 49. YAWING MOMENT COEFFICIENT VERSUS AILERON DEFLECTION FOR VARIOUS ANGLES-OF-ATTACK (AT THREE SIDESLIP ANGLES)

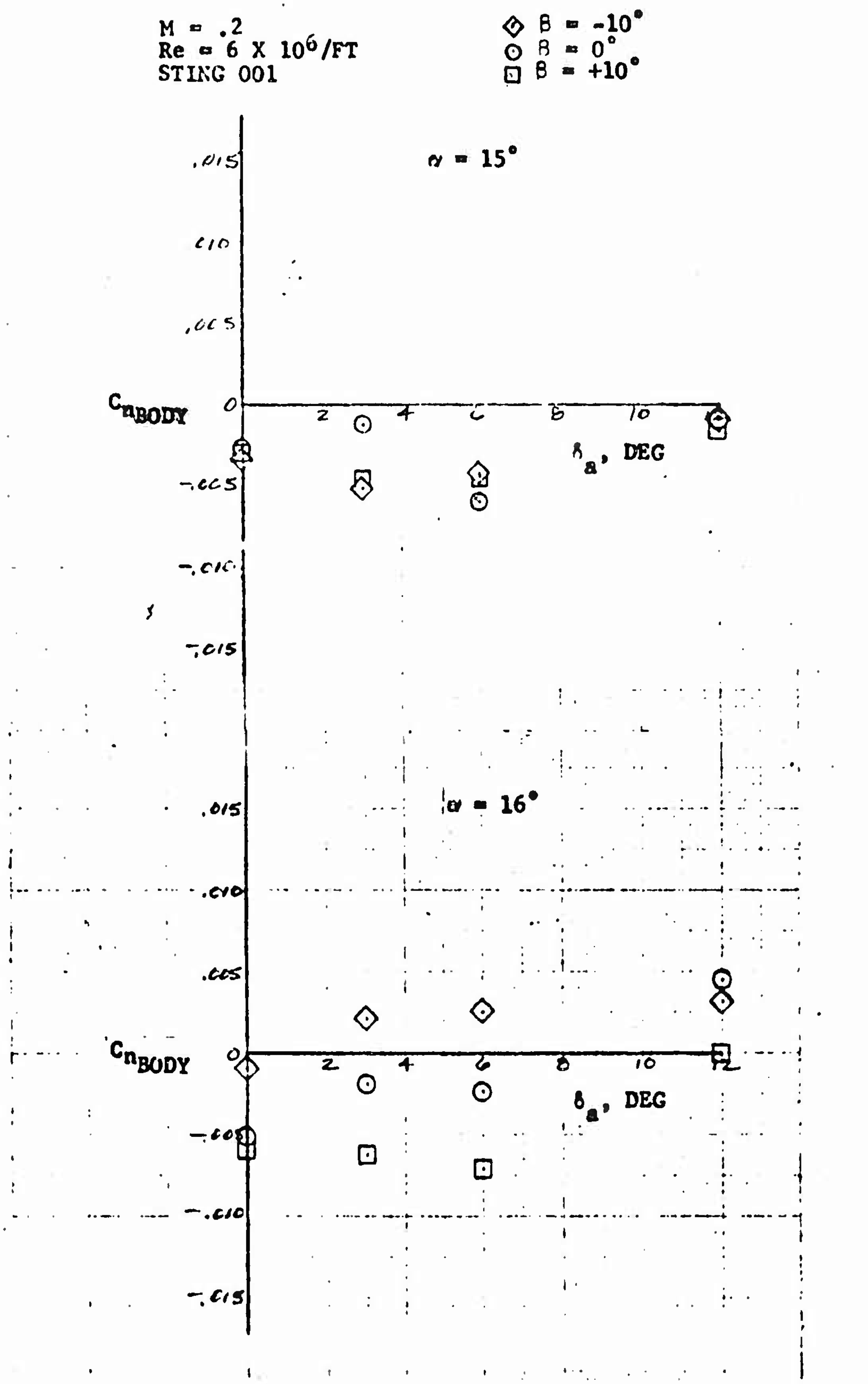

FIGURE 49. YAWING MOMENT COEFFICIENT VERSUS AILERON DEFLECTION (CONT) FOR VARIOUS ANGLES-OF-ATTACK (AT THREE SIDESLIP ANGLES)

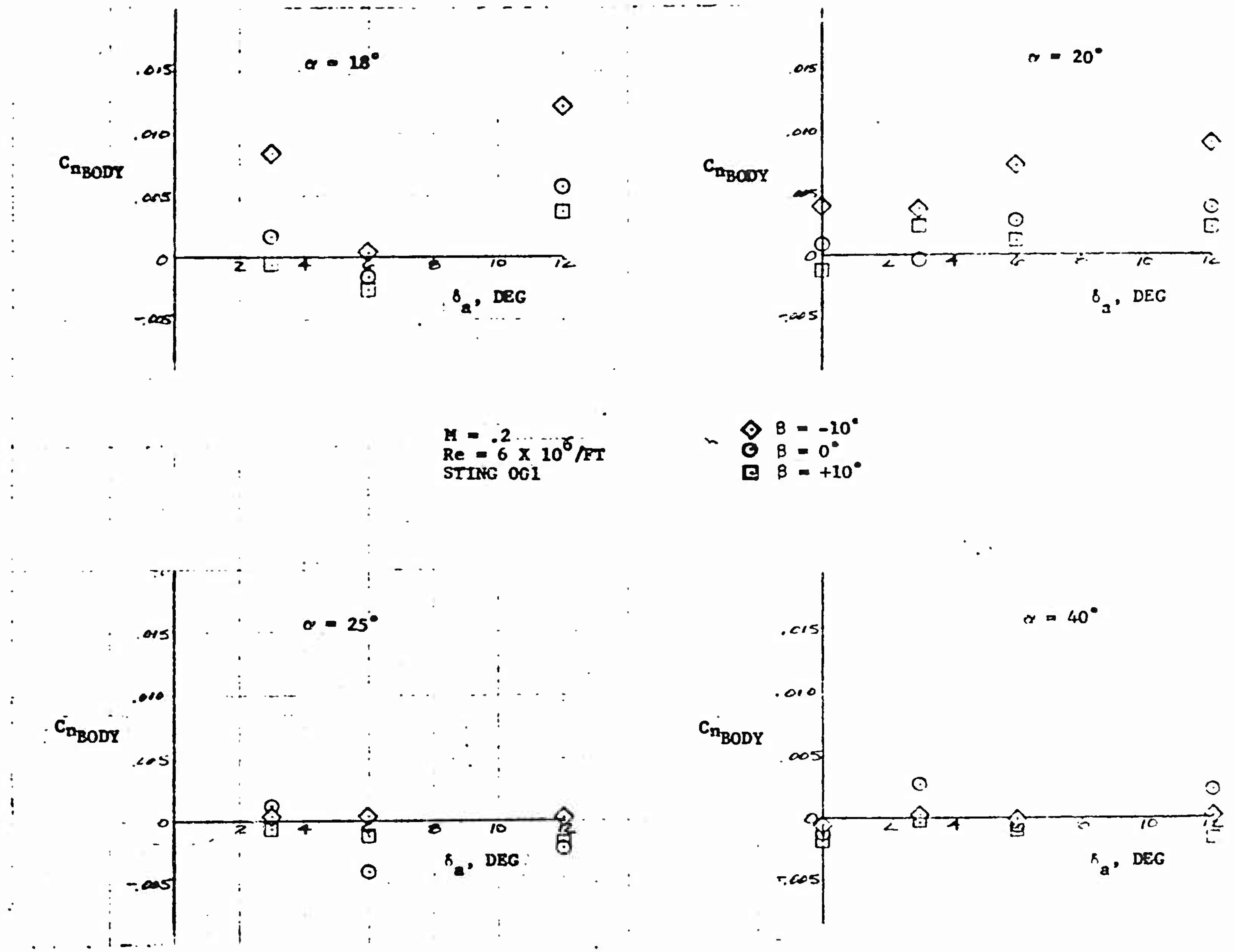

FIGURE 49. YAWING MOMENT COEFFICIENT VERSUS AILERON DEFLECTION FOR VARIOUS ANGLES-OF-ATTACK (CONT) (AT THREE SIDESLIP ANGLES)

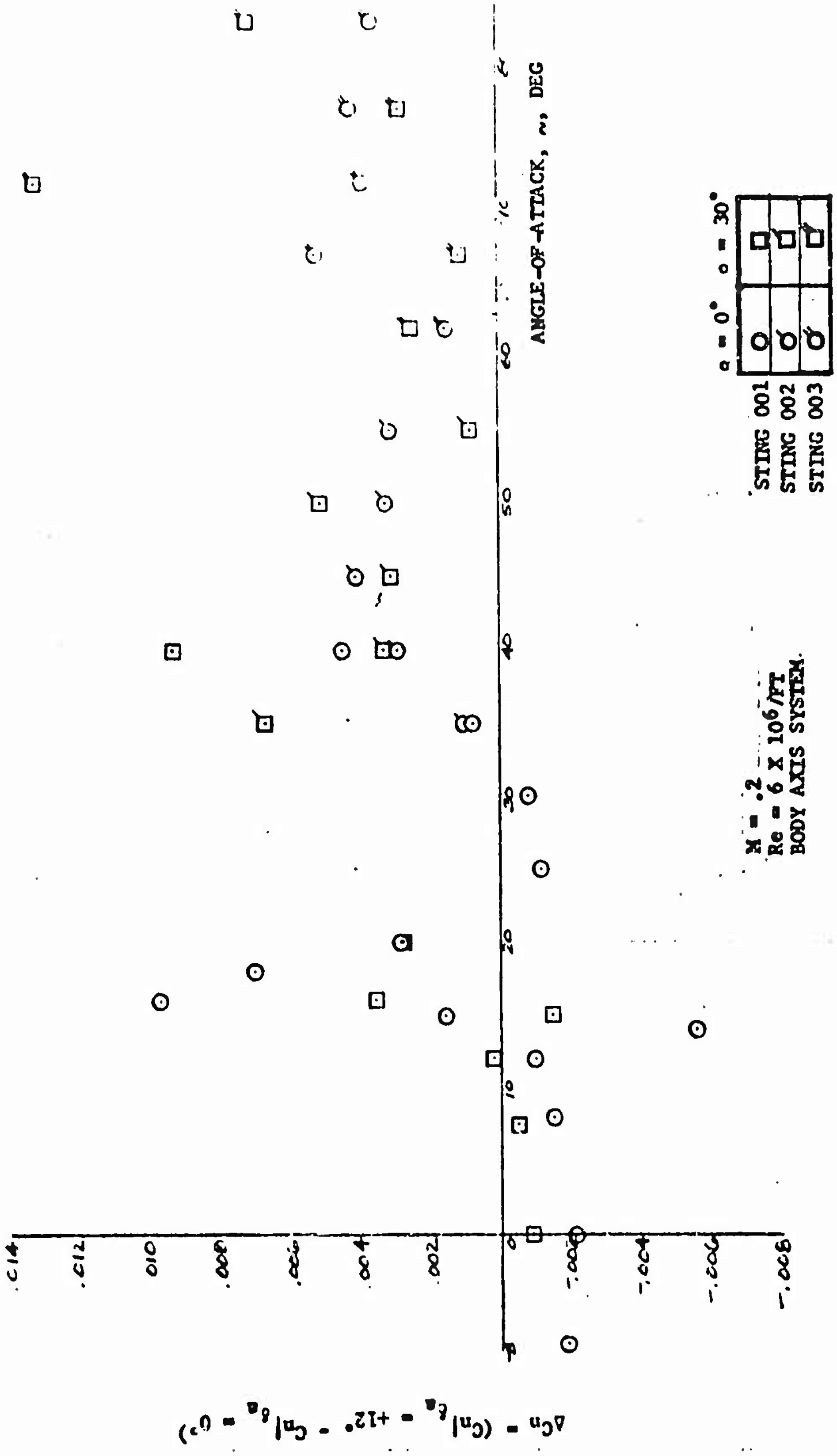

FIGURE 50. CHANGE IN YAWING MOMENT COEFFICIENT DUE TO FULL POSITIVE AILERON DEFLECTION VERSUS ANGLE-OF-ATTACK (FOR TWO SIDESLIP ANGLES)

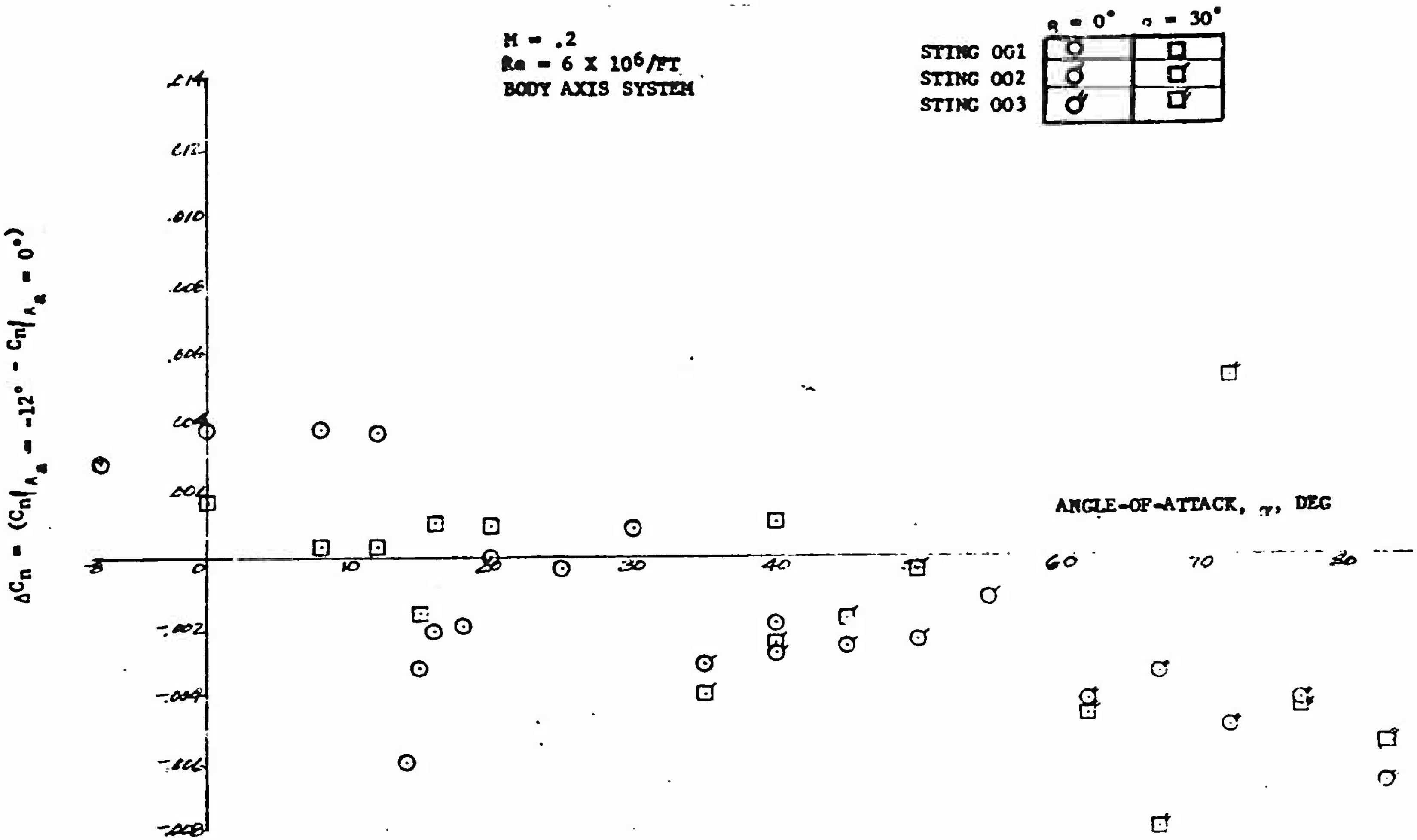

FIGURE 51. CHANGE IN YAWING MOMENT COEFFICIENT DUE TO FULL NEGATIVE AILERON DEFLECTION VERSUS ANGLE-OF-ATTACK (FOR TWO SIDESLIP ANGLES)

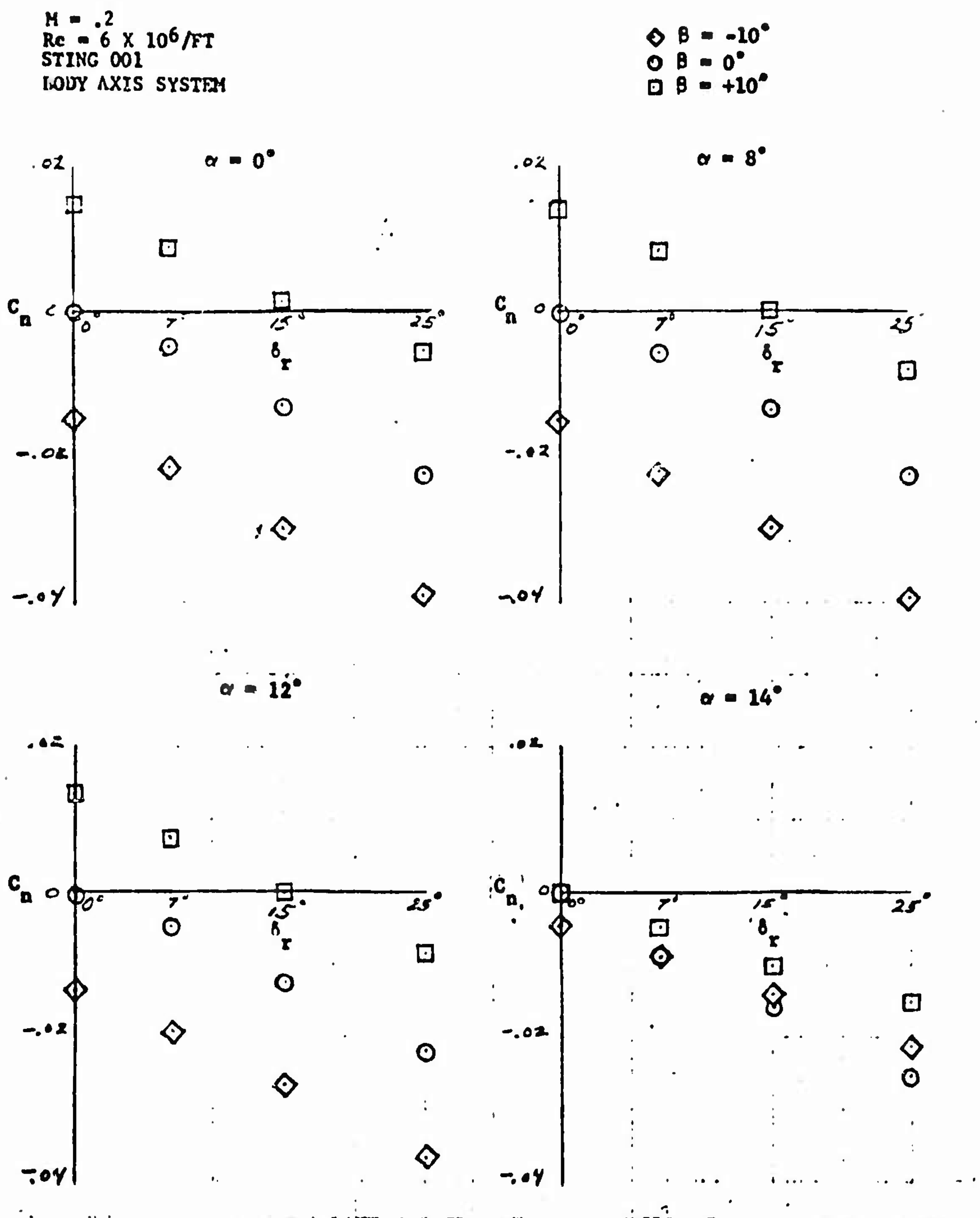

FIGURE 52. YAWING MOMENT COEFFICIENT VERSUS RUDDER DEFLECTION FOR VARIOUS ANGLES-OF-ATTACK (FOR THREE SIDESLIP ANGLES)

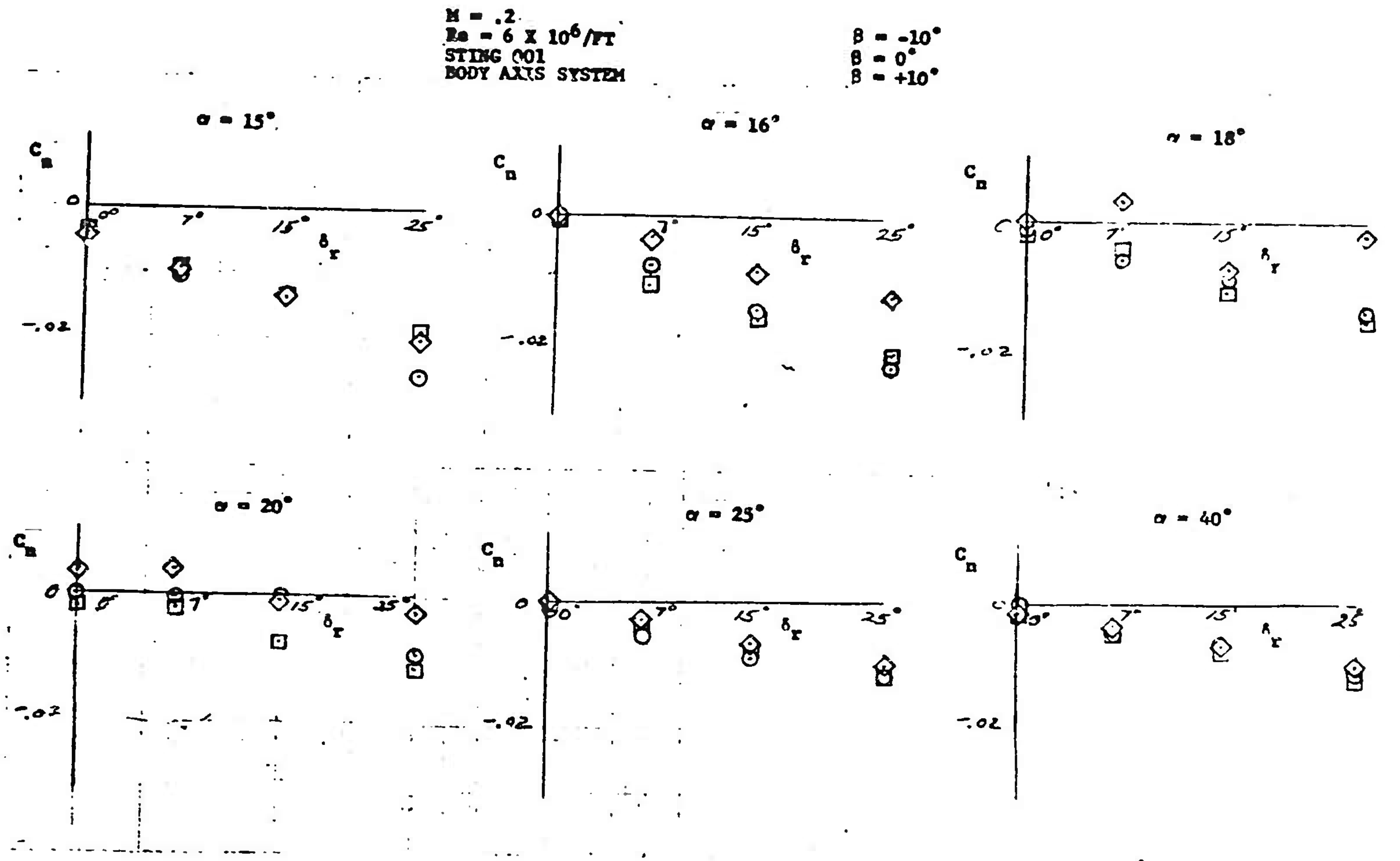

FIGURE 52. YAWING MOMENT COEFFICIENT VERSUS RUDDER DEFLECTION FOR VARIOUS ANGLES-OF-ATTACK
(CONT.) (FOR THREE SIDESLIP ANGLES)

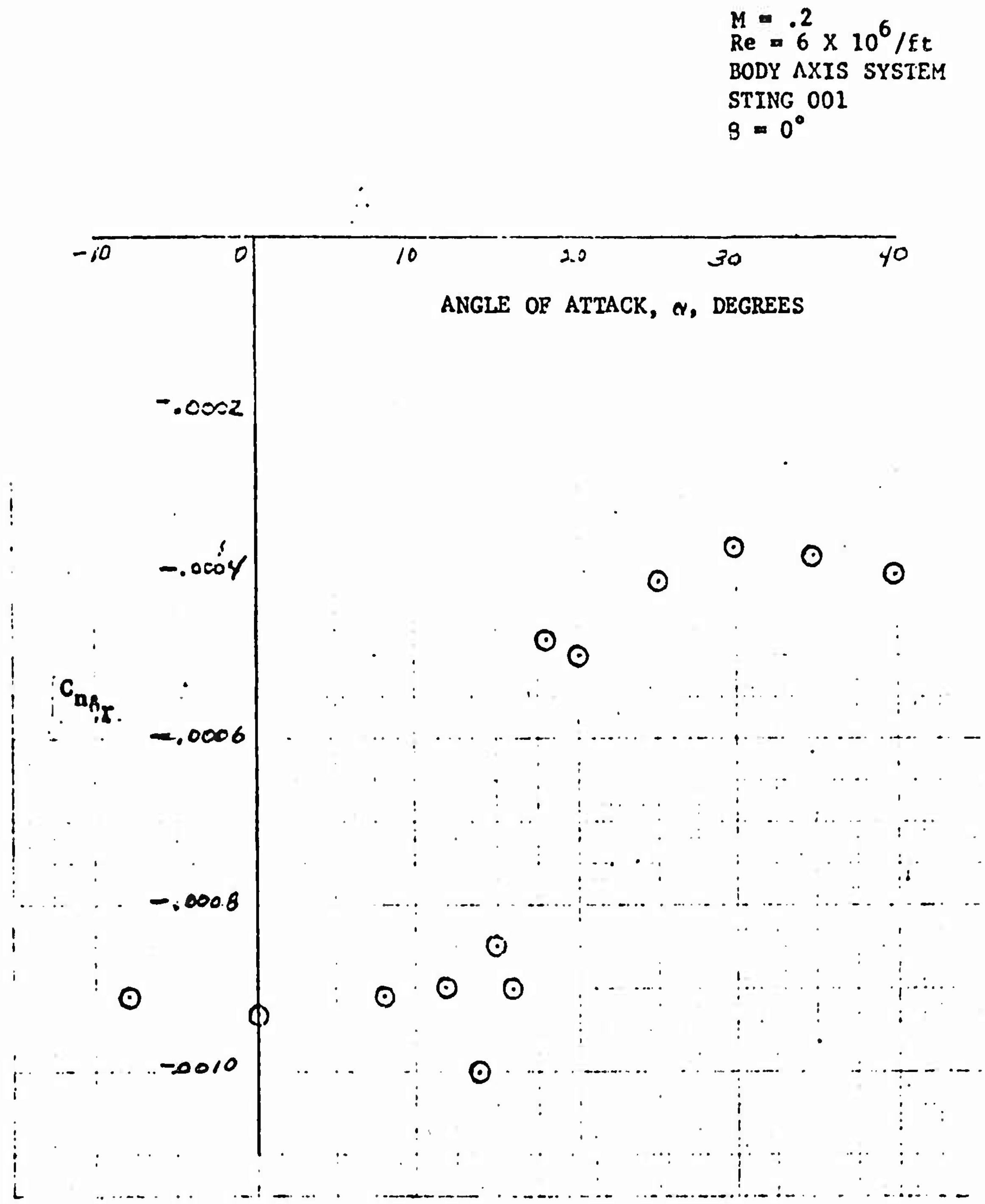

FIGURE 53. RUDDER EFFECTIVENESS VERSUS ANGLE-OF-ATTACK

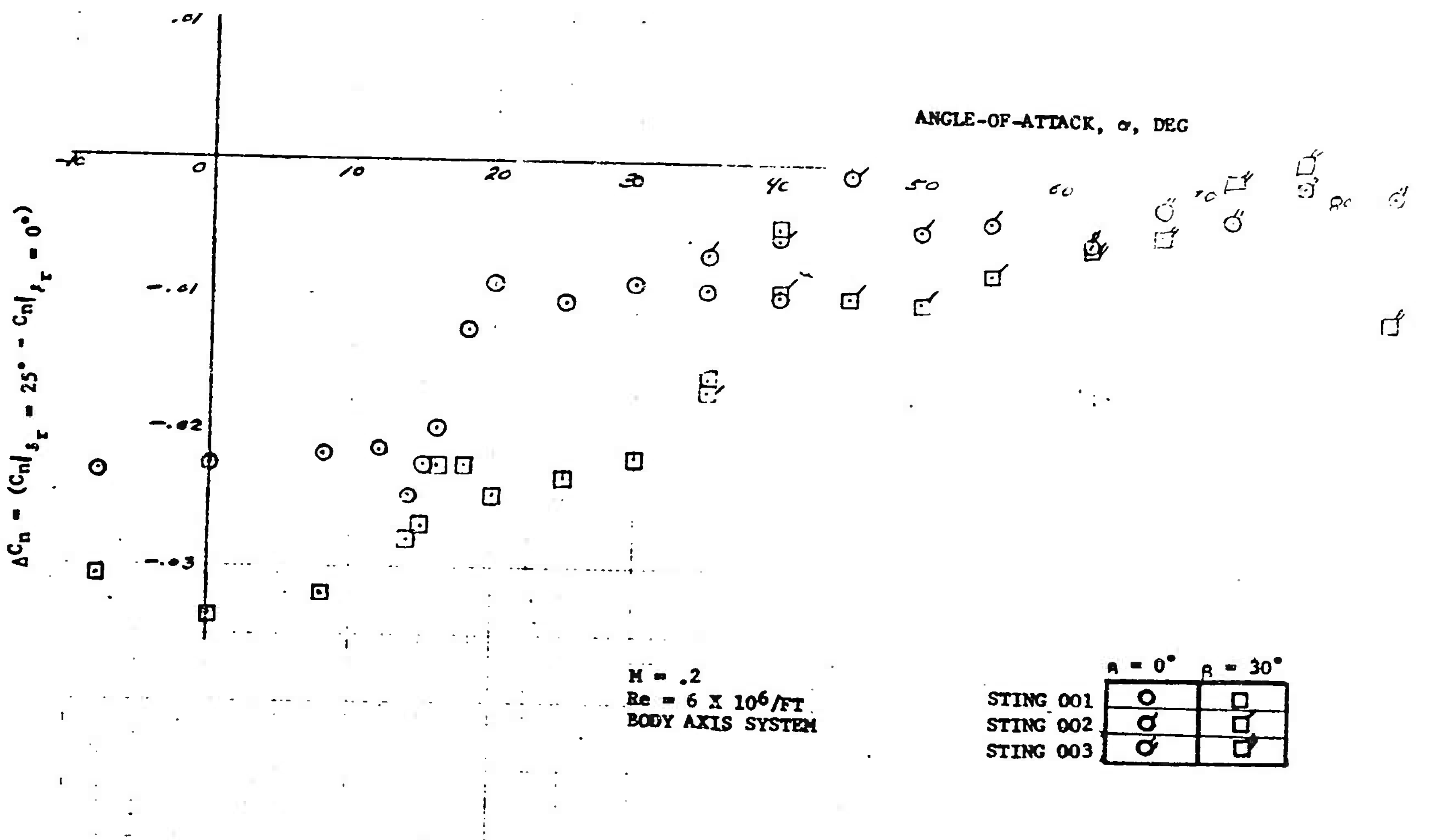

FIGURE 54. CHANGE IN YAWING MOMENT COEFFICIENT DUE TO FULL POSITIVE RUDDER DEFLECTION VERSUS ANGLE-OF-ATTACK (FOR TWO SIDESLIP ANGLES)

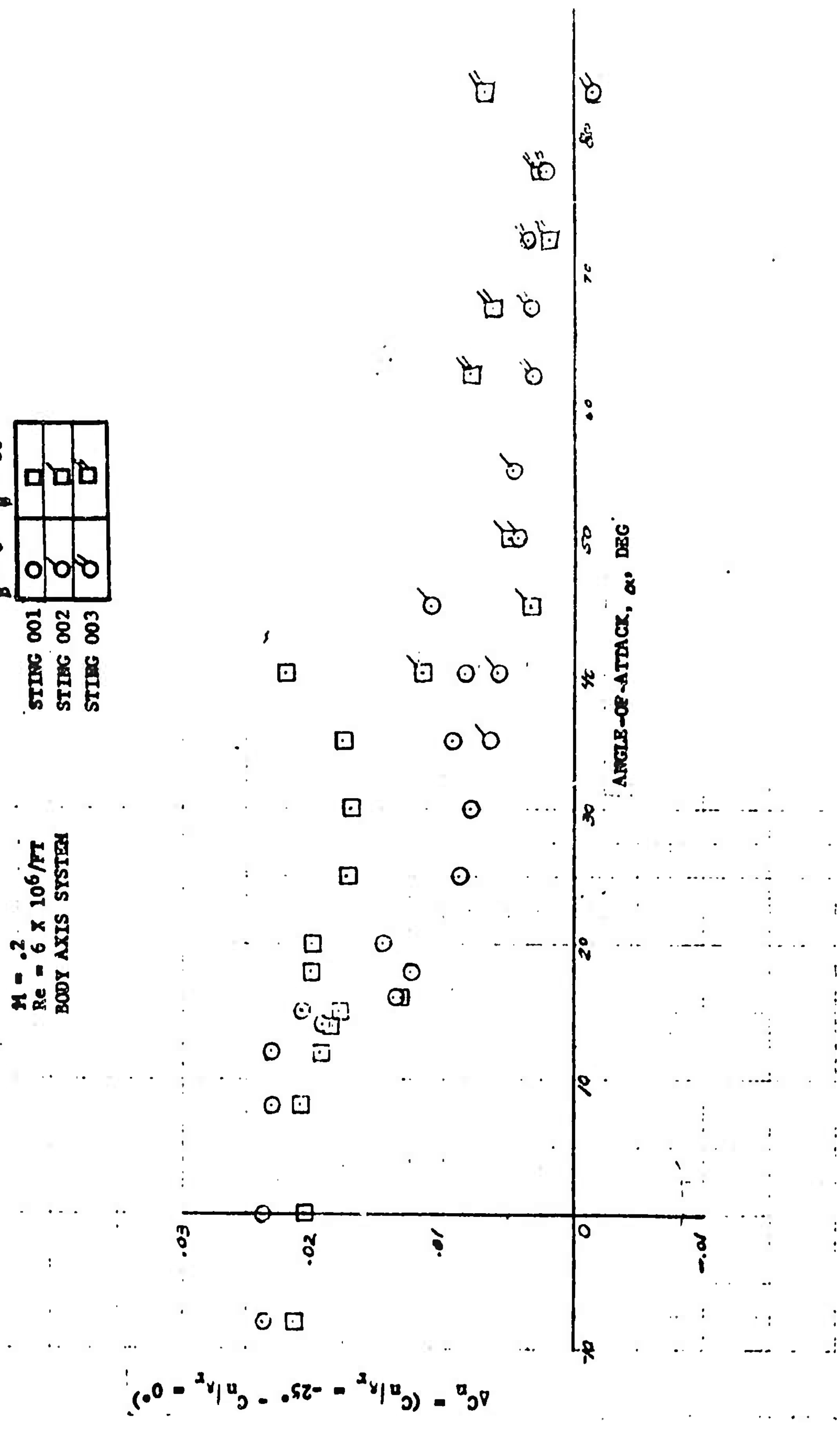

FIGURE 55. CHANGE IN YAWING MOMENT COEFFICIENT DUE TO FULL NEGATIVE RUDDER DEFLECTION VERSUS ANGLE-OF-ATTACK (FOR TWO SIDESLIP ANGLES)

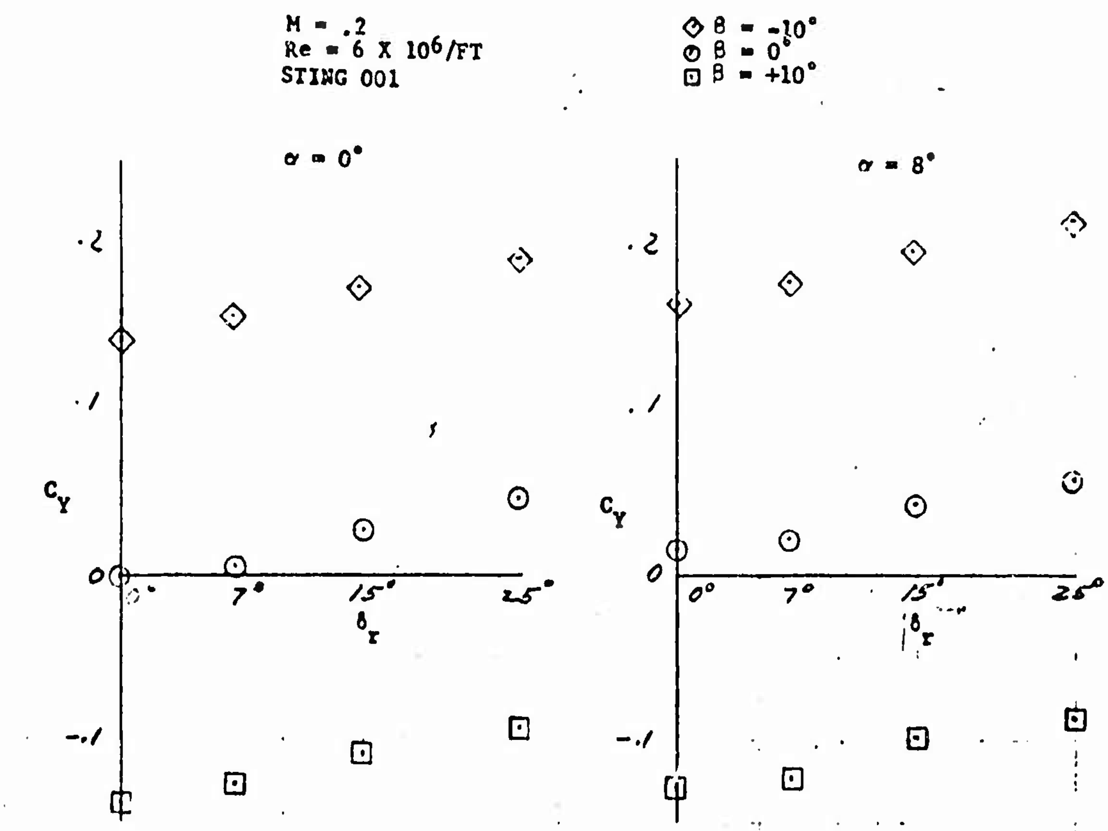

FIGURE 56. SIDEFORCE COEFFICIENT VERSUS RUDDER DEFLECTION FOR VARIOUS ANGLES-OF-ATTACK (FOR TWO SIDESLIP ANGLES)

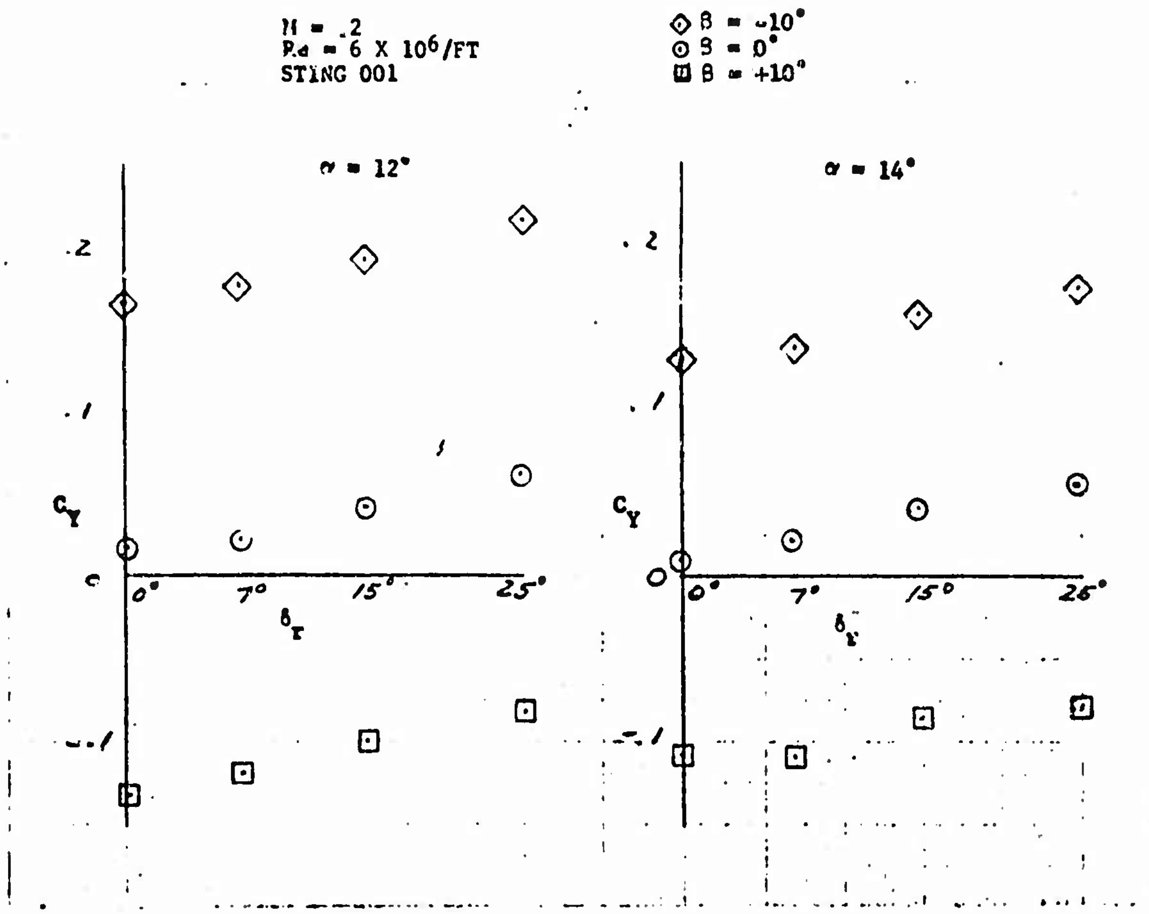

FIGURE 56. SIDEFORCE COEFFICIENT VERSUS RUDDER DEFLECTION FOR (CONT) VARIOUS ANGLES-OF-ATTACK (FOR TWO SIDESLIP ANGLES)

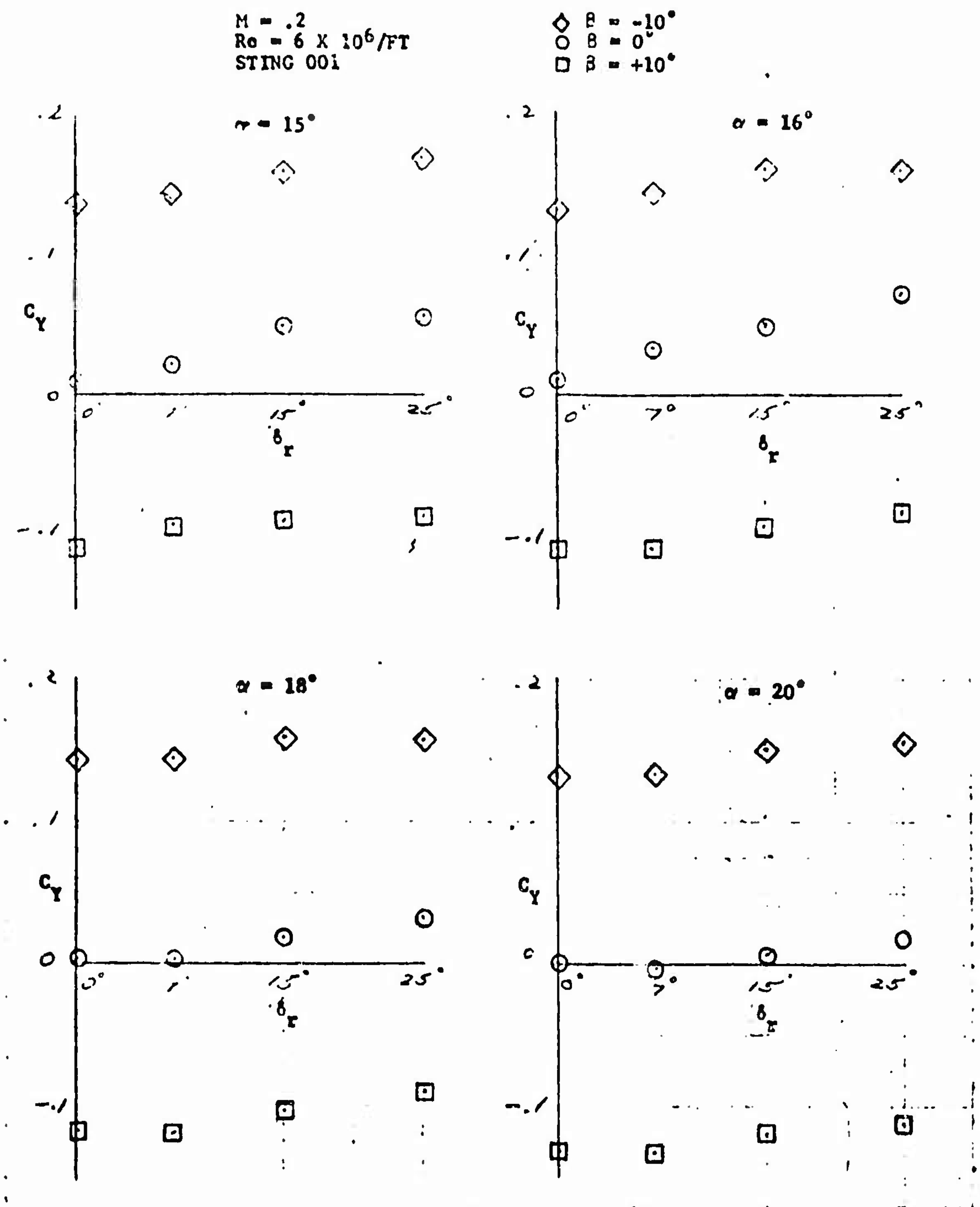

FIGURE 56. SIDEFORCE COEFFICIENT VERSUS RUDDER DEFLECTION FOR VARIOUS
(CONT) ANGLES-OF-ATTACK (FOR TWO SIDESLIP ANGLES)

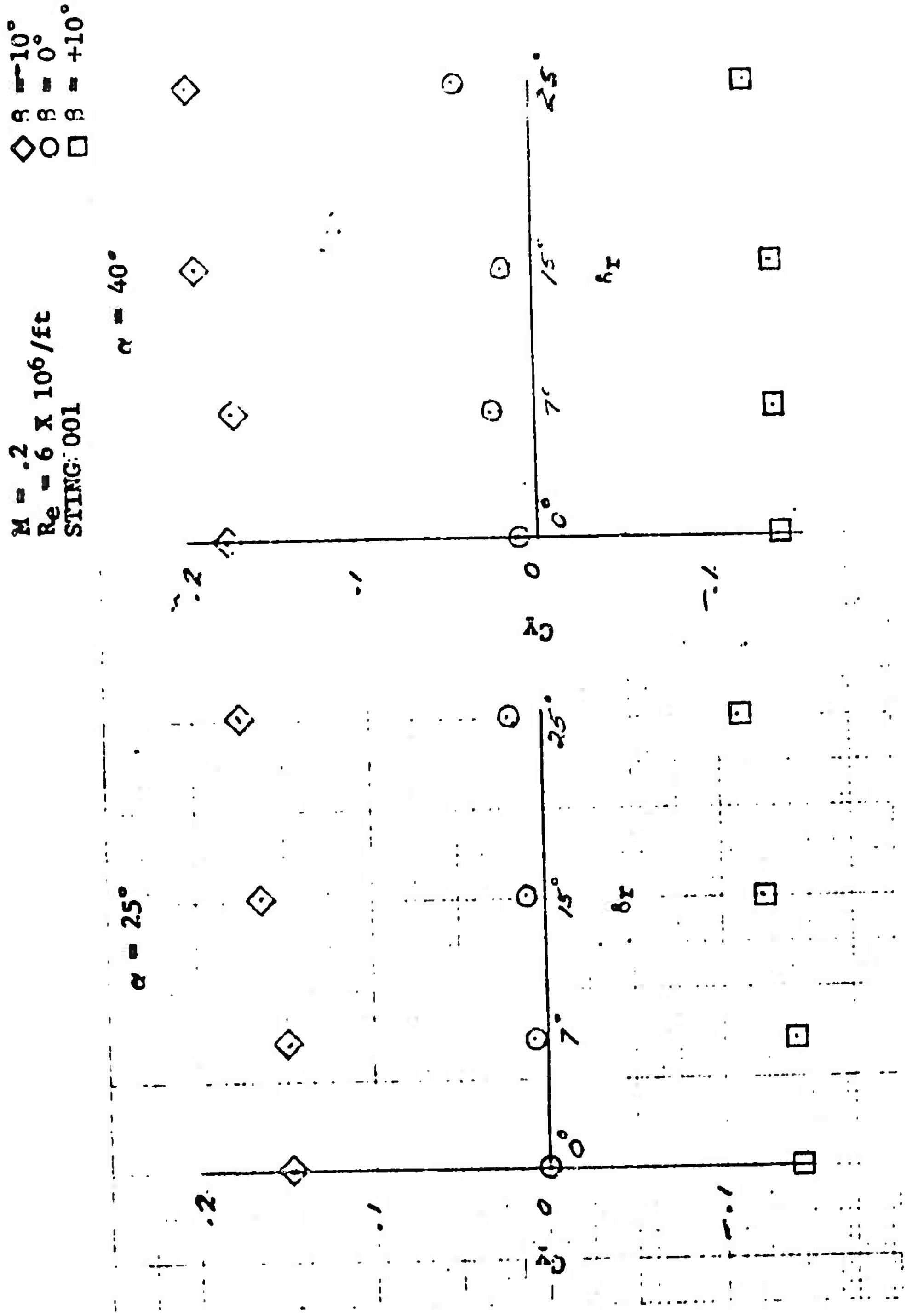

FIGURE 56. SIDEFORCE COEFFICIENT VERSUS RUDDER DEFLECTION FOR VARIOUS ANGLES OF ATTACK (FOR TWO SIDESLIP ANGLES) (CONT)

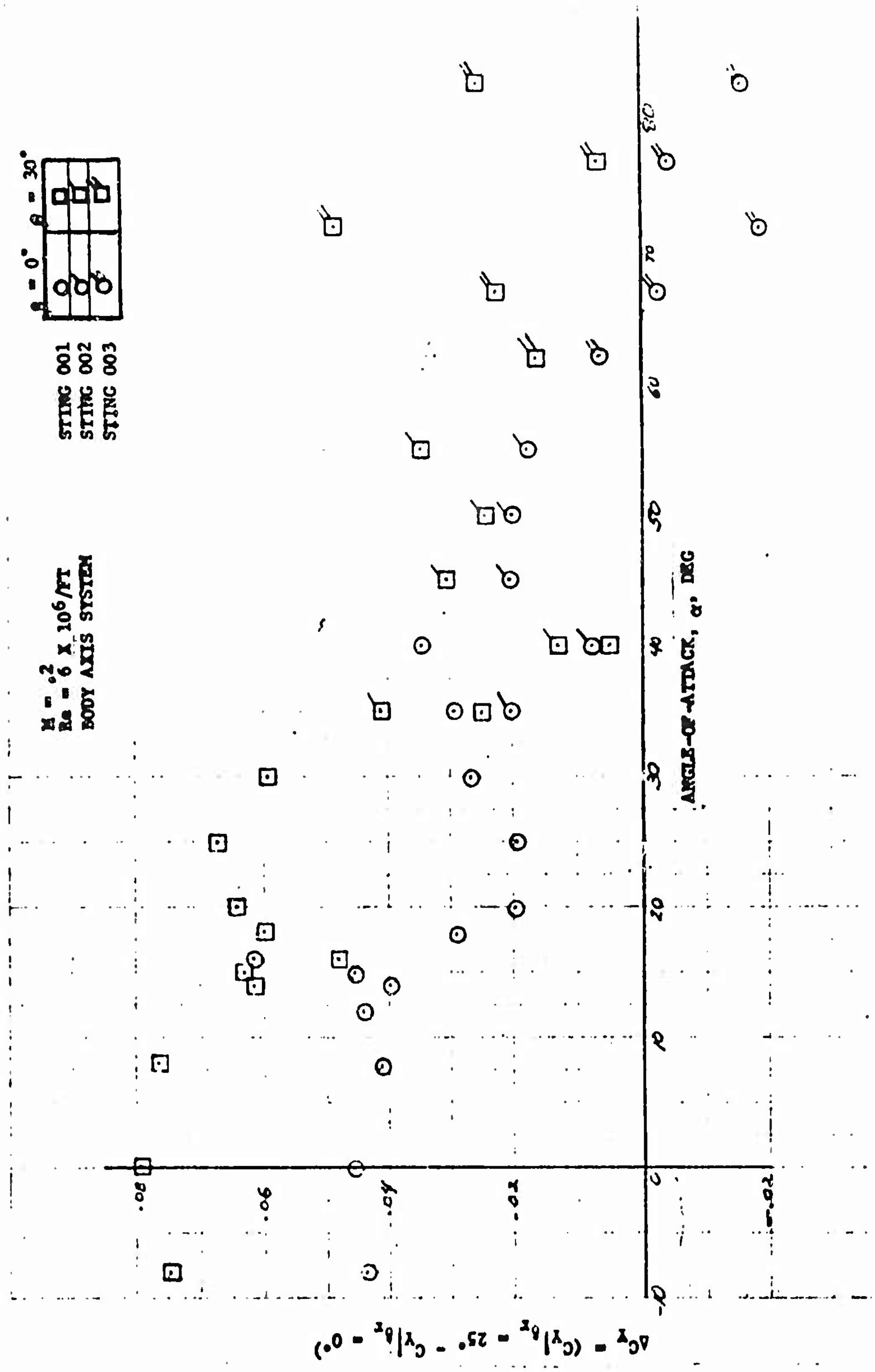

FIGURE 57. CHANGE IN SIDEFORCE COEFFICIENT DUE TO FULL POSITIVE RUDDER DEFLECTION VERSUS ANGLE-OF-ATTACK (FOR TWO SIDESLIP ANGLES)

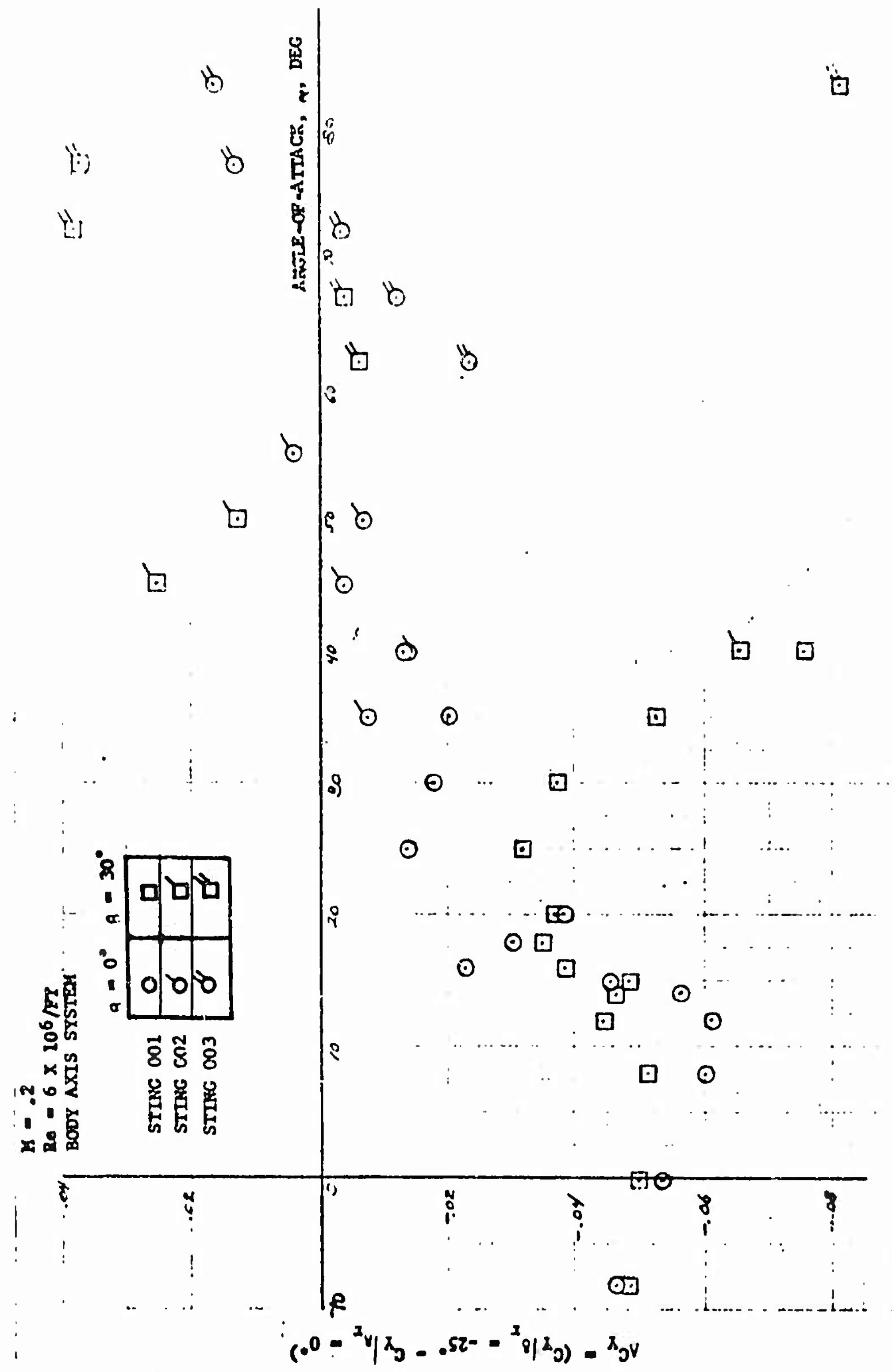

FIGURE 58. CHANGE IN SIDEFORCE COEFFICIENT DUE TO FULL NEGATIVE RUDDER DEFLECTION VERSUS ANGLE-OF-ATTACK (FOR TWO SIDESLIP ANGLES)

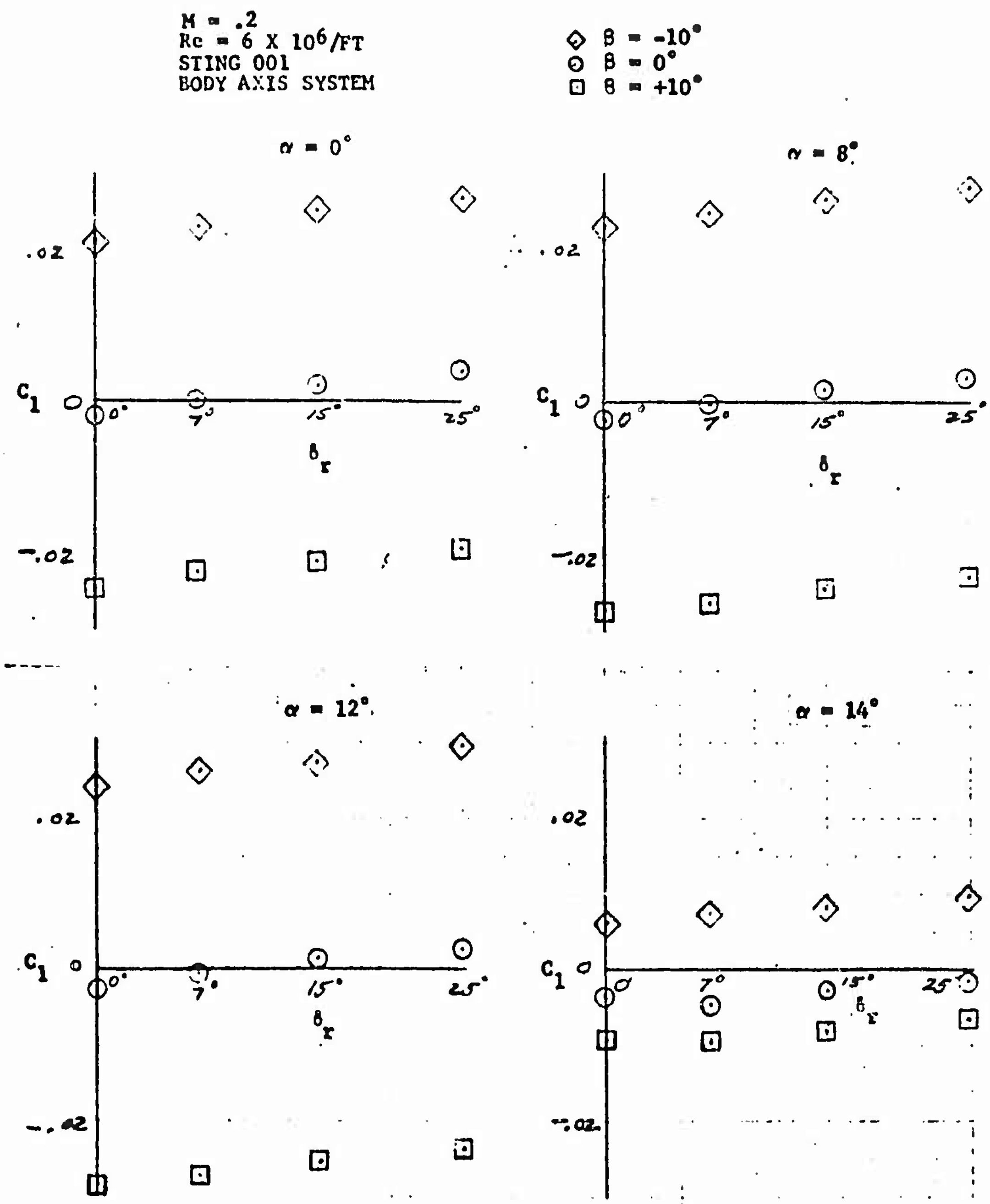

FIGURE 59. ROLLING MOMENT COEFFICIENT VERSUS RUDDER DEFLECTION FOR VARIOUS ANGLES-OF-ATTACK (FOR THREE SIDESLIP ANGLES)

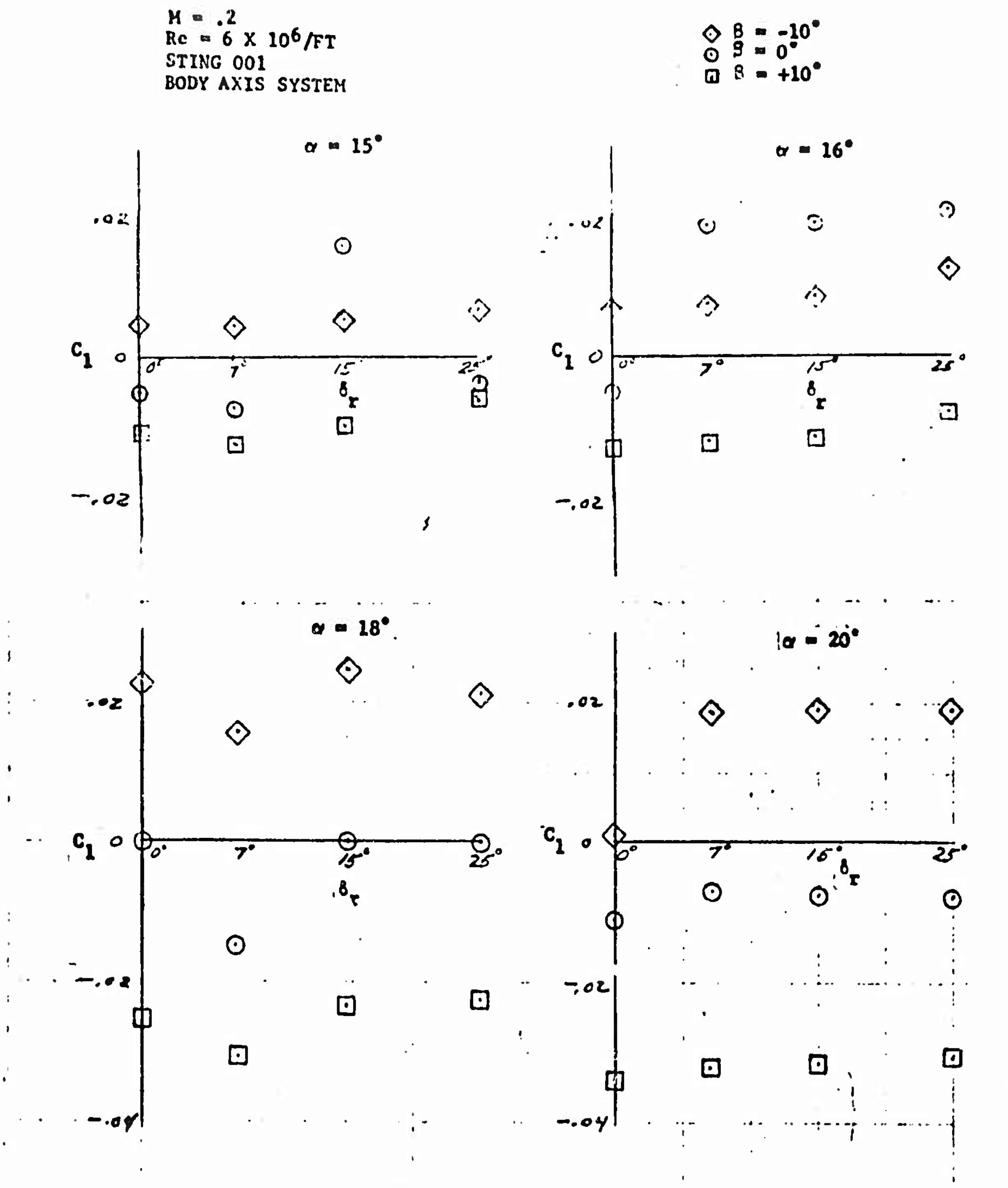

FIGURE 59. (CONT) ROLLING MOMENT COEFFICIENT VERSUS RUDDER DEFLECTION FOR VARIOUS ANGLES-OF-ATTACK (FOR THREE SIDESLIP ANGLES)

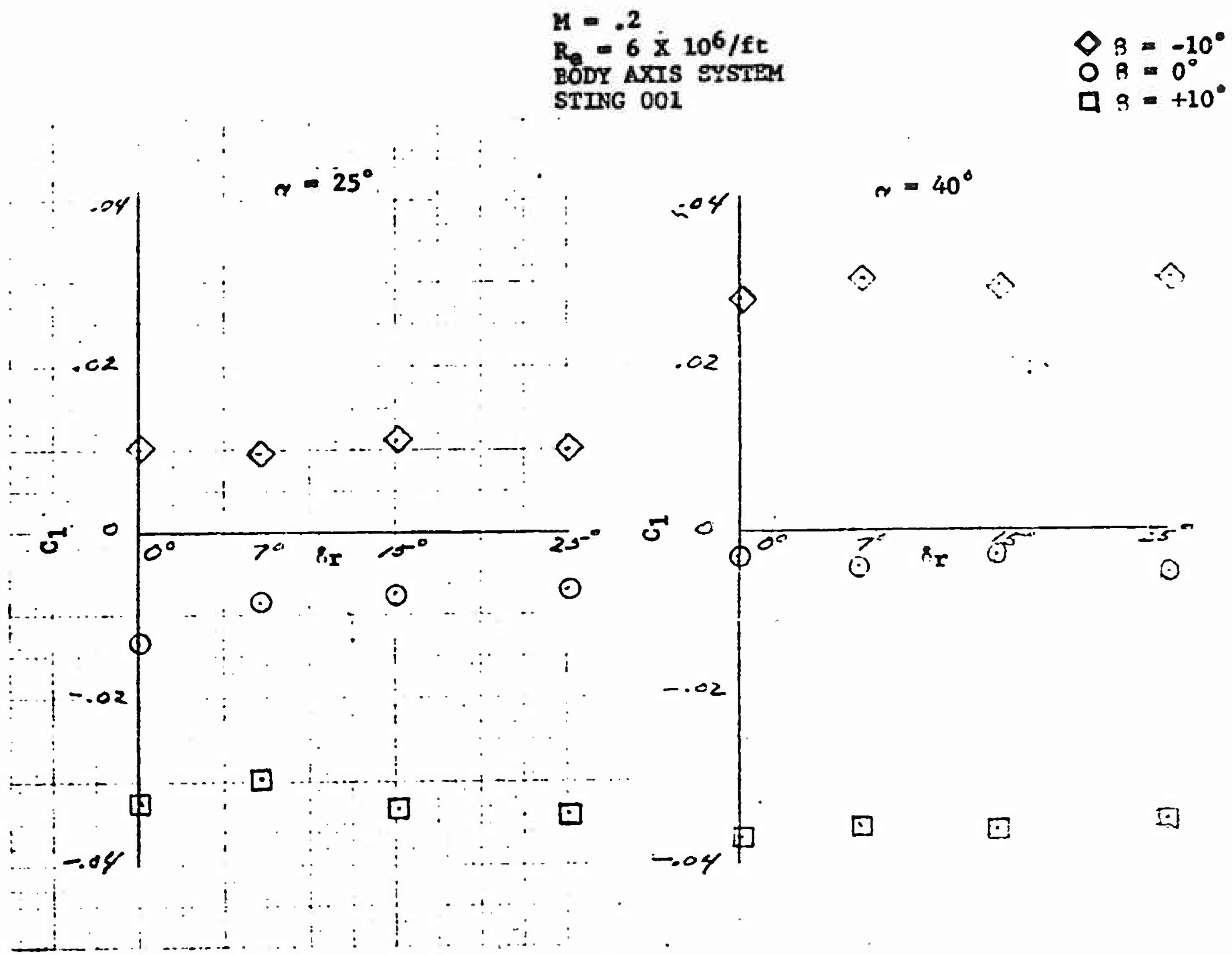

FIGURE 59. ROLLING MOMENT COEFFICIENT VERSUS RUDDER DEFLECTION FOR (CONT) VARIOUS ANGLES-OF-ATTACK (FOR THREE SIDESLIP ANGLES)

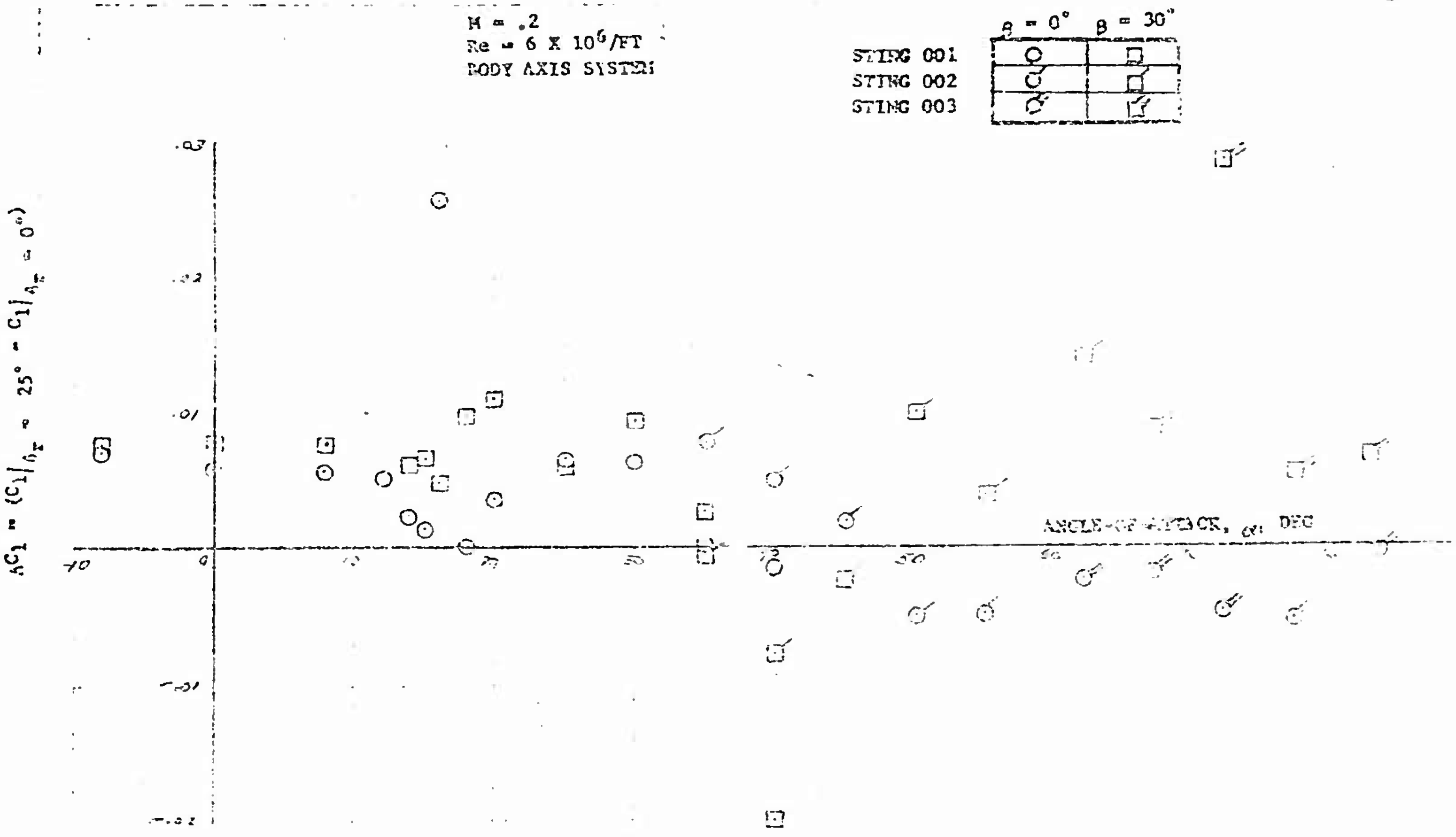

FIGURE 80. CHANGE IN ROLLING MOMENT COEFFICIENT DUE TO FULL POSITIVE RUDDER DEFLECTION VERSUS ANGLE-OF-ATTACK (FOR TWO SIDESLIP ANGLES)

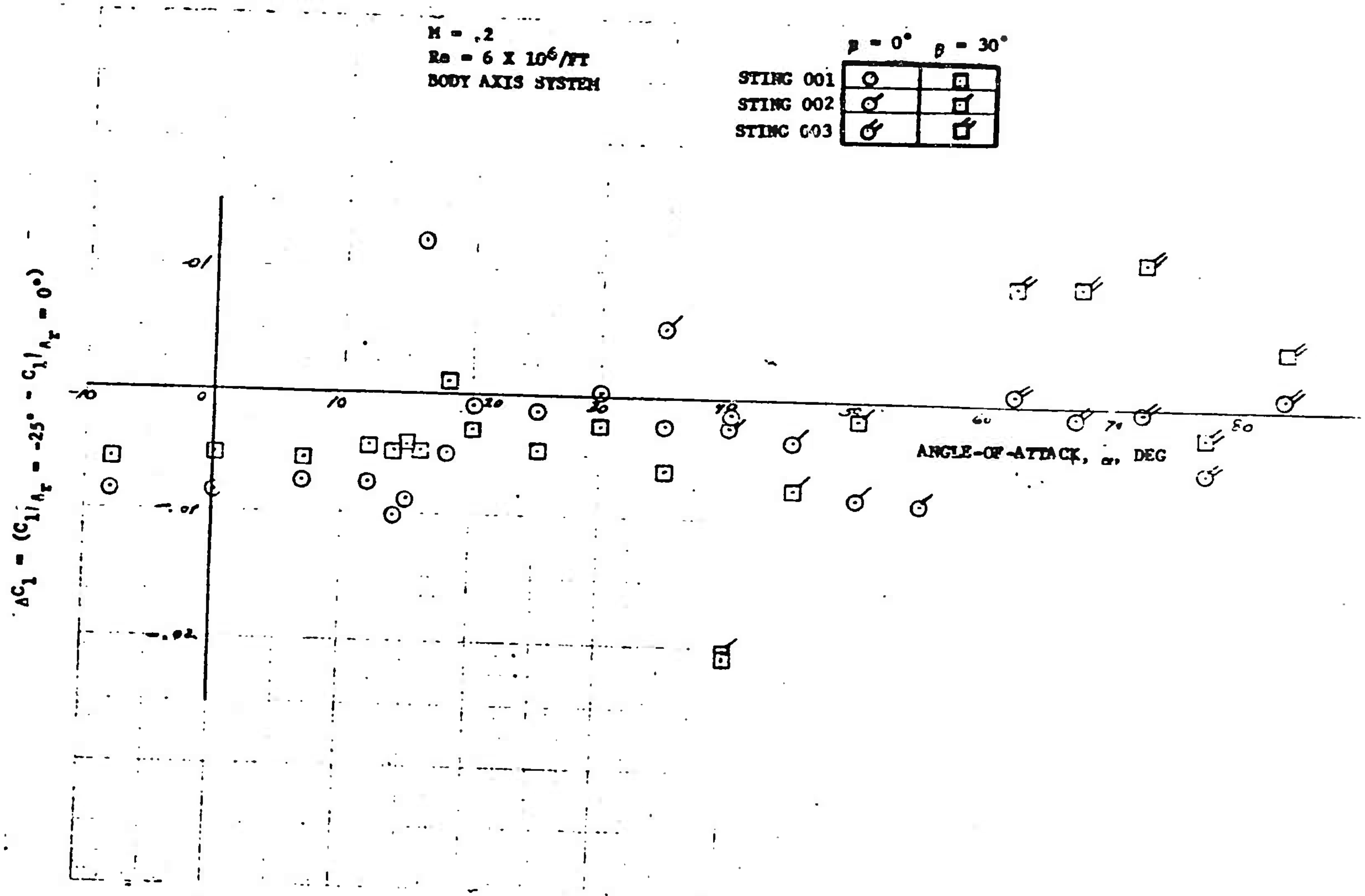

FIGURE 61. CHANGE IN ROLLING MOMENT COEFFICIENT DUE TO FULL NEGATIVE RUDDER DEFLECTION VERSUS ANGLE-OF-ATTACK (FOR TWO SIDESLIP ANGLES)

TABLE I
TRANSITION STRIPS[1]

SURFACE	GRIT STRIP LOCATION
Wing	Spanwise along upper surface at 5% of local chord[2]
Horizontal Stabilizer	Spanwise along upper surface at 5% of local chord[2]
Vertical Stabilizer	Extending vertically along 5% local chord[2]
Dorsal Fin	Along 5% local chord[2]
Nose	Ring 1.0 inch from tip of nose[2]
Upper Fuselage	Longitudinal, just below and parallel to canopy rail beginning 5.4 inches aft of the nose and extending 10.5 inches
Lower Fuselage	Longitudinal, immediately above outer curvature of engine nacelles beginning 7.4 inches aft of the nose and extending 17.0 inches

[1].08 inch wide bands of #90 carborundum grit

[2]streamwise distance to forward edge of transition strip

APPENDIX A
RUN SCHEDULE

RUN SCHEDULE

RUN NUMBER	MACH NUMBER	$R_e \times 10^{-6}$ (1/FT)	ALPHA SCHEDULE (DEG)	BETA SCHEDULE (DEG)	STING CONFIG. NUMBER	AILERON POSITION (δ_a, DEG)	ELEVATOR POSITION (δ_e, DEG)	RUDDER POSITION (δ_r, DEG)	GRIT	REMARKS
1	0.2	6.0	α(1)	0	1	0	0	0	Yes	Date: 5-8-73
2	0.2	6.0	0	β(1)	1	0	0	0	Yes	
3	0.2	6.0	8	β(1)	1	0	0	0	Yes	α(1): -8, -4,
4	0.2	6.0	12	β(1)	1	0	0	0	Yes	0, 4, 8, 12, 14,
5	0.2	6.0	16	β(1)	1	0	0	0	Yes	15, 16, 18, 20,
6	0.2	6.0	20	β(1)	1	0	0	0	Yes	25, 30, 35, 40°
7	0.2	6.0	40	β(1)	1	0	0	0	Yes	
8	0.2	5.0	α(1)	0	1	0	0	0	Yes	β(1): -10, 0, 2,
9	0.2	5.0	0	β(1)	1	0	0	0	Yes	5, 10, 15, 20,
10	0.2	5.0	8	β(1)	1	0	0	0	Yes	25, 30°
11	0.2	5.0	12	β(1)	1	0	0	0	Yes	
12	0.2	5.0	16	β(1)	1	0	0	0	Yes	
13	0.2	5.0	20	β(1)	1	0	0	0	Yes	
14	0.2	5.0	40	β(1)	1	0	0	0	Yes	
15	0.2	4.0	α(1)	0	1	0	0	0	Yes	
16	0.2	4.0	0	β(1)	1	0	0	0	Yes	
17	0.2	4.0	8	β(1)	1	0	0	0	Yes	
18	0.2	4.0	12	β(1)	1	0	0	0	Yes	
19	0.2	4.0	16	β(1)	1	0	0	0	Yes	
20	0.2	4.0	20	β(1)	1	0	0	0	Yes	

Preceding page blank

RUN SCHEDULE

RUN NUMBER	MACH NUMBER	$R_e \times 10^{-6}$ (1/FT)	ALPHA SCHEDULE (DEG)	BETA SCHEDULE (DEG)	STING CONFIG. NUMBER	AILERON POSITION (δ_a, DEG)	ELEVATOR POSITION (δ_e, DEG)	RUDDER POSITION (δ_r, DEG)	GRIT	REMARKS
21	0.2	4.0	40	β(1)	1	0	0	0	Yes	
22	0.2	3.0	α(1)	0	1	0	0	0	Yes	
23	0.2	3.0	0	β(1)	1	0	0	0	Yes	
24	0.2	3.0	8	β(1)	1	0	0	0	Yes	
25	0.2	3.0	12	β(1)	1	0	0	0	Yes	
26	0.2	3.0	16	β(1)	1	0	0	0	Yes	
27	0.2	3.0	20	β(1)	1	0	0	0	Yes	
28	0.2	3.0	40	β(1)	1	0	0	0	Yes	
29	0.2	2.0	α(1)	0	1	0	0	0	Yes	
30	0.2	2.0	0	β(1)	1	0	0	0	Yes	
31	0.2	2.0	8	β(1)	1	0	0	0	Yes	
32	0.2	2.0	12	β(1)	1	0	0	0	Yes	
33	0.2	2.0	16	β(1)	1	0	0	0	Yes	
34	0.2	2.0	20	β(1)	1	0	0	0	Yes	
35	0.2	2.0	40	β(1)	1	0	0	0	Yes	
36	0.2	1.0	α(1)	0	1	0	0	0	Yes	
37	0.2	1.0	0	β(1)	1	0	0	0	Yes	
38	0.2	1.0	8	β(1)	1	0	0	0	Yes	
39	0.2	1.0	12	β(1)	1	0	0	0	Yes	
40	0.2	1.0	16	β(1)	1	0	0	0	Yes	

RUN SCHEDULE

RUN NUMBER	MACH NUMBER	$R_e \times 10^{-6}$ (1/FT)	ALPHA SCHEDULE (DEG)	BETA SCHEDULE (DEG)	STING CONFIG. NUMBER	AILERON POSITION (δ_a, DEG)	ELEVATOR POSITION (δ_e, DEG)	RUDDER POSITION (δ_r, DEG)	GRIT	REMARKS
41	0.2	1.0	20	β(1)	1	0	0	0	Yes	
42	0.2	1.0	40	β(1)	1	0	0	0	Yes	
43	0.2	4.0	-8	β(2)	1	0	0	0	Yes	β(2): -10, -5,
44	0.2	4.0	-4	β(2)	1	0	0	0	Yes	-2, 0, 2, 5, 10,
45	0.2	4.0	0	β(2)	1	0	0	0	Yes	15, 20, 25, 30°
46	0.2	4.0	4	β(2)	1	0	0	0	Yes	
47	0.2	4.0	8	β(2)	1	0	0	0	Yes	
48	0.2	4.0	12	β(2)	1	0	0	0	Yes	
49	0.2	4.0	14	β(2)	1	0	0	0	Yes	
50	0.2	4.0	16	β(2)	1	0	0	0	Yes	
51	0.2	4.0	18	β(2)	1	0	0	0	Yes	
52	0.2	4.0	20	β(2)	1	0	0	0	Yes	
53	0.2	4.0	22	β(2)	1	0	0	0	Yes	
54	0.2	4.0	25	β(2)	1	0	0	0	Yes	
55	0.2	4.0	30	β(2)	1	0	0	0	Yes	
56	0.2	4.0	35	β(2)	1	0	0	0	Yes	
57	0.2	4.0	40	β(2)	1	0	0	0	Yes	
58	0.4	4.0	-8	β(2)	1	0	0	0	Yes	
59	0.4	4.0	-4	β(2)	1	0	0	0	Yes	
60	0.4	4.0	0	β(2)	1	0	0	0	Yes	

RUN SCHEDULE

RUN NUMBER	MACH NUMBER	$R_e \times 10^{-6}$ (1/FT)	ALPHA SCHEDULE (DEG)	BETA SCHEDULE (DEG)	STING CONFIG. NUMBER	AILERON POSITION (δ_a, DEG)	ELEVATOR POSITION (δ_e, DEG)	RUDDER POSITION (δ_r, DEG)	GRIT	REMARKS
61	0.4	4.0	4	β(2)	1	0	0	0	Yes	
62	0.4	4.0	8	β(2)	1	0	0	0	Yes	
63	0.4	4.0	12	β(2)	1	0	0	0	Yes	
64	0.4	4.0	14	β(2)	1	0	0	0	Yes	
65	0.4	4.0	15	β(2)	1	0	0	0	Yes	
66	0.4	4.0	16	β(2)	1	0	0	0	Yes	
67	0.4	4.0	18	β(2)	1	0	0	0	Yes	
68	0.4	4.0	20	β(2)	1	0	0	0	Yes	
69	0.4	4.0	25	β(2)	1	0	0	0	Yes	
70	0.2	6.0	0	β(1)	1	0	0	0	Yes	
71	0.2	6.0	8	β(1)	1	0	0	0	Yes	
72	0.2	6.0	12	β(1)	1	0	0	0	Yes	
73	0.2	6.0	15	β(1)	1	0	0	0	Yes	
74	0.2	6.0	16	β(1)	1	0	0	0	Yes	
75	0.2	6.0	20	β(1)	1	0	0	0	Yes	
76	0.2	6.0	40	β(1)	1	0	0	0	Yes	
77	0.2	6.0	-8	β(1)	1	0	-25	0	Yes	
78	0.2	6.0	-4	β(1)	1	0	-25	0	Yes	
79	0.2	6.0	0	β(1)	1	0	-25	0	Yes	
80	0.2	6.0	4	β(1)	1	0	-25	0	Yes	

RUN SCHEDULE

RUN NUMBER	MACH NUMBER	$R_e \times 10^{-6}$ (1/FT)	ALPHA SCHEDULE (DEG)	BETA SCHEDULE (DEG)	STING CONFIG. NUMBER	AILERON POSITION (δ_a, DEG)	ELEVATOR POSITION (δ_e, DEG)	RUDDER POSITION (δ_r, DEG)	GRIT	REMARKS
81	0.2	6.0	8	β(1)	1	0	-25	0	Yes	
82	0.2	6.0	12	β(1)	1	0	-25	0	Yes	
83	0.2	6.0	14	β(1)	1	0	-25	0	Yes	
84	0.2	6.0	15	β(1)	1	0	-25	0	Yes	
85	0.2	6.0	16	β(1)	1	0	-25	0	Yes	
86	0.2	6.0	18	β(1)	1	0	-25	0	Yes	
87	0.2	6.0	20	β(1)	1	0	-25	0	Yes	
88	0.2	6.0	25	β(1)	1	0	-25	0	Yes	
89	0.2	6.0	30	β(1)	1	0	-25	0	Yes	
90	0.2	6.0	35	β(1)	1	0	-25	0	Yes	
91	0.2	6.0	40	β(1)	1	0	-25	0	Yes	
92	0.2	6.0	α(1)	0	1	0	+15	0	Yes	
93	0.2	6.0	-8	β(1)	1	0	+15	0	Yes	
94	0.2	6.0	-4	β(1)	1	0	+15	0	Yes	
95	0.2	6.0	0	β(1)	1	0	+15	0	Yes	
96	0.2	6.0	4	β(1)	1	0	+15	0	Yes	
97	0.2	6.0	8	β(1)	1	0	+15	0	Yes	
98	0.2	6.0	12	β(1)	1	0	+15	0	Yes	
99	0.2	6.0	14	β(1)	1	0	+15	0	Yes	
100	0.2	6.0	15	β(1)	1	0	+15	0	Yes	

RUN SCHEDULE

RUN NUMBER	MACH NUMBER	$R_e \times 10^{-6}$ (1/FT)	ALPHA SCHEDULE (DEG)	BETA SCHEDULE (DEG)	STING CONFIG. NUMBER	AILERON POSITION (δ_a, DEG)	ELEVATOR POSITION (δ_e, DEG)	RUDDER POSITION (δ_r, DEG)	GRIT	REMARKS
101	0.2	6.0	16	β(1)	1	0	+15	0	Yes	
102	0.2	6.0	18	β(1)	1	0	+15	0	Yes	
103	0.2	6.0	20	β(1)	1	0	+15	0	Yes	
104	0.2	6.0	25	β(1)	1	0	+15	0	Yes	
105	0.2	6.0	30	β(1)	1	0	+15	0	Yes	
106	0.2	6.0	35	β(1)	1	0	+15	0	Yes	
107	0.2	6.0	40	β(1)	1	0	+15	0	Yes	
108	0.2	6.0	-8	β(1)	1	-12	0	0	Yes	
109	0.2	6.0	-4	β(1)	1	-12	0	0	Yes	
110	0.2	6.0	0	β(1)	1	-12	0	0	Yes	
111	0.2	6.0	4	β(1)	1	-12	0	0	Yes	
112	0.2	6.0	8	β(1)	1	-12	0	0	Yes	
113	0.2	6.0	12	β(1)	1	-12	0	0	Yes	
114	0.2	6.0	14	β(1)	1	-12	0	0	Yes	
115	0.2	6.0	15	β(1)	1	-12	0	0	Yes	
116	0.2	6.0	16	β(1)	1	-12	0	0	Yes	
117	0.2	6.0	18	β(1)	1	-12	0	0	Yes	
118	0.2	6.0	20	β(1)	1	-12	0	0	Yes	
119	0.2	6.0	25	β(1)	1	-12	0	0	Yes	
120	0.2	6.0	30	β(1)	1	-12	0	0	Yes	

RUN SCHEDULE

RUN NUMBER	MACH NUMBER	$R_e \times 10^{-6}$ (1/FT)	ALPHA SCHEDULE (DEG)	BETA SCHEDULE (DEG)	STING CONFIG. NUMBER	AILERON POSITION (δ_a, DEG)	ELEVATOR POSITION (δ_e, DEG)	RUDDER POSITION (δ_r, DEG)	GRIT	REMARKS
121	0.2	6.0	35	B(1)	1	-12	0	0	Yes	
122	0.2	6.0	40	B(1)	1	-12	0	0	Yes	
123	0.2	6.0	-8	B(1)	1	+12	0	0	Yes	
124	0.2	6.0	-4	B(1)	1	+12	0	0	Yes	
125	0.2	6.0	0	B(1)	1	+12	0	0	Yes	
126	0.2	6.0	4	B(1)	1	+12	0	0	Yes	
127	0.2	6.0	8	B(1)	1	+12	0	0	Yes	
128	0.2	6.0	12	B(1)	1	+12	0	0	Yes	
129	0.2	6.0	14	B(1)	1	+12	0	0	Yes	
130	0.2	6.0	15	B(1)	1	+12	0	0	Yes	
131	0.2	6.0	16	B(1)	1	+12	0	0	Yes	
132	0.2	6.0	18	B(1)	1	+12	0	0	Yes	
133	0.2	6.0	20	B(1)	1	+12	0	0	Yes	
134	0.2	6.0	25	B(1)	1	+12	0	0	Yes	
135	0.2	6.0	30	B(1)	1	+12	0	0	Yes	
136	0.2	6.0	35	B(1)	1	+12	0	0	Yes	
137	0.2	6.0	40	B(1)	1	+12	0	0	Yes	
138	0.2	6.0	-8	B(1)	1	0	0	-25	Yes	
139	0.2	6.0	-4	B(1)	1	0	0	-25	Yes	
140	0.2	6.0	0	B(1)	1	0	0	-25	Yes	

RUN SCHEDULE

RUN NUMBER	MACH NUMBER	$R_e \times 10^{-6}$ (1/FT)	ALPHA SCHEDULE (DEG)	BETA SCHEDULE (DEG)	STING CONFIG. NUMBER	AILERON POSITION (δ_a, DEG)	ELEVATOR POSITION (δ_e, DEG)	RUDDER POSITION (δ_r, DEG)	GRIT	REMARKS
141	0.2	6.0	4	β(1)	1	0	0	-25	Yes	
142	0.2	6.0	8	β(1)	1	0	0	-25	Yes	
143	0.2	6.0	12	β(1)	1	0	0	-25	Yes	
144	0.2	6.0	14	β(1)	1	0	0	-25	Yes	
145	0.2	6.0	15	β(1)	1	0	0	-25	Yes	
146	0.2	6.0	16	β(1)	1	0	0	-25	Yes	
147	0.2	6.0	18	β(1)	1	0	0	-25	Yes	
148	0.2	6.0	20	β(1)	1	0	0	-25	Yes	
149	0.2	6.0	25	β(1)	1	0	0	-25	Yes	
150	0.2	6.0	30	β(1)	1	0	0	-25	Yes	
151	0.2	6.0	35	β(1)	1	0	0	-25	Yes	
152	0.2	6.0	40	β(1)	1	0	0	-25	Yes	
153	0.2	6.0	-8	β(1)	1	0	0	+25	Yes	
154	0.2	6.0	-4	β(1)	1	0	0	+25	Yes	
155	0.2	6.0	0	β(1)	1	0	0	+25	Yes	
156	0.2	6.0	4	β(1)	1	0	0	+25	Yes	
157	0.2	6.0	8	β(1)	1	0	0	+25	Yes	
158	0.2	6.0	12	β(1)	1	0	0	+25	Yes	
159	0.2	6.0	14	β(1)	1	0	0	+25	Yes	
160	0.2	6.0	15	β(1)	1	0	0	+25	Yes	

RUN SCHEDULE

RUN NUMBER	MACH NUMBER	$R_e \times 10^{-6}$ (1/FT)	ALPHA SCHEDULE (DEG)	BETA SCHEDULE (DEG)	STING CONFIG. NUMBER	AILERON POSITION (δ_a, DEG)	ELEVATOR POSITION (δ_e, DEG)	RUDDER POSITION (δ_r, DEG)	GRIT	REMARKS
161	0.2	6.0	16	β(1)	1	0	0	+25	Yes	
162	0.2	6.0	18	β(1)	1	0	0	+25	Yes	
163	0.2	6.0	20	β(1)	1	0	0	+25	Yes	
164	0.2	6.0	25	β(1)	1	0	0	+25	Yes	
165	0.2	6.0	30	β(1)	1	0	0	+25	Yes	
166	0.2	6.0	35	β(1)	1	0	0	+25	Yes	
167	0.2	6.0	40	β(1)	1	0	0	+25	Yes	
168	0.2	6.0	-8	β(1)	1	0	-10	0	Yes	
169	0.2	6.0	-4	β(1)	1	0	-10	0	Yes	
170	0.2	6.0	0	β(1)	1	0	-10	0	Yes	
171	0.2	6.0	4	β(1)	1	0	-10	0	Yes	
172	0.2	6.0	8	β(1)	1	0	-10	0	Yes	
173	0.2	6.0	12	β(1)	1	0	-10	0	Yes	
174	0.2	6.0	14	β(1)	1	0	-10	0	Yes	
175	0.2	6.0	15	β(1)	1	0	-10	0	Yes	
176	0.2	6.0	16	β(1)	1	0	-10	0	Yes	
177	0.2	6.0	18	β(1)	1	0	-10	0	Yes	
178	0.2	6.0	20	β(1)	1	0	-10	0	Yes	
179	0.2	6.0	25	β(1)	1	0	-10	0	Yes	
180	0.2	6.0	30	β(1)	1	0	-10	0	Yes	

RUN SCHEDULE

RUN NUMBER	MACH NUMBER	$R_e \times 10^{-6}$ (1/FT)	ALPHA SCHEDULE (DEG)	BETA SCHEDULE (DEG)	STING CONFIG. NUMBER	AILERON POSITION (δ_a, DEG)	ELEVATOR POSITION (δ_e, DEG)	RUDDER POSITION (δ_r, DEG)	GRIT	REMARKS
181	0.2	6.0	35	β(1)	1	0	-10	0	Yes	
182	0.2	6.0	40	β(1)	1	0	-10	0	Yes	
183	0.2	6.0	-8	β(1)	1	0	+10	0	Yes	
184	0.2	6.0	-4	β(1)	1	0	+10	0	Yes	
185	0.2	6.0	0	β(1)	1	0	+10	0	Yes	
186	0.2	6.0	4	β(1)	1	0	+10	0	Yes	
187	0.2	6.0	8	β(1)	1	0	+10	0	Yes	
188	0.2	6.0	12	β(1)	1	0	+10	0	Yes	
189	0.2	6.0	14	β(1)	1	0	+10	0	Yes	
190	0.2	6.0	15	β(1)	1	0	+10	0	Yes	
191	0.2	6.0	16	β(1)	1	0	+10	0	Yes	
192	0.2	6.0	18	β(1)	1	0	+10	0	Yes	
193	0.2	6.0	20	β(1)	1	0	+10	0	Yes	
194	0.2	6.0	25	β(1)	1	0	+10	0	Yes	
195	0.2	6.0	30	β(1)	1	0	+10	0	Yes	
196	0.2	6.0	35	β(1)	1	0	+10	0	Yes	
197	0.2	6.0	40	β(1)	1	0	+10	0	Yes	
198	0.2	6.0	-8	β(1)	1	0	-15	0	Yes	
199	0.2	6.0	-4	β(1)	1	0	-15	0	Yes	
200	0.2	6.0	0	β(1)	1	0	-15	0	Yes	

RUN SCHEDULE

RUN NUMBER	MACH NUMBER	$R_e \times 10^{-6}$ (1/FT)	ALPHA SCHEDULE (DEG)	BETA SCHEDULE (DEG)	STING CONFIG. NUMBER	AILERON POSITION (δ_a, DEG)	ELEVATOR POSITION (δ_e, DEG)	RUDDER POSITION (δ_r, DEG)	GRIT	REMARKS
201	0.2	6.0	4	β(1)	1	0	-15	0	Yes	
202	0.2	6.0	8	β(1)	1	0	-15	0	Yes	
203	0.2	6.0	12	β(1)	1	0	-15	0	Yes	
204	0.2	6.0	14	β(1)	1	0	-15	0	Yes	
205	0.2	6.0	15	β(1)	1	0	-15	0	Yes	
206	0.2	6.0	16	β(1)	1	0	-15	0	Yes	
207	0.2	6.0	18	β(1)	1	0	-15	0	Yes	
208	0.2	6.0	20	β(1)	1	0	-15	0	Yes	
209	0.2	6.0	25	β(1)	1	0	-15	0	Yes	
210	0.2	6.0	30	β(1)	1	0	-15	0	Yes	
211	0.2	6.0	35	β(1)	1	0	-15	0	Yes	
212	0.2	6.0	40	β(1)	1	0	-15	0	Yes	
213	0.2	6.0	α(1)	12.5	1	0	0	0	Yes	
214	0.2	6.0	α(1)	17.5	1	0	0	0	Yes	
215	0.2	6.0	-8	β(1)	1	0	0	0	Yes	
216	0.2	6.0	-4	β(1)	1	0	0	0	Yes	
217	0.2	6.0	0	β(1)	1	0	0	0	Yes	
218	0.2	6.0	4	β(1)	1	0	0	0	Yes	
219	0.2	6.0	14	β(1)	1	0	0	0	Yes	
220	0.2	6.0	15	β(1)	1	0	0	0	Yes	

RUN SCHEDULE

RUN NUMBER	MACH NUMBER	$R_e \times 10^{-6}$ (1/FT)	ALPHA SCHEDULE (DEG)	BETA SCHEDULE (DEG)	STING CONFIG. NUMBER	AILERON POSITION (δ_a, DEG)	ELEVATOR POSITION (δ_e, DEG)	RUDDER POSITION (δ_r, DEG)	GRIT	REMARKS
221	0.2	6.0	16	β(1)	1	0	0	0	Yes	
222	0.2	6.0	18	β(1)	1	0	0	0	Yes	
223	0.2	6.0	25	β(1)	1	0	0	0	Yes	
224	0.2	6.0	30	β(1)	1	0	0	0	Yes	
225	0.2	6.0	35	β(1)	1	0	0	0	Yes	
226	0.2	6.0	α(1)	-10	1	+3	0	0	Yes	
227	0.2	6.0	α(1)	0	1	+3	0	0	Yes	
228	0.2	6.0	α(1)	10	1	+3	0	0	Yes	
229	0.2	6.0	-8	β(1)	1	+6	0	0	Yes	
230	0.2	6.0	-4	β(1)	1	+6	0	0	Yes	
231	0.2	6.0	0	β(1)	1	+6	0	0	Yes	
232	0.2	6.0	4	β(1)	1	+6	0	0	Yes	
233	0.2	6.0	8	β(1)	1	+6	0	0	Yes	
234	0.2	6.0	12	β(1)	1	+6	0	0	Yes	
235	0.2	6.0	14	β(1)	1	+6	0	0	Yes	
236	0.2	6.0	15	β(1)	1	+6	0	0	Yes	
237	0.2	6.0	16	β(1)	1	+6	0	0	Yes	
238	0.2	6.0	18	β(1)	1	+6	0	0	Yes	
239	0.2	6.0	20	β(1)	1	+6	0	0	Yes	
240	0.2	6.0	25	β(1)	1	+6	0	0	Yes	

RUN SCHEDULE

RUN NUMBER	MACH NUMBER	$R_e \times 10^{-6}$ (1/FT)	ALPHA SCHEDULE (DEG)	BETA SCHEDULE (DEG)	STING CONFIG. NUMBER	AILERON POSITION (δ_a, DEG)	ELEVATOR POSITION (δ_e, DEG)	RUDDER POSITION (δ_r, DEG)	GRIT	REMARKS
241	0.2	6.0	30	β(1)	1	+6	0	0	Yes	
242	0.2	6.0	35	β(1)	1	+6	0	0	Yes	
243	0.2	6.0	40	β(1)	1	+6	0	0	Yes	
244	0.2	6.0	-8	β(1)	1	0	0	+7	Yes	
245	0.2	6.0	-4	β(1)	1	0	0	+7	Yes	
246	0.2	6.0	0	β(1)	1	0	0	+7	Yes	
247	0.2	6.0	4	β(1)	1	0	0	+7	Yes	
248	0.2	6.0	8	β(1)	1	0	0	+7	Yes	
249	0.2	6.0	12	β(1)	1	0	0	+7	Yes	
250	0.2	6.0	14	β(1)	1	0	0	+7	Yes	
251	0.2	6.0	15	β(1)	1	0	0	+7	Yes	
252	0.2	6.0	16	β(1)	1	0	0	+7	Yes	
253	0.2	6.0	18	β(1)	1	0	0	+7	Yes	
254	0.2	6.0	20	β(1)	1	0	0	+7	Yes	
255	0.2	6.0	25	β(1)	1	0	0	+7	Yes	
256	0.2	6.0	30	β(1)	1	0	0	+7	Yes	
257	0.2	6.0	35	β(1)	1	0	0	+7	Yes	
258	0.2	6.0	40	β(1)	1	0	0	+7	Yes	
259	0.2	6.0	-8	β(1)	1	0	0	+15	Yes	
260	0.2	6.0	-4	β(1)	1	0	0	+15	Yes	

RUN SCHEDULE

RUN NUMBER	MACH NUMBER	$R_e \times 10^{-6}$ (1/FT)	ALPHA SCHEDULE (DEG)	BETA SCHEDULE (DEG)	STING CONFIG. NUMBER	AILERON POSITION (δ_a, DEG)	ELEVATOR POSITION (δ_e, DEG)	RUDDER POSITION (δ_r, DEG)	GRIT	REMARKS
261	0.2	6.0	0	B(1)	1	0	0	+15	Yes	
262	0.2	6.0	4	B(1)	1	0	0	+15	Yes	
263	0.2	6.0	8	B(1)	1	0	0	+15	Yes	
264	0.2	6.0	12	B(1)	1	0	0	+15	Yes	
265	0.2	6.0	14	B(1)	1	0	0	+15	Yes	
266	0.2	6.0	15	B(1)	1	0	0	+15	Yes	
267	0.2	6.0	16	B(1)	1	0	0	+15	Yes	
268	0.2	6.0	18	B(1)	1	0	0	+15	Yes	
269	0.2	6.0	20	B(1)	1	0	0	+15	Yes	
270	0.2	6.0	25	B(1)	1	0	0	+15	Yes	
271	0.2	6.0	30	B(1)	1	0	0	+15	Yes	
272	0.2	6.0	35	B(1)	1	0	0	+15	Yes	
273	0.2	6.0	40	B(1)	1	0	0	+15	Yes	
274	0.2	6.0	-8	B(1)	1	0	-25	+25	Yes	
275	0.2	6.0	-4	B(1)	1	0	-25	+25	Yes	
276	0.2	6.0	0	B(1)	1	0	-25	+25	Yes	
277	0.2	6.0	4	B(1)	1	0	-25	+25	Yes	
278	0.2	6.0	8	B(1)	1	0	-25	+25	Yes	
279	0.2	6.0	12	B(1)	1	0	-25	+25	Yes	
280	0.2	6.0	14	B(1)	1	0	-25	+25	Yes	

RUN SCHEDULE

RUN NUMBER	MACH NUMBER	$R_e \times 10^{-6}$ (1/FT)	ALPHA SCHEDULE (DEG)	BETA SCHEDULE (DEG)	STING CONFIG. NUMBER	AILERON POSITION (δ_a, DEG)	ELEVATOR POSITION (δ_e, DEG)	RUDDER POSITION (δ_r, DEG)	GRIT	REMARKS
281	0.2	6.0	15	β(1)	1	0	-25	+25	Yes	
282	0.2	6.0	16	β(1)	1	0	-25	+25	Yes	
283	0.2	6.0	18	β(1)	1	0	-25	+25	Yes	
284	0.2	6.0	20	β(1)	1	0	-25	+25	Yes	
285	0.2	6.0	25	β(1)	1	0	-25	+25	Yes	
286	0.2	6.0	30	β(1)	1	0	-25	+25	Yes	
287	0.2	6.0	35	β(1)	1	0	-25	+25	Yes	
288	0.2	6.0	40	β(1)	1	0	-25	+25	Yes	
289	0.2	6.0	-8	β(1)	1	+12	-25	+25	Yes	
290	0.2	6.0	-4	β(1)	1	+12	-25	+25	Yes	
291	0.2	6.0	0	β(1)	1	+12	-25	+25	Yes	
292	0.2	6.0	4	β(1)	1	+12	-25	+25	Yes	
293	0.2	6.0	8	β(1)	1	+12	-25	+25	Yes	
294	0.2	6.0	12	β(1)	1	+12	-25	+25	Yes	
295	0.2	6.0	14	β(1)	1	+12	-25	+25	Yes	
296	0.2	6.0	15	β(1)	1	+12	-25	+25	Yes	
297	0.2	6.0	16	β(1)	1	+12	-25	+25	Yes	
298	0.2	6.0	18	β(1)	1	+12	-25	+25	Yes	
299	0.2	6.0	20	β(1)	1	+12	-25	+25	Yes	
300	0.2	6.0	25	β(1)	1	+12	-25	+25	Yes	

RUN SCHEDULE

RUN NUMBER	MACH NUMBER	$R_e \times 10^{-6}$ (1/FT)	ALPHA SCHEDULE (DEG)	BETA SCHEDULE (DEG)	STING CONFIG. NUMBER	AILERON POSITION (δ_a, DEG)	ELEVATOR POSITION (δ_e, DEG)	RUDDER POSITION (δ_r, DEG)	GRIT	REMARKS
301	0.2	6.0	30	β(1)	1	+12	-25	+25	Yes	
302	0.2	6.0	35	β(1)	1	+12	-25	+25	Yes	
303	0.2	6.0	40	β(1)	1	+12	-25	+25	Yes	
304	0.2	6.0	-8	β(1)	1	0	0	0	No	
305	0.2	6.0	-4	β(1)	1	0	0	0	No	
306	0.2	6.0	0	β(1)	1	0	0	0	No	
307	0.2	6.0	4	β(1)	1	0	0	0	No	
308	0.2	6.0	8	β(1)	1	0	0	0	No	
309										No Run No. 309
310	0.2	6.0	12	β(1)	1	0	0	0	No	
311	0.2	6.0	14	β(1)	1	0	0	0	No	
312	0.2	6.0	15	β(1)	1	0	0	0	No	
313	0.2	6.0	16	β(1)	1	0	0	0	No	
314	0.2	6.0	18	β(1)	1	0	0	0	No	
315	0.2	6.0	20	β(1)	1	0	0	0	No	
316	0.2	6.0	25	β(1)	1	0	0	0	No	
317	0.2	6.0	30	β(1)	1	0	0	0	No	
318	0.2	6.0	35	β(1)	1	0	0	0	No	
319	0.2	6.0	40	β(1)	1	0	0	0	No	
320	0.2	6.0	30	β(2)	2	0	0	0	No	

RUN SCHEDULE

RUN NUMBER	MACH NUMBER	$R_e \times 10^{-6}$ (1/FT)	ALPHA SCHEDULE (DEG)	BETA SCHEDULE (DEG)	STING CONFIG. NUMBER	AILERON POSITION (δ_a, DEG)	ELEVATOR POSITION (δ_e, DEG)	RUDDER POSITION (δ_r, DEG)	GRIT	REMARKS
321	0.2	6.0	35	β(2)	2	0	0	0	No	
322	0.2	6.0	40	β(2)	2	0	0	0	No	
323	0.2	6.0	45	β(2)	2	0	0	0	No	
324	0.2	6.0	50	β(2)	2	0	0	0	No	
325	0.2	6.0	55	β(2)	2	0	0	0	No	
326	0.2	6.0	35	β(2)	2	0	+15	0	No	
327	0.2	6.0	40	β(2)	2	0	+15	0	No	
328	0.2	6.0	45	β(2)	2	0	+15	0	No	
329	0.2	6.0	50	β(2)	2	0	+15	0	No	
330	0.2	6.0	55	β(2)	2	0	+15	0	No	
331	0.2	6.0	35	β(2)	2	0	-25	0	No	
332	0.2	6.0	40	β(2)	2	0	-25	0	No	
333	0.2	6.0	45	β(2)	2	0	-25	0	No	
334	0.2	6.0	50	β(2)	2	0	-25	0	No	
335	0.2	6.0	55	β(2)	2	0	-25	0	No	
336	0.2	6.0	35	β(2)	2	0	-25	+25	No	
337	0.2	6.0	40	β(2)	2	0	-25	+25	No	
338	0.2	6.0	45	β(2)	2	0	-25	+25	No	
339	0.2	6.0	50	β(2)	2	0	-25	+25	No	
340	0.2	6.0	55	β(2)	2	0	-25	+25	No	

RUN SCHEDULE

RUN NUMBER	MACH NUMBER	$R_e \times 10^{-6}$ (1/FT)	ALPHA SCHEDULE (DEG)	BETA SCHEDULE (DEG)	STING CONFIG NUMBER	AILERON POSITION (δ_a, DEG)	ELEVATOR POSITION (δ_e, DEG)	RUDDER POSITION (δ_r, DEG)	GRIT	REMARKS
341	0.2	6.0	35	β(2)	2	+12	-25	+25	No	
342	0.2	6.0	40	β(2)	2	+12	-25	+25	No	
343	0.2	6.0	45	β(2)	2	+12	-25	+25	No	
344	0.2	6.0	50	β(2)	2	+12	-25	+25	No	
345	0.2	6.0	55	β(2)	2	+12	-25	+25	No	
346	0.2	6.0	35	β(2)	2	+12	0	0	No	
347	0.2	6.0	40	β(2)	2	+12	0	0	No	
348	0.2	6.0	45	β(2)	2	+12	0	0	No	
349	0.2	6.0	50	β(2)	2	+12	0	0	No	
350	0.2	6.0	55	β(2)	2	+12	0	0	No	
351	0.2	6.0	35	β(2)	2	-12	0	0	No	
352	0.2	6.0	40	β(2)	2	-12	0	0	No	
353	0.2	6.0	45	β(2)	2	-12	0	0	No	
354	0.2	6.0	50	β(2)	2	-12	0	0	No	
355	0.2	6.0	55	β(2)	2	-12	0	0	No	
356	0.2	6.0	35	β(2)	2	0	0	+25	No	
357	0.2	6.0	40	β(2)	2	0	0	+25	No	
358	0.2	6.0	45	β([illegible]	2	0	0	+25	No	
359	0.2	6.0	50		2	0	0	+25	No	
360	0.2	6.0	55	β(2)	2	0	0	+25	No	

RUN SCHEDULE

RUN NUMBER	MACH NUMBER	$R_e \times 10^{-6}$ (1/FT)	ALPHA SCHEDULE (DEG)	BETA SCHEDULE (DEG)	STING CONFIG. NUMBER	AILERON POSITION (δ_a, DEG)	ELEVATOR POSITION (δ_e, DEG)	RUDDER POSITION (δ_r, DEG)	GRIT	REMARKS
361	0.2	6.0	35	β(2)	2	0	0	-25	No	
362	0.2	6.0	40	β(2)	2	0	0	-25	No	
363	0.2	6.0	45	β(2)	2	0	0	-25	No	
364	0.2	6.0	50	β(2)	2	0	0	-25	No	
365	0.2	6.0	55	β(2)	2	0	0	-25	No	
366	0.2	6.0	30	β(2)	2	0	0	0	No	
367	0.2	6.0	35	β(2)	2	0	0	0	No	
368	0.2	6.0	40	β(2)	2	0	0	0	No	
369	0.2	6.0	45	β(2)	2	0	0	0	No	
370	0.2	6.0	50	β(2)	2	0	0	0	No	
371	0.2	6.0	55	β(2)	2	0	0	0	No	
372	0.2	6.0	62	β(2)	3	0	0	0	No	
373	0.2	6.0	67	β(2)	3	0	0	0	No	
374	0.2	6.0	72	β(2)	3	0	0	0	No	
375	0.2	6.0	77	β(2)	3	0	0	0	No	
376	0.2	6.0	83	β(2)	3	0	0	0	No	
377	0.2	6.0	62	β(2)	3	0	+15	0	No	
378	0.2	6.0	67	β(2)	3	0	+15	0	No	
379	0.2	6.0	72	β(2)	3	0	+15	0	No	
380	0.2	6.0	77	β(2)	3	0	+15	0	No	

RUN SCHEDULE

RUN NUMBER	MACH NUMBER	$R_e \times 10^{-6}$ (1/FT)	ALPHA SCHEDULE (DEG)	BETA SCHEDULE (DEG)	STING CONFIG. NUMBER	AILERON POSITION (δ_a, DEG)	ELEVATOR POSITION (δ_e, DEG)	RUDDER POSITION (δ_r, DEG)	GRIT	REMARKS
381	0.2	6.0	83	β(2)	3	0	+15	0	No	
382	0.2	6.0	62	β(2)	3	0	-25	0	No	
383	0.2	6.0	67	β(2)	3	0	-25	0	No	
384	0.2	6.0	72	β(2)	3	0	-25	0	No	
385	0.2	6.0	77	β(2)	3	0	-25	0	No	
386	0.2	6.0	83	β(2)	3	0	-25	0	No	
387	0.2	6.0	62	β(2)	3	0	0	-25	No	
388	0.2	6.0	67	β(2)	3	0	0	-25	No	
389	0.2	6.0	72	β(2)	3	0	0	-25	No	
390	0.2	6.0	77	β(2)	3	0	0	-25	No	
391	0.2	6.0	83	β(2)	3	0	0	-25	No	
392	0.2	6.0	62	β(2)	3	-12	0	0	No	
393	0.2	6.0	67	β(2)	3	-12	0	0	No	
394	0.2	6.0	72	β(2)	3	-12	0	0	No	
395	0.2	6.0	77	β(2)	3	-12	0	0	No	
396	0.2	6.0	83	β(2)	3	-12	0	0	No	
397	0.2	6.0	62	β(2)	3	+12	0	0	No	
398	0.2	6.0	67	β(2)	3	+12	0	0	No	
399	0.2	6.0	72	β(2)	3	+12	0	0	No	
400	0.2	6.0	77	β(2)	3	+12	0	0	No	

RUN SCHEDULE

RUN NUMBER	MACH NUMBER	$R_e \times 10^{-6}$ (1/FT)	ALPHA SCHEDULE (DEG)	BETA SCHEDULE (DEG)	STING CONFIG. NUMBER	AILERON POSITION (δ_a, DEG)	ELEVATOR POSITION (δ_e, DEG)	RUDDER POSITION (δ_r, DEG)	GRIT	REMARKS
401	0.2	6.0	83	β(2)	3	+12	0	0	No	
402	0.2	6.0	62	β(2)	3	0	0	+25	No	
403	0.2	6.0	67	β(2)	3	0	0	+25	No	
404	0.2	6.0	72	β(2)	3	0	0	+25	No	
405	0.2	6.0	77	β(2)	3	0	0	+25	No	
406	0.2	6.0	83	β(2)	3	0	0	+25	No	
407	0.2	6.0	62	β(2)	3	0	-25	+25	No	
408	0.2	6.0	67	β(2)	3	0	-25	+25	No	
409	0.2	6.0	72	β(2)	3	0	-25	+25	No	
410	0.2	6.0	77	β(2)	3	0	-25	+25	No	
411	0.2	6.0	83	β(2)	3	0	-25	+25	No	
412	0.2	6.0	62	β(2)	3	+12	-25	+25	No	
413	0.2	6.0	67	β(2)	3	+12	-25	+25	No	
414	0.2	6.0	72	β(2)	3	+12	-25	+25	No	
415	0.2	6.0	77	β(2)	3	+12	-25	+25	No	
416	0.2	6.0	83	β(2)	3	+12	-25	+25	No	

APPENDIX B
GEOMETRIC PARAMETERS OF FULL-SCALE T-2

APPENDIX B
GEOMETRIC PARAMETERS OF FULL-SCALE T-2
(from reference (c))

WING

S_W	Total area (includes flap, aileron and 39.39 ft^2 covered by fuselage)	254.86 ft^2
A_W	Net surface area (wetted)	424.85 ft^2
b_W	Span (perpendicular to plane of symmetry) including tiptanks	38.13 ft
AR_w	Aspect Ratio	5.07
λ_w	Taper Ratio	.496
Γ_w	Dihedral Angle	+3°
	Chord (in streamline direction)	
c_r	Root (Wing Sta. 0)	114.20 in
c_t	Tip Chord (Wing Sta. 214.242)	56.63 in
	(Equivalent)	
$\bar{c}_w$	Mean aerodynamic chord	88.88 in
	(Wing Sta. 95.078)	
	Location of 25% MAC	F.S. 219.697
Λ_w	Sweepback of 25% element	2°17'
i_w	Incidence angle	
	Root Chord	2°
	Tip Chord	-1°
	Airfoil Section (root and tip in streamline direction)	NASA64_1A212 2 = .8* (MOD) (flaps and ailerons rigged 3° up)
	*NAA Modified	
Ω_w	Rate of Taper	0.2671

Preceding page blank

FLAP (Data for One)

	Type	Single Slotted
S_f	Area	22.78 ft^2
b_f	Span (perpendicular to plane of symmetry)	101.75 in
c_i	Inboard chord (Wing Sta. 27.09)	39.39 in
c_o	Outboard chord (Wing Sta. 127.54)	29.63 in
c_f/c_w	Ratio flap chord to wing chord (avg.)	.37
$b_f/b_{\frac{w}{2}}$	Ratio flap span to wing semi-span	.475
δ_f	Flap deflection, maximum (from uprigged position)	33°
	Flap in neutral position	3° Up

AILERON

	Type	Straight Sided
S_a	Area (aft of hinge line and including tab)	9.5 ft^2
b_a	Span (perpendicular to plane of symmetry)	79.57 in
c_i	Inboard chord (Wing Sta. 128.69)	20 in
c_o	Outboard chord (Wing Sta. 208.26)	14.66 in
c_a/c_w	Ratio aileron chord (aft H.L.) to wind chord	.25
$b_a/b_{\frac{w}{2}}$	Ratio aileron span to wind semi-span	.374
δ_a	Aileron deflection, maximum (from neutral position)	-12° Up, +13° Dn
	Aileron in neutral position	3° Up
	Aerodynamic Balance	Sealed paddle balance
S_b	Balance area forward of the H.L. (including 50% of fabric seal)	4.45 ft^2
c_b/c_a	Ratio balance chord to aileron chord	.42

AILERON - (Cont'd)

	Static balance	Weighted paddle balance
	Irreversible full power system	Hydraulic

AILERON TRIM TAB

	Ground adjustable fixed tab on each aileron	
S_a	Area (each)	.07 ft^2

HORIZONTAL TAIL*

S_h	Total area (includes 3.07 ft^2 covered by vertical tail and fairing)	72.29 ft^2
S_{net_h}	Net area	69.22 ft^2
A_h	Net surface area (wetted)	146.38 ft^2
b_h	Span	17.91 ft
AR_h	Aspect Ratio	4.42
λ_h	Taper Ratio	0.50
Γ_h	Dihedral Angle	0°
Λ_h	Sweepback of 25% element	15°
	Chord (in streamline direction)	
c_r	Root (H.T. Sta. 0)	64.61 in
c_t	Equivalent tip chord	33.05 in
	(H.T. Sta. 106.488)	
$\bar{c}_h$	Mean aerodynamic chord	50.447 in
	(H.T. Sta. 47.78)	
i_h	Incidence angle	0°
	Airfoil section (root and tip in streamline direction)	NASA 65A012

*Percent lines base on horizontal prior to addition of trailing edge extension.

HORIZONTAL TAIL - (Cont'd)

l_h	Tail length (.25 $\bar{c}_w$ to .25 $\bar{c}_h$)	202.58 in

HORIZONTAL STABILIZER

S_s	Area stabilizer, total	42.5 ft^2
i_s	Stabilizer incidence angle	0°

ELEVATOR

S_e	Total area (excluding balance area forward of the hinge line)	21.00 ft^2
b_e	Span (between equivalent chords) (one elevator only)	101.97 in
c_i	Inboard chord (B.P. 3.906)	18.85 in
c_o	Outboard chord (B.P. 105.877)	10.52 in
c_e/c_h	Ratio elevator chord (aft H.L.) to horizontal tail chord	.310
b_e/b_h	Ratio elevator span to horizontal tail span	0.936
δ_e	Elevator deflection maximum	27° Up, 15° Dn
	Boost: Push force 2.95:1 Pull force 2.95:1 to 8 lbs then 6.0:1	Hydraulic
	Static balance	Weighted Leading Edge
	Aerodynamic balance	Overhang
S_b	Balance area forward of hinge line	5.72 ft^2
c_b/c_e	Ratio balance chord to elevator chord	0.322
	Nose factor	0.60
	Point of tangency for nose factor is at elevator hinge line	

ELEVATOR TRIM TAB

S_t	Area (each)	2.36 ft^2
b_t	Span, Equivalent (B.P. 8.93 to 54.53)	46.10 in
c_t	Chord, constant	6.5 in
b_t/b_e	Ratio tab span to elevator span	0.462 in
δ_t	Tab deflection	L.H. 10° Up, 13° Dn R.H. 0° Up, 13° Dn

VERTICAL TAIL

S_v	Total area (includes 4.38 ft^2 blanketed by fuselage plus 2.14 ft^2 blanketed by horizontal tail)	40.33 ft^2
S_{net_v}	Net area	33.86 ft^2
A_v	Net surface area (wetted)	79.18 ft^2
A_d	Net surface area of dorsal fin (wetted)	18.12 ft^2
b_v	Span, unblanketed	8.04 ft
AR_v	Aspect Ratio	1.80
λ_v	Taper Ratio	.375
c_r	Chord (in streamline direction)	
	Root (W.P. + 33.000)	78.14 in
c_t	Equivalent Tip Chord (W.P. + 129.41)	29.38 in
$\bar{c}_v$	Mean aerodynamic chord (W.P. + 73.92)	58.47 in
Λ_v	Sweepback (25% chord)	30°
	Airfoil Section	NASA 63A012
l_v	Tail length (.25 $\bar{c}_w$ to .25 $\bar{c}_v$)	194.05 in

VERTICAL FIN

S_f	Area (including 2.14 ft^2 blanketed by horizontal tail and excluding dorsal fin)	29.87

VERTICAL FIN (Cont'd)

i_f	Angle with respect to airplane plane of symmetry	0°

RUDDER

S_r	Total area	9.13 ft^2
	S_{r_u} Upper surface	3.23 ft^2
	S_{r_l} Lower surface	5.90 ft^2
b_r	Span, equivalent	
	b_{r_u} Upper surface	31.94 in
	b_{r_l} Lower surface	42.99
c_{r_u}	Upper chord (W.P. 96.00)	12.59 in
c_{r_l}	Lower chord (W.P. + 9.91)	22.45 in
c_r/c_v	Ratio rudder chord (aft H.L.) to vertical tail chord	
	c_r/c_v Upper surface @ W.P. 96.00	.266
	c_r/c_v Lower surface	.250
δ_r	Rudder deflection, maximum	25° Rt., 25° Lt.
	Boost	None
	Aerodynamic balance	Overhang
S_b	Balance area forward of hinge line	2.41 ft^2
c_b/c_r	Ratio balance chord to rudder chord	
	c_b/c_{r_u} Upper surface @ W.P. 96.00	.234
	c_b/c_r Lower surface	.24
	Static balance	Weighted leading edge
	Nose factor	0.40
	Point of tangency for nose factor is at rudder hinge line	

RUDDER TRIM TAB

S_t	Area	1.60 ft^2
b_t	Span, equivalent (W.P. 14.94 to W.P. 53.00)	38.06 in
c_t	Chord, constant	6.0 in
b_t/b_r	Ratio tab span to rudder span	.508
δ_t	Tab deflection, maximum	7° Rt., 7° Lt.

FUSELAGE

l_f	Length (actual)	34.58 ft
F_f	Maximum frontal area (basic fuselage)	15.75 ft^2
w_f	Maximum width (basic fuselage) F.S. 169	54 in
h_f	Maximum depth	
	Basic fuselage over canopy (F.S. 169)	88.1 in
	Including ducts (F.S. 214)	73.9 in
A_f	Net surface area	221.11 ft^2
L/D	Fineness ratio (actual)	5.91

CANOPY

l_c	Length (actual)	19.75 ft
F_c	Maximum frontal area	3.70 ft^2
A_c	Net surface area	73.10 ft^2
L/D_c	Fineness ratio (actual)	8.8

NACELLE

l_n	Length (actual)	23.71 ft
F_n	Maximum frontal area	10.50 ft^2
A_n	Net surface area	206.0 ft^2
	Inlet area (includes gutters)	3.1 ft^2
L/D_n	Fineness ratio (actual)	5.025

SPEED BRAKE (Data for one side only)

	Type	One Piece
	Location	Side of Aft Fuselage
	Number	Two
S_j	Area (Planform)	8.00 ft^2
F_j	Area (frontal)	4.24 ft^2
δ_j	Maximum deflection	32°

TIP TANK (Data for one tank only)

l_{tt}	Overall length	142.75 in
d_{tt}	Maximum diameter (Tank Sta. 61.875)	20.00 in
L/D	Fineness ratio	7.14
Ss_{tt}	Side area (projected)	14.1 ft^2
Sp_{tt}	Planform area (projected)	14.2 ft^2
	Volume	15.3 ft^3
A_{tt}	Total Surface Area	44.30 ft^2
$A_{net_{tt}}$	Net Surface Area (wetted)	42.40 ft^2

APPENDIX C
SELECTED EXCERPTS FROM BAR REPORT

Wind Tunnel Tests of a 9 Percent Scale T-2C Model at the NASA Ames Research Center 12-Foot Pressure Tunnel, Final Data Acquisition Report

by William Bihrle, Jr.
Bihrle Applied Research, Inc.
Oyster Bay, N.Y. 11771

Dated 20 August 1973. Prepared under contract N62269-73-C-0687. Report number 73-20.

Reynolds Number Effect

Tables C-I, C-II, and C-III in this section present tabulated values of C_m, C_ℓ, and C_n, respectively for a range of angles of attack and sideslip angles as a function of Reynolds number.

It can be seen in Table C-I that no significant change in pitch is realized with varying Reynolds number at and below 12 degrees angle of attack. Above α = 12 degrees, the influence of Reynolds numbers can be detected. The magnitude of this Re effect is illustrated in Figures C-1, C-2, C-3, C-4, and C-5 at β = 0, -10, 10, 20, and 30 degrees, respectively. It should be noted that the Re effect is magnified in these figures since the pitching moment coefficient is plotted to a .05/inch (normally plotted .10/inch) scale. In all instances it can be seen that the largest variation is obtained between the 1.0 and 6.0 X 10^6/ft Reynolds number data.

The reason that Reynolds number plays a significant role only above 12 degrees angle of attack can be obtained from Figure C-6 which presents the lift coefficient as a function of angle of attack. This figure shows that:

a. the lift curve is linear throughout the unstalled angle-of-attack region and is unaffected by Reynolds number above 1.0 X 10^6/ft.

b. the angle of attack at which stall occurs and the magnitude of $C_{L_{MAX}}$ are directly related to the value of the Reynolds number. Consequently, the stall angle is in the vicinity of 12.5 and 14.5 degrees for a Reynolds number of 1.0 and 6.0 X 10^6/ft, respectively. The corresponding values for $C_{L_{MAX}}$ are 1.02 and 1.19.

c. the greatest discrepancy from the Re = 6.0 X 10^6/ft data occurs at Re = 1.0 X 10^6/ft. The magnitude of this discrepancy is appreciably reduced for Re values of 3.0 X 10^6/ft and above.

Preceding pages blank

Obviously, the stall pattern of the wing associated with a given value of Reynolds numbers is responsible for the observed pitching moment variation with Reynolds numbers.

On Tables C-II and C-III boundaries have been drawn. The values below these boundaries deviate more than ±5 percent (an arbitrary value) from the values obtained at Re = 6.0 X 10^6/ft. It can be seen that the roll and yaw characteristics fall within this tight band for all values of Reynolds number above 1.0 X 10^6/ft below stall. However, for all intents and purposes, from stall to 40 degrees angle of attack the Re = 6.0 X 10^6/ft data cannot be duplicated consistently within 5 percent for any Re value less than 6.0 X 10^6/ft. This tabulated data can also be examined for values of β = -10, 10° and β = 0, 20, 30° in Figures C-7 and C-8, respectively for roll and Figures C-9 and C-10, respectively for yaw. From these figures it can be seen that

a. both roll and yaw are unaffected (although not within the 5% band) by Reynolds number at α = 40 degrees within the β = ±10 range.

b. Reynolds number has its largest influence on both roll and yaw between stall and 20 degrees angle of attack.

c. the left model wing panel stalls before the right panel.

d. both roll and yaw are significantly affected by Reynolds number at α = 40 degrees when β = 30 degrees.

From these initial tests, it was apparent that the full-scale aerodynamic characteristics could be realized with the 9 percent T-2C model for angles of attack below stall at a Reynolds number of 2.0 X 10^6/ft. However, the angle of attack at which stall occurs was dependent on the magnitude of the Reynolds number and all the aerodynamic characteristics were significantly influenced by the stall characteristics.

Based on these results, it was deemed necessary that all the T-2C control configurations be tested at a Reynolds number of 6.0 X 10^6/ft since the complete angle of attack range (i.e., -8 to 40°) was to be run during a given test.

Effect of Transition Grit Pattern

Again, because the complete angle of attack range of -8 to 40 degrees was to be run during a given test, grit was applied both to the fuselage and airfoil sections in the manner previously described. The significance of having this grit pattern on the model was determined by testing the $\delta_e = \delta_r = \delta_a = 0°$ configuration without grit at a Reynolds number of 6.0 X 10^6/ft.

From Figure C-11 it would appear that transition was set with the applied grit since C_{D_O} is higher with the transition band. Since the model had no ducting, inlet spillage associated with a given mass flow, base drag, etc. were not simulated and the absolute values of drag measured during these tests are,

therefore, not significant. It can be seen in Figure C-6 that the lift versus angle of attack relationship was unaffected by grit. Since it was found (see previous section) that the wing stall pattern influenced the pitching, rolling, and yawing moment characteristics of the T-2C configuration, one would expect that the moments measured without grit would be the same as those obtained with the grit pattern.

Tables C-IV, C-V, and C-VI in this section present tabulated values of C_m, C_ℓ, and C_n, respectively for a range of angles of attack and sideslip angles as a function of grit being on or off the model.

This tabulated data can also be examined for sideslip values of -10, 0, 10, 20 and 30 degrees in Figures C-12 through C-15. The effect of grit on the yawing moment in Figures C-14 and C-13, respectively. An inspection of these tables or figures indicates the premise based on the lift characteristics to be correct. Except for a few isolated data points just above stall, the data obtained without the grit transition pattern duplicates the data obtained with grit throughout the angle-of-attack range. On this bases, the model tests with sting 002 and 003 were conducted with a clean model.

The significance of these results cannot be conclusively stated since a Reynolds number variation was not conducted with the clean model. (Although these tests had been scheduled they were deleted because of program slippages that resulted from model, instrumentation and tunnel problems.) One could conclude that these results indicate that supercritical flow conditions had been realized at or in the vicinity of a Reynolds number of 5.0 X 10^6/ft. On the other hand, the position could be taken that the grit pattern was not applied in an optimum fashion (whatever that might be) and that the Reynolds number variation obtained with the gritted model would have been duplicated with the clean model. If the later were the case, the full-scale stalled aerodynamic characteristics may not necessarily have been obtained. The inability to demonstrate conclusively that the full-scale stalled aerodynamic characteristics have been documented during a wind tunnel investigation is a problem which confronts all investigators. The T-2C configuration fortunately seems to be sensitive to Reynolds number in a very limited angle of attack range (i.e., between 14 and 20 degrees). Although the author is inclined to conclude that supercritical flow conditions were achieved during these tests, it is recommended that this opinion be further substantiated with a very short wind tunnel investigation. This recommendation is being made only in light of the needs of the parameter identification program.

Repeatability

Tables C-IV, C-V, and C-VI tabulate data that were obtained several times during the investigation for the basic (i.e., $\delta_e = \delta_a = \delta_r = 0^\circ$) gritted model at a Reynolds number of 6.0 X 10^6/ft. It can be seen that these data fall well within the accuracy commonly expected during a wind tunnel investigation. In fact, the comparison between data obtained with the gritted and clean model (see Figures C-12 through C-15) can also be used to illustrate this point.

Table C-I Tabulation of C_n as a Function of α and β for a Range of Reynolds Numbers (Configuration [illegible]).

α (deg)	$R_e \times 10^{6}$ (/ft)	β = -10 (deg)	0 (deg)	2 (deg)	5 (deg)	10 (deg)	15 (deg)	20 (deg)	25 (deg)	30 (deg)
6	6.0	-.0581	-.0202	-.0229	-.0321	-.0567	-.0503	-.0682	-.0650	-.0655
	5.0	-.0572	-.0118	-.0147	-.0216	-.0482	-.0419	-.0610	-.0570	-.0564
	4.0	-.0473	-.0082	-.0094	-.0187	-.0429	-.0357	-.0457	-.0491	-.0518
	3.0	-.0480	-.0103	-.0129	-.0237	-.0457	-.0405	-.0485	-.0528	-.0565
	2.0	-.0412	-.0026	-.0051	-.0135	-.0359	-.0316	-.0357	-.0437	-.0465
	1.0	-.0309	.0046*	.0011	-.0002	-.0274	-.0152	-.0249	-.0221	-.0331
8	6.0	-.1954	-.1534	-.1569	-.1657	-.1937	-.1535	-.1555	-.1456	-.1159
	5.0	-.1850	-.1442	-.1480	-.1551	-.1849	-.1436	-.1449	-.1364	-.1051
	4.0	-.1851	-.1448	-.1482	-.1555	-.1819	-.1394	-.1391	-.1339	-.1005
	3.0	-.1922	-.1546	-.1568	-.1641	-.1889	-.1452	-.1453	-.1330	-.1069
	2.0	-.1885	-.1491	-.1526	-.1592	-.1800	-.1348	-.1361	-.1246	-.0987
	1.0	-.1795	-.1520	-.1496	-.1556	-.1786	-.1408	-.1350	-.1001	-.0951
12	6.0	-.2701	-.2264	-.2248	-.2407	-.2666	-.2656	-.2168	-.2353	-.2191
	5.0	-.2627	-.2195	-.2212	-.2312	-.2576	-.2567	-.2386	-.2218	-.2071
	4.0	-.2560	-.2146	-.2179	-.2291	-.2549	-.2496	-.2317	-.2129	-.1964
	3.0	-.2601	-.2189	-.2227	-.2339	-.2610	-.2451	-.2346	-.2149	-.2013
	2.0	-.2532	-.2163	-.2202	-.2334	-.2473	-.2350	-.2254	-.2027	-.1917
	1.0	-.2581	-.2210	-.2261	-.2380	-.2371	-.2300	-.2055	-.1728	-.1553
16	6.0	-.3579	-.3218	-.3194	-.3418	-.3515	-.3245	-.3048	-.2957	-.2913
	5.0	-.3474	-.3011	-.3098	-.3274	-.3281	-.3127	-.3008	-.2795	-.2731
	4.0	-.3170	-.2989	-.2994	-.3129	-.3140	-.2938	-.2832	-.2655	-.2728
	3.0	-.3321	-.2900	-.2900	-.3002	-.3058	-.2872	-.2783	-.2614	-.2655
	2.0	-.2927	-.2746	-.2733	-.2847	-.2974	-.2874	-.2830	-.2556	-.2592
	1.0	-.2875	-.2574	-.2521	-.2598	-.2713	-.2700	-.2560	-.2203	-.2164
20	6.0	-.4249	-.3489	-.3391	-.3505	-.3634	-.3752	-.4040	-.3590	-.3579
	5.0	-.4114	-.3408	-.3328	-.3374	-.3493	-.3585	-.3745	-.3369	-.3451
	4.0	-.3682	-.3346	-.3374	-.3463	-.3411	-.3554	-.3723	-.3441	-.3406
	3.0	-.3588	-.3275	-.3255	-.3369	-.3378	-.3560	-.3772	-.3442	-.3577
	2.0	-.3321	-.2157	-.3297	-.3177	-.3314	-.3669	-.3687	-.3375	-.3462
	1.0	-.3190	-.2721	-.2871	-.2874	-.3022	-.3361	-.3446	-.2969	-.2901
40	6.0	-.5710	-.6057	-.5967	-.5522	-.5607	-.5469	-.5002	-.3937	-.3648
	5.0	-.5563	-.5832	.5816	-.5676	-.5471	-.5265	-.4575	-.4320	-.4000
	4.0	-.5468	-.5746	-.5713	-.5626	-.5455	-.5257	-.4866	-.4450	-.4218
	3.0	-.5467	-.5732	-.5715	-.5633	-.5344	-.5322	-.4449	-.4538	-.4525
	2.0	-.5342	-.5566	-.5526	-.5492	[illegible]	-.5045	-.4797	-.4422	-.4428
	1.0	-.5245	-.5446	-.5346	-.5233	-.4144	-.4524	-.4369	-.3119	-.2537

*Bad data point

Table C-II Tabulation of C_l as a Function of α and β for a Range of Reynolds Numbers (Clark-Y Model).

α_u (deg)	R_e $\times 10^{-6}$ (/ft)	β: -10 (deg)	0 (deg)	2 (deg)	5 (deg)	10 (deg)	15 (deg)	20 (deg)	25 (deg)	30 (deg)
0	6.0	.0211	-.0019	-.0060	-.0129	-.0240	-.0329	-.0428	-.0497	-.0568
	5.0	.0201	-.0019	-.0070	-.0134	-.0244	-.0335	-.0431	-.0501	-.0567
	4.0	.0212	-.0014	-.0059	-.0131	-.0239	-.0325	-.0424	-.0496	-.0558
	3.0	.0211	-.0017	-.0060	-.0133	-.0241	-.0330	-.0427	-.0496	-.0558
	2.0	.0210	-.0011	-.0059	-.0129	-.0241	-.0326	-.0421	-.0494	-.0554
	1.0	.0207	-.0006	-.0055	-.0121	-.0233	-.0317	-.0432	-.0504	-.0565
8	6.0	.0209	-.0020	-.0070	-.0144	-.0247	-.0331	-.0401	-.0451	-.0488
	5.0	.0203	-.0019	-.0068	-.0139	-.0253	-.0334	-.0407	-.0456	-.0489
	4.0	.0212	-.0016	-.0065	-.0139	-.0247	-.0331	-.0408	-.0458	-.0487
	3.0	.0210	-.0020	-.0068	-.0142	-.0250	-.0329	-.0412	-.0458	-.0487
	2.0	.0205	-.0022	-.0068	-.0139	-.0244	-.0319	-.0397	-.0448	-.0478
	1.0	.0207	-.0012	-.0061	-.0121	-.0219	-.0315	-.0388	-.0459	-.0505
12	6.0	.0207	-.0022	-.0072	-.0148	-.0251	-.0330	-.0347	-.0412	-.0457
	5.0	.0207	-.0022	-.0071	-.0144	-.0249	-.0331	-.0364	-.0418	-.0458
	4.0	.0206	-.0015	-.0065	-.0138	-.0244	-.0328	-.0366	-.0422	-.0456
	3.0	.0192	-.0033	-.0080	-.0155	-.0254	-.0282	-.0375	-.0427	-.0459
	2.0	.0194	-.0028	-.0075	-.0148	-.0153	-.0266	-.0367	-.0415	-.0452
	1.0	.0197	.0005	-.0035	-.0071	-.0146	-.0267	-.0385	-.0434	-.0487
16	6.0	.0009	-.0277	.0097	.0008	-.0154	-.0327	-.0451	-.0482	-.0495
	5.0	.0215	-.0127	.0070	-.0018	-.0144	-.0369	-.0496	-.0566	-.0610
	4.0	.0170	.0079	.0024	.0060	-.0164	-.0361	-.0531	-.0598	-.0627
	3.0	.0260	.0074	.0022	-.0059	-.0214	-.0406	-.0539	-.0578	-.0616
	2.0	.0252	.0061	.0020	-.0066	-.0233	-.0376	-.0469	-.0538	-.0612
	1.0	.0235	.0001	-.0068	-.0162	-.0284	-.0406	-.0488	-.0538	-.0636
20	6.0	.0134	-.0111	-.0146	-.0191	-.0291	-.0448	-.0601	-.0788	-.0866
	5.0	.0144	-.0112	-.0134	-.0188	-.0286	-.0407	-.0597	-.0792	-.0871
	4.0	.0049	-.0123	-.0094	-.0194	-.0373	-.0556	-.0672	-.0731	-.0842
	3.0	.0261	-.0013	-.0043	-.0088	-.0315	-.0493	-.0650	-.0713	-.0805
	2.0	.0262	.0051	.0009	-.0097	-.0298	-.0466	-.0604	-.0689	-.0795
	1.0	.0248	-.0017	.0021	-.0186	-.0305	-.0466	-.0597	-.0673	-.0787
[illegible]	6.0	.0210	-.0020	-.0083	-.0166	-.0279	-.0386	-.0438	-.0519	-.0515
	5.0	.0225	-.0036	-.0094	-.0154	-.0282	-.0410	-.0472	-.0565	-.0627
	4.0	.0234	-.0035	-.0085	-.0167	-.0315	-.0418	-.0495	-.0615	-.0668
	3.0	.0258	-.0034	-.0094	-.0191	-.0316	-.0430	-.0537	-.0675	-.0747
	2.0	.0218	-.0061	-.0103	-.0202	-.0310	-.0443	-.0545	-.0674	-.0771
	1.0	.0234	-.0055	-.0104	-.0183	-.0287	-.0378	-.0489	-.0531	-.0574

Table C-III [illegible] Values of C_n as a Function of α and β for a [illegible]

α (deg)	$R_e \times 10^{-6}$ (1/ft)	β −10 (deg)	0 (deg)	2 (deg)	5 (deg)	10 (deg)	15 (deg)	20 (deg)	25 (deg)	30 (deg)
0	6.0	-.0145	.0002	.0031	.0083	.0147	.0185	.0299	.0377	.0441
	5.0	-.0145	.0001	.0034	.0083	.0150	.0188	.0300	.0375	.0448
	4.0	-.0146	-.0003	.0031	.0080	.0145	.0180	.0294	.0374	.0431
	3.0	-.0147	-.0003	.0032	.0081	.0145	.0182	.0289	.0367	.0433
	2.0	-.0149	-.0008	.0030	.0079	.0142	.0185	.0283	.0370	.0434
	1.0	-.0151	-.0012	.0027	.0079	.0150	.0201	.0349	.0425	.0474
8	6.0	-.0179	0	.0042	.0096	.0175	.0167	.0271	.0373	.0436
	5.0	-.0172	.0004	.0041	.0097	.0176	.0168	.0272	.0371	.0432
	4.0	-.0172	.0001	.0041	.0095	.0172	.0163	.0271	.0365	.0428
	3.0	-.0168	.0001	.0042	.0096	.0168	.0161	.0270	.0366	.0429
	2.0	-.0169	-.0005	.0040	.0096	.0169	.0159	.0267	.0366	.0435
	1.0	-.0159	-.0002	.0031	.0101	.0172	.0182	.0288	.0411	.0463
12	6.0	-.0176	0	.0046	.0108	.0196	.0250	.0271	.0386	.0438
	5.0	-.0172	.0003	.0047	.0108	.0192	.0245	.0289	.0388	.0433
	4.0	-.0169	.0002	.0045	.0107	.0184	.0233	.0282	.0375	.0427
	3.0	-.0172	-.0006	.0039	.0095	.0169	.0154	.0277	.0376	.0426
	2.0	-.0171	-.0003	.0044	.0097	.0060	.0154	.0275	.0371	.0432
	1.0	-.0165	.0008	.0076	.0086	.0092	.0175	.0303	.0408	.0453
16	6.0	-.0040	.0017	-.0052	-.0043	-.0031	.0048	.0221	.0282	.0332
	5.0	-.0104	.0034	-.0057	-.0061	-.0005	.0061	.0189	.0260	.0291
	4.0	-.0028	.0061	.0048	-.0033	-.0003	.0088	.0188	.0242	.0293
	3.0	-.0136	-.0058	-.0033	-.0016	-.0002	.0082	.0153	.0212	.0335
	2.0	-.0047	-.0061	-.0041	-.0031	-.0014	.0060	.0129	.0264	.0397
	1.0	-.0020	-.0025	-.0002	.0011	.0003	.0050	.0140	.0280	.0414
20	6.0	-.0002	.0048	.0064	.0079	.0097	.0168	.0186	.0262	.0369
	5.0	-.0010	.0044	.0056	.0073	.0098	.0165	.0225	.0262	.0396
	4.0	-.0027	.0010	.0007	.0034	.0033	.0055	.0164	.0253	.0405
	3.0	-.0057	-.0004	.0004	.0006	.0028	.0075	.0156	.0263	.0415
	2.0	-.0043	-.0053	-.0035	.0003	.0025	.0051	.0125	.0252	.0409
	1.0	-.0069	.0005	-.0018	.0062	.0094	.0072	.0140	.0270	.0426
40	6.0	-.0202	.0015	.0065	.0127	.0219	.0345	.0405	.0479	.0377*
	5.0	-.0207	.0015	.0074	.0108	.0208	.0348	.0444	.0554	.0602
	4.0	-.0225	.0007	.0062	.0134	.0230	.0391	.0474	.0596	.0634
	3.0	-.0241	.0009	.0076	.0123	.0238	.0403	.0489	.0641	.0746
	2.0	-.0214	.0030	.0095	.0140	.0229	.0371	.0475	.0597	.0737
	1.0	-.0193	.0025	.0078	.0137	.0243	.0337	.0454	.0466	.0411

*Bad data point.

C-IV [illegible] α [illegible] β [illegible]

α (deg)	CRIT	β (deg) -10	0	[illegible]	5	10	15	20	25	30
-8	OFF	.0706	.1103	.1033	.0976	.0674	.0501	.0354	.0173	[illegible]
↓	ON	.0683	.1067	.1050	.0980	.0712	.0557	.0423	.0417	.0199
-4	OFF	-.0205	.0313	.0345	.0207	.0002	-.0102	-.0317	-.0315	-.0107
↓	ON	.0021	.0440	.0415	.0317	.0062	.0005	-.0225	-.0258	-.0345
0	OFF	-.0731	-.0371	-.0402	-.0480	-.0694	-.0650	-.0785	-.0755	-.0716
	ON	-.0691	-.0307	-.0322	-.0408	-.0630	-.0569	-.0710	-.0671	-.0682
		-.0619	-.0242	-.0255	-.0349	-.0568	-.0528	-.0673	-.0657	-.0607
↓	↓	-.0581	-.0202	-.0229	-.0321	-.0567	-.0503	-.0682	-.0650	-.0655
4	OFF	-.1452	-.1069	-.1098	-.1178	-.1356	-.1097	-.1164	-.1091	-.0979
↓	ON	-.1399	-.0980	-.1005	-.1102	-.1287	-.1035	-.1107	-.1038	-.0938
8	OFF	-.2128	-.1724	-.1753	-.1836	-.2060	-.1977	-.1582	-.1479	-.1132
	ON	-.2014	-.1617	-.1642	-.1720	-.1961	-.1529	-.1555	-.1423	-.1157
↓	↓	-.1954	-.1534	-.1569	-.1657	-.1937	-.1535	-.1555	-.1456	-.1159
12	OFF	—	-.2427	-.2449	-.2520	-.2777	-.2791	-.2515	-.2307	-.2177
	ON	-.2738	-.2330	-.2369	-.2463	-.2711	-.2684	-.2466	-.2272	-.2107
↓	↓	-.2704	-.2264	-.2298	-.2407	-.2666	-.2656	-.2168	-.2353	-.2191
14	OFF	-.3177	-.2827	-.2850	-.2951	-.3273	-.2936	-.2802	-.2685	-.2733
↓	ON	-.3085	-.2743	-.2743	-.2860	-.3194	-.2848	-.2776	-.2641	-.2707
15	OFF	-.3385	-.3155	-.3033	-.3414	-.3428	-.3118	-.2990	-.2896	-.2966
	ON	-.3297	-.2911	-.3170	-.3331	-.3401	-.3034	-.2939	-.2840	-.2938
↓	↓	-.3323	-.2975	-.2917	-.3330	-.3393	-.3031	-.2907	-.2840	-.2925
16	OFF	-.3632	-.3246	-.3335	-.3560	-.3641	-.3338	-.3049	-.2925	-.3035
	ON	-.3538	-.3191	-.3204	-.3475	-.3592	-.3240	-.3030	-.2896	-.3067
		-.3583	-.3257	-.3263	-.3494	-.3623	-.3216	-.3079	-.3006	-.3088
↓	↓	-.3519	-.3218	-.3194	-.3418	-.3515	-.3245	-.3048	-.2957	-.2913
18	OFF	-.4042	-.3623	-.3629	-.3688	-.3580	-.3563	-.3422	-.3191	-.3235
↓	ON	-.3701	-.3418	-.3448	-.3540	-.3557	-.3707	-.3433	-.3175	-.3201
20	OFF	-.4266	-.3418	-.3383	-.3434	-.3622	-.3811	-.3945	-.3675	-.3663
	ON	-.4271	-.3499	-.3466	-.3487	-.3556	-.3816	-.3751	-.3540	-.3626
↓	↓	-.4249	-.3489	-.3371	-.3505	-.3634	-.3752	-.4040	-.3590	-.3579
25	OFF	-.4634	-.4436	-.4502	-.4467	-.4409	-.4569	-.4497	-.4417	-.4453
↓	ON	-.4553	-.4424	-.4311	-.4334	-.4344	-.4475	-.4452	-.4317	[illegible]
30	OFF	-.4832	-.4950	-.4941	-.4744	-.4713	-.4715	-.4413	-.4697	[illegible]
↓	ON	-.4748	-.4958	-.4763	-.4900	-.4809	-.4645	-.4239	-.4559	-.4556
35	OFF	-.5237	-.5573	-.5554	-.5473	-.5126	-.4939	-.4645	-.4522	[illegible]
↓	ON	-.5187	-.5548	-.5515	-.5442	-.5133	-.4922	-.4603	-.4238	[illegible]
40	OFF	-.5627	-.6076	-.6031	-.5844	-.5611	-.5397	-.5087	-.4514	[illegible]
	ON	-.5618	-.5965	-.5933	-.5864	-.5580	-.5421	-.4951	-.4332	[illegible]
↓	↓	-.5710	-.6051	-.5961	-.5822	-.5601	-.5469	-.5002	-.3937	[illegible]

Table [illegible] Tabulation of C_l as a Function of α and β for a Gritted and Clean Model at a Reynolds Number of 6.0×10^6/ft.

α_u (deg)	GRIT	β (deg)								
		-10	0	2	5	10	15	20	25	30
-8	OFF	.0197	-.0026	-.0077	-.0141	-.0256	-.0352	-.0468	-.0538	-.0622
	ON	.0194	-.0025	-.0072	-.0142	-.0251	-.0351	-.0471	-.0539	-.0615
-4	OFF	.0199	-.0025	-.2071	-.0143	-.0257	-.0348	-.0452	-.0521	-.0597
	ON	.0194	-.0026	-.0071	-.0139	-.0255	-.0341	-.0452	-.0518	-.0588
0	OFF	.0200	-.0028	-.0077	-.0147	-.0258	-.0345	-.0445	-.0516	-.0572
	ON	.0201	-.0027	-.0077	-.0147	-.0258	-.0346	-.0448	-.0514	-.0568
		.0208	-.0021	-.0065	-.0136	-.0250	-.0341	-.0439	-.0507	-.0568
		.0211	-.0019	-.0060	-.0129	-.0240	-.0329	-.0428	-.0497	-.0568
4	OFF	.0197	-.0027	-.0078	-.0152	-.0260	-.0345	-.0430	-.0491	-.0539
	ON	.0200	-.0028	-.0078	-.0151	-.0256	-.0342	-.0426	-.0487	-.0533
8	OFF	.0197	-.0032	-.0085	-.0154	-.0264	-.0349	-.0411	-.0465	-.0495
	ON	.0206	-.0027	-.0073	-.0148	-.0254	-.0333	-.0408	-.0454	-.0487
		.0209	-.0020	-.0070	-.0144	-.0247	-.0331	-.0401	-.0451	-.0488
12	OFF	——	-.0029	-.0085	-.0159	-.0261	-.0340	-.0365	-.0424	-.0457
	ON	.0206	-.0027	-.0074	-.0151	-.0254	-.0332	-.0361	-.0410	-.0452
		.0207	-.0022	-.0072	-.0148	-.0251	-.0330	-.0397	-.0412	-.0457
14	OFF	.0031	-.0082	-.0128	-.0191	-.0090	-.0263	-.0376	-.0424	-.0452
	ON	.0048	-.0065	-.0122	-.0187	-.0095	-.0261	-.0373	-.0423	-.0446
15	OFF	.0003	-.0225	-.0164	.0024	-.0093	-.0266	-.0407	-.0452	-.0458
	ON	.0009	-.0082	.0096	.0013	-.0122	-.0274	-.0389	-.0433	-.0465
		.0057	-.0036	-.0064	.0043	-.0103	-.0254	-.0380	-.0432	-.0453
16	OFF	-.0011	.0139	.0088	-.0004	-.0149	-.0357	-.0454	-.0487	-.0477
	ON	.0081	.0136	.0094	.0019	-.0154	-.0329	-.0435	-.0483	-.0511
		.0102	-.0248	.0156	.0084	-.0107	-.0298	-.0407	-.0499	-.0496
		.0009	-.0277	.0097	.0008	-.0154	-.0327	-.0451	-.0482	-.0495
18	OFF	.0154	-.0167	-.0203	-.0264	-.0303	-.0466	-.0612	-.0513	-.0600
	ON	.0215	-.0031	-.0066	-.0159	-.0246	-.0416	-.0619	-.0627	-.0731
20	OFF	.0187	-.0081	-.0095	-.0167	-.0334	-.0469	-.0655	-.0714	-.0869
	ON	.0100	-.0140	-.0138	-.0216	-.0354	-.0520	-.0663	-.0741	-.0851
		.0134	-.0111	-.0146	-.0191	-.0291	-.0448	-.0609	-.0788	-.0866
25	OFF	.0080	.0104	-.0116	-.0159	-.0310	-.0414	-.0570	-.0708	-.0847
	ON	.0099	-.0085	-.0097	-.0160	-.0294	-.0383	-.0538	-.0701	-.0831
30	OFF	.0137	-.0144	-.0156	-.0240	-.0328	-.0453	-.0598	-.0745	-.0547
	ON	.0151	-.0107	-.0165	-.0220	-.0312	-.0446	-.0601	-.0715	-.0560
35	OFF	.0257	-.0041	-.0079	-.0186	-.0320	-.0471	-.0541	-.0670	-.0729
	ON	.0253	-.0020	-.0083	-.0164	-.0324	-.0464	-.0528	-.0658	-.0727
40	OFF	.0213	-.0053	-.0125	-.0199	-.0316	-.0447	-.0487	-.0569	-.0574
	ON	.0201	.0050	-.0120	-.0190	-.0305	-.0413	-.0454	-.0555	-.0643
		.0210	-.0020	-.0085	-.0166	-.0274	-.0386	-.0438	-.0519	-.0515

C-VI

α_u (deg)	GRIT	β (deg)							
		-10	0	2	5	10	15	20	25	[illegible]
-8	OFF	-.0147	.0012	.0048	.0018	.0173	.0229	.0324	.0354	[illegible]
	ON	-.0151	.0016	.0052	.0107	.0178	.0226	.0328	.0366	[illegible]
-4	OFF	-.0150	.0007	.0039	.0091	.0165	.0207	.0314	.0373	[illegible]
	ON	-.0151	.0010	.0045	.0097	.0171	.0205	.0317	.0367	[illegible]
0	OFF	-.0153	.0001	.0032	.0064	.0152	.0190	.0303	.0391	[illegible]
	ON	-.0151	.0007	.0039	.0091	.0156	.0191	.0304	.0355	[illegible]
		-.0153	-.0003	.0029	.0052	.0148	.0189	.0296	.0375	[illegible]
		-.0145	.0002	.0031	.0083	.0177	.0185	.0299	.0377	[illegible]
4	OFF	-.0173	-.0002	.0034	.0084	.0165	.0185	.0293	.0396	.0462
	ON	-.0170	.0003	.0037	.0095	.0166	.0186	.0293	.0392	[illegible]
8	OFF	-.0183	.0003	.0040	.0101	.0189	.0226	.0279	.0392	[illegible]
	ON	-.0182	-.0000	-.0039	-.0099	.0178	.0172	.0274	.0382	.0455
		-.0179	.0020	.0042	.0096	.0175	.0167	.0271	.0373	.0436
12	OFF	⟶	-.0011	-.0046	.0111	.0207	.0266	.0299	.0403	[illegible]
	ON	-.0184	-.0001	.0045	.0108	.0196	.0255	.0297	.0397	.0445
		-.0176	-.0000	.0046	.0108	.0196	.0250	.0271	.0386	[illegible]
14	OFF	-.0073	-.0022	.0030	.0094	.0020	.0113	.0264	.0373	.0430
	ON	-.0054	-.0011	.0026	.0094	.0017	.0126	.0265	.0373	.0424
15	OFF	-.0071	-.0007	.0023	.0001	.0017	.0104	.0245	.0358	.0420
	ON	-.0056	-.0016	-.0028	-.0022	-.0004	.0093	.0252	.0347	.0410
		-.0050	-.0017	.0046	-.0016	-.0009	.0102	.0252	.0358	.0413
16	OFF	-.0028	-.0057	-.0046	-.0032	-.0021	.0062	.0213	.0287	.0350
	ON	-.0004	-.0070	-.0056	[illegible]	-.0029	.0075	.0227	.0303	.0313
		-.0013	.0027	[illegible]	[illegible]	-.0019	.0097	.0228	.0318	.0361
		[illegible]	.0017	[illegible]	-.0045	-.0031	.0098	.0221	[illegible]	[illegible]
18	OFF	.0014	.0005	.0023	.0044	.0076	.0128	.0190	.0295	.0417
	ON	-.0072	-.0003	.0023	.0043	.0057	.0092	.0217	.0272	[illegible]
20	OFF	-.0010	.0054	.0073	.0092	.0136	.0173	.0173	.0277	[illegible]
	ON	-.0001	.0000	.0067	.0056	.0113	.0165	.0225	.0285	.0355
		-.0002	.0048	[illegible]	[illegible]	.0077	.0108	.0186	.0262	[illegible]
25	OFF	-.0041	.0026	.0026	.0046	.0136	.0188	.0271	.0357	[illegible]
	ON	-.0045	[illegible]	[illegible]	[illegible]	.0136	.0183	.0263	[illegible]	[illegible]
30	OFF	-.0121	[illegible]	[illegible]	[illegible]	[illegible]	.0255	.0303	[illegible]	[illegible]
	ON	-.0124	[illegible]	[illegible]	[illegible]	[illegible]	.0247	.0298	[illegible]	[illegible]
35	OFF	-.0182	[illegible]	.0072	[illegible]	[illegible]	.0326	.0412	[illegible]	[illegible]
	ON	-.0175	[illegible]	.0077	.0111	.0213	.0312	.0390	[illegible]	[illegible]
40	OFF	[illegible]	[illegible]	[illegible]	[illegible]	[illegible]	[illegible]	[illegible]	[illegible]	[illegible]
	ON	-.0181	[illegible]	[illegible]	[illegible]	[illegible]	[illegible]	[illegible]	[illegible]	[illegible]
		[illegible]	[illegible]	[illegible]	[illegible]	[illegible]	[illegible]	[illegible]	[illegible]	[illegible]

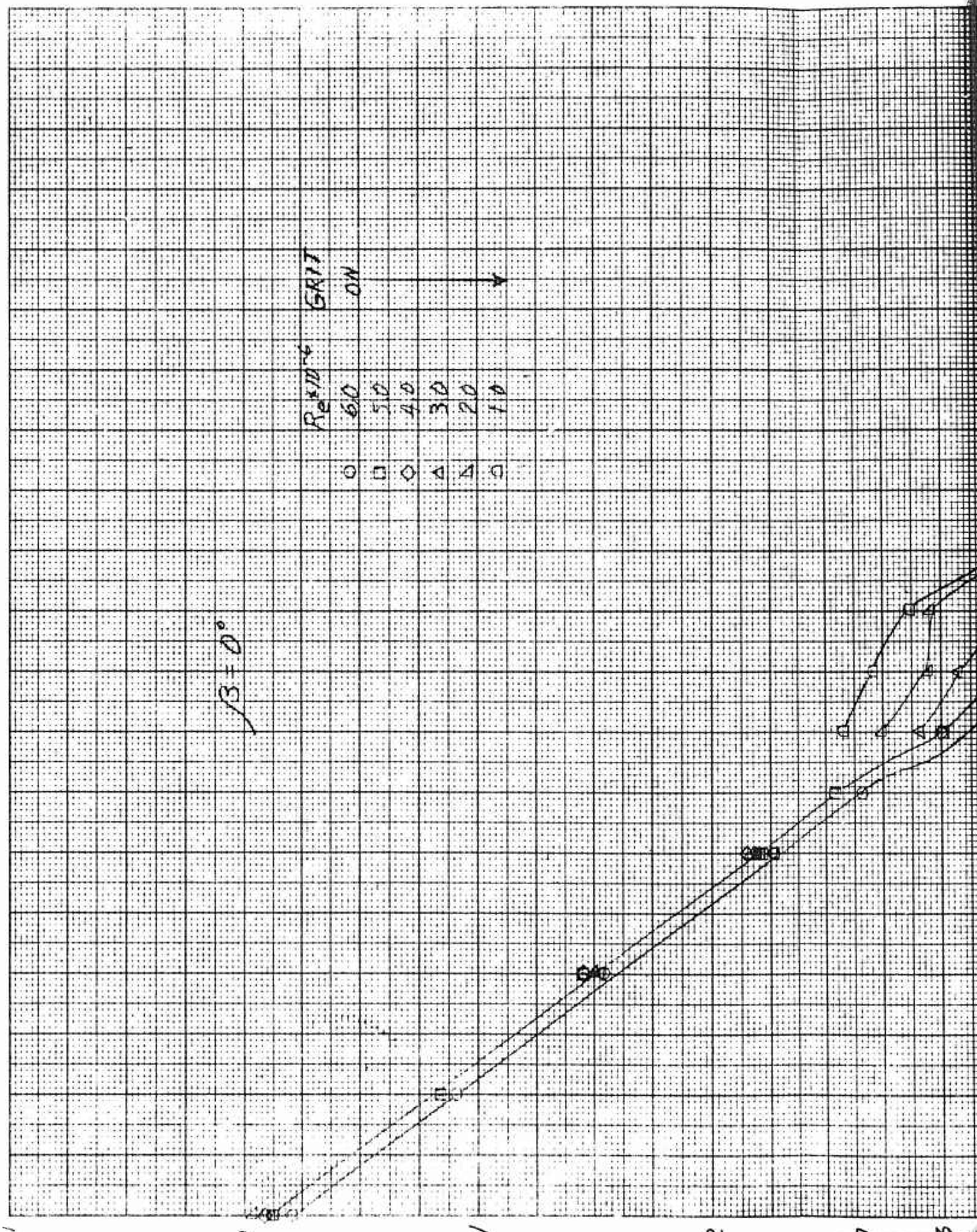

$R_e \times 10^{-6}$
GRIT ON
6.0
5.0
4.0
3.0
2.0
1.0
$\beta = 0°$
0
1
2
3

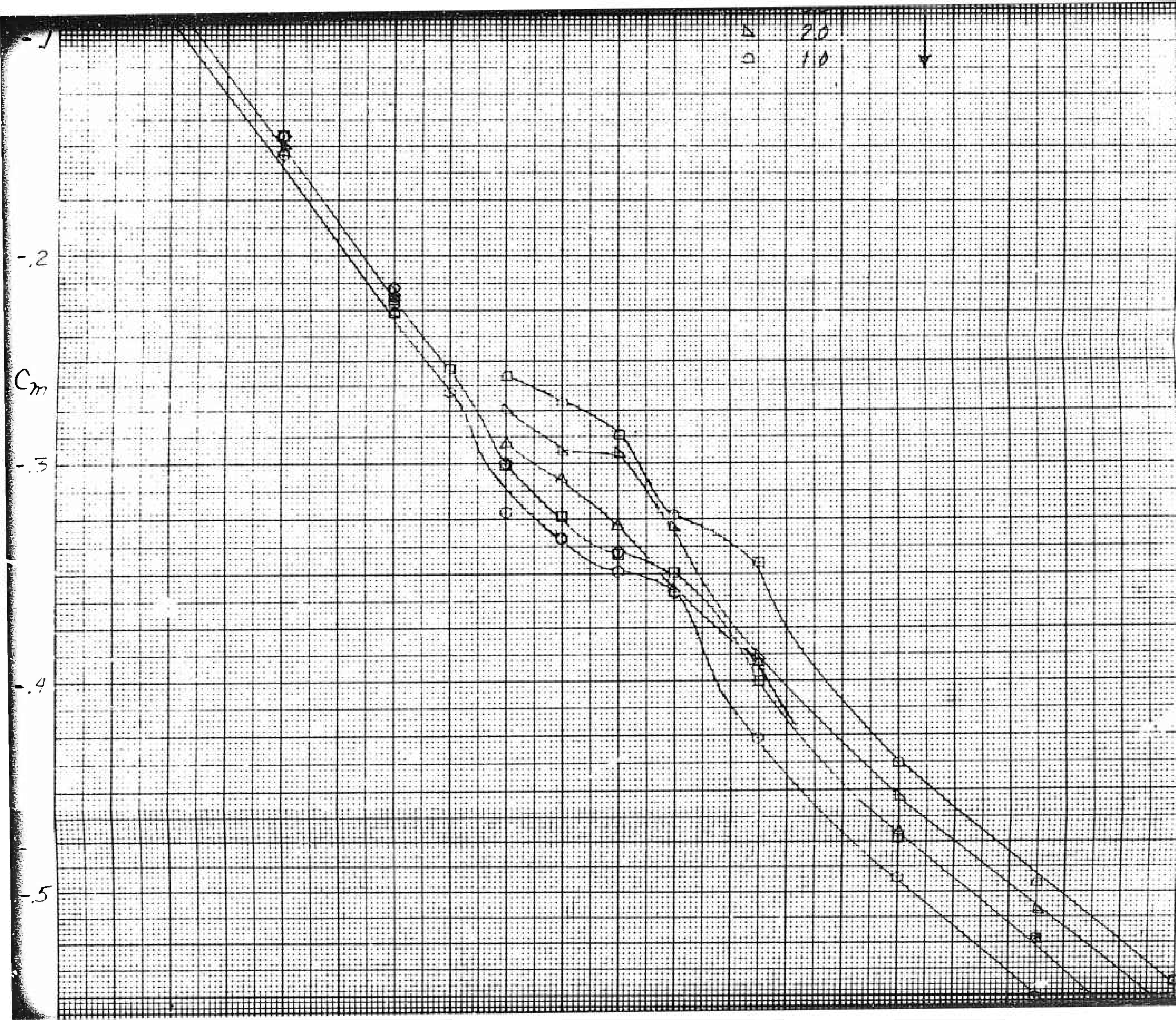

2.0
1.0
-.1
-.2
C_m
-.3
-.4
-.5

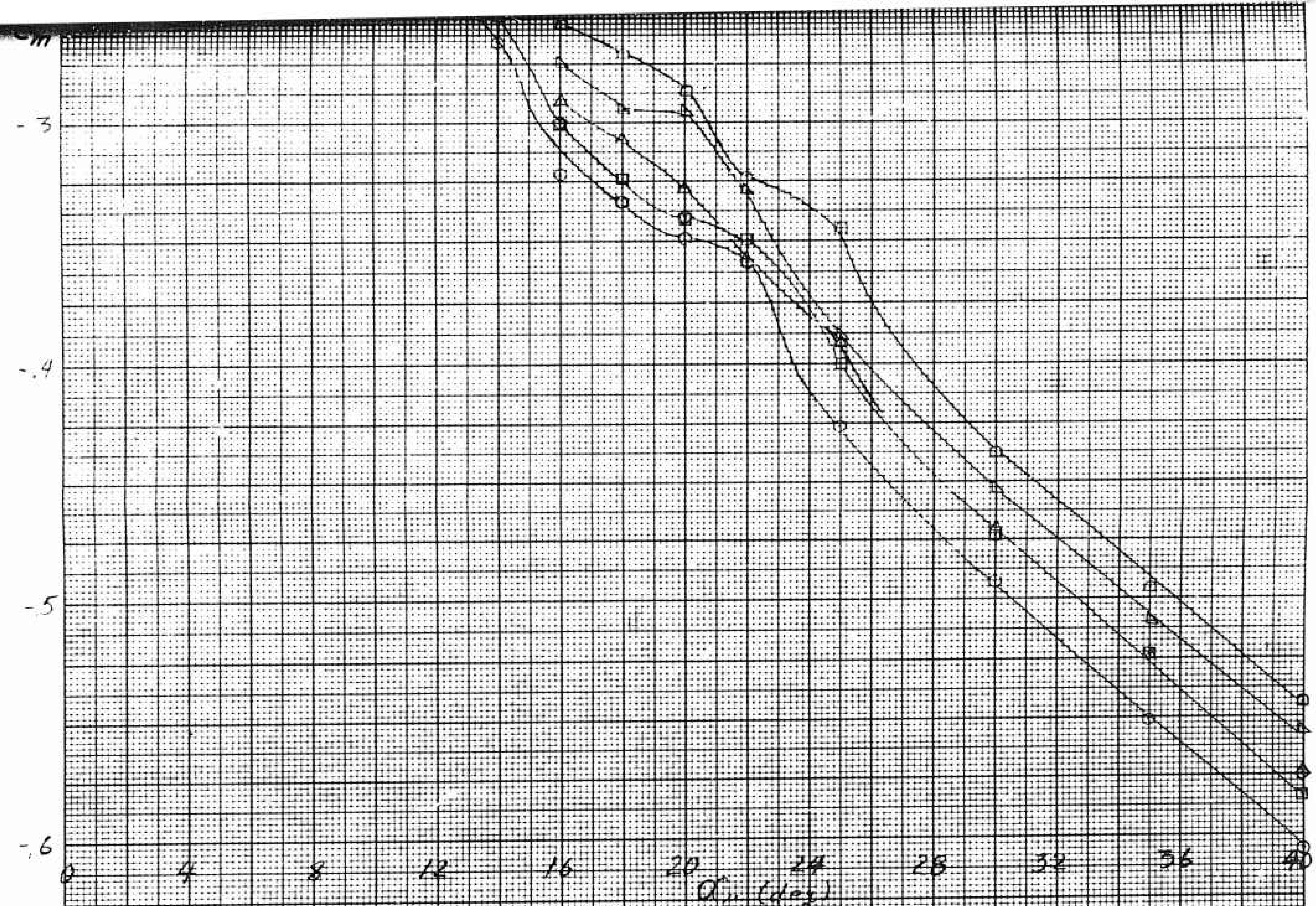

Figure C-1 Influence of Reynolds Number on the Pitch Characteristics of a Gritted Model ($M = 2.0$, $\delta_e = \delta_a = \delta_R = 0^{\circ}$, $\beta = 0^{\circ}$).

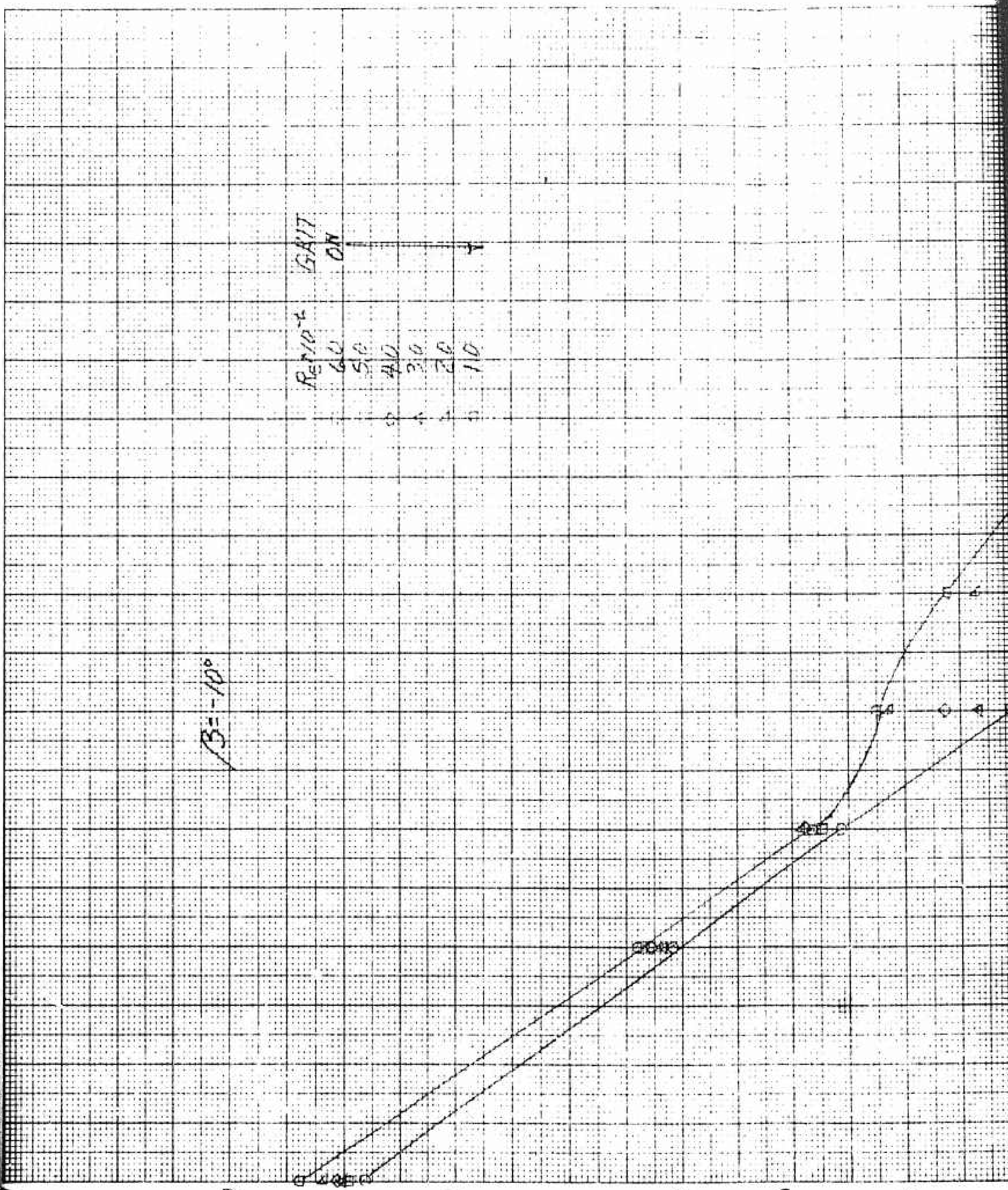

Preceding page blank

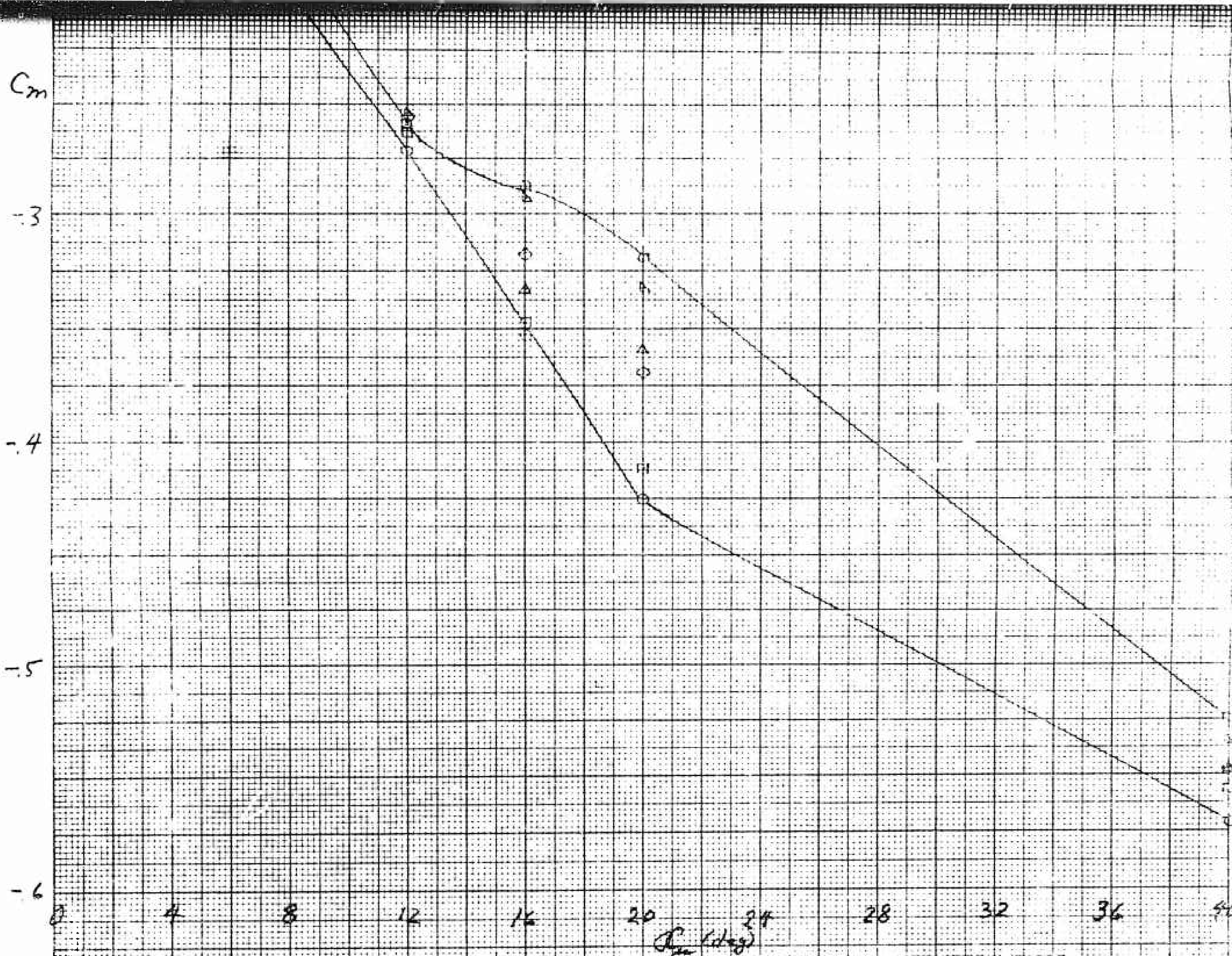

Figure C-2 Influence of Reynolds Number on the Pitch Characteristics of a Gritted Model ([illegible], $\delta_e = \delta_a = \delta_r$ [illegible] β = [illegible]).

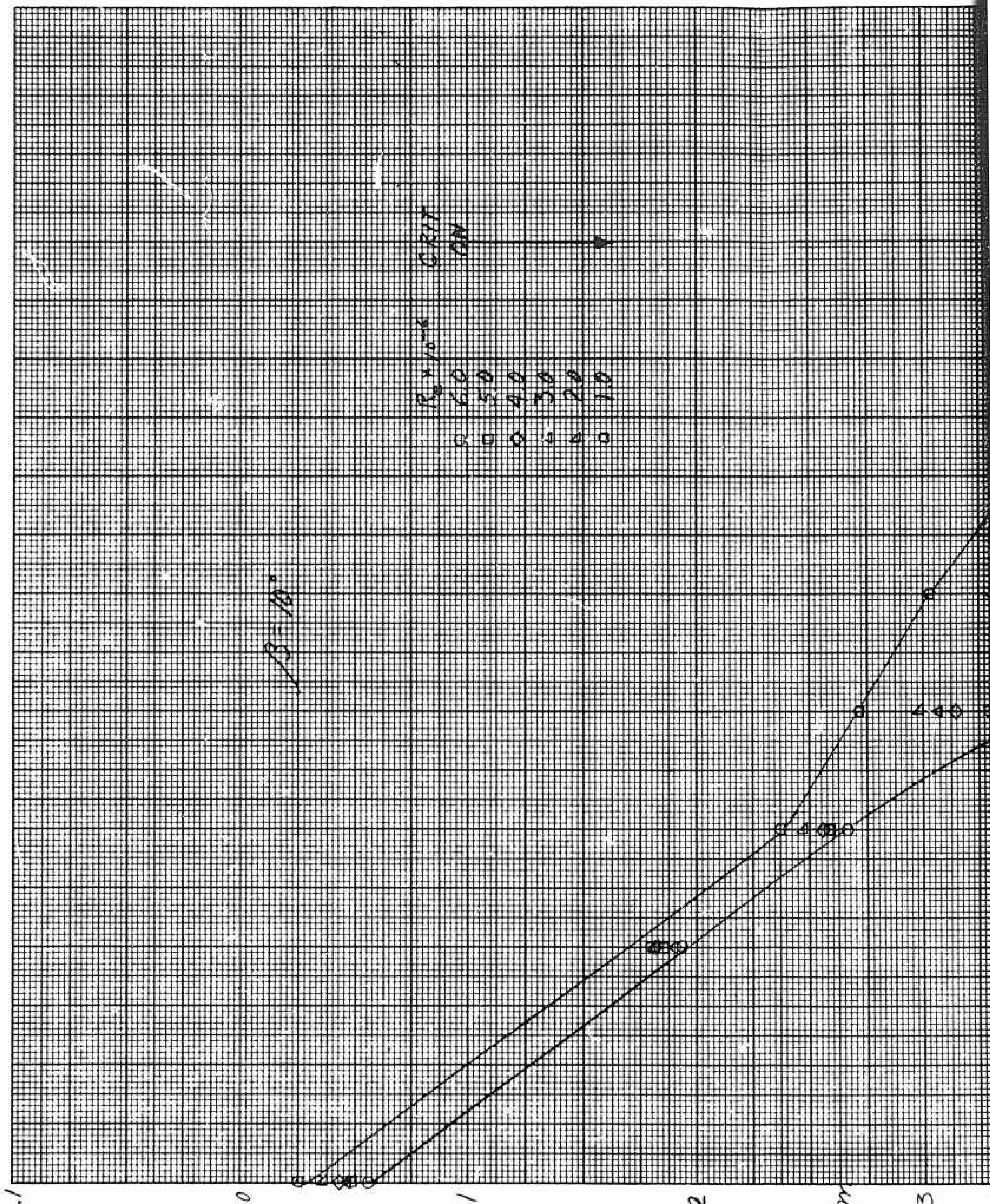

Preceding page blank

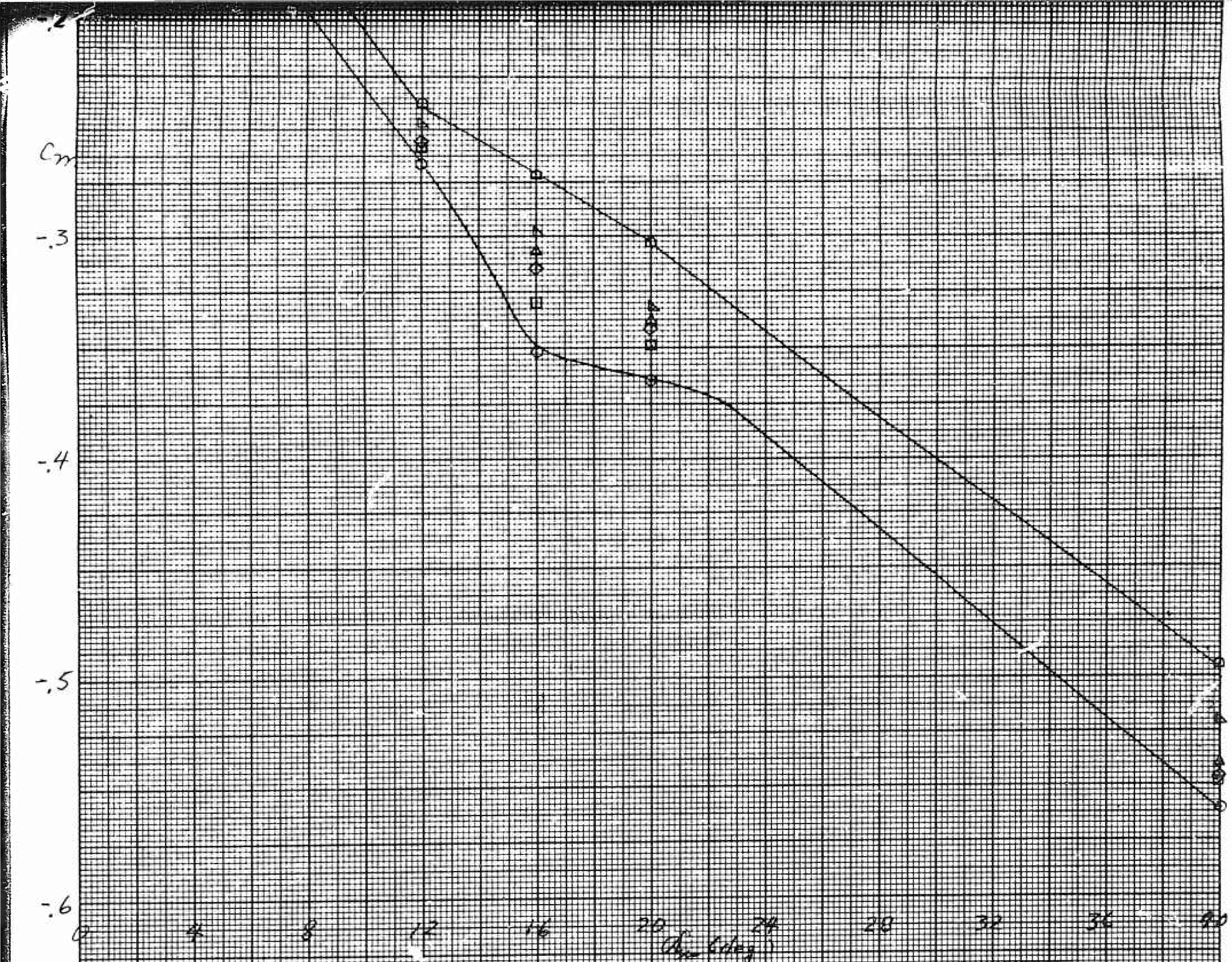

Figure C-3 Influence of Reynolds Number on the Pitch Characteristics of a Gritted Model ($M = 2.0$, $\delta_e = \delta_a = \delta_R = 0^0$, $\underline{\beta = 10^0}$).

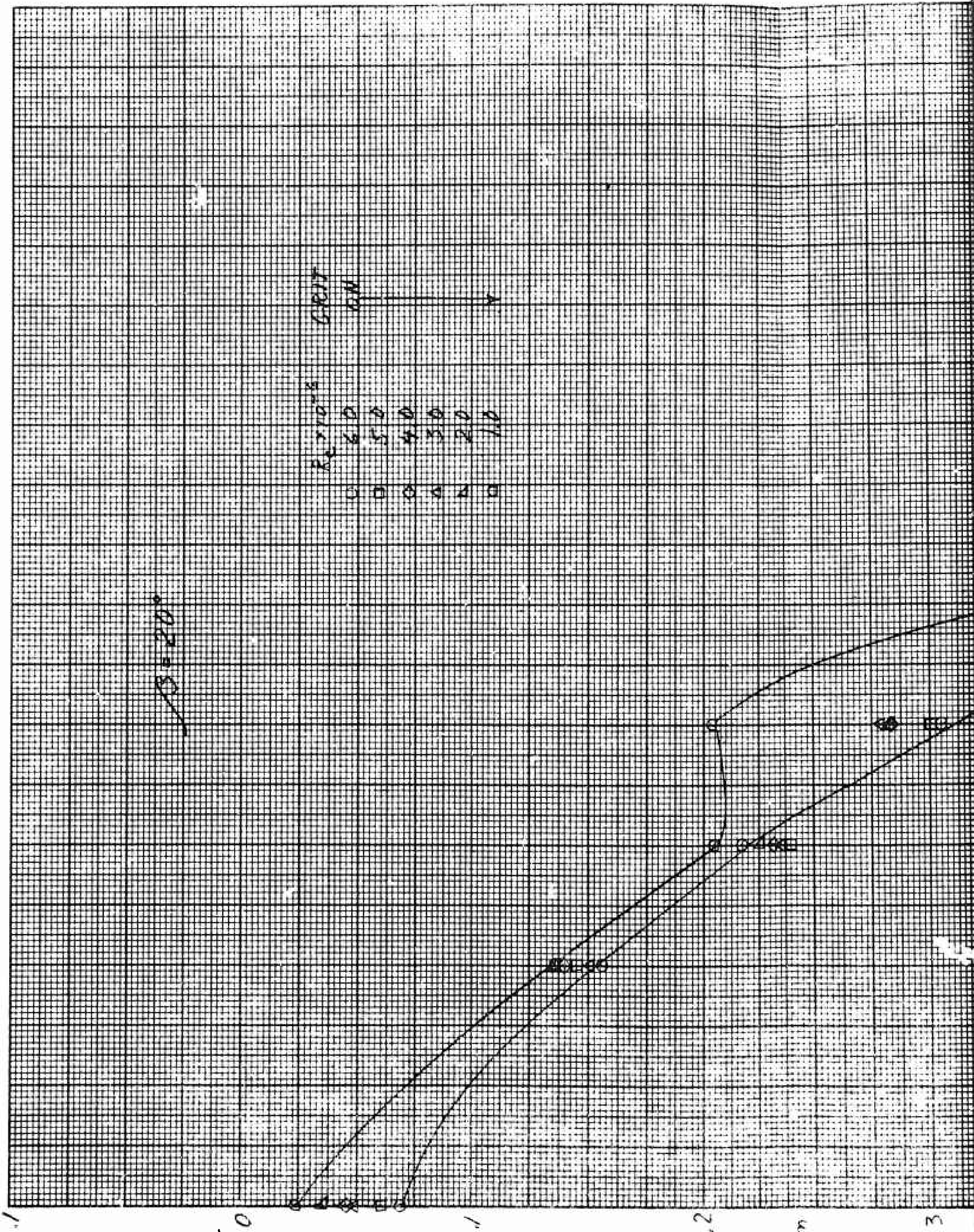

Preceding page blank

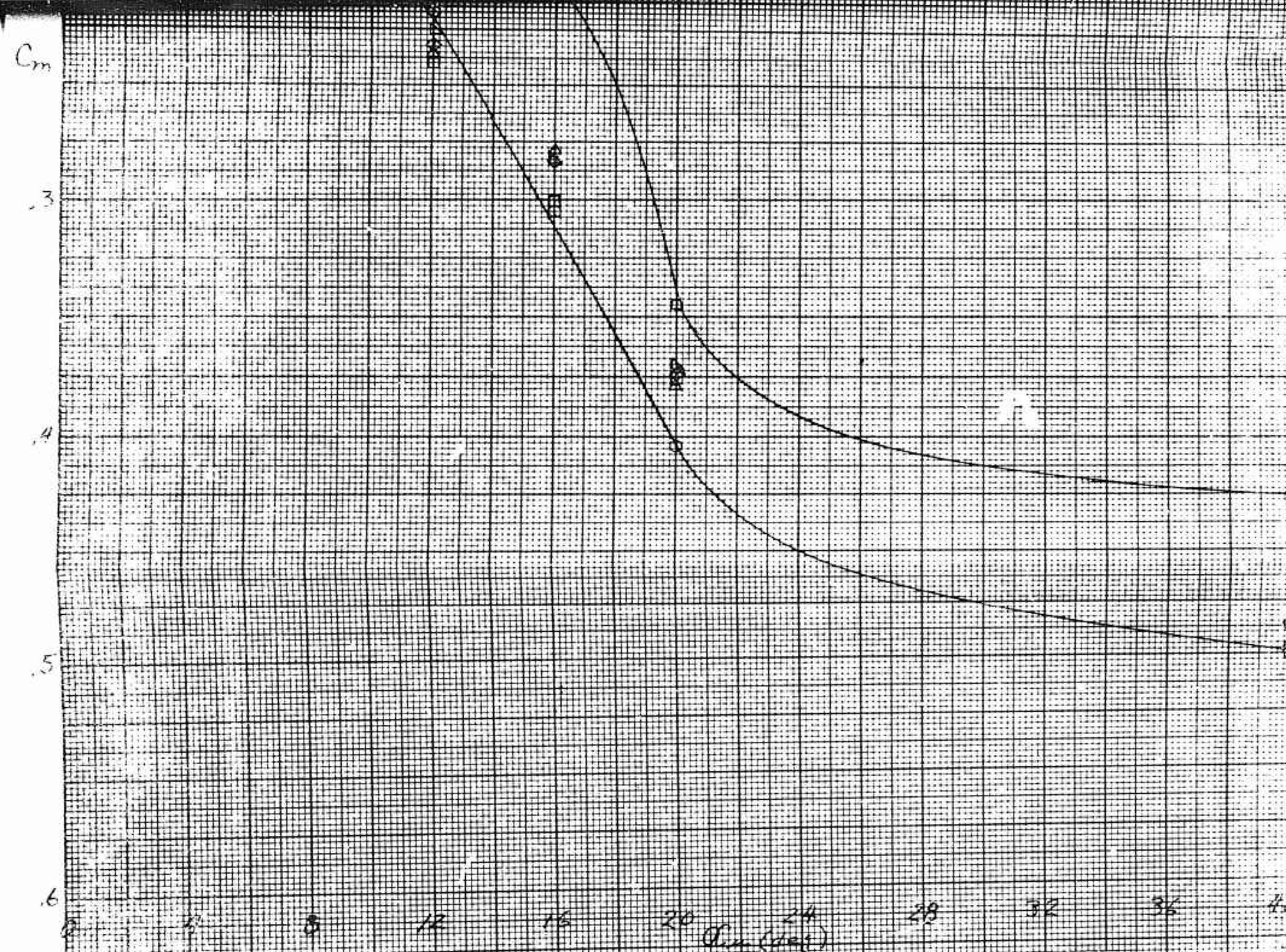

Figure C-4 Influence of Reynolds Number on the Pitch Characteristics of a Gritted Model ($M = 2.0$, $\delta_e = \delta_a = \delta_R = 0^\circ$, $\beta = 20^\circ$).

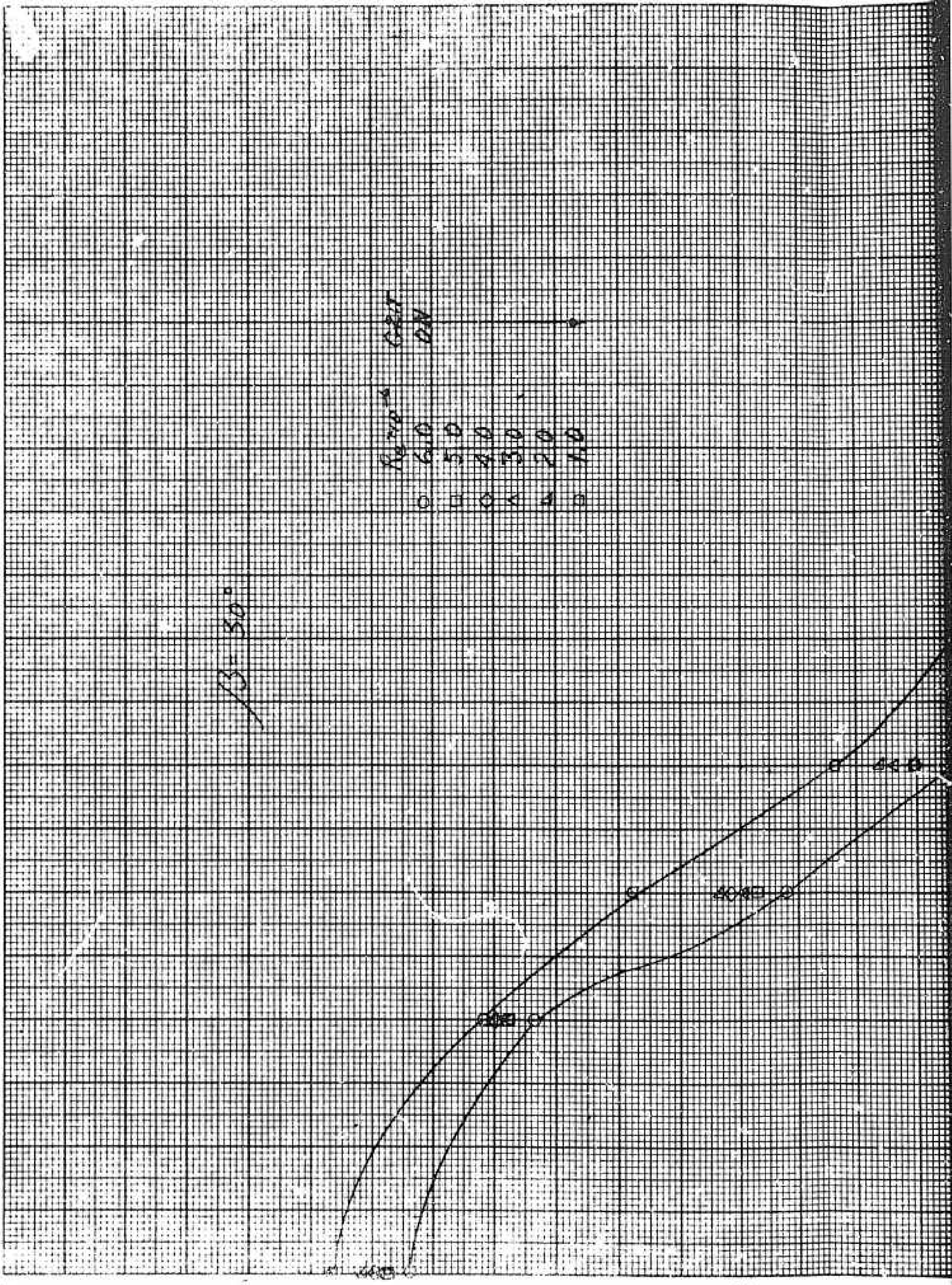

Preceding page blank

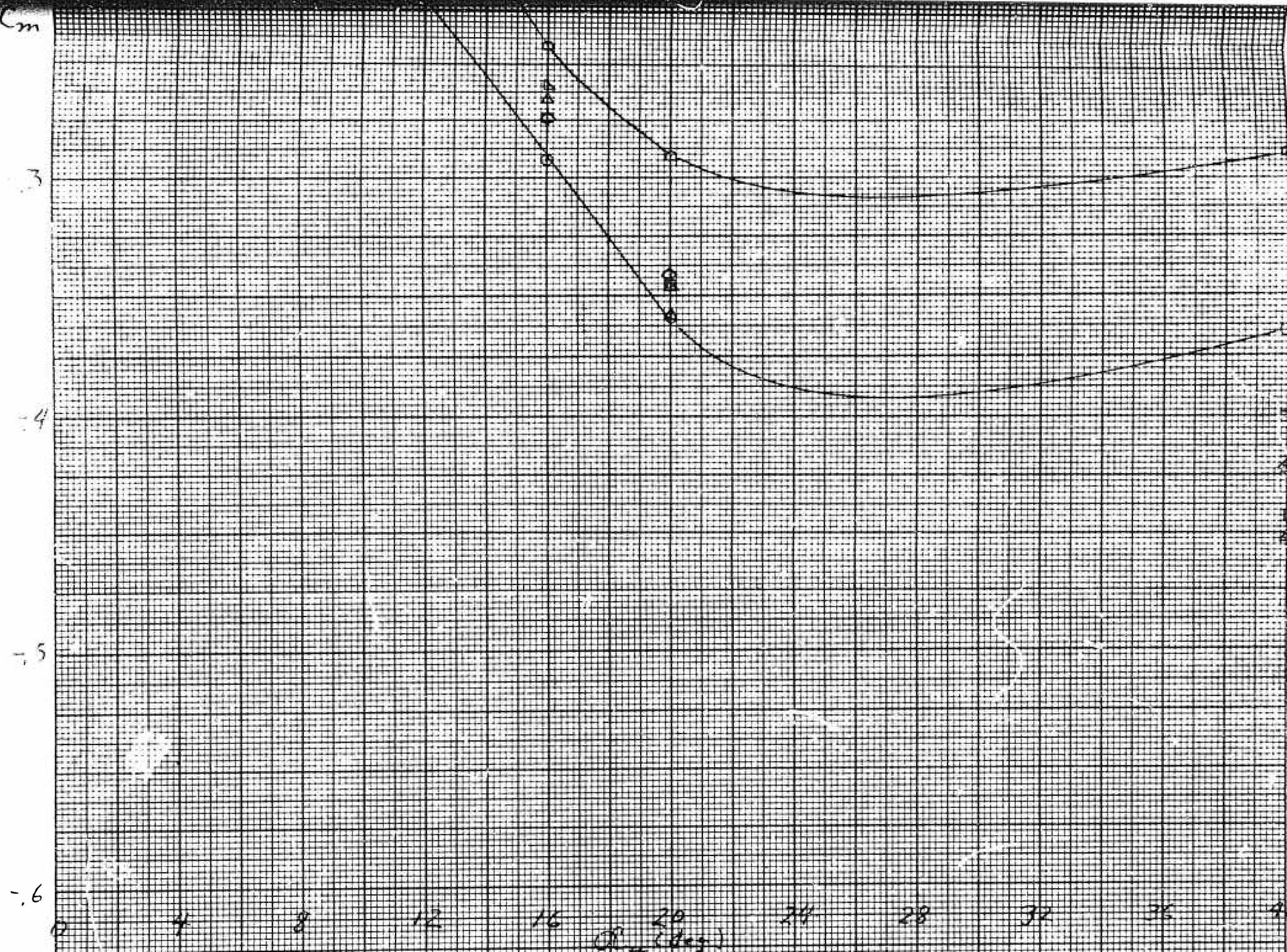

Figure C-5 Influence of Reynolds Number on the Pitch Characteristics of a Gritted Model ($M = 2.0$, $\delta_e = \delta_a = \delta_R = 0^{\circ}$, $\beta = 30^{\circ}$).

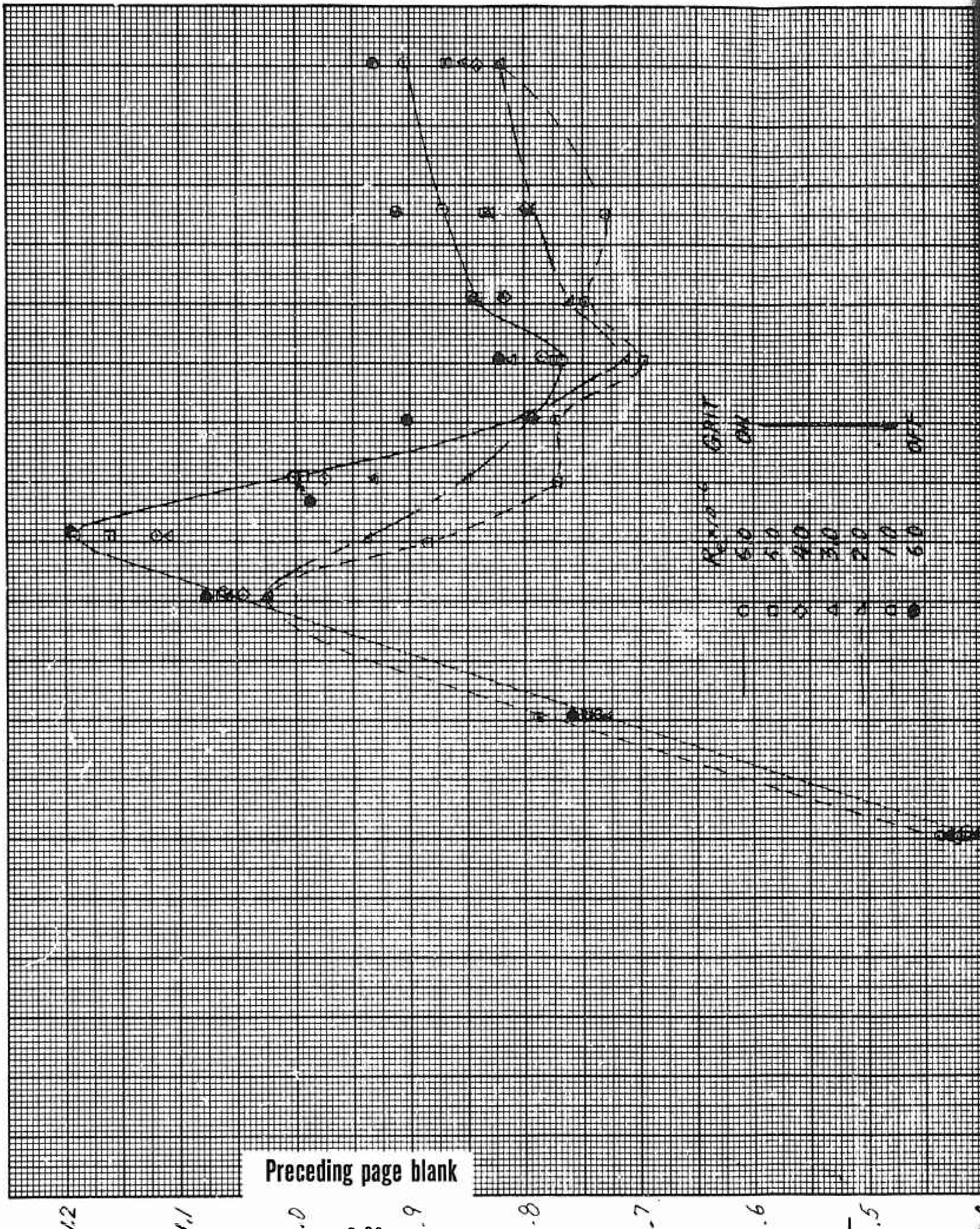

Preceding page blank

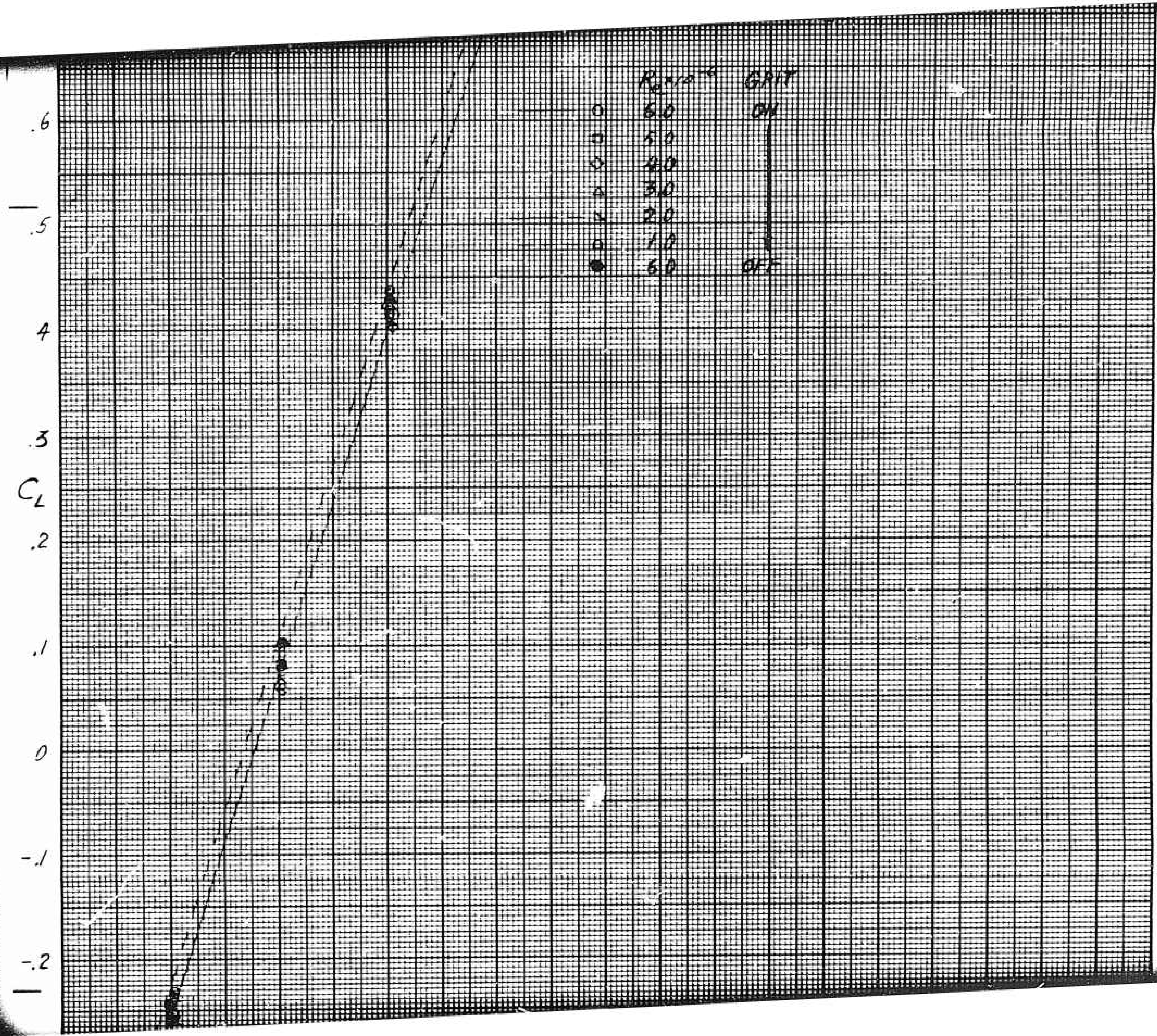
$R_e \times 10^{-6}$ GRIT
6.0 ON
5.0
4.0
3.0
2.0
1.0
6.0 OFF
C_L
.6
.5
.4
.3
.2
.1
0
-.1
-.2

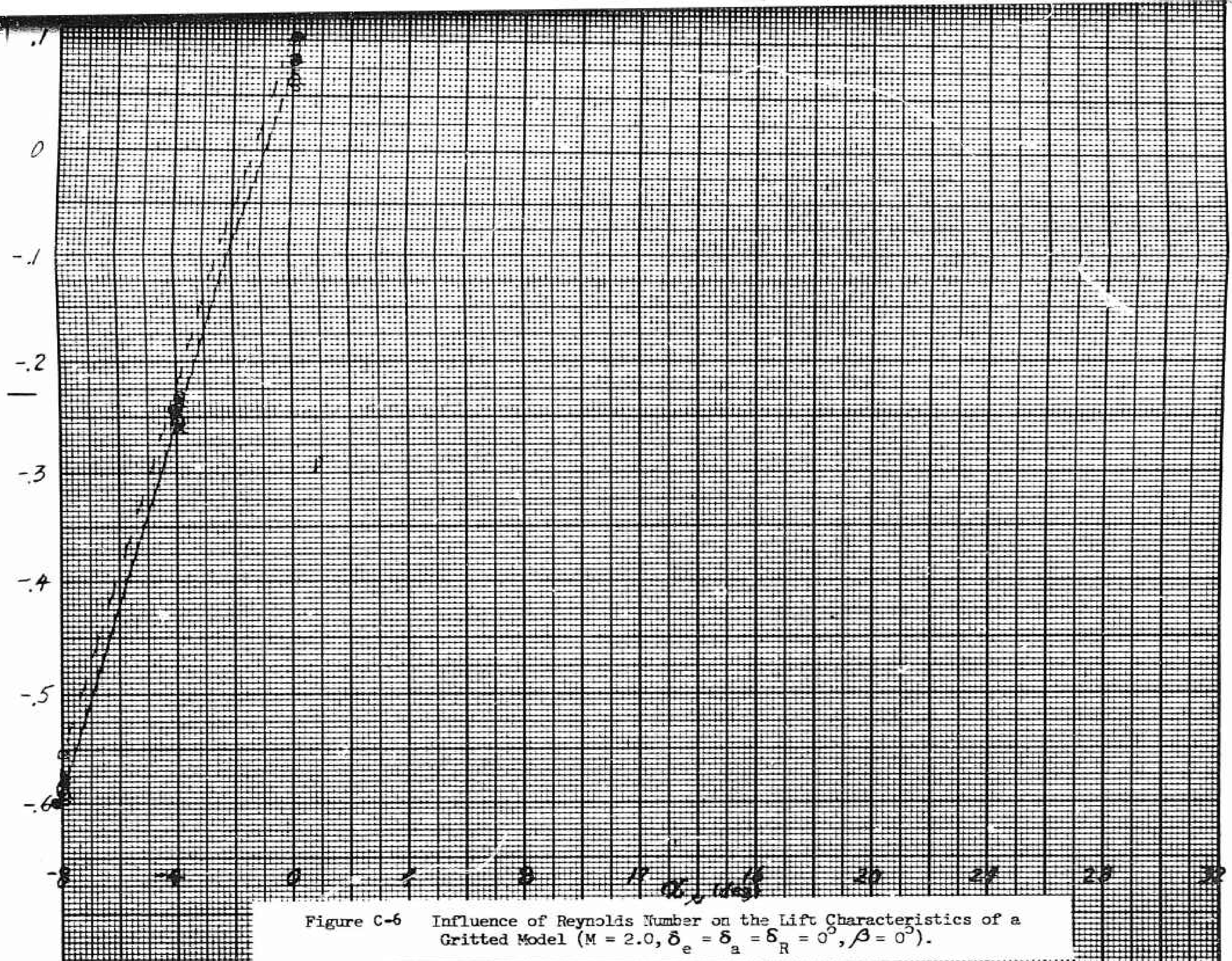

Figure C-6 Influence of Reynolds Number on the Lift Characteristics of a Gritted Model ($M = 2.0, \delta_e = \delta_a = \delta_R = 0^\circ, \beta = 0^\circ$).

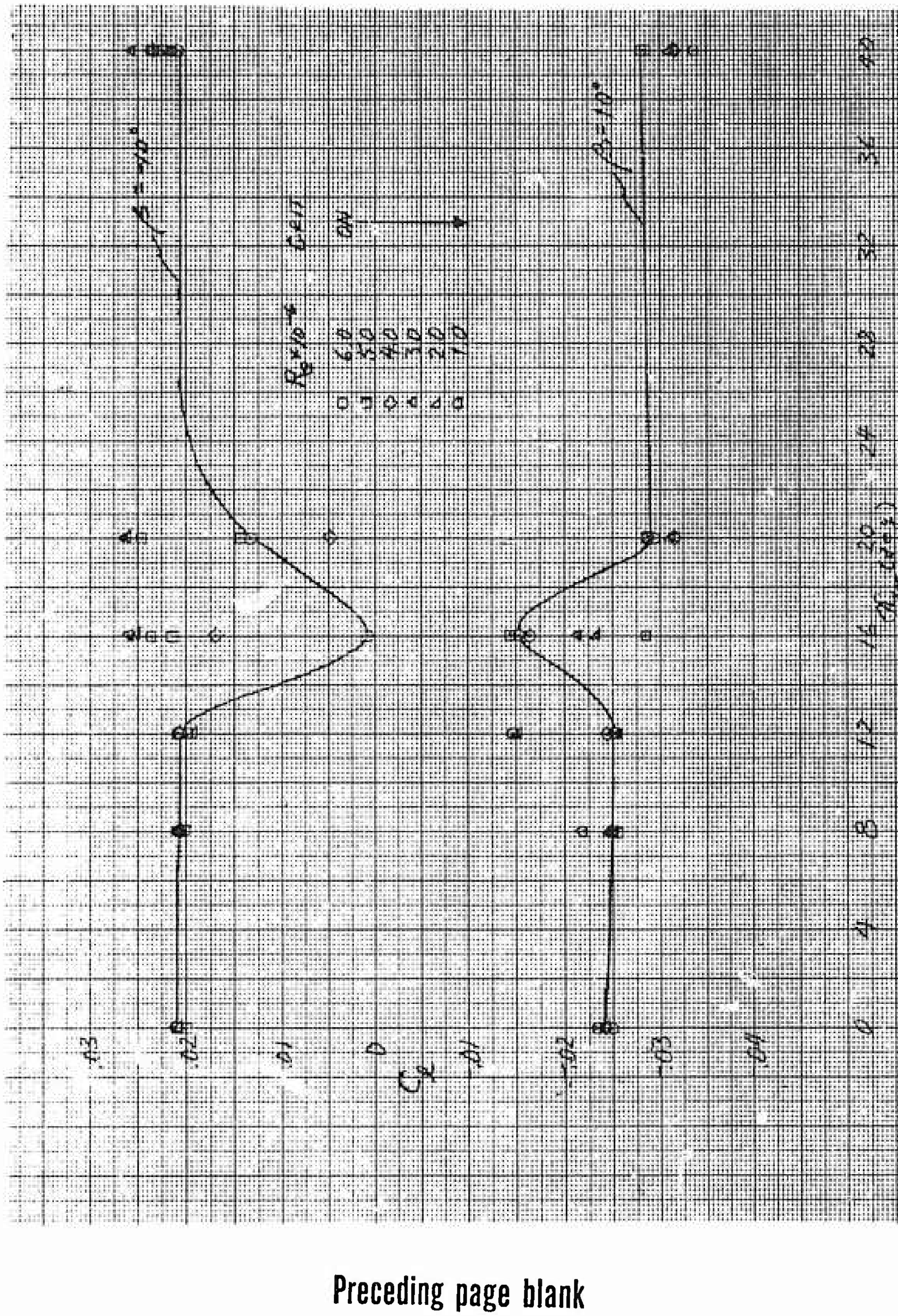

Figure C-7 Influence of Reynolds Number on the Roll Characteristics of a Gritted Model($M = 2.0$, $\delta_e = \delta_a = \delta_R = 0°$, $\beta = -10, 10°$).

Preceding page blank

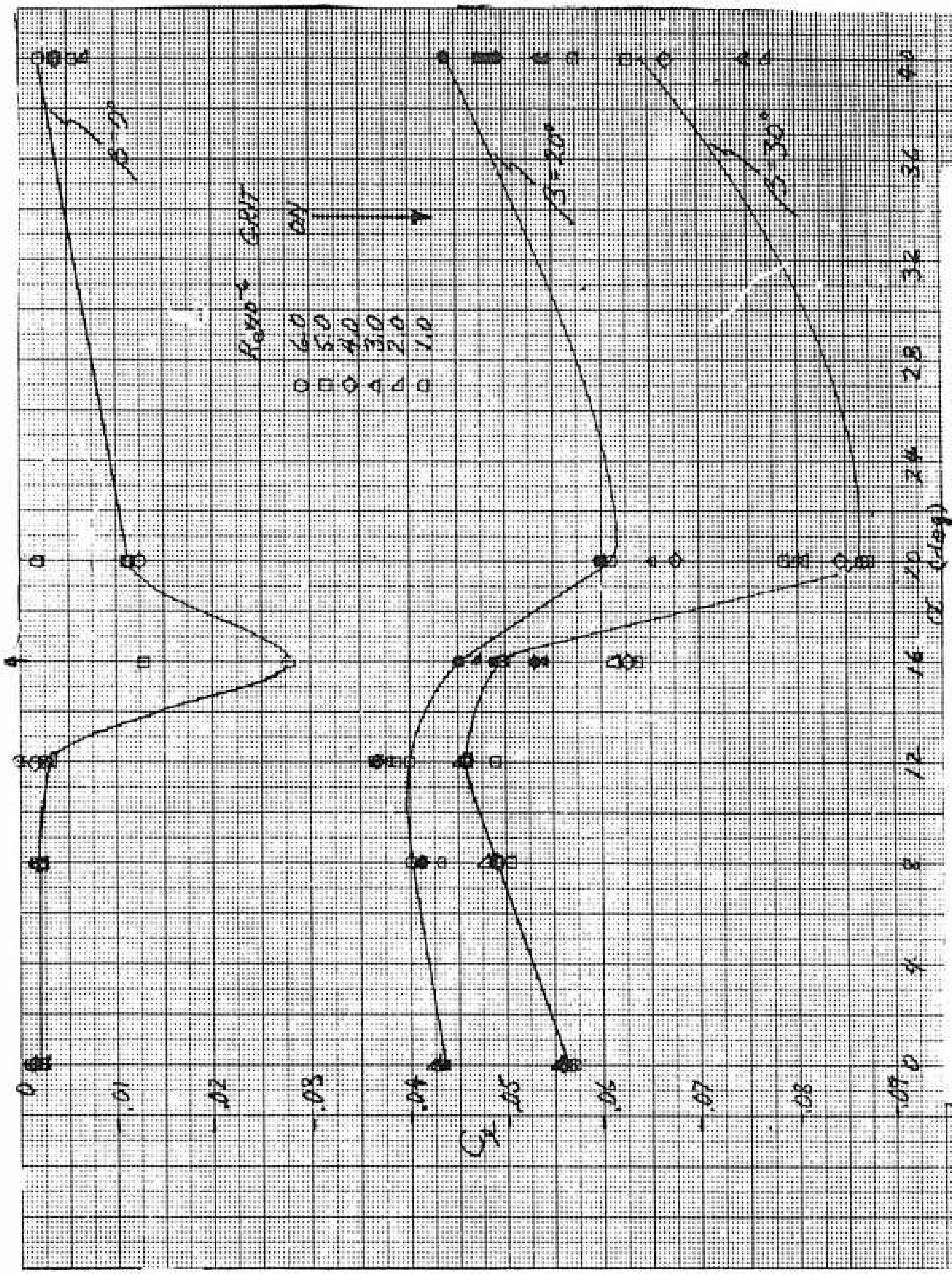

Figure C-8 Influence of Reynolds Number on the Roll Characteristics of a Gritted Model ($M = 0, \delta_a = \delta_e = \delta_R = 0°, \beta = 0, 20, 30°$).

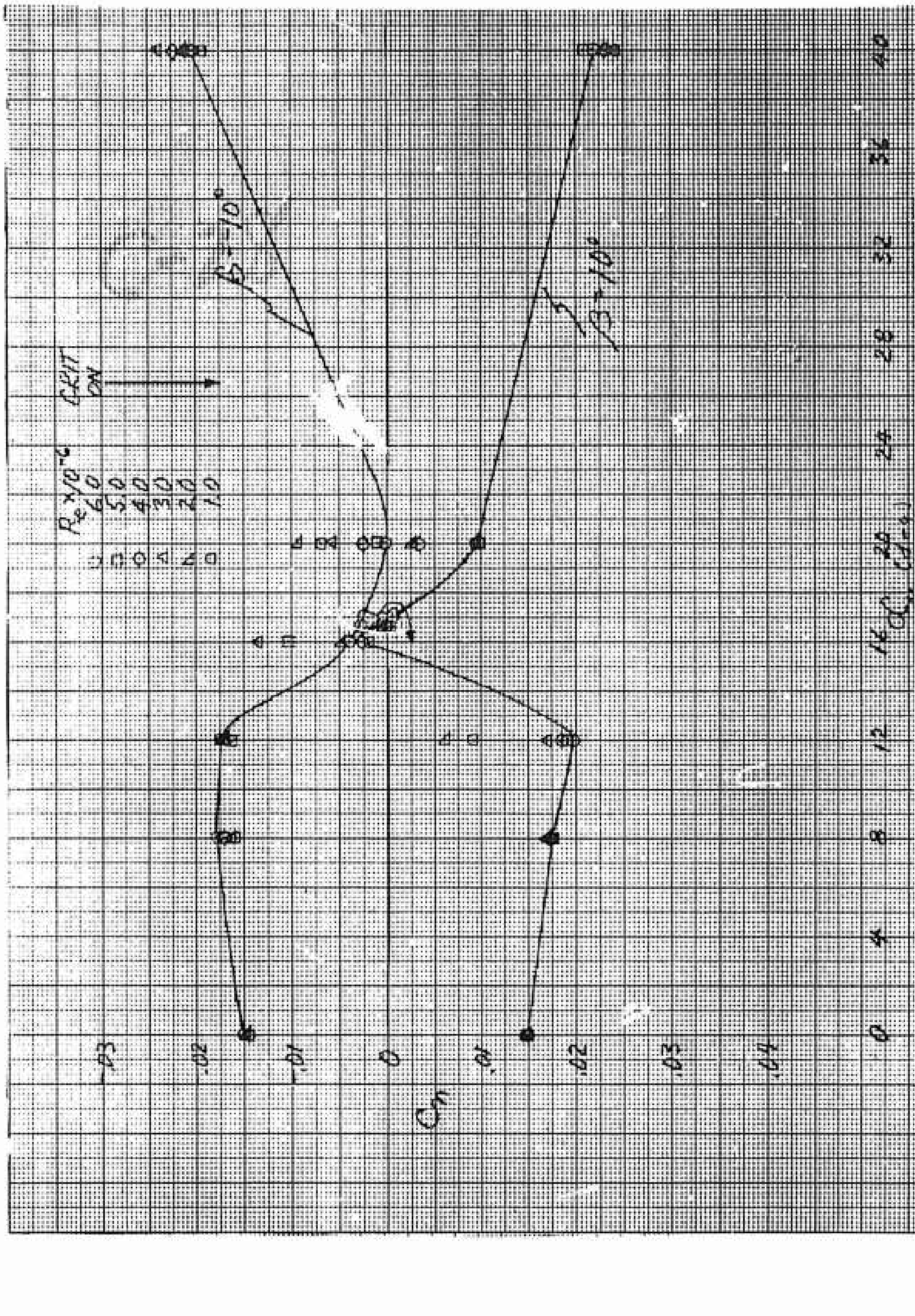

Figure C-9 Influence of Reynolds Number on the Yaw Characteristics of a Gritted Model ($M = 2.0, \delta_e = \delta_a = \delta_R = 0°, \beta = -10, 10°$).

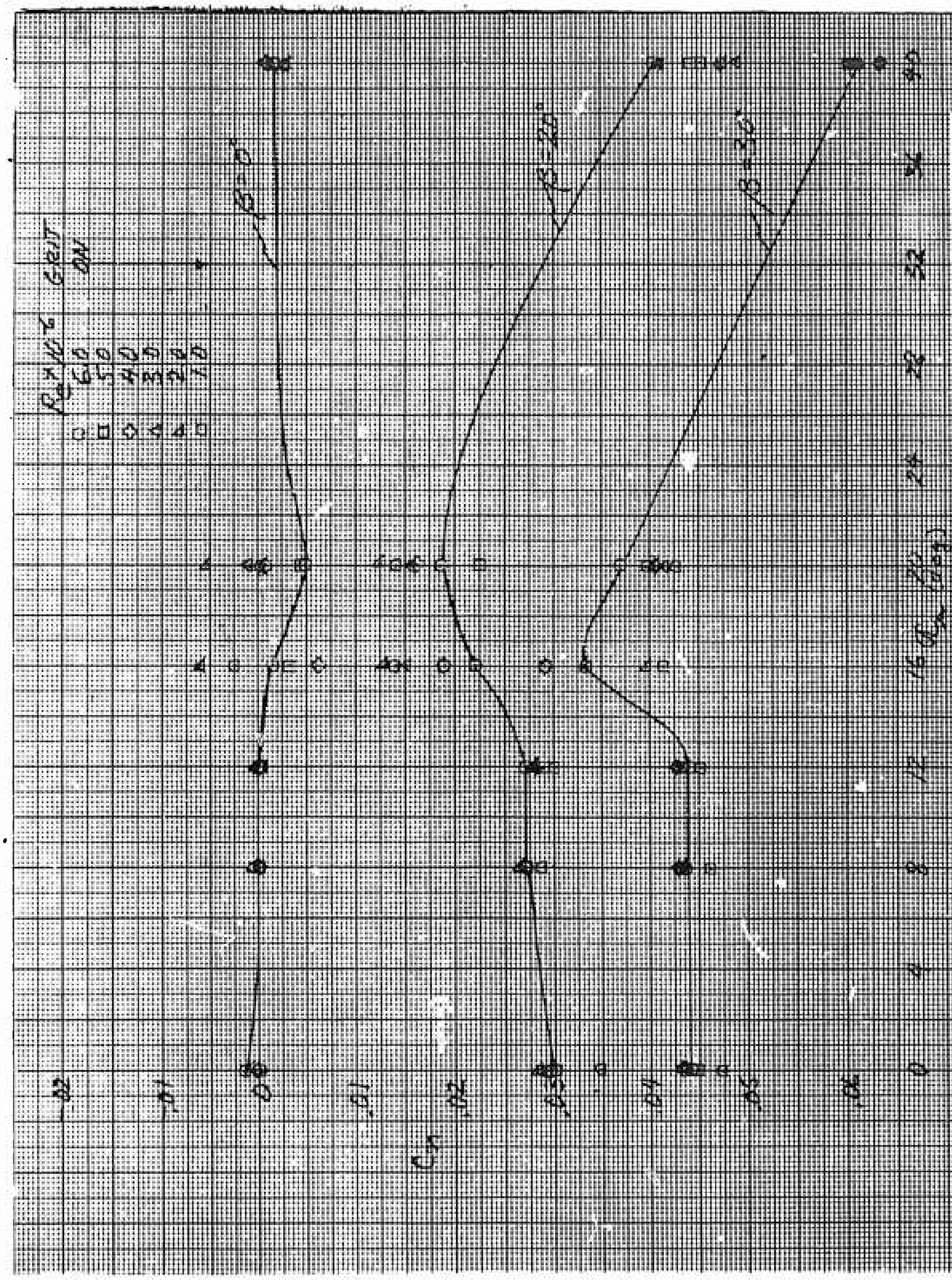

Figure C-10 Influence of Reynolds Number on the Yaw Characteristics of a Gritted Model ($M = 2.0$, $\delta_e = \delta_a = \delta_R = 0^\circ$, $\beta = 0, 20, 30^\circ$).

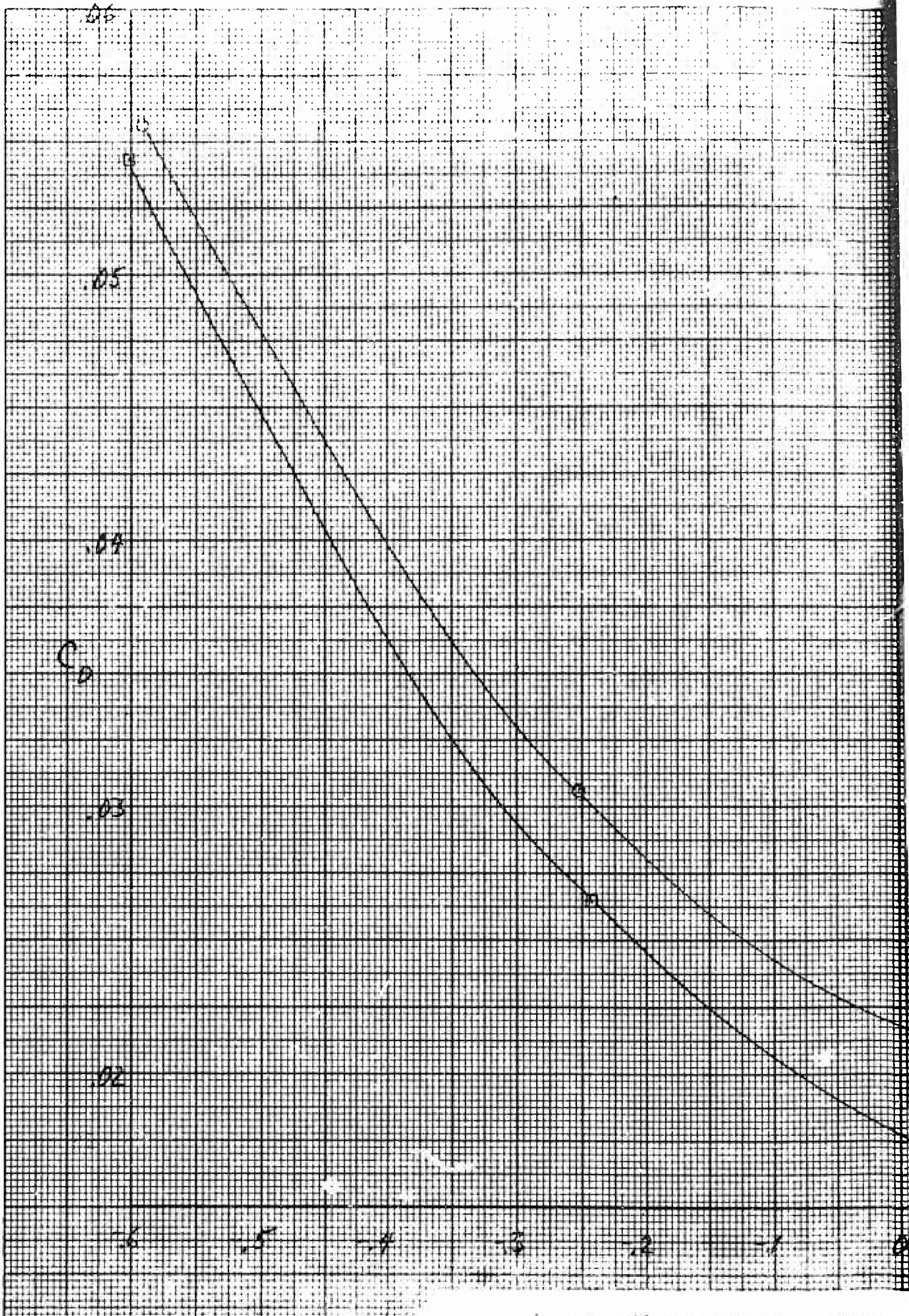

[illegible] transitio[illegible]

[illegible] (M[illegible]

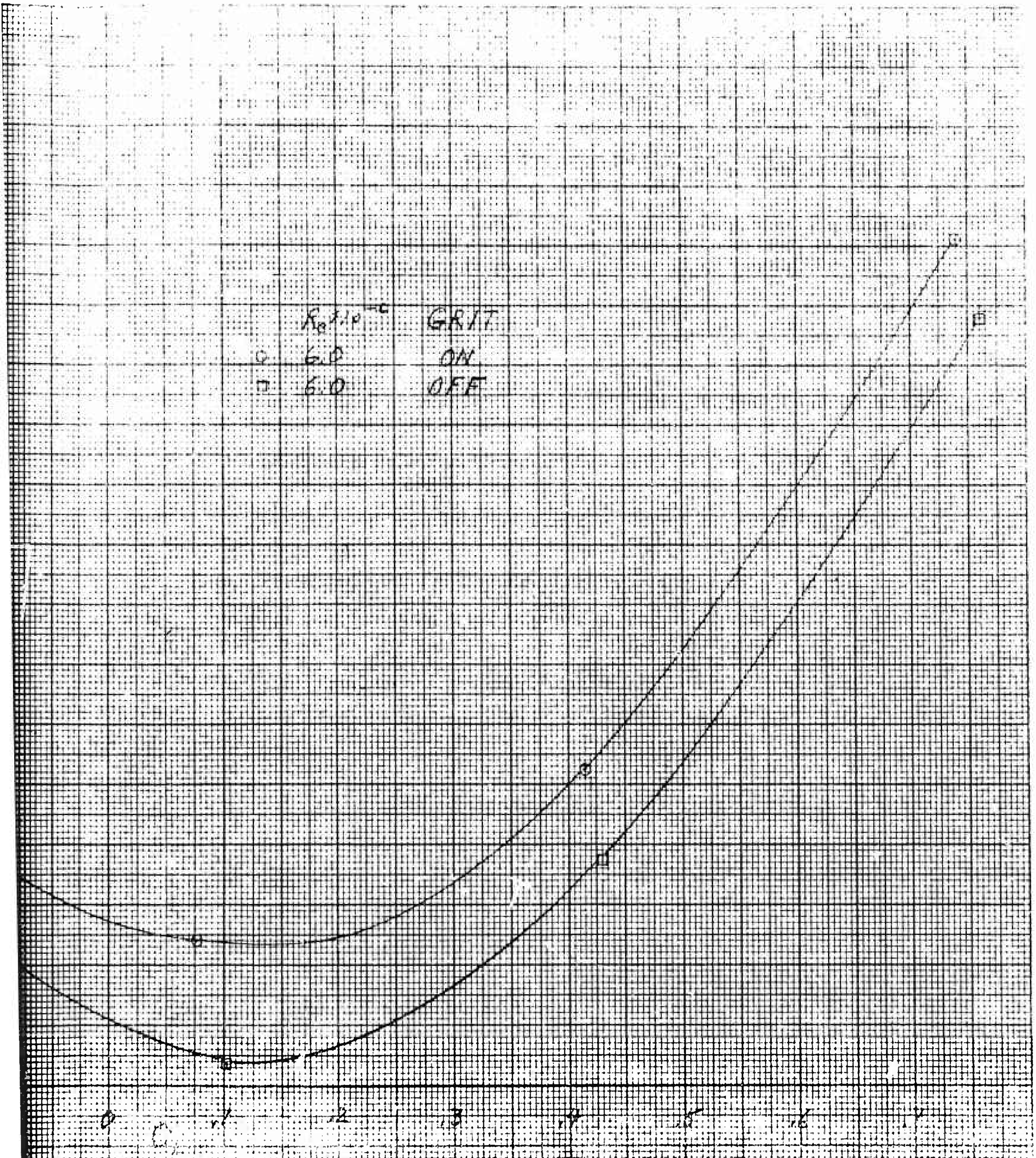
R_θ x10^-6 GRIT
6.0 ON
6.0 OFF
0
.1
.2
.3
.4
.5
.6
.7

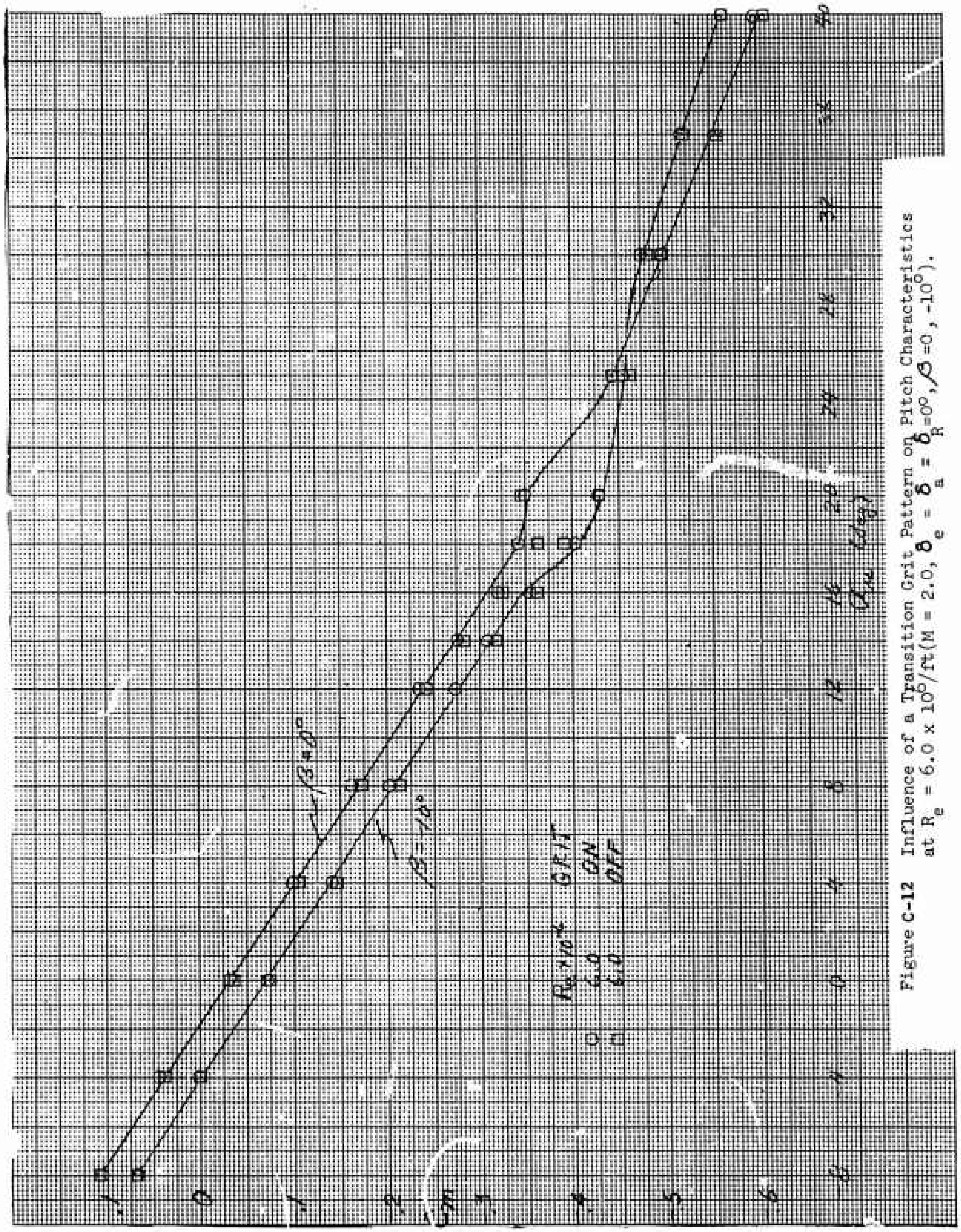

Figure C-12 Influence of a Transition Grit Pattern on Pitch Characteristics at $R_e = 6.0 \times 10^6$/ft ($M = 2.0$, $\delta_e = \delta_a = \delta_R = 0°$, $\beta = 0, -10°$).

Preceding page blank

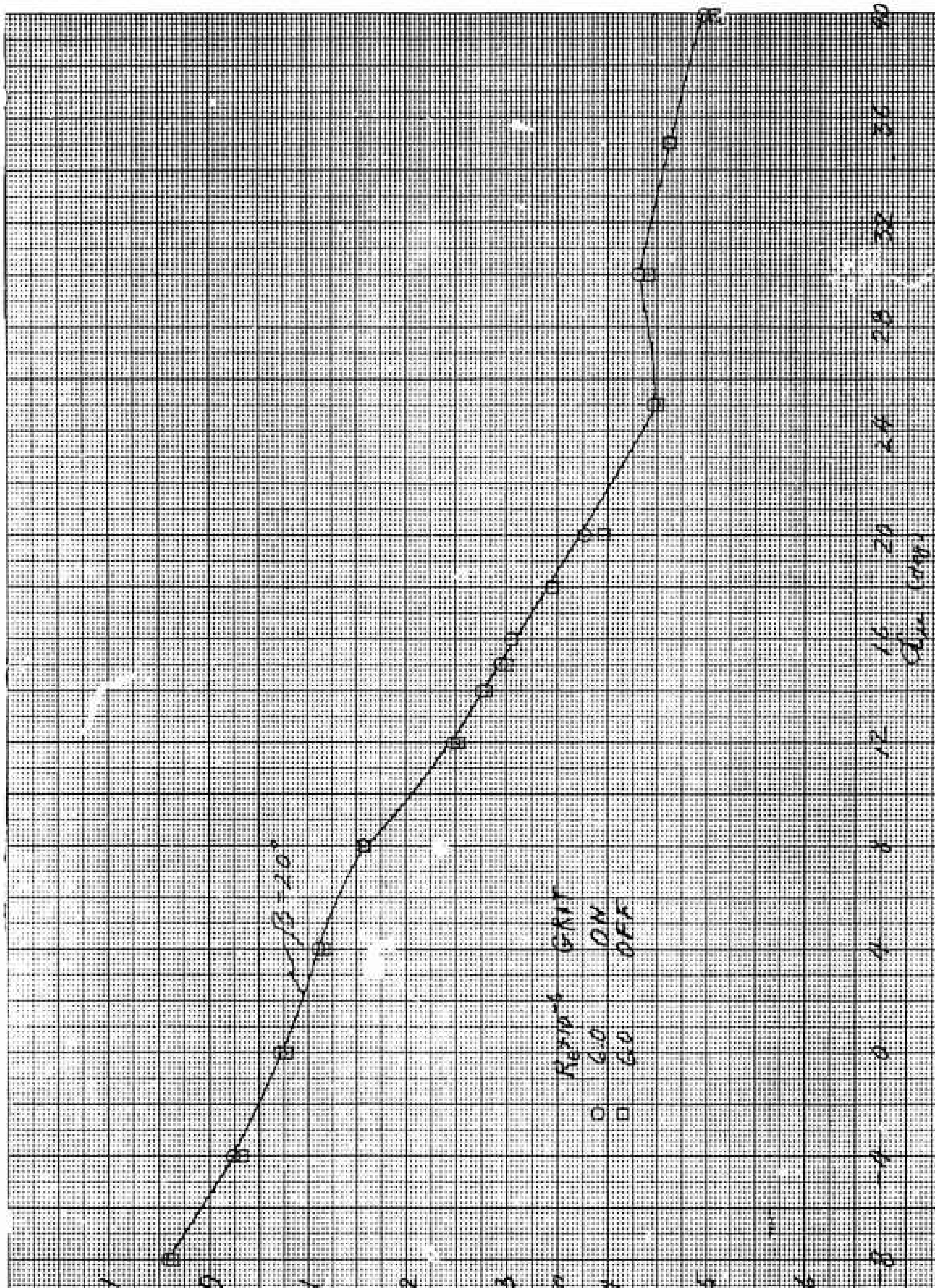

Figure C-13 Influence of a Transition Grit Pattern on Pitch Characteristics at $R_e = 6.0 \times 10^6$/ft, ($M=2.0$, $\delta_e = \delta_a = \delta_R = 0°$, $\beta = 20°$).

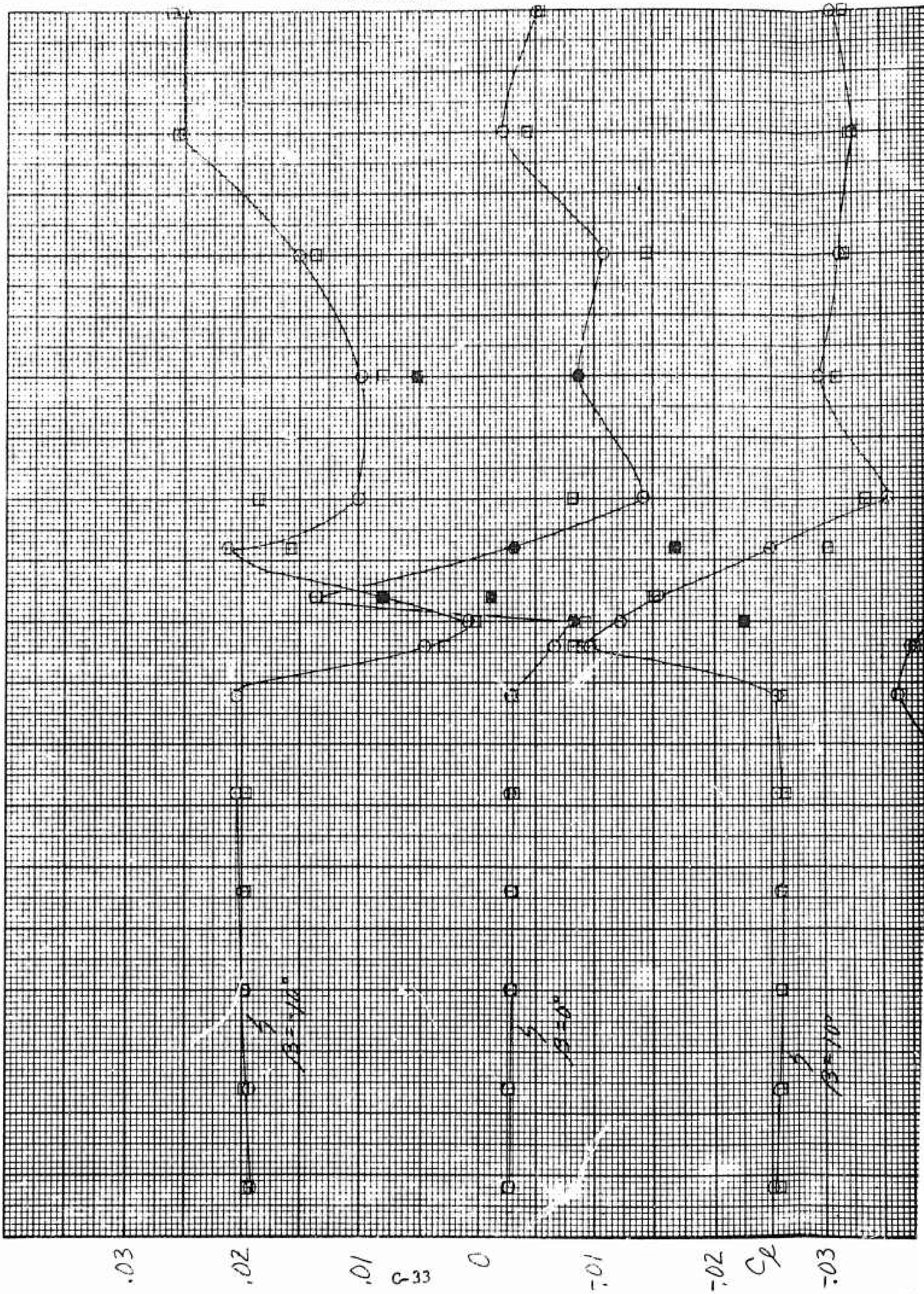
.03
.02
.01
0
-.01
-.02
C_ℓ
-.03
β=+10°
β=0°
β=-10°

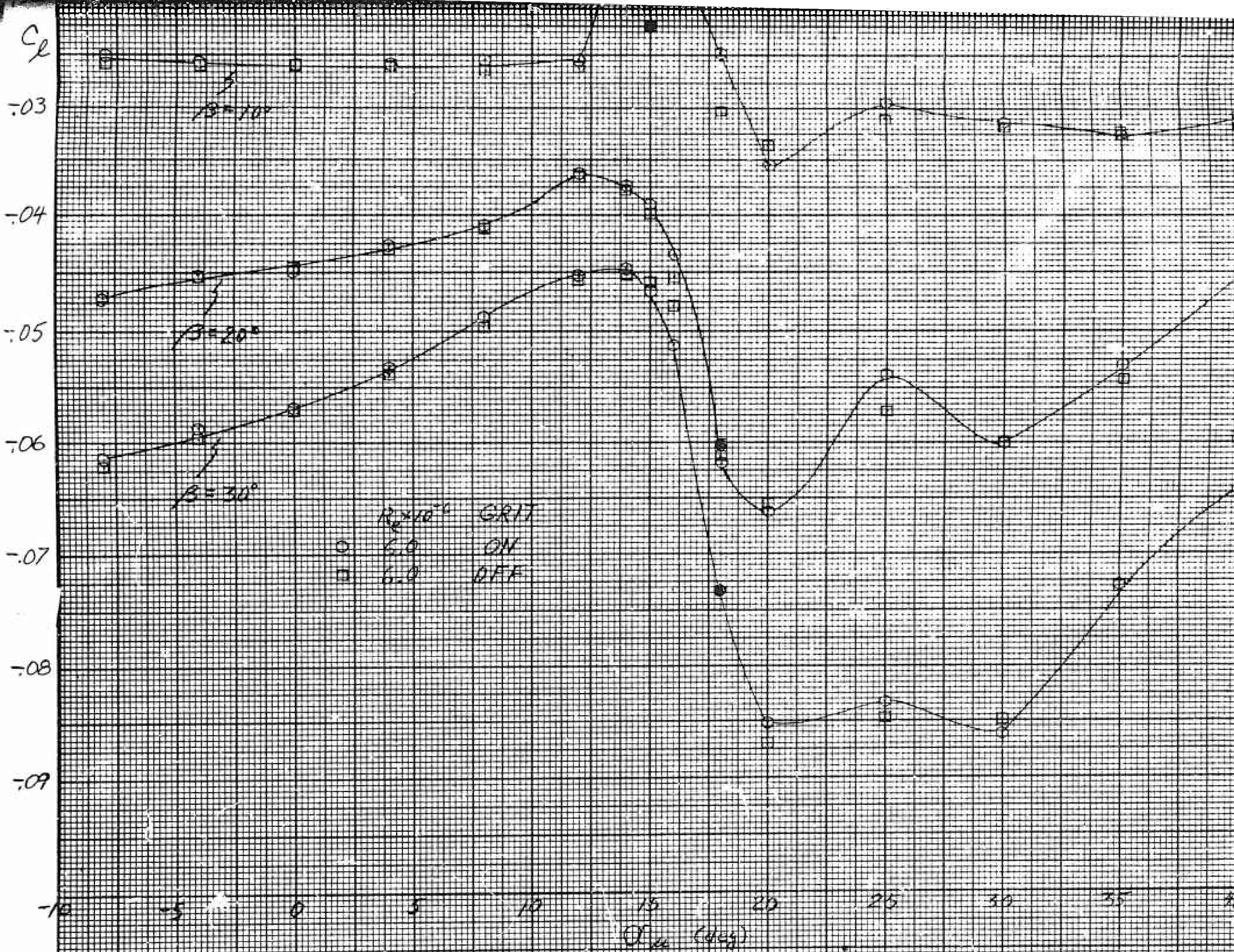

Figure C-14 Influence of a Transition Grit Pattern on Roll Characteristics at $R_e = 6.0 \times 10^6$/ft, ($M=2.0$, $\delta_e = \delta_a = \delta_R = 0°$, $\beta = -10, 0, 10, 20, 30°$).

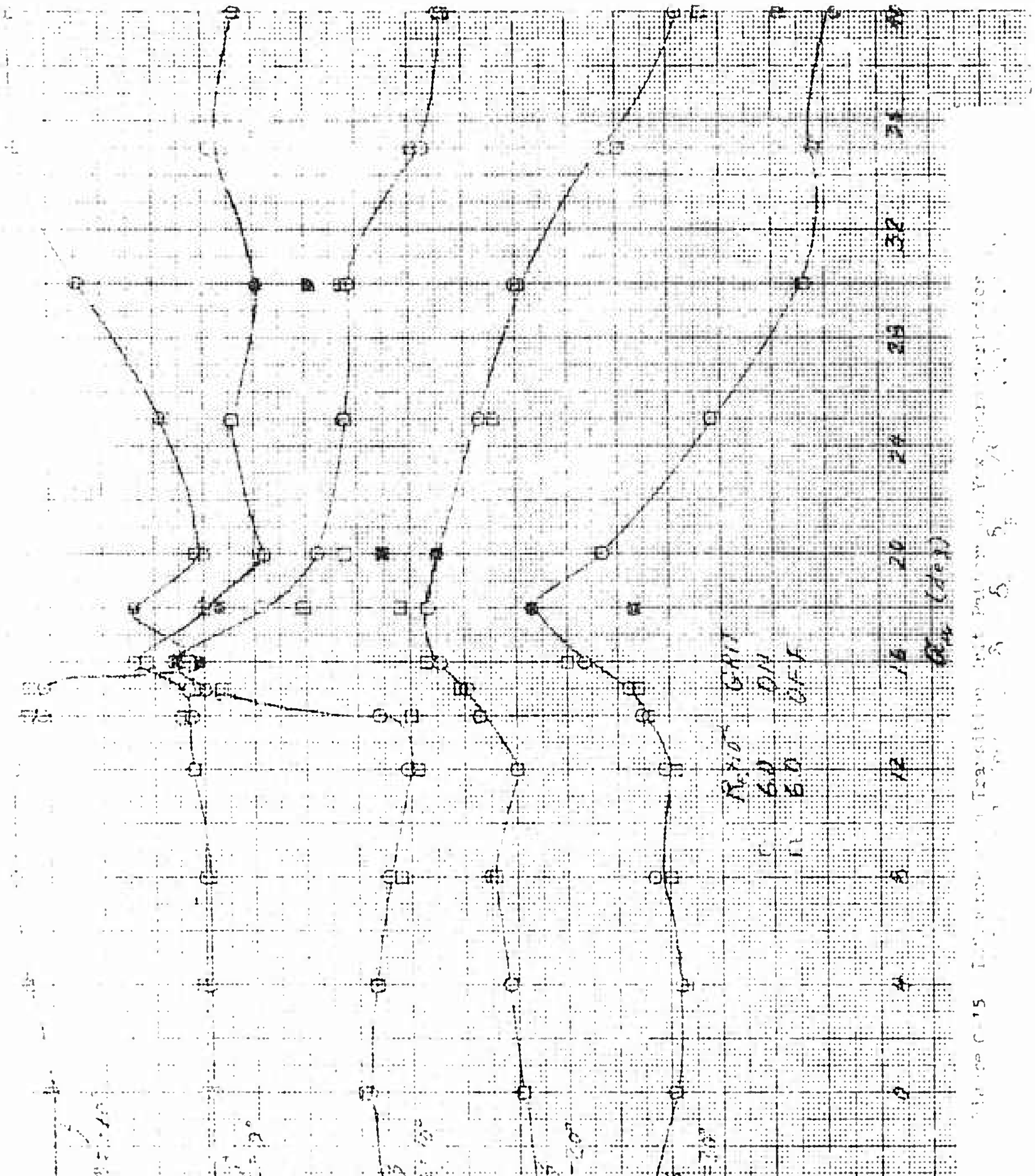

Preceding page blank